Halogen Bonding Fluorescent Receptors for Sensing Hydrosulfide and Other Anions

Edward Joseph Mitchell

Linacre College



A thesis submitted for the degree of Doctor of Philosophy

in Inorganic Chemistry

Trinity 2021

Halogen Bonding Fluorescent Receptors for Sensing Hydrosulfide and Other Anions

Edward Joseph Mitchell, Linacre College, University of Oxford

Abstract of thesis submitted for the degree of D.Phil, Trinity 2021

This thesis describes the preparation and study of fluorescent iodotriazole containing host molecules exploiting halogen bonding for the selective molecular recognition and sensing of hydrosulfide and other anions.

Chapter One introduces the field of anion supramolecular chemistry, highlighting the areas of relevance to this thesis, including the non-covalent interaction halogen bonding (XB), and reviews artificial molecular receptors for the selective recognition and sensing of anion guest species, in particular hydrosulfide.

Chapter Two describes the development of a series of halogen bonding coumarin based receptors, including acyclic, macrocyclic and mechanically interlocked systems. The synthetic procedures and characterisation of each receptor are described. The capability of each receptor to recognise anions in organic solvent media, coupled with the coumarin fluorophore's ability to relay and sense the binding event via changes in fluorescence, is explored using ^{1}H NMR and fluorescence emission spectroscopy titration experiments.

Chapter Three builds on the results of Chapter 2, detailing the synthesis and characterisation of two generations of acyclic water-soluble halogen bonding coumarin receptors. The receptors, each employing water solubilising TEG groups, are investigated for their ability to recognise and sense hydrosulfide and other anions in pure and buffered water. Computational Density Functional Theory (DFT) and Molecular Dynamics simulations are used to corroborate the experimental anion binding observations.

Chapter Four investigates the use of BODIPY as a fluorescent reporter group in anion receptor design. A variety of BODIPY-iodotriazole containing receptors are prepared, including acyclic receptors, mechanically interlocked molecules, and porphyrin-BODIPY [2]rotaxanes. The anion recognition and fluorescence emission sensing properties of each receptor are investigated in organic and organic-aqueous solvent mixtures.

Chapter Five provides a summary of the main conclusions of this thesis.

Chapter Six details the experimental procedures employed in this work, including synthetic protocols and characterisation data for novel compounds.

Acknowledgments

Firstly, I would like to extend a great thank you to Professor Paul Beer for giving me the opportunity of a lifetime to come and study at the University of Oxford. As a supervisor he has been encouraging and tremendously helpful. His patient and laid-back approach has allowed me to pursue wider interests and has made my degree an enjoyable endeavour. The taxpayer, through RWM and the EPSRC, has provided the funds for the work in this thesis; I'll make sure to pay back to society in many positive ways over my lifetime.

Reaching the end would have been near impossible had it not been for the camaraderie of the Beer and Langton groups, with whom many pints were sunk in the multitude of great Oxford pubs. My first and last fumehood companion Robert Hein has always been enthusiastic and engaging — a good friend who is also a marvellous chemist. My early weeks and months were made welcoming by the support of George Li who would never-end to inspire me with his exciting chemistry ideas.

The long hours in the lab were made enjoyable by the friendships built over these past four years. Jessica Pancholi's great taste in tunes made every day more entertaining, whilst the compromise struck with Jane on podcasts and Laura on music meant we all came to share similar interests that would erupt into hours of debate. Enjoyable political exchanges were never far from conversation with Zongyao and Krzysztof, whilst reminiscing of old Durham days with Toby was a form of sweet escapism. Weekend sessions in the lab listening and chatting about the R&S OST with Aidan stand as some of my favourite memories. A big thank you to everyone else who made S7 a vibrant place to work.

I would like to give a special thank you to my part II student Adam Beecroft, whose work was pivotal to the completion of this thesis. Cheers for all the great conversations and fun games of slither.io and backgammon to beat the long hours of waiting for titrations and NMRs.

Beyond the lab I have been privileged to make many brilliant friends in Oxford. I would like to thank my first-year housemates from 49 Walton Street who made returning home something to look forward to, whether for the long kitchen debates or for one of the many events we would attend together. Within the Linacre College Common Room I give thanks to the many diverse, interesting and enriching friends I made, without which I would have never taken on the positions of Social Secretary or President. The final year of my DPhil was dominated by the pandemic, but I was fortunate to make a family out of my household bubble; Vihanga, Dilhan,

Sol, Rana and Ziyue, thank you for a brilliant final year of late-night parties and hours of music into the night.

Of course, none of this would ever have been achieved if it was not for my family. I would like to thank my Mum, Chris, Dad, Amanda and Duncan for their unwavering support. A special thank you goes to Granny Laura for her support of my formal dinner filled, socialite Oxford lifestyle.

Finally, I want to thank my friends from my undergraduate days in Durham. Though we no longer live in the same city, we have all endeavoured to meet as regularly as possible, go on holidays together, and call during the long lockdowns. They have given my life stability and sanctuary when I have needed it. I want to specifically thank Hannah, Jack, Vincent and Tia for their tremendous support over these years.

'Each of these lives is the right one.

Every path is the right path.

Everything could have been anything else and it would have just as much meaning.'

Nemo — Mr Nobody; paraphrasing Tennessee Williams

Publications

Hydrosulfide (HS^-) Recognition and Sensing in Water by Halogen Bonding Hosts

Edward J. Mitchell, Adam J. Beecroft, Jonathan Martin, Sally Thompson, Igor Marques, Vítor Félix, Paul D. Beer, *Angew. Chemie - Int. Ed., 2021, **60**, 24048-24053*

Halogen Bonding Strapped Porphyrin BODIPY Rotaxanes for Dual Optical and Electrochemical Anion Sensing

Richard Yuen C. Tse, Robert Hein, Edward J. Mitchell, Zongyao Zhang and Paul D. Beer, *Chem. Eur. J., 2021, **27**, 14550-14559*

Poster Presentations

Supramolecular Environmental Sulphide Sensing. *14th International Symposium on Macrocyclic and Supramolecular Chemistry, June 2019, Lecce, Italy.*

Supramolecular Environmental Sulphide Sensing. *RSC Macrocyclic and Supramolecular Chemistry, December 2018, Lancaster, U.K.*

Abbreviations

δ	chemical shift
β_x	binding constant
λ	wavelength
μ	micro
Δ	change in (a physical quantity)
Å	Ångstrom
a.u.	arbitrary units
ACQ	Aggregation-caused quenching
AMT	active metal template
br.	broad
BODIPY	boron-dipyrromethene (4,4-difluoro-4-bora-3a,4a-diaza-s-indacene)
cat.	catalytic
CuAAC	copper(I)-catalysed azide-alkyne cycloaddition
DBU	1,8-diazabicycloundec-7-ene
DMAP	4-dimethylaminopyridine
DMF	N,N-dimethylformamide
DMSO	dimethyl sulfoxide
DNA	deoxyribonucleic acid
e.g.	*exempli gratia*
EDTA	ethylenediaminetetraacetate
eq	equivalents
ESI	electrospray ionisation (mass spectrometry)
g	gram
G	Gibbs free energy
Grubbs' I/ II	Grubbs' first/ second generation catalyst
H	enthalpy
HB	hydrogen bonding
HRMS	high resolution mass spectrometry
Hz	Hertz
ICT	Isothermal titration calorimetry
i.e.	id est
J	coupling constant
K	Kelvin (Temperature SI Unit)
K_a	association constant
K_d	dissociation constant
L	litre
M	molar (moles per litre)
m/z	mass to charge ratio
Me	methyl
MIM	mechanically-interlocked molecule
MS	mass spectrometry

Ms	mesyl
NMR	nuclear magnetic resonance
PEG	polyethylene glycol
PET	photo-induced electronic transfer
ppm	parts per million
PTLC	preparative thin layer chromatography
rt / RT	room temperature
RCM	ring-closing metathesis
Rf	retention factor
ROESY	rotating-frame nuclear Overhauser effect correlation spectroscopy
S	entropy
TBA	tetrabutylammonium
TBTA	tris[(1-benzyl-1,2,3-triazol-4-yl)methyl]amine
TEG	triethylene glycol
TFA	trifluoroacetic acid
THF	tetrahydrofuran
TLC	thin layer chromatography
TMS	trimethylsilyl (protecting group)
Ts	tosyl
UV	ultra-violet
v/v	volume/ volume percent
vis.	visible
XB	halogen bonding

Contents

Abstract i
Acknowledgments ii
Publications v
Abbreviations vi
Contents viii
Chapter 1 Introduction 1
1. Introduction 2
1.1. Supramolecular Chemistry 2
1.2. Host-Guest Chemistry 2
1.2.1. The Importance of Anions 3
1.2.2. The Challenges of Anion Recognition 4
1.2.3. Anion Recognition Toolkit 7
1.2.3.1. Complementarity 7
1.2.3.2. Preorganisation 7
1.2.3.3. Non-covalent interactions for anion recognition 8
1.2.3.3.1. Electrostatic forces — Ions & Dipoles 8
1.2.3.3.2. Hydrogen bonding 9
1.2.3.3.3. Halogen Bonding 9
1.2.3.3.4. Anion-π interactions 10
1.2.4. Host Systems for Anion Recognition 10
1.2.4.1. Natural Hosts 11
1.2.4.2. Positively Charged Receptors 12
1.2.4.2.1. Protonated amine, quaternary ammonium- and guanidinium-based receptors 12
1.2.4.2.2. Imidazolium, Triazolium and Pyridinium receptors 13
1.2.4.3. Neutral Receptors 17
1.2.4.3.1. Amide, Urea/Thio-Urea and Squaramide Receptors 17
1.2.4.3.2. Pyrrole receptors 19
1.2.4.3.3. Triazoles and campestarene receptors 20
1.2.4.3.4. Chalcogen Bonding Receptors 22
1.2.4.4. Water soluble Hosts 22
1.2.4.5. Mechanically Interlocked Anion Hosts 24
1.3. Anion Sensing 29
1.3.1. Optical anion sensing 30
1.3.1.1 Fluorescence and luminescence anion sensing 30
1.3.1.2. Colorimetric anion sensing 34
1.3.2. Electrochemical anion sensing 35
1.3.3. Surface assembled anion sensors 36
1.4. Hydrogen sulfide and the hydrosulfide anion 38
1.4.1. Hydrosulfide recognition and sensing 38
1.4.1.1. Chemodosimeters 39
1.4.1.2. Supramolecular approaches and challenges to hydrosulfide recognition 40
1.5. Objectives 43
1.6. References 44

Chapter 2 Coumarin-based Anion Receptors **49**
2. Coumarin-based Anion Receptors 50
2.1. Introduction 50
2.1.1. Coumarin anion sensors 50
2.1.2. Chapter Objectives 51
2.2. Acyclic Halogen Bonding Coumarin Receptor 52
2.2.1. Synthesis 53
2.2.2. Anion Binding Studies 54
2.2.2.1. ^{1}H NMR Titrations 54
2.2.2.2. Fluorescence Titrations 57
2.2.3. Summary 61
2.3. Macrocyclic Halogen Bonding Coumarin Receptors 61
2.3.1. Synthesis 61
2.3.1.1. Synthesis of a bis-coumarin-azide compound 61
2.3.1.2. Attempted copper (I) catalysed azide-alkyne macrocyclization 63
2.3.1.3. Synthesis of a bis-coumarin-alkene derivative 64
2.3.1.4. Ring-closing metathesis (RCM) reactions 65
2.3.2. Anion Binding Studies 68
2.3.2.1. 1H NMR titrations 69
2.3.2.2. Fluorescence Titrations 70
2.3.3. Summary 72
2.4. Rotaxane Coumarin Receptors 72
2.4.1. Synthesis 75
2.4.1.1. Synthesis of bis azide axle precursor 75
2.4.1.2. Stopper synthesis 76
2.4.1.3. Active metal templation rotaxane synthesis 76
2.4.1.4. Rotaxane 2.32 characterisation 77
2.4.1.5. Synthesis of stopper bromide 79
2.4.1.6. Synthesis of pyridinium axle 79
2.4.1.7. Chloride templated ring-closing-metathesis rotaxanation 80
2.4.1.8. Rotaxane 2.40 characterisation 81
2.4.2. Anion Binding Studies 83
2.4.2.1 Fluorescence Titrations 83
2.4.3. Summary 86
2.5. Conclusion and Summary 87
2.6. References 88
Chapter 3 Water Soluble Halogen Bonding Receptors for Hydrosulfide **89**
3. Water Soluble Halogen Bonding Receptors for Hydrosulfide 90
3.1. Introduction 90
3.1.1. Photo-physical Sensing in Water 90
3.1.3. Chapter Objectives 91
3.2. Generation 1 Water Soluble XB Receptors 93
3.2.1. Synthesis 93
3.2.1.1. Synthesis of TEG tertiary amine coumarin azide 93
3.2.1.2. Synthesis of bis-iodoalkyne amine 94
3.2.1.3. Synthesis of acyclic receptors 94
3.2.2. Anion Binding Studies 98
3.2.2.1. 1H NMR Titration studies 98

3.2.2.1.1. Preliminary studies in acetone 98
3.2.2.1.2. Receptor 3.11 ^{1}H NMR Titration Studies in Acetone 99
3.2.2.1.3. Protonation Studies 100
3.2.2.1.4. Receptor 3.12 ^{1}H NMR Titration Studies in Acetonitrile 101
3.2.2.2. Fluorescence Titration Studies 102
3.2.2.2.1. Receptor 3.11 Fluorescence Titration Studies 103
3.2.2.2.2. Receptor 3.12 Fluorescence Titration Studies 105
3.2.3 Summary 106
3.3. Generation 2 Water Soluble XB Receptors 106
3.3.1. Synthesis 106
3.3.1.1. Synthesis of benzyl TEG azide 106
3.3.1.2. Synthesis of receptors 108
3.3.1.2.1. Synthesis of XB and HB pyridine receptors 110
3.3.1.2.2. Synthesis of XB and HB pyridinium receptors 112
3.3.2. Anion Binding Studies 114
3.3.2.1. ^{1}H NMR Studies 115
3.3.2.2. pKa determination of secondary amine XB and HB receptors 118
3.3.2.3. Photophysical Studies 120
3.3.2.3.1. XB receptor 3.20H^{+} and HB receptor 3.22H^{+} Fluorescence Titration Studies 122
3.3.2.3.2. XB receptor 3.23 and HB receptor 3.24 Fluorescence Titration Studies 125
3.3.2.3.3. XB receptor 3.25 and HB receptor 3.26 Fluorescence Titration Studies 128
3.3.3. Reversibility Studies 130
3.3.4. Limit of Detection 132
3.3.5. Molecular Modelling 134
3.3.6. Summary 136
3.4. Conclusions and Future Work 136
3.5. References 139
Chapter 4 BODIPY-Based Halogen Bonding Receptors 141
4. BODIPY-based Halogen Bonding Receptors 142
4.1. Introduction 142
4.1.1. BODIPY receptor systems 142
4.1.2. Chapter Objectives 143
4.2. Iodotriazole BODIPY 144
4.2.1. Mono-Iodotriazole Synthesis 144
4.2.2. Anion Binding Studies 145
4.2.2.1. 1H NMR Titration Studies 145
4.2.2.2. Fluorescence Titration Studies 146
4.2.3. Summary 148
4.2.4. Bis-Iodotriazole BODIPY 148
4.2.5. Bis-Iodotriazole BODIPY Generation 1 Synthesis 149
4.2.6. Anion Binding Studies 150
4.2.6.1. Fluorescence Titration Studies 150
4.2.7. Bis-Iodotriazole BODIPY Generation 2 Synthesis 152
4.2.8. Fluorescence Titration Studies 154
4.2.8.1. Titration Studies in Acetonitrile 154
4.2.8.2. Titration Studies in Water-Acetonitrile Mixtures 157

4.2.9. Summary 163
4.3. BODIPY Rotaxanes 164
4.3.1. BODIPY Stopper Synthesis 166
4.3.2. Axle and Rotaxane Synthesis 167
4.3.2.1. Rotaxane Characterization 168
4.3.3. Rotaxane and Axle Anion Binding Studies 170
4.3.3.1. 1H NMR Chloride Anion Titration Studies 170
4.3.3.2. Rotaxane Decomposition 173
4.3.3.3. XB Axle 4.21 and HB Axle 4.22 Fluorescence Titration Studies 174
4.3.4. Summary 175
4.4. BODIPY-Porphyrin Rotaxanes 175
4.4.1. Introduction to Porphyrin Receptors 175
4.4.2. BODIPY Phenyl Spacer Rotaxane Synthesis & Characterisation 177
4.4.3. BODIPY Perfluoroaryl Spacer Rotaxane Synthesis & Characterisation 180
4.4.4. Anion Binding Studies 183
4.4.4.1. Fluorescence Titrations 183
4.4.5. Summary 188
4.5. Conjugated XB BODIPY Receptor 189
4.5.1. Synthesis 189
4.5.2. Preliminary Anion Binding Studies 190
4.5.2.1. 1H NMR titrations 190
4.5.2.2. Fluorescence Titrations 190
4.5.3. Summary 193
4.6. Conclusions and Future Work 193
4.7. References 195
Chapter 5 Conclusions **197**
5.1. Conclusions 198
Chapter 6 Experimental **201**
6. Experimental 202
6.1. General Information 202
6.1.1. Instruments 203
6.2. Solution Titration Protocols 203
6.2.1. Tetrabutylammonium (TBA) Salts for Titration 203
6.2.2. 1H NMR Titrations 203
6.2.3. Fluorescence Titrations 204
6.3. Synthesis from Chapter 2 205
6.4. Synthesis from Chapter 3 223
6.5. Synthesis from Chapter 4 239
6.6. References 254

Chapter 1

Introduction

1. Introduction

1.1. Supramolecular Chemistry

Supramolecular chemistry is at the forefront of our ability to manipulate matter. It concerns the non-covalent intermolecular bonds that bring two or more molecules together; individually each intermolecular bond is weaker than their covalent counterpart, but when in concert the strength is remarkable. Many fundamental biological systems and processes are built on supramolecular interactions. Even duplex DNA, present in every cell in the body, consists of two entwined molecular helixes bridged by intermolecular hydrogen bonding. [1]

The expanding field of supramolecular chemistry draws its inspiration from the fundamentals of nature and the complexity in biological processes. From its origins in host-guest chemistry, the field has now come to encompass an enormous number of disciplines such as molecular self-assembly, molecular recognition and nanotechnology,[2] the research of which promises to take us into the future with technologies such as smart materials, targeted medicine, and biological computers.[3] The field of supramolecular chemistry has enhanced our fundamental understanding of the world around us and has been the subject for which two Nobel prizes have been awarded.

1.2. Host-Guest Chemistry

In 1987 Pedersen, Lehn and Cram were jointly awarded the Nobel Prize in chemistry for their work on establishing the field of host-guest chemistry. Their pivotal research was based on Fischer's fundamental work on biological enzyme substrate interactions, elegantly described in 1884 as a 'lock and key' analogy.[4] This ingenious metaphor correctly identified a complementarity between the species involved. It is this complementarity of shape, size and chemical functionality between a host (lock) and guest (key) which forms the basis of all host-guest chemistry.

By using these principles Pedersen demonstrated host-guest size complementarity between crown ethers and group 1 metal cations, such as dibenzo-18-crown-6 being selective for potassium (Figure 1.1a).[5] Enhanced group 1 metal cation recognition was achieved with the three-dimensional cryptands developed by Lehn[6] (Figure 1.1b) and the preorganised spherands by Cram (Figure 1.1c).[7] Each of these hosts contain cavities large enough to encapsulate unsolvated metal cations via favourable ion-dipole interactions.

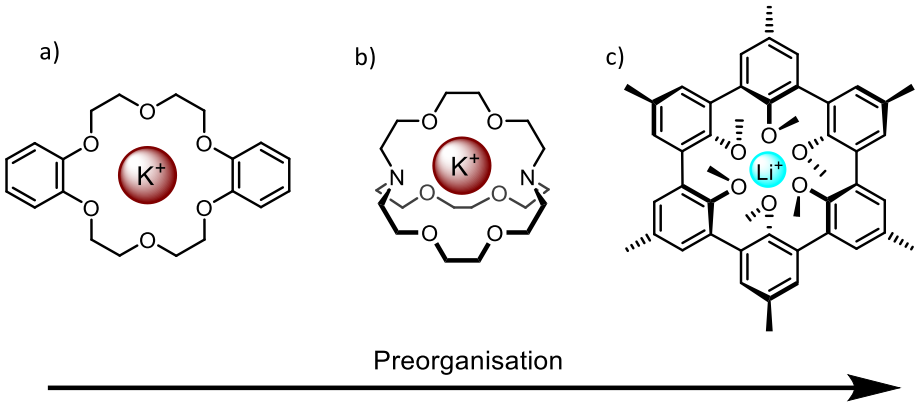


Figure 1.1: *Host-guest complexes* ***a)*** *Pedersen's potassium cation dibenzo[18]-crown-6 complex* ***b)*** *Lehn's potassium cation [2.2.2]cryptand complex* ***c)*** *Cram's lithium cation spherand complex*

Parallel to the early advancements in cation host-guest chemistry, anion coordination was also being investigated, with the first synthetic anion receptors being developed by Park and Simmons in 1968.[8] Analogous to Lehn's cryptands, the receptors adopted a macrobicyclic three-dimensional shape with bridgehead nitrogens. Termed katapinands, once protonated the hosts were found to be capable of binding and encapsulating halides in acidic aqueous solution via favourable electrostatics and hydrogen bonding (Figure 1.2). Although further anion host receptors were developed, such as Lehn's cryptates,[9] progress remained sporadic in the subsequent decades compared to the growth in field of cation coordination. By the 1990s the field was evolving and the inherent challenges of binding anions was reflected in increasingly imaginative host receptors.

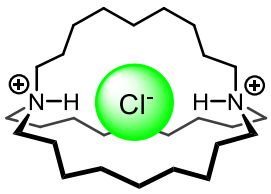


Figure 1.2: *Katapinand – chloride diazabicyclo[9.9.9]alkane ammonium ion complex*

1.2.1. The Importance of Anions

The critical role of anions in the world around us cannot be understated. Anions fulfil a plethora of functions in biological systems with the majority of all enzyme substrates and co-factors existing as anions under physiological conditions: adenosine triphosphate (ATP), responsible for regulating intercellular energy transfer, and the very backbone of biological information, DNA and RNA, all exist as polyanionic phosphate esters. [1,10]

The simpler halides also play an important role *in vivo*. Chloride is present extensively in extracellular fluid and is essential for regulating blood pressure and in a number of homeostatic, osmotic and respiratory processes.[11] Hereditary defects in the ability of membrane channel proteins to regulate intercellular transport of chloride is responsible for the disease cystic fibrosis.[12] Similarly, misregulation of iodide is the cause of a number of thyroid related diseases, as it plays a critical function in the biosynthesis of hormones in the gland.[13] Although only important as a trace element, bromide and the bromosulfonium ion are needed in the production of specific proteins for tissue development.[14]

Anions make up many of the key macronutrients absorbed by plant roots. In particular, nitrates and phosphates are essential for growth and see extensive industrial production for use as fertilisers. Over many decades, the overuse of these fertilisers in intensive arable farming has caused environmental damage from algal blooms or eutrophication, a process that can deplete oxygen-water levels to the point of eco-system collapse.[15] Other by-products of humanity have also polluted parts of the environment with dangerous levels of anions. Extensive use of cyanide in metal extraction has left areas of land and water systems toxic.[11] Nitrates and sulfates produced from burning fossil fuels are responsible for spreading acid rain across parts of the globe.[15] Pertechnetate, produced from reprocessing nuclear fuel, can leave aquatic environments radioactive for centuries.[16] The negative effects of anthropogenic anions are evident all around us and are a significant cause for concern, one of which is the naturally occurring hydrosulfide anion which will be addressed in section 1.4. Hydrogen sulfide and the hydrosulfide ion.

In all of these processes and environments anions play a multitude of roles as nucleophiles, bases and catalysts. The fundamental and topical importance of anions has made the continued search for synthetic receptors capable of sensing or sequestering anions highly desirable.

1.2.2. The Challenges of Anion Recognition

Nature has had millennia to perfect the complex task of anion selectivity in natural processes. In spite of this, the fundamental challenges of anion recognition still compromise many functions. In mammals, bromide can be misrecognised as iodide and cause harmful goitrogen effects.[17,18] Although with fault, the systems that govern anion recognition in biology are remarkable and provide the inspiration behind many synthetic receptor designs. The challenges stem from a number of intrinsic properties related to anions that make distinguishing one anion from another and outcompeting solvent interactions a difficult task.

Generally, anions are far larger and consequently less electron dense than their isoelectric cationic counter parts (Table 1.1). This leads to a significant decrease in Coulombic attraction, requiring receptors to utilise more interactions to compensate. The diffuse nature of anions however, does create a higher degree of polarizability which permits dispersion forces to have a greater contribution towards host-guest complexation.

Table 1.1: *Ionic radii and free energies of hydration for anions and cations* [19,20]

Anion	Ionic Radius / Å	Δ G_{hyd} /kJ mol^{-1}	Cation	Ionic Radius / Å	Δ G_{hyd} /kJ mol^{-1}
F^-	1.19	-465	Na^+	1.16	-365
Cl^-	1.67	-340	K^+	1.52	-295
Br^-	1.82	-315	Rb^+	1.66	–
I^-	2.06	-275	Cs^+	1.81	-250

Anions also adopt a range of geometries (Figure 1.3), varying from simple spheres to complex chiral amino acids. This diversity allows for the rational design of receptors containing cavities of complementary shape and size for specific anion targets.

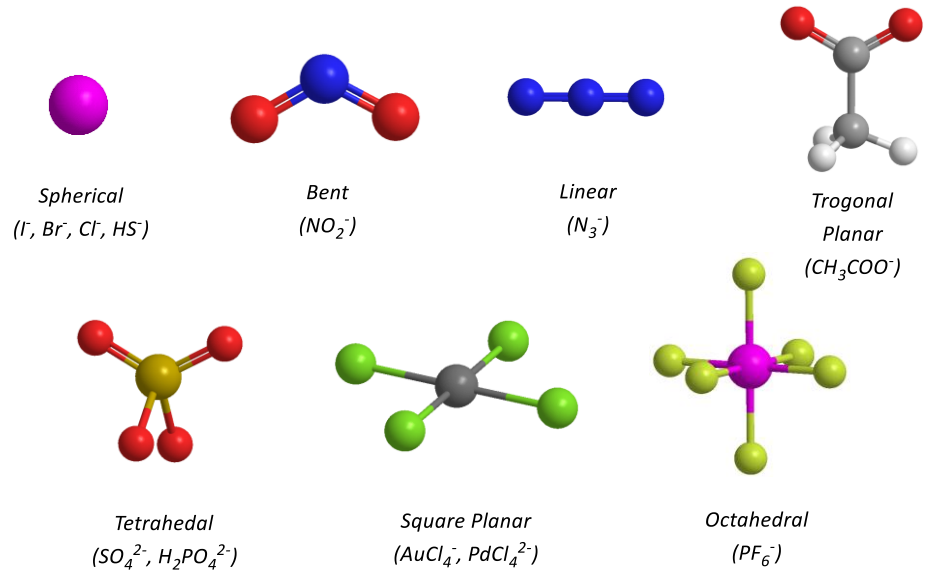


Figure 1.3: *Basic Anion Geometries*

The majority of anions are susceptible to protonation i.e. they are pH dependent. Consequently, solvent pH is of critical importance. Many receptors rely on *in situ* protonation

for binding, such as polyammonium host systems which would cease to function above certain high pH thresholds. Accordingly, there is a critical pH window in which recognition can take place when the anion is present and the receptor is protonated and functional (Figure 1.4). Furthermore, anions such as cyanide and fluoride, which are highly basic, may de-protonate a receptor, preventing effective recognition.[21]

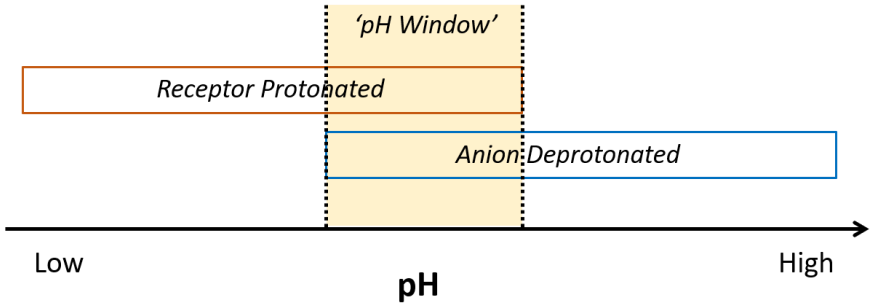


Figure 1.4: *Receptor pH window, in which a receptor can operate and an anion is not protonated*

Anions exhibit high free energies of solvation, particularly in protic polar solvents such as water (Table 1.1). As a consequence, potential anion binding receptors must compete with the solvent environment and overcome the desolvation energy barrier. Compared to similar sized cations this energetic cost is much greater for anions; F^- and Na^+, for example, have similar ionic radii, however the free energy of hydration is much larger for the halide (Table 1.1). Numerous neutral anion receptors commonly only function in aprotic solvents, such a chloroform, where the desolvation energy barrier is relatively low — strong and selective anion binding in aqueous media, especially in pure water, remains a key challenge.

The *Hofmeister series*,[22] originally established from studying salt effects on the solubility of proteins, ranks anions according to their hydrophobicity, which is reflected in their respective hydration energies (Figure 1.5). Larger, more charge diffuse anions such as I^- tend to be more hydrophobic and less solvated than the more charge dense anions such as F^-, which is much more hydrophilic. The collective Lewis acid property terms 'hard' and 'soft' align with the *Hofmeister series*. 'Hard' anions refer to those that have a smaller ionic radius, have higher charge states, and are less easily polarised. 'Soft' refers to anions with larger ionic radii, lower charge states, and are more easily polarised. Kosmotropic anions contribute to the stability of water-water interactions and as a result can induce aggregation of hydrophilic molecules in solution. Chaotropic anions disrupt water-water interactions, thereby increasing the solubility of hydrophilic solutes and disrupting their aggregation. As illustrated in the section reviewing

water soluble anion host systems, the selective binding of hydrophobic anions is achieved by employing lipophilic host cavities.[22]

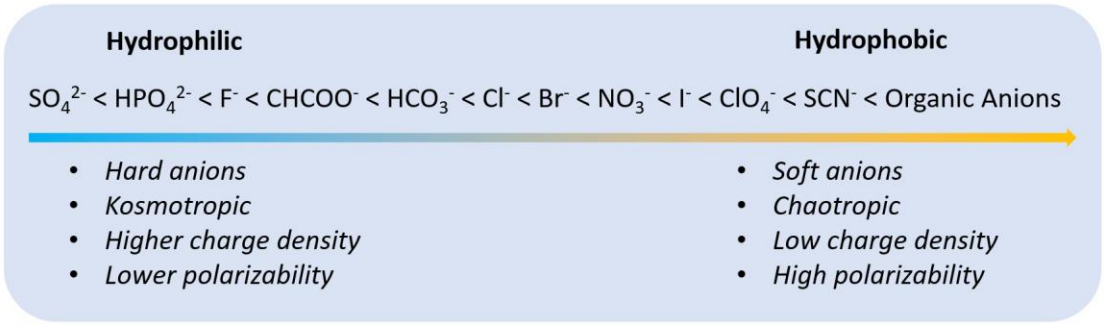


Figure 1.5: *Hofmeister Series and general trends*

1.2.3. Anion Recognition Toolkit

Anion recognition is achieved through complementary non-covalent attraction between host and guest. The key concepts for host-guest recognition in general and the specific non-covalent interactions considered and exploited by supramolecular chemists in the pursuit of anion recognition are discussed in the following sections.

1.2.3.1. Complementarity

The concept of 'lock and key' and the later 'induced fit' model, whereby enzymes undergo conformational changes to bind to guests, are the foundations of host-guest complementarity. Both of these concepts highlight the requirement that in order to maximise host-guest non-covalent interactions, the host contains a cavity that complements the guest's shape and size. The supramolecular chemist can tune a host's geometric and stereoelectronic characteristics to increase selectivity over non-complementary guests of the wrong shape and size.

1.2.3.2. Preorganisation

The concept of preorganisation was introduced by Cram who stated " the more highly hosts and guests are organised for binding and low solvation prior to their complexation, the most stable will be their complexes".[23] This occurs because of both entropic and enthalpic favourability — a lower enthalpic penalty and a more favourable entropy owing to a reduction in the degrees of freedom lost upon association. This was elegantly demonstrated by the comparison between acyclic hosts and their crown ether analogues for group 1 metal cation recognition. Crown ethers exhibit far greater binding associations; this is termed the macrocyclic effect.[24] As seen with cryptand and spherand molecules (Figure 1.1), likewise for

the acyclic, macrocyclic and cryptand polyammonium anion host systems shown in Figure 1.6, where increasing preorganisation results in enhanced anion association.[25,26,27]

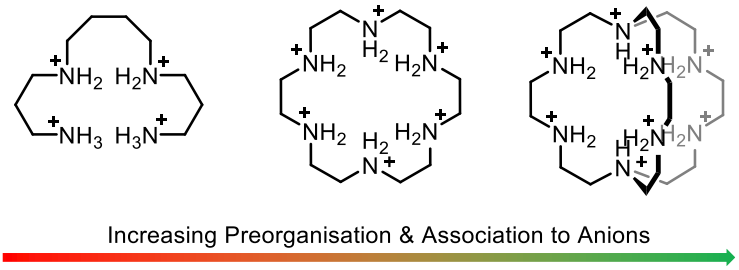


Figure 1.6: *Increase in preorganisation and anion association — acyclic, macrocyclic and cryptand*

1.2.3.3. Non-covalent interactions for anion recognition

This sub-section will briefly explore the non-covalent interactions most commonly used for host-guest anion association.

1.2.3.3.1. Electrostatic forces — Ions & Dipoles

The electrostatic forces that dictate attraction and repulsion between charged species is governed by Coulomb's law (Equation 1.1). The law states that the electrostatic force of attraction is equal to the multiple of two charged species divided by the square distance between them, all multiplied by Coulombs' constant.

Equation 1.1: Coulomb's law

$$F = k\frac{q_1 q_2}{r^2}$$

F = The electric force between the two charges

k = Coulombs' constant (8.99 x 10^9 kg m^3 s^{-2} C^{-2})

q_x = Charge of species

r = Distance of separation

Ion-ion (100–300 kJ mol^{-1}), ion-dipole (50–200 kJ mol^{-1}) and dipole-dipole (5–50 kJ mol^{-1}) interactions all have varying degrees of strength based on their charge and the distances involved, with the strongest being the attractive force between two ions. To take advantage of this attraction many anion host receptors are cationic, such as Schmidtchen's quaternary ammonium cage (Figure 1.7) which is capable of binding chloride in water.[28]

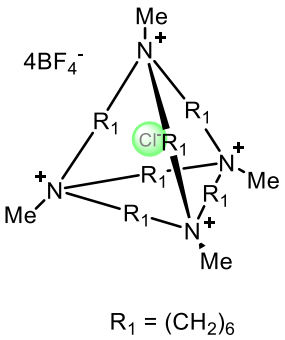


Figure 1.7: *Schmidtchen's quaternary ammonium cage complexed with chloride*

1.2.3.3.2. Hydrogen bonding

Hydrogen bonding is the quintessential intermolecular interaction employed for anion recognition. It is a special class of dipole-anion interaction and primarily electrostatic in character.[29] It results from the attraction between a highly polarised hydrogen covalently bonded to an electronegative atom, such as N, O or F, and a Lewis base such as an anion. The strength of the interaction can range from 5–120 kJ mol^{-1}.[30]

1.2.3.3.3. Halogen Bonding

Analogous to the hydrogen bond (HB), halogen bonding (XB) is the net attraction between an electrophilic region associated with a halogen atom and a Lewis base (anion) or nucleophilic region associated in another atom.[31] As halogen atoms are themselves electronegative, acting as Lewis acids appears counter intuitive. However, this can be resolved by considering the localised electron distribution density on a halogen atom when bonded to an electron-withdrawing group (Figure 1.8). At the pole of the halogen, parallel to the bonding axis, is an electrophilic region known as a 'sigma (σ)-hole', accountable for the attractive interaction with a Lewis base and for the stringent linearity commonly observed in XB. In contrast, the 'equatorial belt' around the halogen is electron dense. The strength of XB is comparable to HB (10-200 $KJmol^{-1}$)[29,30] and increases with increasing polarizability of the halogen atom i.e. iodine is a stronger XB donor than bromine and chlorine. Electrostatic surface potentials (Figure 1.8) highlight the changing nature of electron density across the halogens, where the red surfaces show regions of reduced electron density and therefore the capability of interacting with a Lewis base.[32] As mentioned above, the geometric restraints of XB make the interaction almost exclusively linear, favouring bonding angles of 180˚.

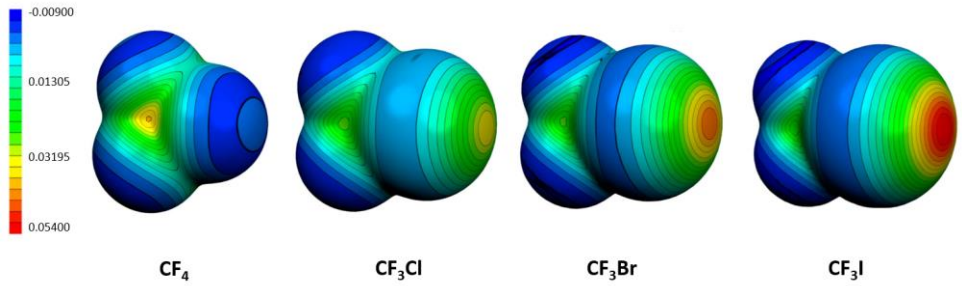


Figure 1.8: *Electrostatic Surface potentials. Reprinted with permission; Copyright 2007 Springer.*[32]

Notably, XB anion recognition has been repeatedly proven to outperform HB, particularly in aqueous solvent environments.[33]

1.2.3.3.4. Anion-π interactions

Anion-π interactions are the result of the electrostatic attraction between an anion and an electron poor aromatic π system.[34] The interaction is relatively weak compared to the aforementioned HB and XB intermolecular bonds, and when observed in a host-anion guest complex it often fulfils a supplementary role to another stronger interaction. This is demonstrated in Johnson's sulphonamide receptor, where a perfluorinated aryl ring was found to assist in the binding of a chloride anion in $CDCl_3$ (K_a = 30 M^{-1}, Figure 1.9a).[35] Nonetheless, anion-π interactions have been used as the primary means of anion association in a number of systems, such as in Stoddart's NDI-based triangular prisms which was able to recognise triiodide in CD_2Cl_2 (K_a = 25 M^{-1}, Figure 1.9b).

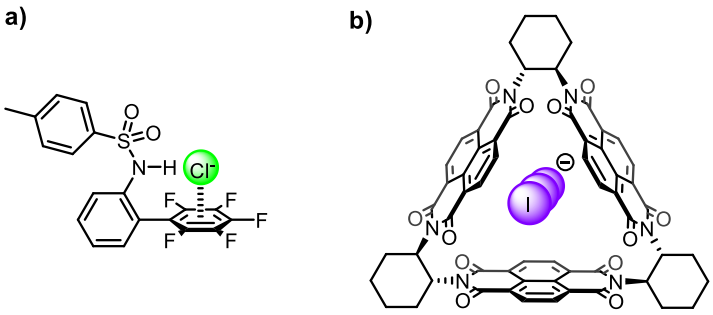


Figure 1.9: a) *Johnson's sulphonamide receptor coordinating with* Cl^- ***b)*** *Stoddart's NDI-based triangular prism complexing with an* I_3^-

1.2.4. Host Systems for Anion Recognition

Primarily influenced by how nature recognises anions, a vast catalogue of anion host systems have been developed over the past decades. These hosts have been designed for many purposes, each adding to the overall understanding of the field.

This section will highlight the range and diversity of anion host systems reported, starting from naturally occurring hosts that have inspired the foundations of the field, to some of the most complex systems synthesised to date.

1.2.4.1. Natural Hosts

Two natural host-anion guest systems are found in bacterial proteins. The sulphate-binding protein (SBP) and the phosphate-binding protein (PBP), exhibit almost exclusive selectivity for their respective oxoanions.[36–38] Both systems almost completely encapsulate the respective negatively charged guest species in complementary sized cavities using multiple hydrogen bonds. SBP adopts a cavity within two polypeptide domains that form seven hydrogen bonds to the sulfate ion from the surrounding amino acid residues (Figure 1.10a). Similarly, PBP achieves recognition by use of 12 hydrogen bonds. Notably, one of these is a hydrogen bond from the HPO_4^{2-} anionic guest to the oxyanion of Asp-56, and another two from the charged guanidinium group present in Arg-135, with additional electrostatic stabilisation (Figure 1.10b).

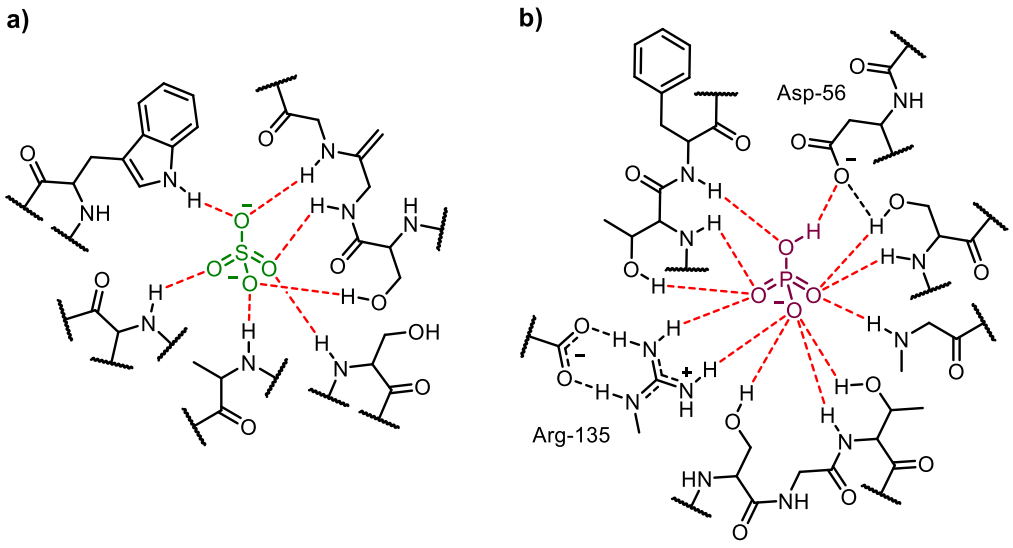


Figure 1.10: *Two dimensional schematics representing x-ray crystal structures of bacteria binding cavities* ***a)*** *SBP coordinating with sulphate* ***b)*** *PBP coordinating with phosphate.*

Extensive macro-molecules, like these proteins, that can fully encapsulate guests and bind with an array of different bonding networks are beyond the scope of current synthetic chemists. However, the principles are the same and continue to influence the design of receptors.

1.2.4.2. Positively Charged Receptors

Cationic receptors exploit charge and charge assisted ion-dipole electrostatic interactions, in particular directional HB and XB, to function in competitive protic solvent media such as methanol and water.

This section reviews some of the most widely used positively charged binding motifs, importantly highlighting the non-covalent binding interactions employed to achieve strong, selective, recognition to overcome competitive protic solvation of the anion guest species.

1.2.4.2.1. Protonated amine, quaternary ammonium- and guanidinium-based receptors

Following Park and Simmons' seminal polyammonium cages that were shown to encapsulate halides (Figure 1.2), a plethora of other cationic polyammonium receptors have been designed. Having already been shown to bind metal cations, Lehn and co-workers were able to reverse the functionality of an azacryptand to develop the first receptor selective for the linear azide anion (Figure 1.11a).[39] At a pH of 5, with six protonated amines, the azide anion was bound with high affinity (log K_a = 4.6) via a combination of favourable electrostatics and HB, and selectively by virtue of the cationic cryptand's complementary ellipsoidal binding cavity. Another azacryptand by Lehn and co-workers (Figure 1.11b) with a smaller binding cavity was able to selectively bind fluoride in aqueous acidic media (log K_a = 10.6).[40,41] In order to overcome the solvent interactions that disrupt the formation of hydrogen bonds between host and guest, Miravet and co-workers developed a shape specific macrocycle (Figure 1.11c).[42] The host bound 1,3,5-benzene tricarboxylate (1,3,5-BTC) selectively in water over other tricarboxylates via HB and shape complementarity.

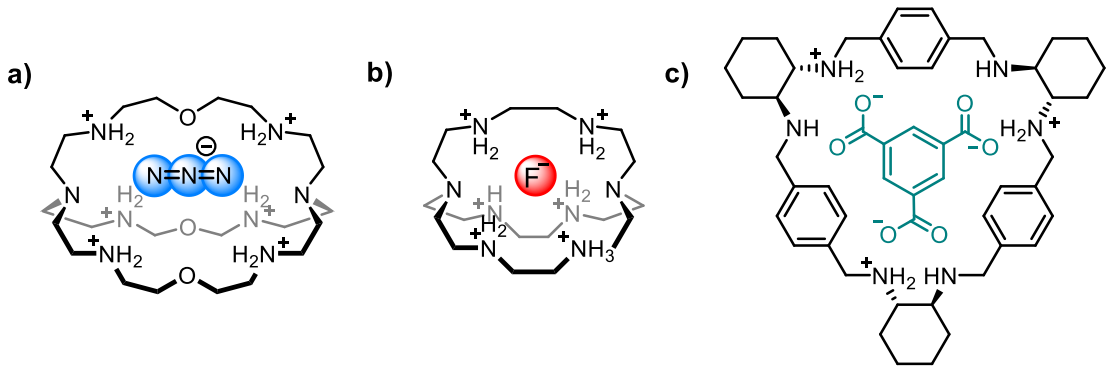


Figure 1.11: *Polyammonium based host receptors* ***a)*** *Lehn's protonated octaazacryptand complexed with an azide anion* ***b)*** *Lehn's protonated cryptand complexed with fluoride* ***c)*** *Miravet's highly shape specific macrocycle complexed with 1,3,5-BTC.*

The restrictive acidic pH window for amine-based receptors limits their wider functionality. Schmidtchen was able to overcome this and establish a new branch of supramolecular receptors by designing pH-independent quaternary ammonium cages (Figure 1.7 and Figure 1.12a).[28,43,44] The cages were found to bind halides and oxyanions in water and methanol, primarily by electrostatic attraction and hydrophobic effects. Varying the length of the alkyl spacer groups between the ammonium bridgeheads of the cage enabled cavity size variation, tuning the complementarity for halides. For example, the larger sized cage ($(CH_2)_8$)) displayed greater affinity for iodide than the smaller cages. To eliminate the influence of counter anions, zwitterionic cages were constructed (Figure 1.12a).[45] The zwitterionic cages displayed enhanced halide binding in water compared to their methylated analogues; for chloride the association constant for the six carbon spacer cage was an order of magnitude greater (K_a = 270 M^{-1} compared to K_a = 20 M^{-1}).

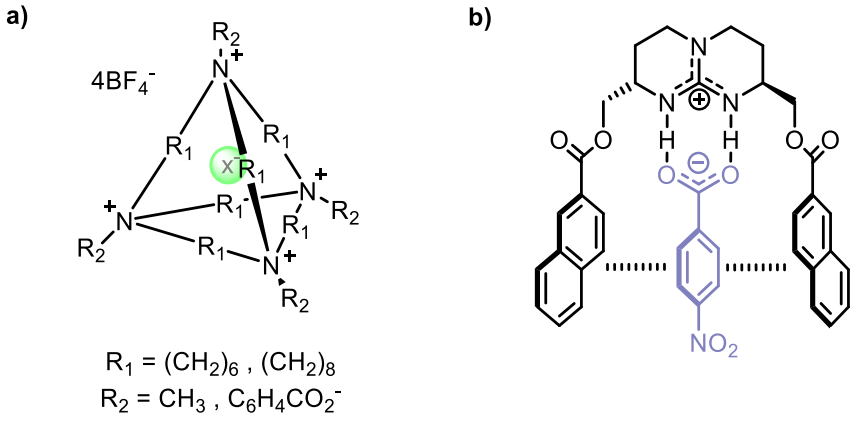


Figure 1.12: a) *Schmidtchen's quaternary ammonium cage encapsulating an anion* ***b)*** *Lehn and Mendoza's chiral acyclic guanidinium receptor coordinating to p-nitrobenzoate.*

An alternative hydrogen bond donor to polyammonium is the guanidinium cation, which with a pK_a = 13.6 has the advantage of remaining protonated over a wider pH range. Lehn and Mendoza incorporated the motif into a chiral acyclic receptor with two naphthoyl side arms (Figure 1.12b).[46] The receptor was able to extract *p*-nitrobenzoate from aqueous solution into chloroform and was found to exhibit enantiomeric selectivity for L-tryptophan. The napthoyl side arms were reported to supplement the guanidinium HB donor motif with the addition of double π-stacking which helped favour certain chiral architectures over their enantiomers.

1.2.4.2.2. Imidazolium, Triazolium and Pyridinium receptors

Unlike amine-based receptors, polarised C–H or C–X donor groups are insensitive to changes in pH. In 1999, having observed strong hydrogen bonding interactions in the solid state

between imidazolium motifs and halides, Sato and co-workers developed the first imidazolium-based acyclic receptor (Figure 1.13a).[47] The receptor utilised three convergent triazolium motifs in a tripodal structure to recognise halides in CD_3CN. Concurrently, Alcalde and co-workers reported the first cyclic imidazolium receptor (Figure 1.13b), which bound fluoride and dihydrogen phosphate in DMSO-d_6.[48] Both receptors benefitted from strong imidazolium C–H---anion hydrogen bonds, in addition to favourable electrostatic attraction. The capability of imidazolium to bind anions has since been demonstrated in a plethora of receptors;[49,50,51,52] notably in 2010 Sessler's 'Texas-sized' molecular box which was found to form 1:1 stoichiometric complexes with di-terephthalate anions in DMSO-d_6 (Figure 1.13c).[53] In 2012 Beer and co-workers reported a series of fluorescent macrocyclic XB haloimidazolium receptors (Figure 1.13d).[54] The bromo- and iodo-imdazolium receptors bound and sensed bromide and iodide anions strongly in CH_3OH/H_2O 9:1, as evidenced by significant emission intensity increases of the respective macrocycle's naphthyl motifs. In comparison, the chloro- and proto-imidazolium macrocyclic analogues were unable to recognise the halides, highlighting the advantage of XB anion binding over HB in competitive aqueous protic solvent media.

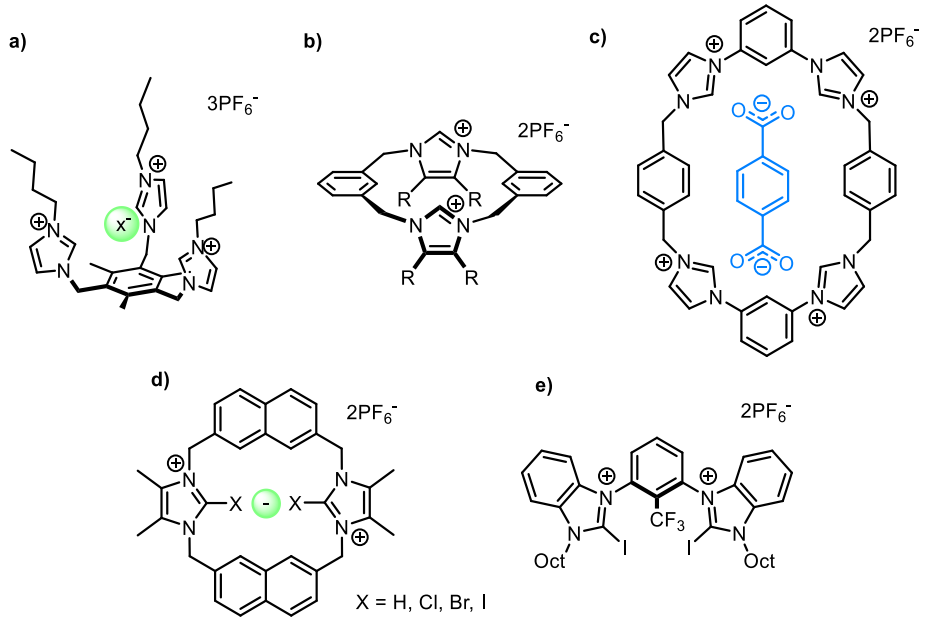


Figure 1.13: *Imidazolium receptors:* ***a)*** *Sato's imidazolium-based acyclic tripodal receptor* ***b)*** *Alcalde's cyclic imidazolium receptor* ***c)*** *Sessler's 'Texas-sized' molecular box complexed with a di-terephthalate anion* ***d)*** *Beer's macrocyclic haloImidazolium receptors complexing with an anion* ***e)*** *Jungbauer and Huber's syn bis-iodotriazolium receptor for organocatalysis.*

Jungbauer and Huber utilised halogen bonding for organocatalysis with a novel bis-iodo-imidazolium receptor (Figure 1.13e).[55] By incorporating a CF_3 group between the two XB

donors they introduced steric restrictions on rotation, creating syn- and anti-isomers. ITC titrations with TBABr in MeCN showed the syn isomer, capable of bidentate XB-bromide coordination, with significantly greater halide affinity than the monotopic anti-isomer (K_{syn} = 3.5 x 10^6 M^{-1}, K_{anti} = 4.4 x 10^4 M^{-1}).

The neutral 1,2,3 triazole motif which is discussed in more detail in the next section, has been shown to be capable of binding anions in aprotic organic solvent media (*see Section 1.2.4.3.3.* Further enhancement of its binding affinity can be achieved through alkylation at the N^3 atom to form the 1,2,3 triazolium motif, which has seen widespread incorporation into a range of receptors both as a HB and a XB donor. In 2007, Pandey and co-workers were the first to publish a triazolium based receptor (Figure 1.14a).[56] Based on a steroidal scaffold, the receptor was found to bind dihydrogen phosphate over the halides in $CDCl_3$ (K_a = 1920 M^{-1}). The first XB iodo-triazolium receptor was reported by Beer and co-workers; with a view to synthesising a higher order XB-based host, a simple acyclic model was synthesised to investigate anion binding. (Figure 1.14b).[57] Utilising a single iodo-triazolium, in the solid state the receptor demonstrated strong XB---halide binding affinity with bond distances between 79 – 84 % of van der Waals radii, with almost linear bond angles. A further example of the anion binding capability of halo-triazoliums was reported by Molina *et al*. [58] A number of their pyrene-based XB triazolium hosts were able to act as chemosensors for anions, particularly $HP_2O_7^{3-}$. Interestingly, ^{1}H NMR and fluorescence studies showed the XB-triazolium host (Figure 1.14c) formed pyrene excimers when binding $HP_2O_7^{3-}$ with greater affinity and fluorescence response than with the HB and mixed HB/XB analogues (K_a= 3032 and 9838 M^{-1} respectively in 9:1 CD_3CN/methanol-d_4). In a more systematic study, Schubert and co-workers investigated the binding affinities of a range of bidentate triazolium host receptors.[59] Their study investigated the influence of XB versus HB, the bidentate bite angle, and receptor charge/polarisation on anion affinities. They found the bis-iodotriazolium receptor (Figure 1.14d) displayed the highest binding strength for anions with a preference for sulphate (K_a= 3400 M^{-1}) in DMSO over the halides. The selectivity was attributed to a favourable host-guest match in size and charge density.

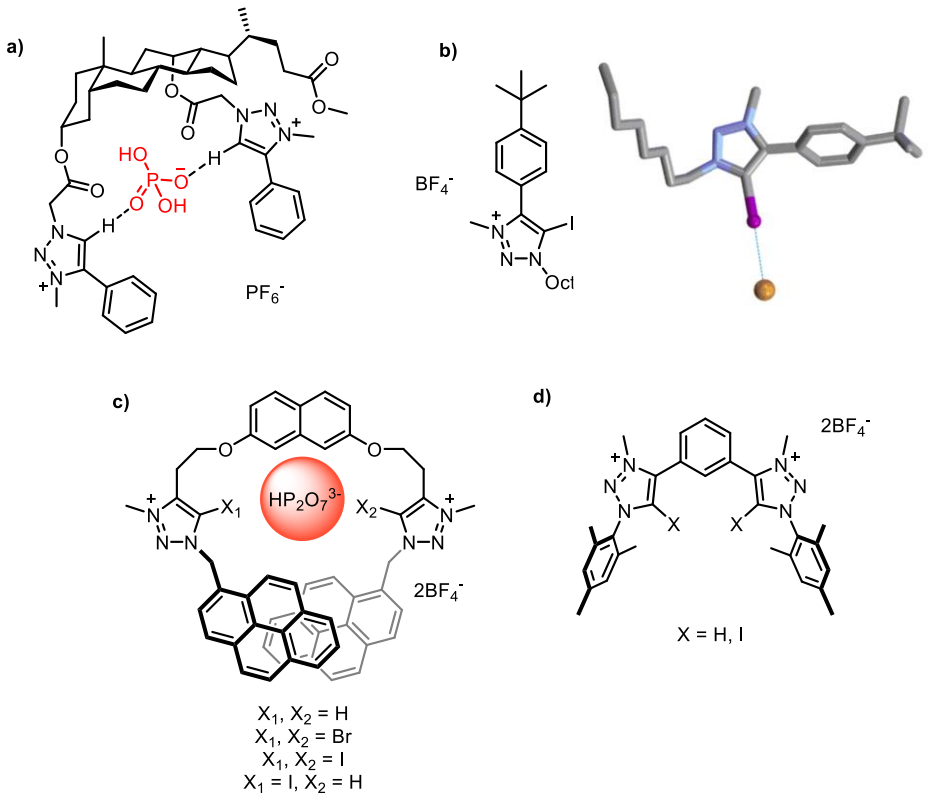


Figure 1.14: *Triazolium host receptors* ***a)*** *Pandey's triazolium receptor coordinating to dihydrogen phosphate* ***b)*** *Beer's first iodo-triazolium receptor and receptor crystal structure* ***c)*** *Molina's pyrene triazolium host complexed with* $HP_2O_7^{3-}$ ***d)*** *Schubert's bidentate triazolium HB/XB host receptor.*

The pyridinium group has seen wide use for its capability to enhance anion binding in XB hosts. A study by Nepal and Scheiner utilising quantum chemical calculations showed that by introducing a pyridinium group into a simple bis-iodotriazole receptor the molecular electrostatic potential (MEP) of the sigma-(σ)-hole on the triazole C-I bond is enlarged, enhancing the electropositive region and significantly increasing anion binding strength.[59] This was experimentally demonstrated by Beer's XB pyridinium bis-iodotriazole motif (Figure 1.15a).[60] The XB-host exhibited such strong halide binding (K_a = >10^4 M^{-1}, CD_3CN), it prompted the use of the more competitive DMSO-d_6. In addition to demonstrating a higher binding affinity than the HB host, the receptor was found to recognise AcO^- selectively over the halides (K_a = 1025 M^{-1}, DMSO-d_6). Of note, was evidence of a significant degree of covalency in the halogen bonding-halide interactions, provided by X-Ray absorption spectra exhibiting charge transfer features between chloride/bromide and the receptor's XB iodotriazole C-I bond.

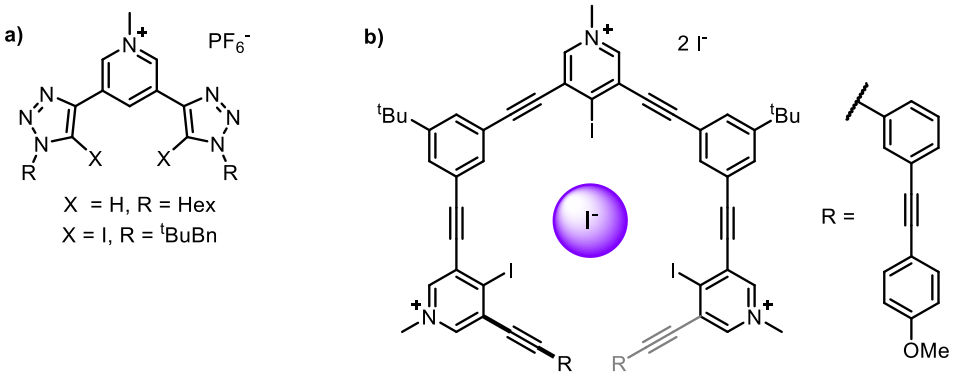


***Figure 1.15**: Pyridinium host receptors a**) Beer's pyridinium bis-iodotriazole/bis-prototriazole receptor **c)** Berryman's pyridinium halogen bonding triple helicate.*

By incorporation of an iodopyridinium XB motif, Berryman and co-workers demonstrated the first XB triple helicate stabilised and assembled by encapsulating iodide anions in organic and aqueous media, as well as in the solid state (Figure 15c).[61]

1.2.4.3. Neutral Receptors

Neutral anion receptors are primarily designed to function in relatively non-polar aprotic organic solvent media, commonly employing convergent hydrogen bonds of various kinds.

1.2.4.3.1. Amide, Urea/Thio-Urea and Squaramide Receptors

In 1986, in an effort to mimic the naturally occurring neutral SBP (see 1.2.4.1. Natural Hosts) Pascal and co-workers published the first amide anion receptor example based on a caged-type structure that was demonstrated to bind fluoride in DMSO-d_6 (Figure 1.16a).[62] In the following years amide motifs were incorporated into a variety of preorganised receptors including macrocycles,[63] tripods,[64,65] and cryptands.[25] A notable publication in 1997 by Crabtree and co-workers described the readily accessible neutral acyclic isophthalamide receptor (Figure 1.16b), that was capable of strongly binding halides in CD_2Cl_2.[66,67] This development propelled the design of many more amide receptors, including the exploitation of related motifs such as ureas, thioureas and squaramides. For example, Umezawa and co-workers showed the urea and thiourea hosts (Figure 1.16c),[68] recognised phosphate in DMSO-d_6 (K_a = 110 M^{-1}, 820 M^{-1} respectively). The greater affinity of the thiourea to bind phosphate was attributed to stronger hydrogen bonds. Aside from acetate (K_a = 43 M^{-1} and 470 M^{-1}), halide anions were bound poorly. In a later study by Gale and co-workers,[69] the pendant butyl groups were substituted for phenyl moieties (Figure 1.16c) which markedly changed the selectivity from phosphate (K_a = 732 M^{-1}) to acetate (K_a = 3210 M^{-1}). They rationalised this change by noting the rigidity introduced from the aromatic groups which

increased preorganisation. These studies highlight the complexity of developing targeted anion hosts; what may appear to be relatively small changes that are not associated with the central binding site can have a significant impact on anion recognition properties.

In a related study, Muthyala and co-workers were able to utilise non-binding carbonyl groups to preorganise an acyclic squaramide receptor to act as a molecular 'valve' (Figure 1.16d).[70] In non-polar solvents, such as $CDCl_3$, the receptor forms intramolecular hydrogen bonds between the carbonyl group and the squaramides. In this 'closed' state the system is incapable of binding chloride. However, in polar solvents, such as CH_3CN, the intramolecular bonds are disrupted and the system is in an 'opened' state, capable of binding chloride (K_a = 517 M^{-1}).

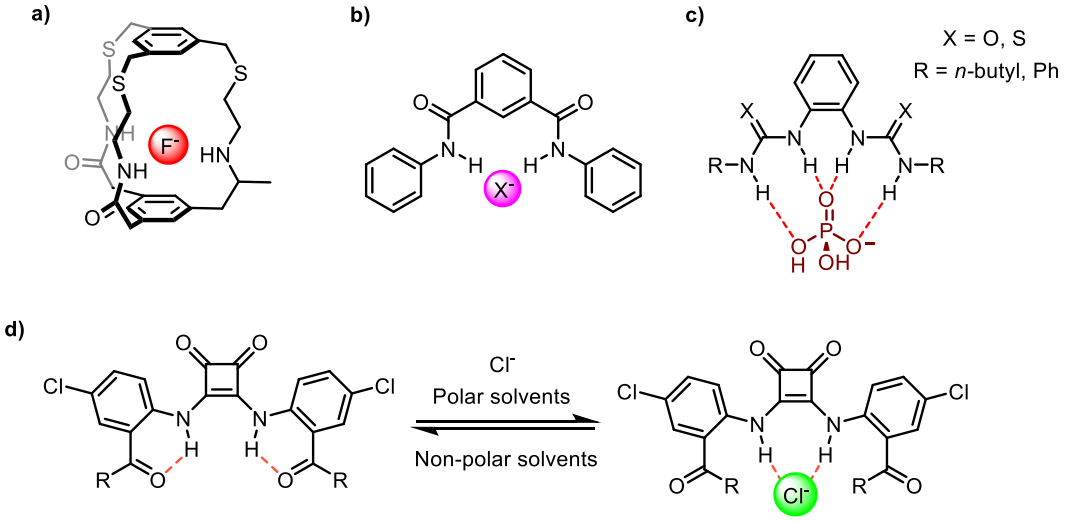


Figure 1.16: *Amido- Urea- type receptors* ***a)*** *Pascal's amide cage complexed with fluoride* ***b)*** *Crabtree's acylic isothalamide receptor* ***c)*** *Umezawa's urea/thiourea hosts coordinating to dihydrogen phosphate* ***d)*** *Muthyala*'s molecular 'valve' Squaramide receptor in its closed and open state.

Coining the term 'molecular oyster', Kubik and co-workers developed a host capable of strongly binding sulphate (K_a = 3.5 x 10^5 M^{-1}) and iodide (K_a = 8900 M^{-1}) in D_2O:CD_3OD 50:50.[71] This innovative receptor containing two cyclic pseudo-peptides bridged with a bis-amide tether, forms 1:1 stoichiometric host-anion guest sandwich complexes (Figure 1.17). The high binding affinities were attributed to a combination of convergent hydrogen bonds and solvophobic interactions which cause a hydrophobic collapse around the binding cavity and anion guest.

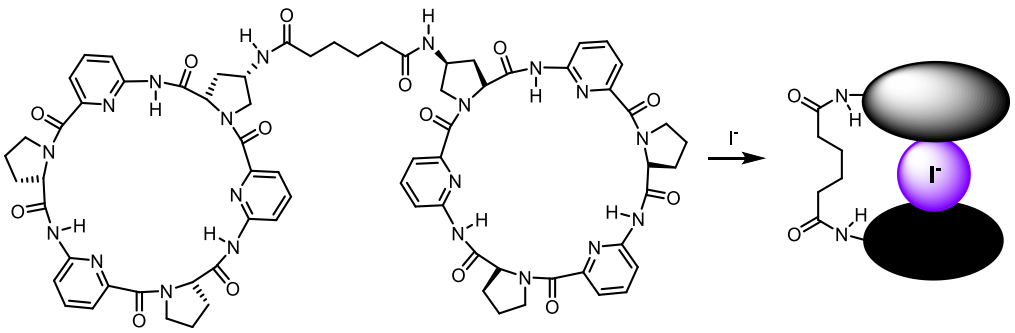


Figure 1.17: *Kubik's 'molecular oyster' complexed with iodide.*

1.2.4.3.2. Pyrrole receptors

Pyrroles have been identified as robust N-H hydrogen bond donor motifs. Unlike their amide and urea counterparts, pyrroles do not contain carbonyl hydrogen bond acceptor groups and therefore have no inherent risk of self-assembly, which can both hamper solubility and directly compete with binding guests.

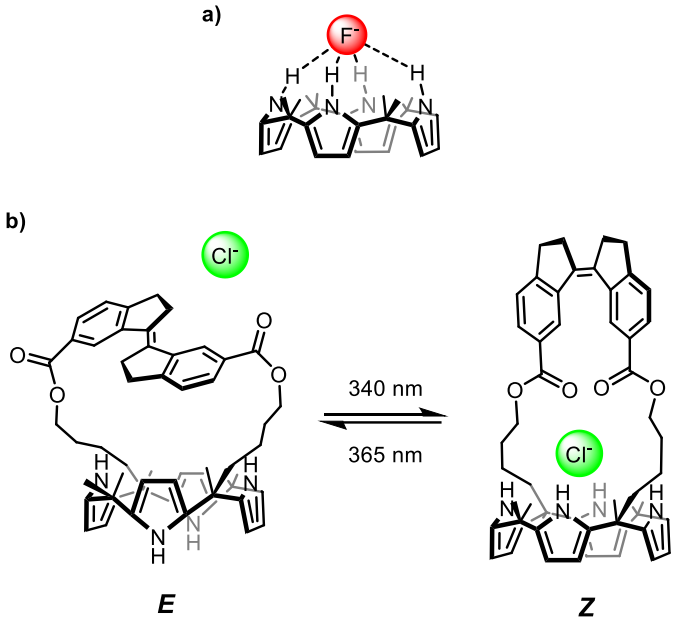


Figure 1.18: *Calix[4]pyrroles* ***a)*** *Sessler's Calix[4]pyrroles coordinating to a fluoride* ***b)*** *Wezenberg's photo-switchable strapped Calix[4]pyrroles receptor in the open and closed state with chloride*

The most distinguished series of pyrrole containing anion receptors are the macrocyclic calix[4]pyrroles (Figure 1.18a).[72] Although originally synthesised in 1886, it was not until 100 years later in 1996 that the system was first reported to bind anions.[73,74] In this seminal work, Sessler and co-workers identified that calix[4]pyrrole (Figure 1.18a) was capable of binding fluoride (K_a = 17170 M^{-1}, CD_2Cl_2) in a 'cone' like shape in which all the pyrrole hydrogen bond donors converge to bind the guest anion. The later development of strapped calix[4]pyrroles[72]

enhanced preorganisation. One recent example incorporated a photo-switchable strap that could inhibit or encourage anion binding (Figure 1.18b).[75] In the open *Z*-isomer the host binds chloride strongly (K_a = 1.6 x 10^6 M^{-1}, CD_3CN), whereas in the *E*-isomer the binding is 8000 times weaker (K_a = 20 M^{-1}, CD_3CN).

1.2.4.3.3. Triazoles and campestarene receptors

Triazole, like its alkylated counterpart, triazolium, has become well established as a potent anion binding motif. In particular, the 1,2,3 triazole is noted for its high anion bind affinity and its synthetic accessibility via the versatile copper(I) mediated azide-alkyne cycloaddition reaction. In early 2008, Flood and co-workers reported a preorganised macrocyclic receptor with four convergent triazoles (Figure 1.19a), reminiscent of Cram's early spherands.[76] The host was found to bind chloride strongly and selectively in CH_2Cl_2 (K_a = 1.3 x 10^5 M^{-1}). Later in that same year, triazole based foldamer receptor structures were reported to recognise halides.[77,78] Since then, a great variety of triazole-based receptors have been developed, including a novel preorganised cryptand-like receptor (Figure 1.19b), displaying remarkably strong binding of chloride (K_a = 10^{17} M^{-1}, CH_2Cl_2) by Flood and co-workers.[79] It is noteworthy that neutral iodotriazole based XB analogues are often shown to outperform the proto-triazole receptor analogues.[52] Beer and co-workers demonstrated this with their simple acyclic 1,3-disubstituted ferrocene receptor (Figure 1.19c), whereby the XB host was able to recognise and redox sense a suite of anions, including azide (K_a = 669 M^{-1}, acetone-d_6) whilst the HB analogue had weaker binding (K_a = 15 M^{-1}, acetone-d_6) and a suppressed redox response.[80]

Schubert and co-workers described a bis-iodotriazole carbazole receptor (Figure 1.19d(i)), preorganised via intramolecular hydrogen bonds formed between the carbazole phenol groups and nitrogen triazole motifs.[81] In comparison with the analogous receptor containing no hydroxyl substituents (K_a = 1.58 x 10^3 M^{-1}, THF) (Figure 1.19d(ii)), the preorganised receptor was found to bind bromide with enhanced affinity (K_a = 3.85 x 10^3 M^{-1}, THF).

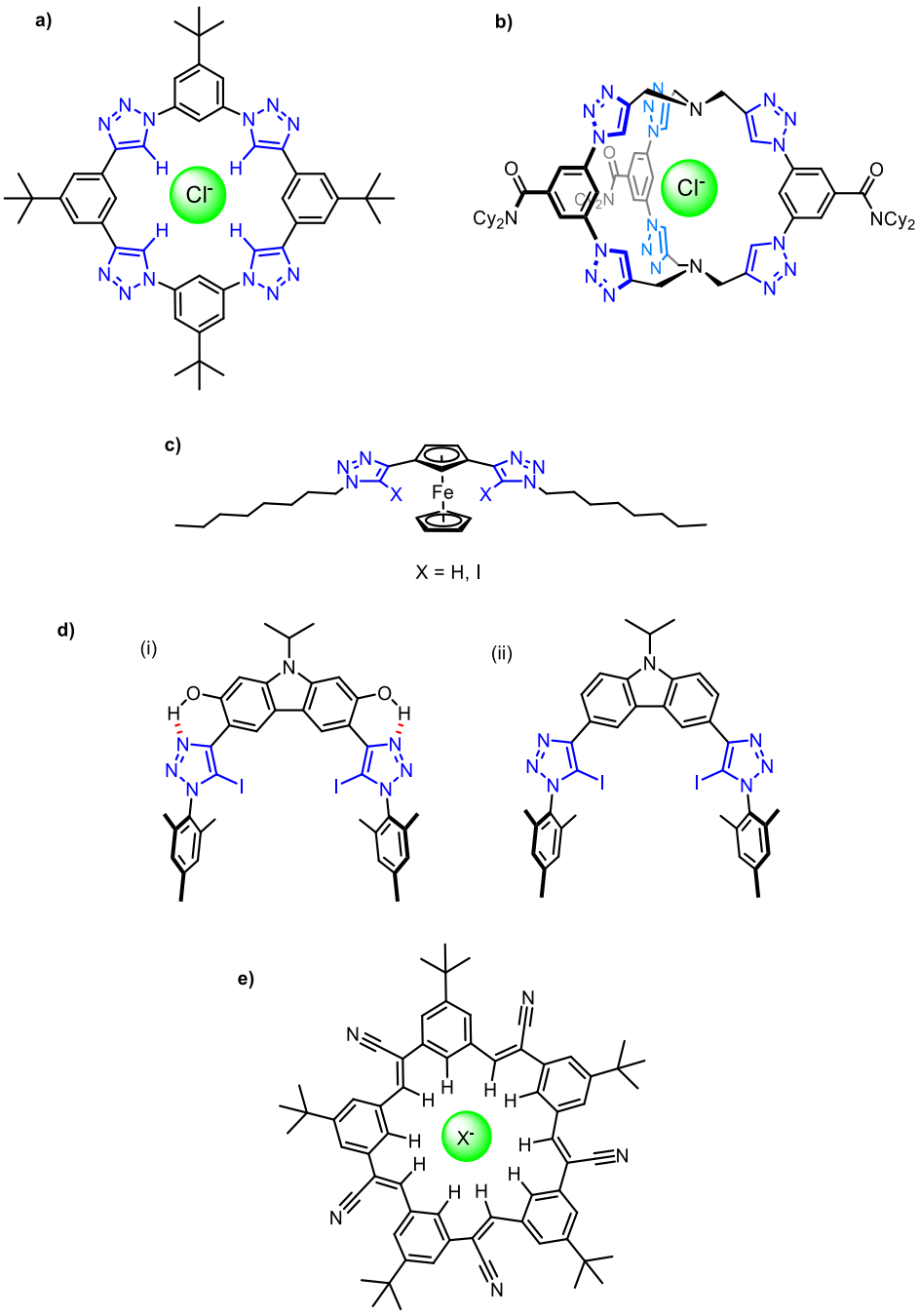


Figure 1.19: *1,2,3 Triazole receptors* ***a)*** *Flood's macrocyclic host complexed with chloride* ***b)*** *Floods cage host receptor complexed with chloride* ***c)*** *Beer's acyclic ferrocene receptor* ***d)*** *Schubert's preorganised cleft-type receptor* ***e)*** *Flood's cyanostar campestarene complexed with an anion.*

Campestarenes are a class of shape persistent macrocycles with 5-fold symmetry.[82] A notable example was Flood and co-workers' cyanostar, composed of repeating cyanostilbene monomers (Figure 1.19e).[83] Unusually, the macrocycle was demonstrated to form 2:1 host-guest complexes with weakly coordinating large anions such as BF_4^-, ClO_4^- and PF_6^- in CD_3OD/CD_2Cl_2 2:3.

1.2.4.3.4. Chalcogen Bonding Receptors

Another type of attractive interaction for anion binding is chalcogen bonding. Similar to XB, chalcogen bonding is the positive attraction between an electropositive σ-hole on a chalcogen (S, Se, Te) and an anion.[84] Currently the number of reported solution phase chalcogen receptors is fairly limited in comparison to XB or HB. One early example in 2016 includes Taylor and Seferos' perfluoroaryl-substituted bis-tellurophene receptor (Figure 1.20).[85] The receptor was found to bind chloride in THF (K_a = 2290 M^{-1}). Although the anion affinity was modest, it demonstrated that chalcogen bonding could be included in the anion recognition toolkit.

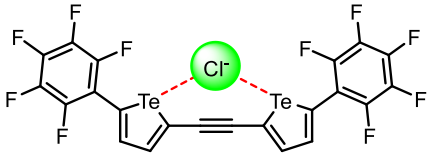


Figure 1.20: *Taylor and Seferos' bis-tellurophene receptor coordinating to chloride*

1.2.4.4. Water soluble Hosts

One of the greatest challenges of anion recognition is overcoming the solvation effects of water.[86] Water forms hydrogen bonds to anions and effectively screens their charge, making recognition difficult. In addition, water acts as a hydrogen bond acceptor and readily interacts with HB motifs designed to bind anions. Finally, to operate in water, receptors need to include solubilising groups. With the exception of polycationic receptors, this often means the inclusion of bulky hydrophilic or ionic appendages, making synthesis more challenging. In spite of these challenges, supramolecular chemists have designed receptors capable of recognising anions in water; notable examples that operate in 100% water include cyclopeptide macrocycles (Figure 1.21a),[71,87] bambus[*n*]urils (Figure 1.21b),[88] biotin[6]-urils (Figure 1.21c),[89,90] and indolocarbazoles (Figure 1.21d).[91]

Kubik and co-workers' cyclopeptide macrocycle (Figure 1.21a), as used in their molecular oyster (see Figure 1.17), was found to be selective for SO_4^- in buffer solution ($\log K_a$ = 5.1, 40 mM acetate buffer, pH 4.8), and was even capable of sulphate recognition in phosphate buffer or in the presence of excess Cl^-.[87] They rationalise this behaviour by the presumed receptor's ability to wrap around the tetrahedral oxyanion with the HB donors converging.

Another family of macrocycles, cyclic glycoluril oligomers — have been shown to exhibit strong binding to anions (Figure 1.21d).[92] Characteristically, bambus[*n*]urils predominately associate with anions thanks to their electropositive interior cavities, well suited to forming inclusion complexes with guests. Sindelar and co-workers, the original

designers of bambus[*n*]urils, modified the solubility by appending carboxylate groups to the structure.[88] Remarkably, despite the receptor being anionic, in water it was found to display Hofmeister selectivity and bound iodide and perchlorate (K_a = 1.0 x 10^7 M^{-1} and 5.5 x 10^7 M^{-1} respectively). Thermodynamic investigations elucidated that the complexation was significantly enthalpic due to a combination of the multiple hydrogen bond donors complexing to the anion guest and the release of high energy water molecules from within the cavity forming stable hydrogen bonds with the bulk water solvent.

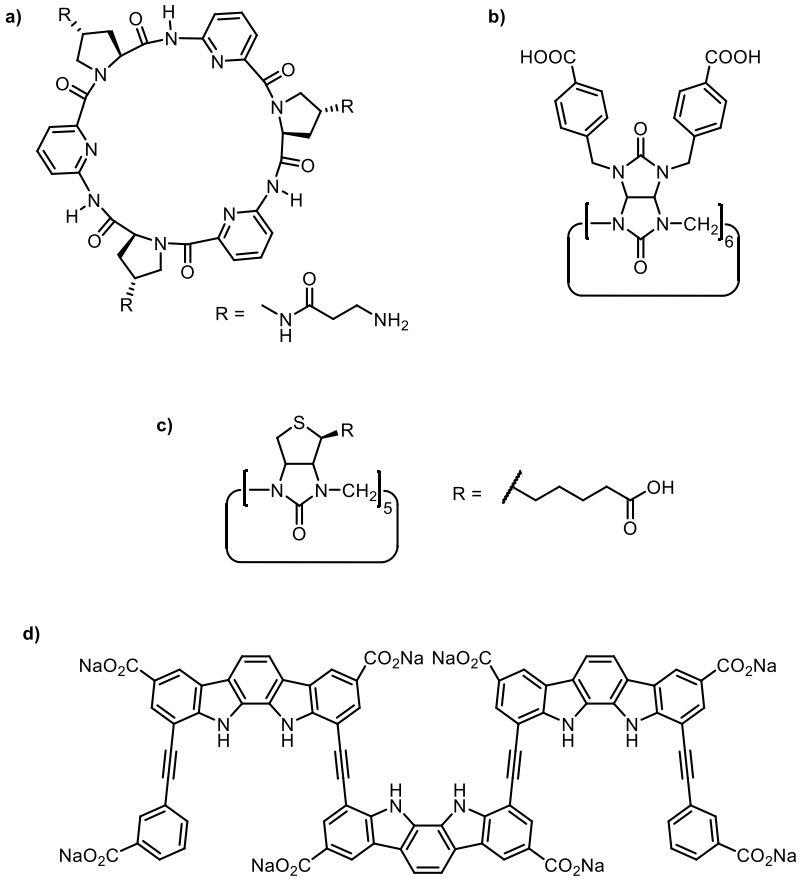


Figure 1.21: *Water soluble anion host receptors* ***a)*** *Kubik's cyclopeptide macrocycle* ***b)*** *Sindelar's bambus[6]uril* ***c)*** *Pittelkow's Biotin[6]uril* ***d)*** *Jeong's indolocarbazole helical foldamer.*

Similar to banbus[*n*]urils, Pittelkow and co-workers demonstrated that their 6+6 biotin formaldehyde macrocycle biotin[6]uril was capable of binding a variety of anionic guests in water (Figure 1.21c).[90] In 100 mM phosphate buffer (pH 7.5) they identified that the receptor recognised a plethora of anions including the halides, N_3^-, NO_3^-, ClO_4^- and notably SCN^- which had the greatest association constant (logK_a = 4.5). Using Isothermal titration calorimetry (ITC) they were able to identify that the binding event is enthalpically led and speculate that the selectivity is governed by a delicate balance between anion size and hardness/softness.

Solubilisation of a indolocarbazole helical foldamer was achieved by Jeong and co-workers by employing water soluble carboxylate sodium salts (Figure 1.21d).[91] Remarkably, by monitoring via ^{1}H NMR spectroscopy, the receptor was able to recognise Cl^- in pure D_2O (K_a = 65 M^{-1}) by way of folding around the guest. Conversely the receptor was unable to recognise I^- and was less selective for Br^- and F^- (K_a = 19 M^{-1} and 46 M^{-1} respectively).

Beer and co-workers were able to solubilize a bis-iodotriazolium-based acyclic receptor in water using polyethylene glycol (PEG) derivatives (Figure 1.22a). They found that the XB system, unlike the HB analogue, was capable of recognising perrhenate (ReO_4^-, K_a = 44 M^{-1}) in water.[93] Employing PEG derivatives again, they were able to solubilise a neutral iodotriazole-based foldamer in water (Figure 1.22b).[94] The host receptor was found to self-assemble around anions with a 2:1 host:guest binding stoichiometry and displayed incredibly strong binding for iodide . Comparisons between the HB, XB and chalcogen bonding (ChB) analogues showed that the HB was incapable of recognising iodide and that the XB outperformed the tellurium ChB. (β_2 = 7.28 x 10^9 M^{-2} and 2.64 x 10^7 M^{-2} respectively).

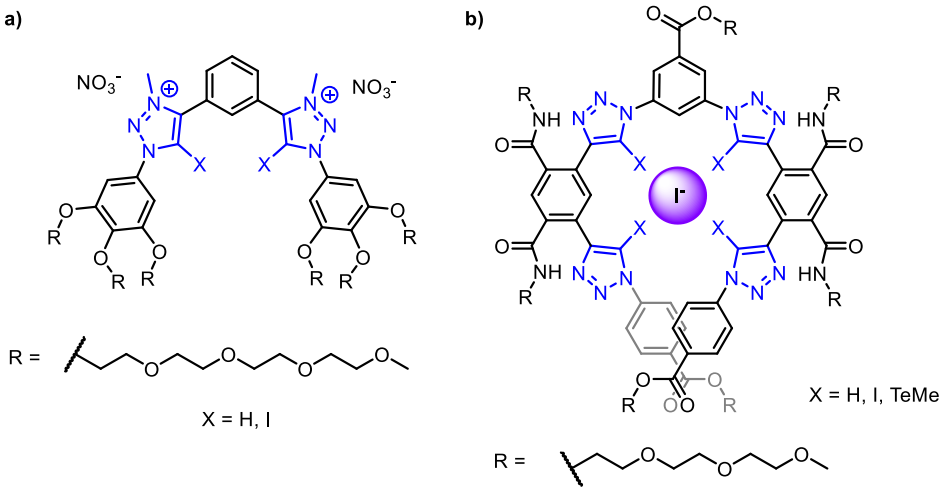


Figure 1.22: *Water soluble receptors* ***a)*** *Beer's acyclic bistriazolium* ***b)*** *Beer's neutral triazole foldamer complexed with iodide.*

1.2.4.5. Mechanically Interlocked Anion Hosts

Mechanically interlocked molecules (MIMs) belong to a category of structures containing two or more molecular components that are linked via a *mechanical bond*, not through a covalent bond. In order to separate the components, the breaking or distortion of a covalent bond is required. Initially targeted as a synthetic challenge, considerable research attention has been devoted to the construction of MIMs in practical yields for their investigation. Due to their mechanically bonded components they contain unique topographic configurations, undergo

molecular motions, and have demonstrated valuable functions in a variety of applications such as in functional materials,[95] sensors,[96] catalysis,[97] polymers,[98] and drug delivery.[99] Moreover, MIMs are well suited for the construction of artificial molecular machines, which in particular has received considerable attention from the supramolecular chemistry community, leading to the award of the 2016 Chemistry Nobel Prize.

The two most prevalent classes of interlocked molecules are [n]catenanes (Figure 1.23a), derived from the Latin for chain *catena*, and [n]rotaxanes (Figure 1.23b) derived from the Latin for wheel *rota* and axle *axis*. The [n] refers to the number of discrete interlocked molecular components. [n]Catenanes consist of two or more linked macrocycles in a chain like manner. Rotaxanes contain a threaded macrocycle and an axle component in a dumbbell type shape. The two ends of the axle consist of stopper groups that are large enough to prevent the macrocycle from slipping off and de-threading. Similarly, pseudorotaxanes (Figure 1.23c) are rotaxane systems where the macrocycle is threaded but is still capable of slipping off, these often only exist if brought together by favourable interactions such as through cooperative binding of a guest.

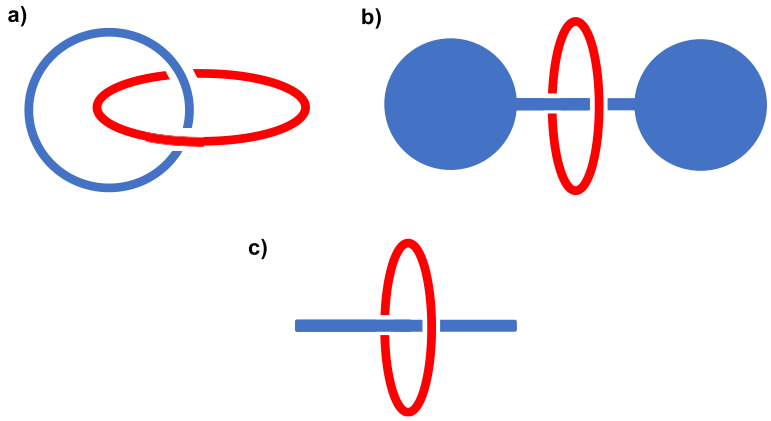


Figure 1.23: *Mechanically interlocked molecules* ***a)*** *[2]Catenane* ***b)*** *[2]Rotaxane* ***c)*** *Pseudorotaxane*

Over the past two decades the unique three dimensional interlocked host cavities of MIMs have been exploited for anion recognition applications.[96] This progress has coincided with the advancement in templation strategies for their construction and has resulted in a variety of elaborate hosts capable of binding anions. These synthetic strategies will be discussed in detail in *Chapter 2, Section 2.4.* Akin to the macrocyclic effect, MIM anion host systems have been shown to display significantly enhanced anion affinities and selectivity in comparison with non-interlocked receptor analogues, attributable to their ability to encapsulate guest anions. Furthermore, the modular synthesis of MIMs allows for the incorporation of reporter groups to provide anion sensing capability.

Beer and co-workers developed a rhenium(I) [2]rotaxane selective for sensing hydrogen sulphate (Figure 1.24a).[100] The rotaxane's synthesis was achieved by ring-closing metathesis (RCM) of a bis-vinyl macrocyclic precursor around a pyridinium axle templated by a chloride anion. The strength of HSO_4^- binding was shown to dramatically increase from macrocyclic precursor, free macrocycle to rotaxane ($K_a = 3.52 \times 10^3\ M^{-1}$, $4.65 \times 10^3\ M^{-1}$, $>10^6\ M^{-1}$ respectively in acetone). By incorporating the luminescent rhenium (I) bipyridyl derivative into the macrocycle component, anion sensing was demonstrated via MLCT emission intensity enhancements, particularly so for hydrogen sulphate.

Gunnlaugsson and co-workers were able to use self-templation of two acyclic precursors for the synthesis of a [2]catenane *via* double-ring cyclisation RCM (Figure 1.24b).[101] The receptor was found to be exclusively selective for $H_2PO_4^-$ in DMSO ($K_a = 55\ M^{-1}$) over the halides and other tetrahedral shaped anions such as SO_4^{2-} due to the favourable interlocked cavity size complementarity.

Jeong and co-workers prepared a fluorescent [2]catenane with two indolocarbazole macrocycle components via chloride anion template RCM (Figure 1.24c).[102] Fluorescence anion titration experiments in H_2O/acetone 1:99 revealed enhancements of the indolocarbazole fluorescence emission intensity, which was greatest for Cl^- as reflected with the catenane host being selective for Cl^- ($K_a = 140000\ M^{-1}$) over other halides and oxyanions. As expected, the corresponding indolocarbazole macrocycle exhibited a 20 fold decrease in Cl^- binding strength ($K_a = 7300\ M^{-1}$), highlighting again the MIM anion host binding effect.

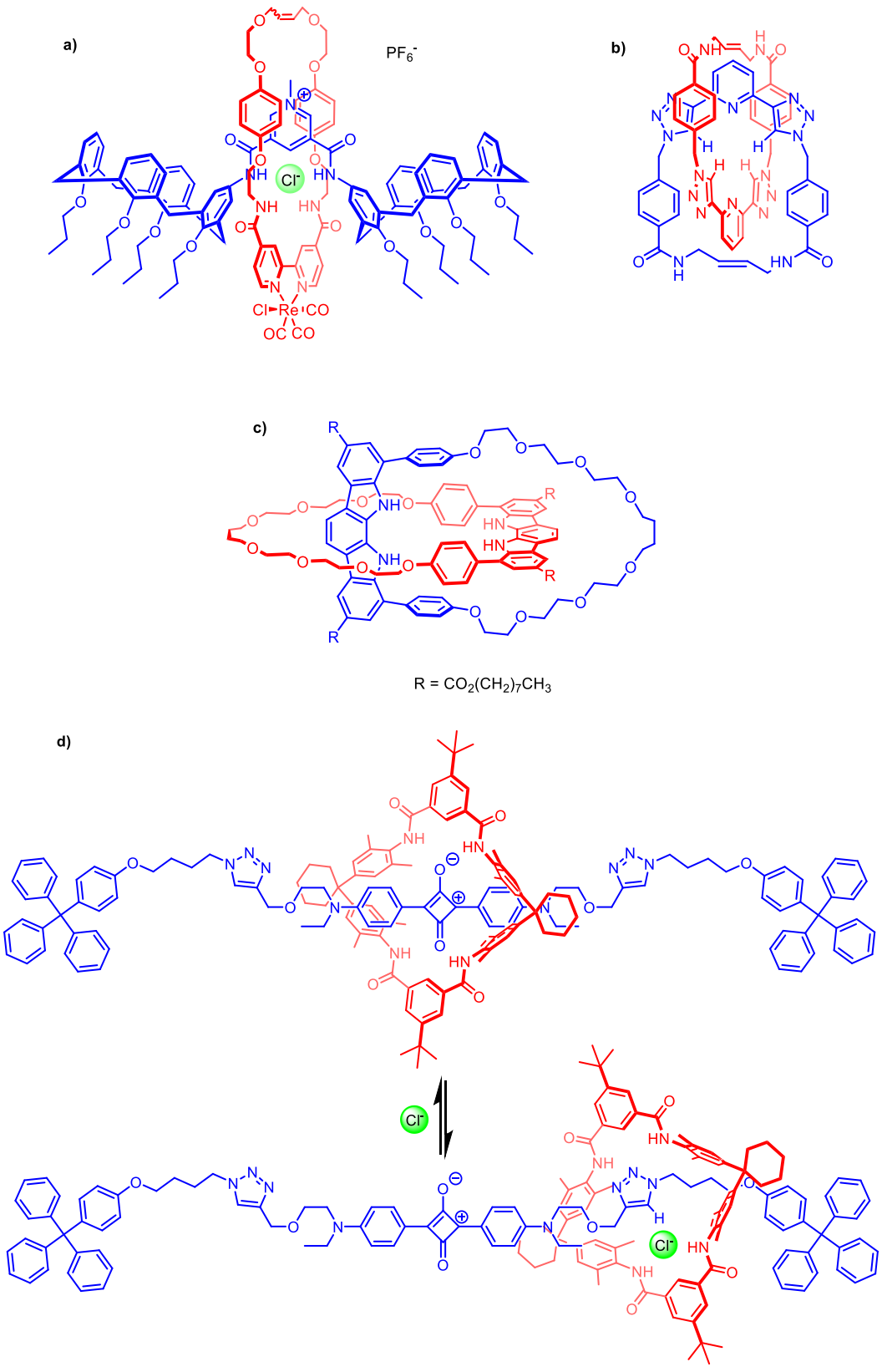


Figure 1.24: *Mechanically interlocked molecular hosts* ***a)*** *Beer's rhenium rotaxane complexed with chloride* ***b)*** *Gunnalaugsson's self-templated [2]catenane* ***c)*** *Jeong's fluorescent indolocarbazole [2]catenane* ***d)*** *Smith's squaraine [2]rotaxane reversible complexing with chloride.*

Building on from an earlier study in which they demonstrated the formation of a quenched squaraine pseudorotaxane,[103,104] Smith and co-workers developed a [2]rotaxane capable of the naked eye sensing of chloride (Figure 1.24d).[105] In chloroform the addition of chloride caused the translocation of the macrocyclic component away from the central photoactive squaraine to an off-centre position in which chloride could be favourably bound. As a consequence of the molecular motion changing the excited state of the fluorophore, a three-fold intensity increase in emission was observed — visible to the naked eye. Interestingly the association constant was found to be significantly lower than the free macrocycle in CH_2Cl_2 (K_a = 340 M^{-1} in $CHCl_3$ compared to K_a = >10^5 M^{-1} in CH_2Cl_2) due to the energetic penalty of translocating the macrocycle away from the squaraine station, a process that disrupts the hydrogen bonding between the macrocycle and squaraine. This example demonstrates that MIMs can be designed to have a unique capability to recognise anions and to act as sensors in novel ways, such as with molecular motion.

In 2014 Beer and co-workers reported a water soluble rotaxane (Figure 1.25) selective for iodide.[33,86] Innovatively, two hydrophilic permethylated β-cyclodextrin groups were included to act as water solubilising groups and as stoppers for the rotaxane. The study compared the binding affinity to halide anions of a halogen bonding system and the analogous hydrogen bonding system. Remarkably the halogen bonding rotaxane bound iodide with high affinity in water (K_a = 2200 M^{-1}), two orders of magnitude greater than the hydrogen bonding analogue (K_a = 20 M^{-1}). Even the free halogen-bonding axle was capable of recognising iodide (K_a = 40 M^{-1}) — comparable to the hydrogen bonding rotaxane. Van't Hoff analysis of the iodide binding event indicated a stark difference in the thermodynamic driving energies of the two receptors. The hydrogen bonding system was predominantly entropically driven, while the halogen bonding rotaxane was enthalpic. This highlights both the charge-transfer contribution of the halogen bonding–anion interaction and the differing desolvation thermodynamics of halogen bonding donors.

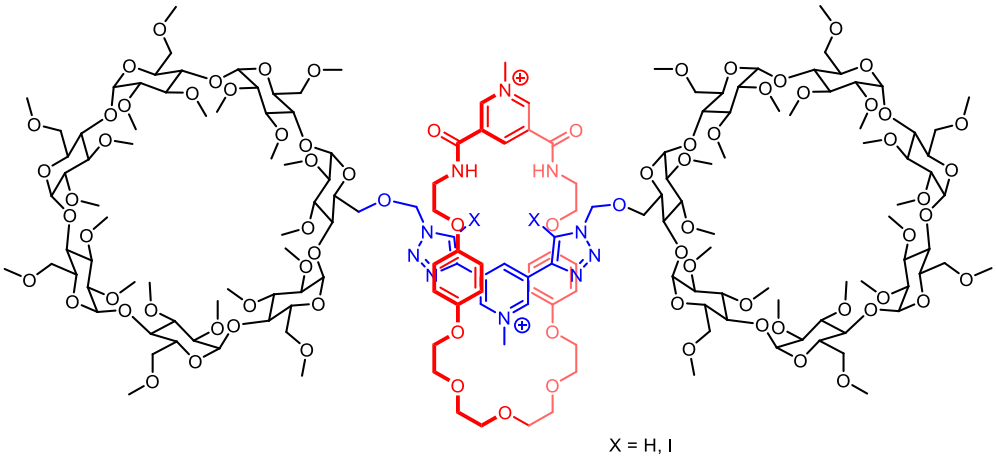


Figure 1.25: *Beer's water soluble rotaxane*

1.3. Anion Sensing

The advances in anion recognition have enabled the development of increasingly more selective and sensitive anion sensors. Sensing refers to the macroscopic detectable signal that results upon an anion recognition event, most commonly a type of photo-physical or electrochemical change. The most prolific category of sensor are chemodosimeters which are non-supramolecular systems that rely on irreversible covalent modification to function (Figure 1.26a) and will therefore not be reviewed in this thesis, except for their extensive use in H_2S sensing (*see 1.4.1. Hydrosulfide recognition and sensing*). Although these sensors can be highly selective their lack of reversibility makes them one-time use systems. Conversely, reversible supramolecular host-guest anion recognition sensors can be repeatedly used. Upon binding to a guest, these systems report a change in signal output from a reporter group that is proximal to the anion recognition site (Figure 1.26b). Another sensing technique are displacement assays in which sensing is induced by a weakly bound dye being displaced by the target analyte (Figure 1.26c).

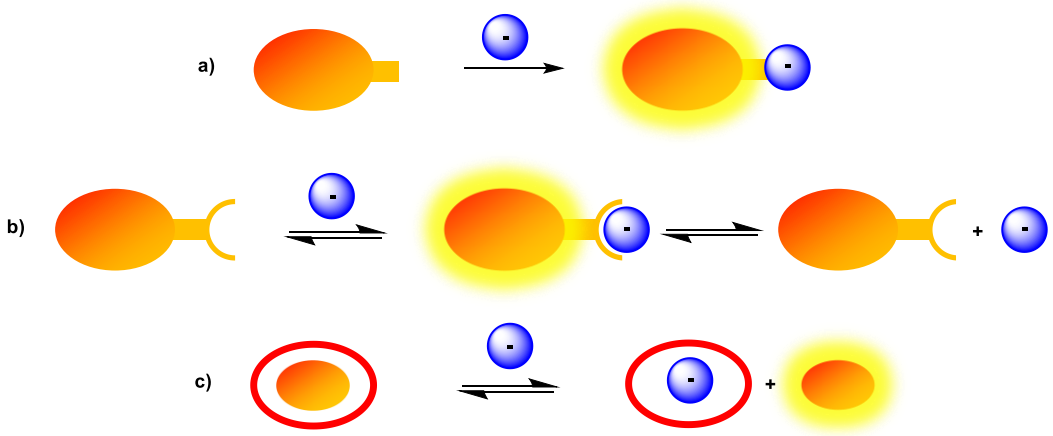


Figure 1.26: *Types of anion sensors* ***a)*** *Chemodosimeter* ***b)*** *Host-Guest* ***c)*** *Displacement assay*

This section will highlight the most well-established sensing methods and mechanisms currently developed for anion sensors and will also examine the evolving field of surface mounted molecular sensors that has the potential to bring the field of host-guest anion sensing into the commercial world.

1.3.1. Optical anion sensing

Coupling optical reporter groups with anion binding motifs has proven a successful strategy in the design of sensors. There are two main types of photo-physical optical sensors, luminescent (fluorescent and phosphorescent) sensors that report a signal based on a change in their emission, and colorimetric sensors that report signal changes from an alteration to their ground state absorbance in the visible spectrum.

1.3.1.1 Fluorescence and luminescence anion sensing

Due to their high sensitivity to changes in their localised environment, fluorophores are widely incorporated into sensors for detecting anions at low concentrations. Upon binding, anions can induce changes to the emission in a number of modes. The most commonly observed changes are photo-induced electron transfer (PET) effects.[106,107] PET caused quenching occurs by the donation of an electron from the anion to the orbital of the excited fluorophore, thereby preventing the singlet decay and emission process (Figure 1.27a). Gunnlaugsson and coworkers demonstrated ideal PET sensor behaviour with their simple thiourea-anthracene receptor.[108,109] On binding to AcO^- and $H_2PO_4^-$ in DMSO a sharp decrease in fluorescence was observed by up to 50% and 70% respectively. Conversely, chloride and bromide only induced minor diminutions (Figure 1.27b).

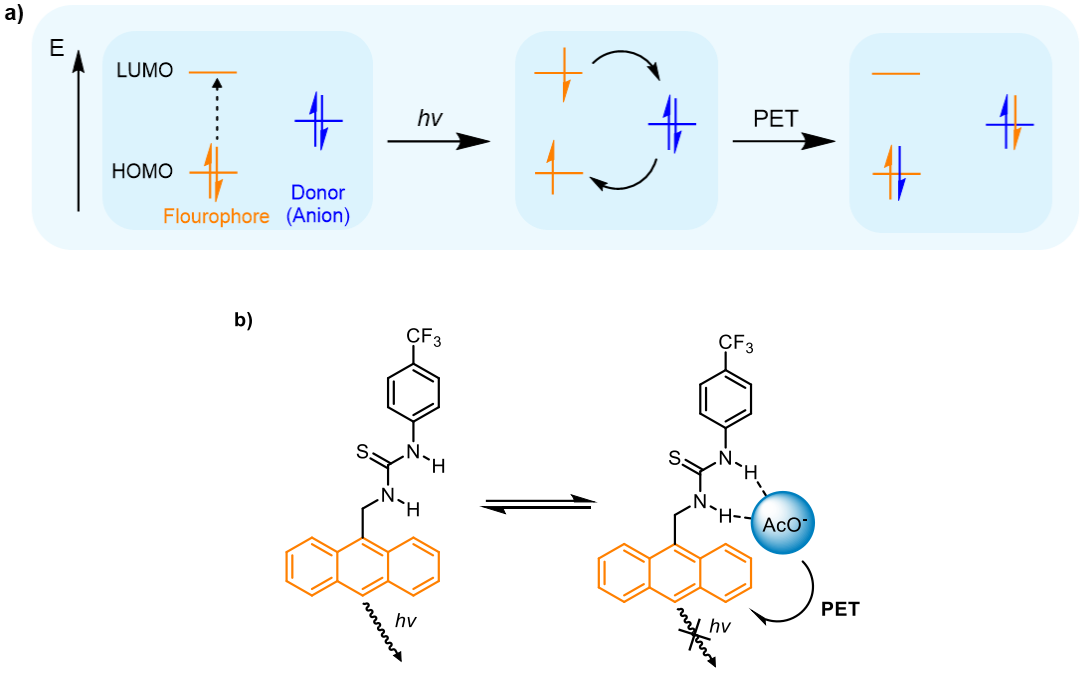


Figure 1.27: *PET quenching* ***a)*** *Mechanism for PET quenching by a proximal donor group* ***b)*** *Gunnlaugsson's thiourea-anthracene sensor that exhibits PET quenching when recognising* AcO^-.

Other mechanisms for fluorescence quenching include Dexter energy transfer (DET) (also commonly known as short-range, collisional or exchange energy transfer), which occurs during the overlap of wavefunctions between the donor and an external acceptor. In a simultaneous transfer, an excited electron is exchanged from the fluorophore to the external group's LUMO, and from the external groups HOMO to the excited fluorophore, thereby returning the fluorophore to the ground state and quenching fluorescence (Figure 1.28a).

Another quenching mechanism is Förster resonance energy transfer (FRET) (also commonly known as resonance or electronic energy transfer), which occurs through proximal distance between two chromophores; a donor and an acceptor.[107] Instead of radiative relaxation of an electron, the donor group transfers energy in a non-radiative resonance process to an acceptor group (Figure 1.28b).

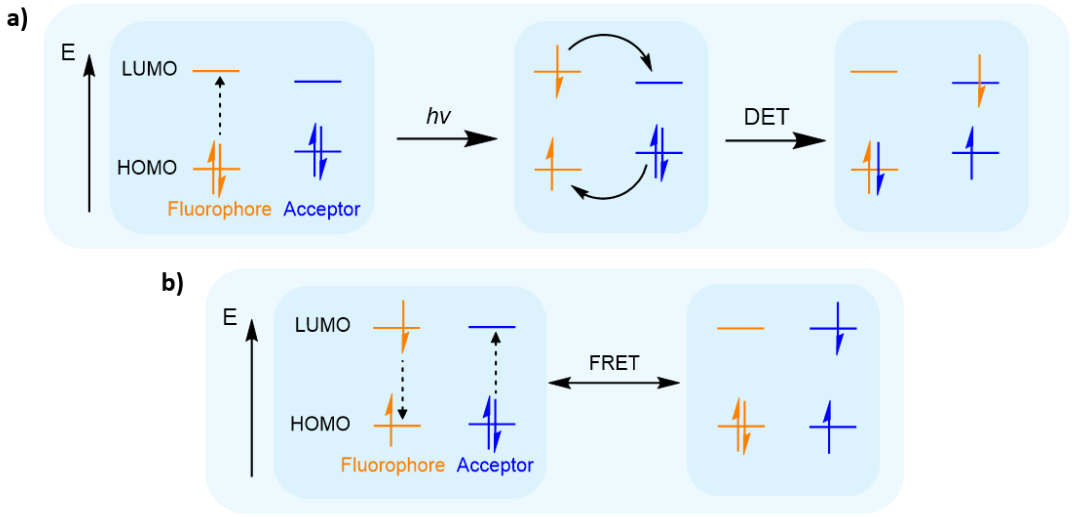


Figure 1.28: a) *Mechanism for DET quenching by an acceptor group with an overlapping wavefunction* ***b)*** *Mechanism for FRET quenching by an acceptor group in close proximity*

A large number of anion induced fluorescence changes can be attributed to the conformational changes that occur on binding. Excimers form when the half-filled orbitals of an excited fluorophore interact with another fluorophore in the ground state (Figure 1.29).[106] This dimer state can then induce a notable broadening and redshift in the emission. Fluorophores with extended conjugated π-systems are particularly susceptible to this interaction due to their favourable ability to π-stack. The introduction of an analyte can induce or break the formation of excimers and therefore has seen considerable interest as a method for sensing. Zapata and co-workers elegantly demonstrated the formation of a pyrene excimer in their triazolium receptor as highlighted earlier (Figure 1.14c). More recently, Caballero and co-workers reported a XB tripod capable of forming anion-induced supramolecular networks of excimers in acetonitrile (Figure 1.29b).[110] On binding to $H_2PO_4^-$, the appended anthracene fluorophores formed excimers with other receptors and induced a unique red shift and broadening to the emission signal.

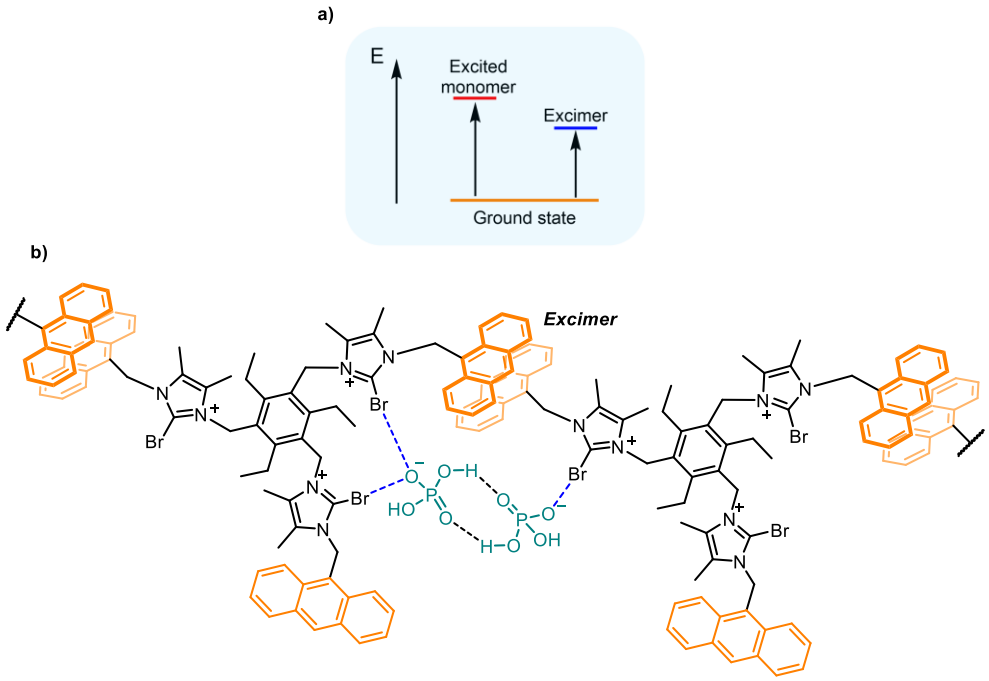


Figure 1.29: a) *Excited monomer and excimer energy differences* ***b)*** *Caballero's $H_2PO_4^-$-induced supramolecular tripod network*

Conformational changes that alter the degrees of freedom in a receptor can have a significant impact on fluorescence. Specifically, rigidity effects, that result from the rigidification of a sensor when coordinating to an anion, can cause fluorescent enhancement.[107] This increase occurs due to the inhibition of vibrational and rotational modes of nonradiative decay that can de-populate the singlet excited state. In addition to a metal-ligand charge transfer (MLCT) blue shift, Beer and co-workers attributed the remarkable MLCT emission enhancement of their calix[4]arene ruthenium(II) bipyridyl receptor to rigidity effects (Figure 1.30a).[111] On binding to $H_2PO_4^-$ in DMSO (K_a = 28000 M^{-1}) they observed a three-fold increase in MLCT emission intensity as the receptor adopted a new conformation best suited for the amide and hydroxyl protons to associate to the anion.

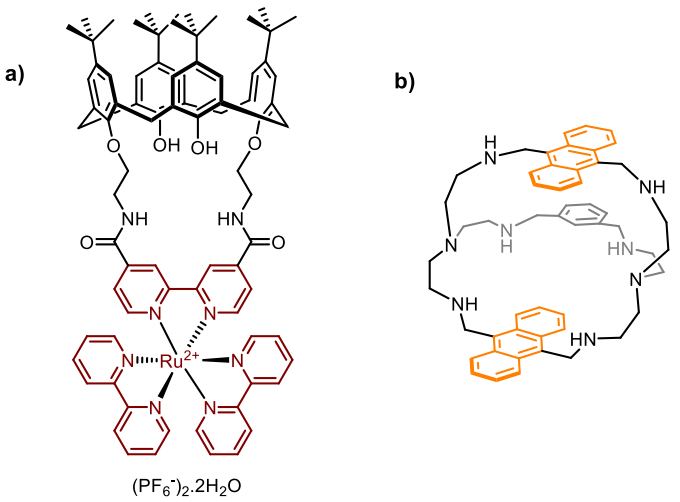


Figure 1.30: a) *Beer's calix[4]arene ruthenium(II) bipyridyl receptor* ***b)*** *Kataev's cryptand*

Changing the composition of the surrounding solvent media can also impact emission intensity. When binding to chaotropic anions, Kataev and co-workers reported that in addition to the interaction between the anion and their receptor, the displacement of water molecules directly caused an increase in fluorescence intensity (Figure 1.30b).[112] They rationalised that the chaotropic nature of the associated analyte disrupted the solvation shell inside and outside the receptor and therefore diminished the rates of nonradiative quenching processes induced by the surrounding water. This method of inducing a detectable signal is relatively unexplored.

1.3.1.2. Colorimetric anion sensing

Sensors capable of a colorimetric response that cause sufficient change for naked-eye detection are highly desirable. Such systems omit the need for expensive detection instruments and are therefore more practical for general use. However, examples of supramolecular host-guest systems that act in this way remain relatively uncommon. Detection of F^- or other basic anions is well reported but the process of induced signal change is more akin to deprotonation or nucleophilic attack rather than anion association.[106,113,114,] Many early colorimetric sensors misinterpreted these interactions as anion association events.[115] Similarly, boron-based receptors, capable of detecting fluoride, form dative bonds instead of supramolecular interactions.[114] Finally, many reversible sensors capable of detecting anions are reported to act as photo-switches but in this process require covalent modification to function. A seminal example of a host-guest colorimetric sensor was reported by Sessler and co-workers in 2000 (Figure 1.31).[116] They rationalised that by directly conjugating an anthraquinone to a calix[4]pyrrole the fluorophore would act as a sink for

vectorial charge-transfer processes when binding and therefore report as an optical sensor. In CH_2Cl_2 the sensor was capable of detecting F^-, Cl^- and $H_2PO_4^-$ by way of a colour change from yellow to orange/red. On the other hand, addition of Br^-, I^- and HSO_4^- did not lead to any noticeable colour change. The group went on to 'colour tune' the system by appending different fluorophores to the host and were able to induce changes from red to blue/purple.[116]

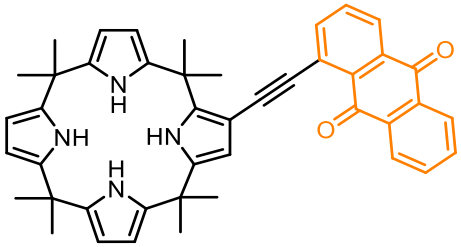


Figure 1.31: *Sessler's colormetric calix[4]pyrrole sensor*

An emerging type of colorimetric sensor and method of inducing naked eye colour changes was demonstrated by Smith and co-workers with their squaraine [2]rotaxane host receptor as discussed earlier (Figure 1.24d).[105] Along with other similar MIM systems, molecular motion, particularly macrocyclic translocation, has been shown to be a formidable method of inducing naked-eye detection for colorimetric sensors.[117–121]

1.3.2. Electrochemical anion sensing

The most common strategy for developing an electrochemical anion sensor is by the incorporation of a redox active reporter group into an anion host receptor. Anion binding events can then cause perturbations in the reporter's voltammetric redox potential which can be sensed. Since Beer's first electrochemical anion sensor in 1989, capable of sensing bromide which upon halide binding induced a 45 mV cathodic shift of the cobaltocene/cobaltocenium redox couple (Figure 1.32a), numerous groups have appended redox active reporter groups onto all manner of anion host receptors.[122,123] Over the decades since, ferrocene has become the most well-established redox reporter group owing to its diagnostic cathodic shifts in the ferrocene/ferrocenium redox couple that occur on binding to anions.[123] Beer and co-workers were able to link their research interests of halogen bonding and redox active sensors with the publication of the first halogen bonding redox-active ferrocene receptors (Figure 1.32b).[124] The halogen bonding sensors were capable of electrochemical sensing chloride and bromide in aqueous-acetonitrile and were found to induce a greater magnitude of cathodic shift on binding than the hydrogen bonding ferrocene receptor analogues. In addition to ferrocene, other metallocenes and organic redox active auxiliaries such as tetrathiafulvalene (TTF) have

been incorporated into host frameworks. Becher and co-workers reported a TTF-calix[4]pyrrole receptor capable of sensing chloride and bromide in acetonitrile (Figure 1.32c).[125] On binding, a large cathodic perturbation of 460 mV was induced for the first TTF oxidation potential for both anions.

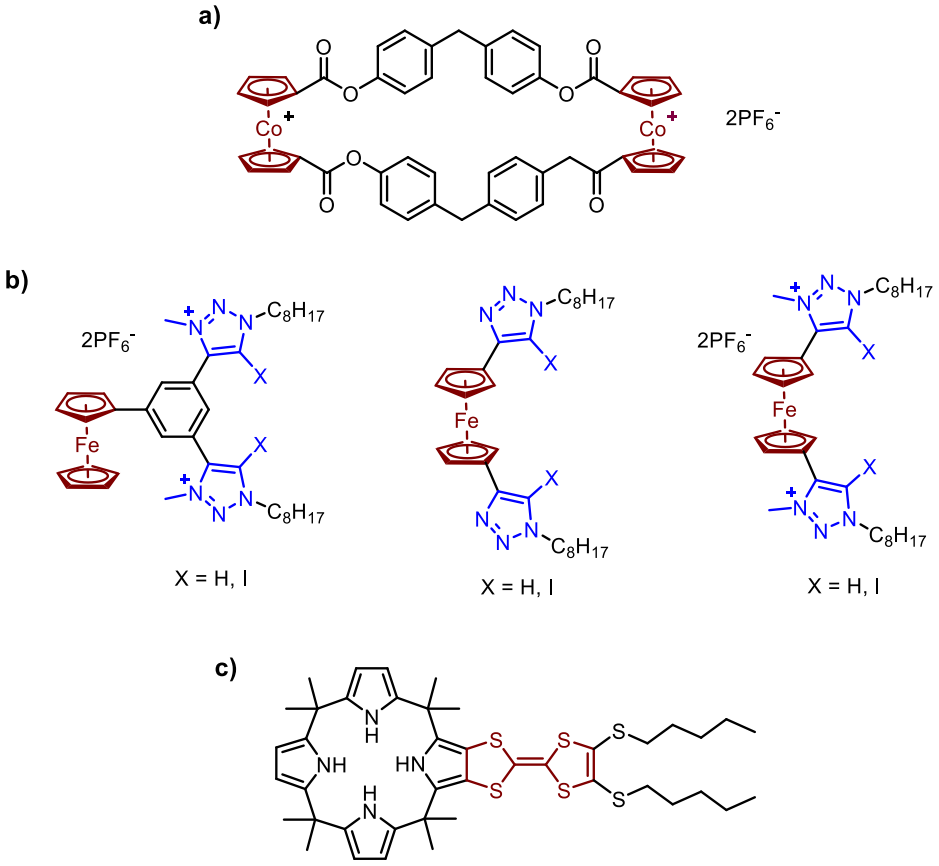


Figure 1.32: a) *Beer's first electrochemical anion sensor* ***b)*** *Beer' halogen bonding redox-active ferrocene receptors* ***c)*** *Becher's TTF-calix[4]pyrrole receptor*

Although most redox-active sensors, as reported in the systems above, sense *via* voltammetric potential changes other techniques such as potentiometric and electrochemical impedance spectroscopy (EIS) offer useful methods of sensing anions. Currently EIS for anion sensing remains rare but recent publications have highlighted the method's great potential for sensing at an interface.[123]

1.3.3. Surface assembled anion sensors

The interfacing of anion sensors onto surfaces, whether it be electroactive surfaces for electrochemical sensing or optically transparent surfaces for photo-physical sensing, is pivotal for the development of real-world sensing devices. Compared to solution phase sensors the field of surface mounted anion, or even cation, sensors is underdeveloped — especially

considering such systems could potentially lead to commercially viable sensing devices. The first example of a self-assembled monolayer (SAM) electrochemical anion sensor was reported by Astruc and co-workers in 1999.[126] The simple amide-ferrocene receptor was functionalised onto a gold surface and was capable of sensing $H_2PO_4^-$ *via* a 290 mV cathodic shift in the ferrocene/ferrocenium redox couple (Figure 1.33a). Subsequent sensors have been mounted onto a variety of surfaces including gold nanoparticles,[127] and for optically active sensors, polymer resins[128] and glass.[129] The close proximity of sensors can result in positive dendritic effects, that cause an enhancement to their sensing properties over their molecular counterparts. Though it is electrochemically inactive unlike gold, glass is widely available, cheap and chemically robust (from H_2S poisoning). Crego-Calama and Reinhoudt *et al* developed a library of fluorescent SAM anion sensors on glass.[130] By functionalising the surface with N-[3-(trimethoxysilyl)propyl]ethylenediamine (TPEDA) they were then able to covalently attach different receptors (Figure 1.33b); thereby omitting the need for solubilising groups needed for solution phase sensing. The sensors were able to discern a variety of anions through quenching or intensity increases in acetonitrile. Although the individual sensors could not entirely discriminate between anions, the implications of the study suggest that an array of different sensors in tandem could allow for a 'fingerprint' reading of analyte mixtures, whereby different compositions of analytes give a distinct combined reading. This methodology deviates from solution phase sensing where significant research has focused on selectivity. Indeed, it may be that surface mounted receptors employing such methods for sensing anions may come to surpass the need for any selectivity.

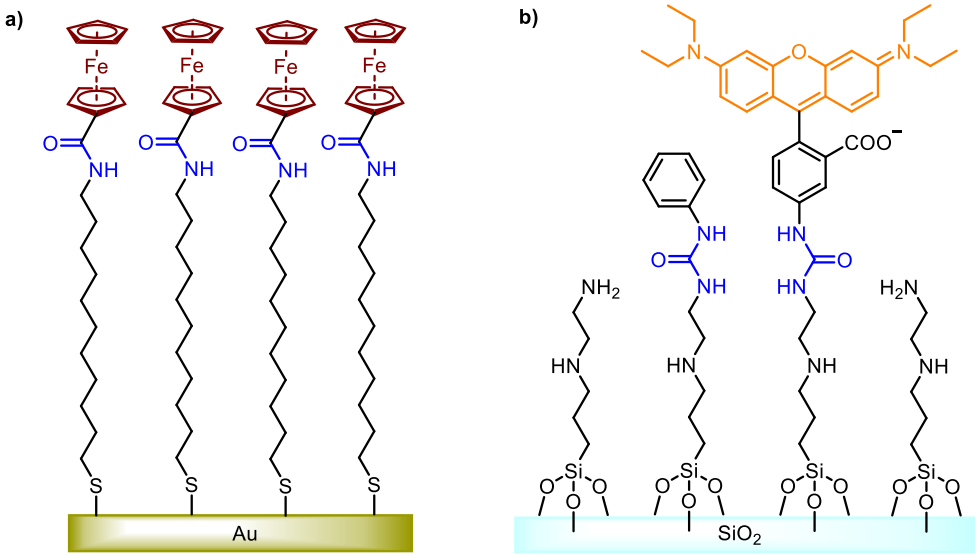


Figure 1.33: a) *Astruc's SAM electrochemical anion sensor* ***b)*** *Crego-Calama and Reinhoudt's fluorescent TPEDA SAM.*

1.4. Hydrogen sulfide and the hydrosulfide anion

The toxicity of hydrogen sulfide (H_2S) towards human health is well known. But in recent years H_2S has been recognised to be of key biological importance as a gasotransmitter produced within living organisms.[131,132,133] Along with carbon monoxide and nitric oxide, it plays a crucial signalling role in a variety of physiological functions including the regulation of the cardiovascular,[134] immune, endocrine and nervous systems.[135,136] In plant physiology it has also been identified to modulate photosynthesis,[137] stomatal closure/aperture,[138] and autophagy regulation.[139,140] However, abnormal concentrations have been implicated in a number of conditions, decreased levels in the brain have been linked with Alzheimer's disease,[141] making H_2S an important diagnostic analyte.

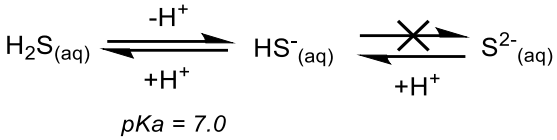
Due to its toxic and corrosive nature, high levels of H_2S in the environment pose a risk to many industries. Importantly, the dominant species of H_2S in aqueous solution is the hydrosulfide anion (HS^-). H_2S/HS^- in flood water can lead to crop poisoning and harvest failure,[142] as a component in crude oil H_2S can corrode pipelines and expose workers to hazardous fumes,[141] and within groundwater H_2S/HS^- can damage long term infrastructure projects and poison livestock.[143,144]

Proposed long term nuclear waste storage involves the burying of vast amounts of radioactive material in what is known as a 'geological disposal facility'. Alarmingly, high levels of H_2S/HS^- in ground water pose a threat to the longevity of this storage.[145] Although cased in a concrete megastructure, over a geological timescale ground motions are expected to cause fractures and allow water to penetrate inside. HS^- in the water could then corrode the copper clad radioactive waste containers and release toxic waste into the environment.[145]

For these reasons, understanding and hence detecting H_2S/HS^- is of critical and growing importance.

1.4.1. Hydrosulfide recognition and sensing

With a pK_a of 7.0, at physiological pH the hydrosulfide anion (HS^-) is the dominant species of H_2S in aqueous solution and in most groundwater environments. The other sulfur anion, sulfide S^{2-}, was recently disproven to exist in aqueous solutions due to its complete conversion to hydrosulfide (Scheme 1.1).[146]



Scheme 1.1: *Equilibrium of Hydrogen sulfide in aqueous conditions.*

Methods used in the detection of H_2S in particular have been mainly confined to irreversible chemodosimeter approaches. The distinction between H_2S and its conjugate base HS^- has been overlooked for these methods due to their analogous reactivity. Nonetheless, the breadth of reported sensors for H_2S/HS^- in aqueous conditions is extensive.

In this section the most well-established chemodosimeter methods of detecting H_2S/HS^- in aqueous conditions will be explored, followed by a review of the fledgling field of supramolecular HS^- recognition and how it may be improved on. Although they have similar reactivity and cooperative roles in biology, detection of important thiol molecules, such as cysteine, is beyond the scope of this study.

1.4.1.1. Chemodosimeters

Traditional methods of detecting H_2S included gas chromatography and electrochemical analysis. Both provided high precision readings but due to their sample destructive methods were denounced for a new wave of sensors that would be biocompatible.[147] Optical probes, whether small molecular or nanomaterials, offered a type of sensor that could give greater real time information and special resolution on biological and environment processes. These strategies take advantage of the reactivity of H_2S/HS^-, using covalent modification to induce a change in a reporter group, whether via a colorimetric or luminescence response.[148,149] There are three major reactive pathways that are adopted for sensing H_2S/HS^-: 1) reduction of nitrates or azides (Figure 1.34a); 2) nucleophilic attack, including substitution (Figure 1.34b), cleavage of a quencher group (Figure 1.34c), breaking of a di-sulfide bond (Figure 1.34d), or another type of reaction such as a Michael addition or the formation of a different substrate (Figure 1.34e); and 3) metal precipitation (Figure 1.34f).[147–150]

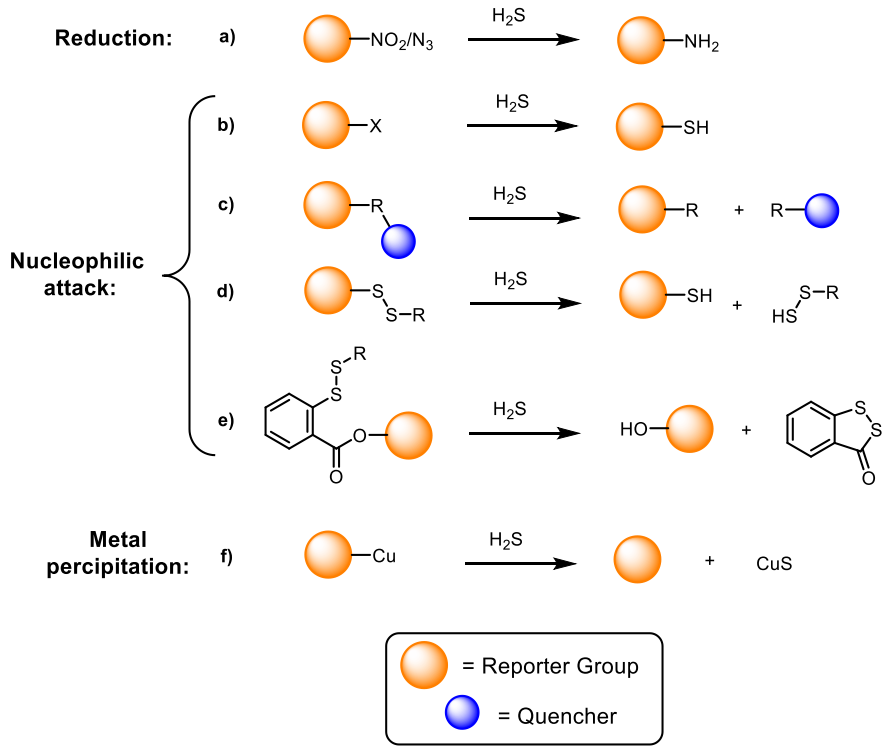


Figure 1.34: *H_2S/HS^- sensing strategies for chemodosimeters*

In spite of the number of available strategies, chemodosimeters are plagued by their inherent irreversibility. A reversible system that has greater longevity and therefore enhanced real-time monitoring has much to offer.

1.4.1.2. Supramolecular approaches and challenges to hydrosulfide recognition

Compared to other anions, HS^- has received scant attention from the host-guest anion recognition community. The first reversible receptors for HS^- were only reported in 2016, and, as of this Thesis, only two more receptor sets since.[151–153] Its recent identification as a biologically important anion has brought it forward as an analyte of interest. However, its basicity, hygroscopicity, and ability to evolve into H_2S makes it more difficult to work with than other anions.

Johnson and co-workers were the first to identify that HS^- had been entirely overlooked.[151] Despite the prevailing assumption that Cl^- and HS^- would have significantly different binding properties based on their differing protonation states, nucleophilicities, hardness/softness, shape and pK_a, they recognised that both have similar ionic radii (S^{2-} = 1.84 Å, Cl^- = 1.81 Å) and play related biological roles. In this light they modified an existing bis(ethynylaniline) receptor reported to recognise Cl^- (Figure 1.35a). For two of their three receptors (Figure 1.35b, 1.1b, 1.1c), the hydrogen bonding ureas were supplemented with an inward facing pyridine to act

as a hydrogen bond acceptor for the HS^- hydrogen. ^1H NMR titration experiments demonstrated all three host systems bound HS^- in d_6-DMSO/CD_3CN (1:9 v/v). However, contrary to expectations, the pyridine receptors exhibited significantly lower binding affinities, suggesting that the hydrogen bond donor element of HS^- is less important in binding HS^- than more anion recognition sites. Importantly each host displayed greater HS^- affinity over Cl^-, this selectivity was more pronounced in the pyridine systems, which was attributed to the weak hydrogen bond formed between the pyridyl nitrogen and SH^- stabilising the association and the repulsion from the pyridyl nitrogen's lone pair to Cl^-. UV-Vis titrations reaffirmed these findings and studies using $Zn(OAc)_2$ to precipitate ZnS confirmed the systems reversibility.

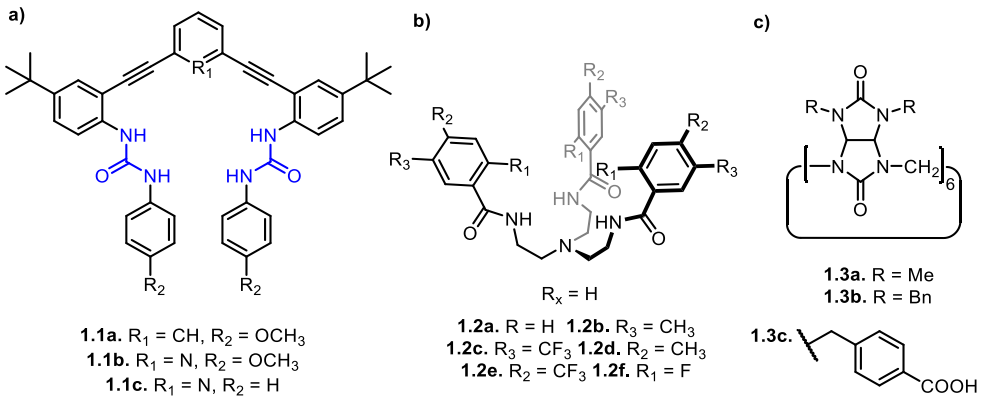


Figure 1.35: *HS^- receptors **a)** Johnson's acyclic receptors **b)** Flood's tripodal receptors **c)** Sindelars bambus[6]urils receptors*

In early 2018, the second set of synthetic receptors for HS^- were reported by Pluth and co-workers — who had previously been in collaboration with the Johnson lab.[152] Using the same logic, previously reported *N,N',N''*-(nitrilotris(ethane-2,1-diyl))tribenzamide tripodal receptors for Cl^- were modified via the addition of electron-withdrawing aryl substituents (Figure 1.35b). Predictably, the p-CF_3- and o-CF_3-aryl containing receptors (Figure 1.35b, 1.2c, 1.2e), exerting the greatest electron-withdrawing inductive effect on the receptors' amide N-H hydrogen bond donors, and displayed greater affinities for HS^- in CD_2Cl_2 than the parent phenyl receptor (1.2e K_a = 3500 M^{-1}, 1.2a K_a = 130 M^{-1}) .

Later the same year Sindelar and co-workers reported that bambus[6]urils, known to bind chloride, were also able to form complexes with HS^- (Figure 1.35c).[153] Using a set of bambus[6]urils with different solubilising groups they demonstrated the first example of HS^- complexation in water. To ensure that HS^- remained the major species in solution, the binding experiments were conducted at a pD of 12.4 in the presence of Na_3PO_4. Interestingly the K_a

values were found to be dependent on the concentration of Na_3PO_4, with lower concentrations resulting in lower association constants (Table 1.2). Contrary to the previous receptors, the binding affinity for HS^- was around 3-fold lower than for Cl^- under similar conditions. Studies in CD_3OD/CD_2Cl_2 1:1, without the use of Na_3PO_4 to increase the pD, found that the receptors bound HS^- with a 1:1 host-guest stoichiometry and with the highest association reported for HS^- (K_a = 77000 M^{-1}, Table 1.2).

The group went on to test the ability of bambus[6]urils complexed with S^{2-} as H_2S releasing agents in water. The complexes were formed by adding Na_2S to a 1:1 CH_2Cl_2:MeOH solution of the bambus[6]urils before removing the solvent. Considering that S^{2-} has been reported to not exist in aqueous solution,[146] it draws questions as to their interpretation of the complex formed.

Table 1.2: *Solvents and association constants for synthetic HS^- receptors*

Receptor	Solvent	K_a / M^{-1}
1.1a	10% d_6-DMSO/CD_3CN	5000
1.2e	CD_2Cl_2	3500 ± 300
1.3c	D_2O[a]	3400
1.3b	CD_3OD/CD_2Cl_2 1:1	77000

[a] = 0.5 M Na_3PO_4 aqueous buffer solution, pD 12.4.

The three sets of HS^- receptors reported thus far highlight the capability of supramolecular systems to recognise this analyte of interest. Modest selectivity over halides in organic solvent media has been demonstrated, and one example of non-selective HS^- binding in water has been achieved. Importantly, this leaves an opportunity for a HS^- selective receptor capable of functioning in competitive aqueous media to be targeted. Additionally, reversible chemosensing of HS^- is unprecedented.

1.5. Objectives

As mentioned in section 1.4, hydrogen sulfide gas and hydrosulfide anion both play pivotal and detrimental roles in many natural biological and industrial processes. Consequently, the selective sensing of H_2S/HS^- is of paramount importance. The capability of supramolecular receptors to recognise HS^- has only recently been realised; the inclusion of reporter groups in such systems could usher in a new age of aqueous HS^- sensors. The presence of HS^- in groundwater is of particular concern for the longevity of radioactive waste storage facilities, such as a GDF. Sensing in deep groundwater environments presents a suite of challenges that must be addressed if accurate sensing of HS^- is to be achieved — the presence of high concentrations of salt (NaCl) in ground water requires any functioning HS^- sensor to operate with near exclusive selectivity over chloride. Current commercialised methods for the detection for H_2S/HS^- have been mainly confined to irreversible chemodosimeter approaches that have limited scope for adaptation to provide real-time information on environmental processes.

The objective of the research in this thesis is concerned with the development of supramolecular halogen bonding receptors capable of recognising and sensing HS^- in aqueous media:

Chapter two describes the development of a series of halogen bonding coumarin based host receptors, including acyclic and mechanically interlocked systems. The capability of halogen bonding motifs to bind anions, coupled with the coumarins fluorophore's ability to relay the binding event via changes in fluorescence is explored.

Chapter three builds on the results of Chapter 2, detailing the synthesis of two generations of water soluble halogen bonding coumarin receptors and investigates their anion binding and sensing properties.

Chapter four investigates the use of BODIPY as a fluorescent reporter group in anion receptors. A series of BODIPY containing receptors are prepared and their sensing capabilities explored.

1.6. References

1 J. D. Watson and F. H. C. Crick, *Nature*, 1953, **171**, 737–738.

2 J. -M Lehn, *Angew. Chem. Int. Ed. English*, 1988, **27**, 89–112.

3 U. Lüning, *Angew. Chem. Int. Ed.*, 2013, **52**, 4724–4724.

4 J. M. Lehn, *Science.*, 1985, **227**, 849–856.

5 C. J. Pedersen, *J. Am. Chem. Soc.*, 1967, **89**, 2495–2496.

6 J. M. Lehn, *Acc. Chem. Res.*, 1978, **11**, 49–57.

7 D. J. Cram, K. Takahiro, R. C. Helgeson and G. M. Lein, *J. Am. Chem. Soc.*, 1979, **101**, 6752–6754.

8 C. H. Park and H. E. Simmons, *J. Am. Chem. Soc.*, 1968, **90**, 2431–2432.

9 E. Graf and J. M. Lehn, *J. Am. Chem. Soc.*, 1976, **98**, 6403–6405.

10 P. Chakrabarti, *J. Mol. Biol.*, 1993, **234**, 463–482.

11 P. A. Gale, E. N. W. Howe and X. Wu, *Chem*, 2016, **1**, 351–422.

12 M. P. Anderson, R. J. Gregory, S. Thompson, D. W. Souza, S. Paul, R. C. Mulligan, A. E. Smith and M. J. Welsh, *Science.*, 1991, **253**, 202–205.

13 F. Delange, *Thyroid*, 1994, **4**, 107–128.

14 A. S. McCall, C. F. Cummings, G. Bhave, R. Vanacore, A. Page-Mccaw and B. G. Hudson, *Cell*, 2014, **157**, 1380–1392.

15 J. L. Hatfield and R. F. Follett, *Nitrogen in the Environment*, Elsevier Inc., 2nd edn., 2008.

16 E. A. Katayev, G. V. Kolesnikov and J. L. Sessler, *Chem. Soc. Rev.*, 2009, **38**, 1572–1586.

17 S. Pavelka, A. Babický, M. Vobecký and J. Lener, *Biol. Trace Elem. Res.*, 2001, **82**, 133–142.

18 S. Pavelka, *Physiol. Res.*, 2004, **53**, 81–90.

19 R. D. Shannon, *Acta Crystallogr. Sect. A*, 1976, **32**, 751–767.

20 J. W. Steed and J. L. Atwood, in *Supramolecular Chemistry*, John Wiley & Sons, Ltd, 2009, 1–31.

21 C. Caltagirone, G. W. Bates, P. A. Gale and M. E. Light, *Chem. Commun.*, 2008, **1**, 61–63.

22 R. S. Carnegie, C. L. D. Gibb and B. C. Gibb, *Angew. Chem. Int. Ed.*, 2014, **53**, 11498–11500.

23 J. B. Wittenberg and L. Isaacs, in *Supramolecular Chemistry*, John Wiley & Sons, Ltd, 2012.

24 C. J. Pedersen, *J. Am. Chem. Soc.*, 1967, **89**, 7017–7036.

25 S. D. Reilly, G. K. Rattan Khalsa, D. K. Ford, J. R. Brainard, B. P. Hay and P. H. Smith, *Inorg. Chem.*, 1995, **34**, 569–575.

26 E. Kimura, T. Yatsunami and M. Kodama, *J. Am. Chem. Soc.*, 1982, **104**, 3182–3187.

27 E. Kimura, A. Sakonaka, T. Yatsunami and M. Kodama, *J. Am. Chem. Soc.*, 1981, **103**, 3041–3045.

28 F. P. Schmidtchen, *Angew. Chem. Int. Ed. English*, 1977, **16**, 720–721.

29 E. Arunan, G. R. Desiraju, R. A. Klein, J. Sadlej, S. Scheiner, I. Alkorta, D. C. Clary, R. H. Crabtree, J. J. Dannenber, P. Hobza, H. G. Kjaergaard, A. C. Legon, B. Mennucci and D. J. Nesbitt, *Pure Appl. Chem.*, 2011, **83**, 1637–1641.

30 J. Emsley, *Chem. Soc. Rev.*, 1980, **9**, 91–124.

31 G. R. Desiraju, P. Shing Ho, L. Kloo, A. C. Legon, R. Marquardt, P. Metrangolo, P. Politzer, G. Resnati and K. Rissanen, *Pure Appl. Chem.*, 2013, **85**, 1711–1713.

32 T. Clark, M. Hennemann, J. S. Murray and P. Politzer, *J. Mol. Model.*, 2007, **13**, 291–296.

33 M. J. Langton, S. W. Robinson, I. Marques, V. Félix and P. D. Beer, *Nat. Chem.*, 2014, **6**, 1039–1043.

34 B. L. Schottel, H. T. Chifotides and K. R. Dunbar, *Chem. Soc. Rev.*, 2008, **37**, 68–83.

35 O. B. Berryman, F. Hof, M. J. Hynes and D. W. Johnson, *Chem. Commun.*, 2006, **5**, 506–508.

36 H. Luecke and F. A. Quiocho, *Nature*, 1990, **347**, 402–406.

37 J. W. Pflugrath and F. A. Quiocho, *J. Mol. Biol.*, 1988, **200**, 163–180.

38 J. W. Pflugrath and F. A. Quiocho, *Nature*, 1985, **314**, 257–260.

39 J. M. Lehn, E. Sonveaux and A. K. Willard, *J. Am. Chem. Soc.*, 1978, **100**, 4914–4916.

40 B. Dietrich, J. M. Lehn, J. Guilhem and C. Pascard, *Tetrahedron Lett.*, 1989, **30**, 4125–4128.

41 S. D. Reilly, G. K. Rattan Khalsa, D. K. Ford, J. R. Brainard, B. P. Hay and P. H. Smith, *Inorg. Chem.*, 1995, **34**, 569–575.

42 J. Hodačová, M. Chadim, J. Závada, J. Aguilar, E. García-España, S. V Luis and J. F. Miravet, *J. Org. Chem.*, 2005, **70**, 2042–2047.

43 F. P. Schmidtchen, *Chem. Ber.*, 1981, **114**, 597–607.

44 F. P. Schmidtchen and G. Müller, *J. Chem. Soc. Chem. Commun.*, 1984, **16**, 1115–1116.

45 K. Worm and F. P. Schmidtchen, *Angew. Chem. Int. Ed. English*, 1995, **34**, 65–66.

46 A. Echavarren, A. Galán, J. M. Lehn and J. De Mendoza, *J. Am. Chem. Soc.*, 1989, **111**, 4994–4995.

47 K. Sato, S. Arai and T. Yamagishi, *Tetrahedron Lett.*, 1999, **40**, 5219–5222.

48 E. Alcalde, C. Alvarez-Rúa, S. García-Granda, E. García-Rodriguez, N. Mesquida and L. Pérez-García, *Chem. Commun.*, 1999, **3**, 295–296.

49 Z. Xu, S. K. Kim and J. Yoon, *Chem. Soc. Rev.*, 2010, **39**, 1457–1466.

50 Y. Hu, S. Long, H. Fu, Y. She, Z. Xu and J. Yoon, *Chem. Soc. Rev.*, 2021, **50**, 589–618.

51 J. Yoon, S. K. Kim, N. J. Singh and K. S. Kim, *Chem. Soc. Rev.*, 2006, **35**, 355–360.

52 J. Pancholi and P. D. Beer, *Coord. Chem. Rev.*, 2020, **416**, 213281.

53 F. P. Schmidtchen, *Angew. Chem.*, 1977, **89**, 751–752.

54 K. Worm, F. P. Schmidtchen, A. Schier, A. Schäfer and M. Hesse, *Angew. Chem. Int. Ed. English*, 1994, **33**, 327–329.

55 S. H. Jungbauer and S. M. Huber, *J. Am. Chem. Soc.*, 2015, **137**, 12110–12120.

56 A. Kumar and P. S. Pandey, *Org. Lett.*, 2008, **10**, 165–168.

57 N. L. Kilah, M. D. Wise, C. J. Serpell, A. L. Thompson, N. G. White, K. E. Christensen and P. D. Beer, *J. Am. Chem. Soc.*, 2010, **132**, 11893–11895.

58 F. Zapata, A. Caballero, P. Molina, I. Alkorta and J. Elguero, *J. Org. Chem.*, 2014, **79**, 6959–6969.

59 R. Tepper, B. Schulze, M. Jäger, C. Friebe, D. H. Scharf, H. Görls and U. S. Schubert, *J. Org. Chem.*, 2015, **80**, 3139–3150.

60 S. W. Robinson, C. L. Mustoe, N. G. White, A. Brown, A. L. Thompson, P. Kennepohl and P. D. Beer, *J. Am. Chem. Soc*, 2015, **137**, 3.

61 C. J. Massena, N. B. Wageling, D. A. Decato, E. Martin Rodriguez, A. M. Rose and O. B. Berryman, *Angew. Chem. - Int. Ed.*, 2016, **55**, 12398–12402.

62 R. A. Pascal, J. Spergel and D. Van Engen, *Tetrahedron Lett.*, 1986, **27**, 4099–4102.

63 A. P. Davis, J. F. Gilmer and J. J. Perry, *Angew. Chem. Int. Ed. English*, 1996, **35**, 1312–1315.

64 P. D. Beer, *Chem. Commun.*, 1996, **6**, 689–696.

65 S. Valiyaveettil, J. F. J. Engbersen, W. Verboom and D. N. Reinhoudt, *Angew. Chem. Int. Ed. English*, 1993, **32**, 900–901.

66 K. Kavallieratos, C. M. Bertao and R. H. Crabtree, *J. Org. Chem.*, 1999, **64**, 1675–1683.

67 K. Kavallieratos, S. R. De Gala, D. J. Austin and R. H. Crabtree, *J. Am. Chem. Soc.*, 1997, **119**, 2325–2326.

68 S. Nishizawa, P. Bühlmann, M. Iwao and Y. Umezawa, *Tetrahedron Lett.*, 1995, **36**, 6483–6486.

69 S. J. Brooks, P. A. Gale and M. E. Light, *Chem. Commun.*, 2005, **1**, 4696–4698.

70 V. Ramalingam, M. E. Domaradzki, S. Jang and R. S. Muthyala, *Org. Lett.*, 2008, **10**, 3315–3318.

71 S. Kubik, R. Kirchner, D. Nolting and J. Seidel, *J. Am. Chem. Soc.*, 2002, **124**, 12752–12760.

72 S. Peng, Q. He, G. I. Vargas-Zúñiga, L. Qin, I. Hwang, S. K. Kim, N. J. Heo, C. H. Lee, R. Dutta and J. L. Sessler, *Chem. Soc. Rev.*, 2020, **49**, 865–907.

73 P. A. Gale, J. L. Sessler, V. Král and V. Lynch, *J. Am. Chem. Soc.*, 1996, **118**, 5140–5141.

74 A. Baeyer, *Berichte der Dtsch. Chem. Gesellschaft*, 1886, **19**, 2184–2185.

75 D. Villarón, M. A. Siegler and S. J. Wezenberg, *Chem. Sci.*, 2021, **12**, 3188–3193.

76 Y. Li and A. H. Flood, *Angew. Chem. - Int. Ed.*, 2008, **47**, 2649–2652.

77 H. Juwarker, J. M. Lenhardt, D. M. Pham and S. L. Craig, *Angew. Chem. Int. Ed.*, 2008, **47**, 3740–3743.

78 R. M. Meudtner and S. Hecht, *Angew. Chem. Int. Ed.*, 2008, **47**, 4926–4930.

79 Y. Liu, W. Zhao, C. H. Chen and A. H. Flood, *Science.*, 2019, **365**, 159–161.

80 J. Y. C. Lim and P. D. Beer, *Eur. J. Inorg. Chem.*, 2017, **2017**, 220–224.

81 R. Tepper, B. Schulze, H. Görls, P. Bellstedt, M. Jäger and U. S. Schubert, *Org. Lett.*, 2015, **17**, 5740–5743.

82 S. Nam, D. C. Ware and P. J. Brothers, *Org. Biomol. Chem.*, 2018, **16**, 6460–6469.

83 S. Lee, C. H. Chen and A. H. Flood, *Nat. Chem.*, 2013, **5**, 704–710.

84 A. Bauzá, T. J. Mooibroek and A. Frontera, *ChemPhysChem*, 2015, **16**, 2496–2517.

85 G. E. Garrett, E. I. Carrera, D. S. Seferos and M. S. Taylor, *Chem. Commun.*, 2016, **52**, 9881–9884.

86 M. J. Langton, C. J. Serpell and P. D. Beer, *Angew. Chem. Int. Ed.*, 2016, **55**, 1974–1987.

87 A. Schaly, R. Belda, E. García-España and S. Kubik, *Org. Lett.*, 2013, **15**, 6238–6241.

88 M. A. Yawer, V. Havel and V. Sindelar, *Angew. Chem. Int. Ed.*, 2015, **54**, 276–279.

89 M. Lisbjerg, H. Valkenier, B. M. Jessen, H. Al-Kerdi, A. P. Davis and M. Pittelkow, *J. Am. Chem. Soc.*, 2015, **137**, 4948–4951.

90 M. Lisbjerg, B. E. Nielsen, B. O. Milhøj, S. P. A. Sauer and M. Pittelkow, *Org. Biomol. Chem.*, 2015, **13**, 369–373.

91 J. M. Suk, M. K. Chae and K. S. Jeong, *Pure Appl. Chem.*, 2012, **84**, 953–964.

92 T. Lizal and V. Sindelar, *Isr. J. Chem.*, 2018, **58**, 326–333.

93 J. Y. C. Lim and P. D. Beer, *Chem. Commun.*, 2015, **51**, 3686–3688.

94 A. Borissov, I. Marques, J. Y. C. Lim, V. Félix, M. D. Smith and P. D. Beer, *J. Am. Chem. Soc.*, 2019, **141**, 4119–4129.

95 S. F. M. van Dongen, Seda Cantekin, J. A. A. W. Elemans, A. E. Rowan and R. J. M. Nolte, *Chem. Soc. Rev.*, 2013, **43**, 99–122.

96 K. M. Bąk, K. Porfyrakis, J. J. Davis and P. D. Beer, *Mater. Chem. Front.*, 2020, **4**, 1052–1073.

97 A. Martinez-Cuezva, A. Saura-Sanmartin, M. Alajarin and J. Berna, *ACS Catal.*, 2020, **10**, 7719–7733.

98 B. Zheng, F. Wang, S. Dong and F. Huang, *Chem. Soc. Rev.*, 2012, **41**, 1621–1636.

99 K. K. Cotí, M. E. Belowich, M. Liong, M. W. Ambrogio, Y. A. Lau, H. A. Khatib, J. I. Zink, N. M. Khashab and J. F. Stoddart, *Nanoscale*, 2009, **1**, 16–39.

100 D. Curiel and P. D. Beer, *Chem. Commun.*, 2005, **14**, 1909–1911.

101 J. P. Byrne, S. Blasco, A. B. Aletti, G. Hessman and T. Gunnlaugsson, *Angew. Chem. Int. Ed.*, 2016, **55**, 8938–8943.

102 M. K. Chae, J. M. Suk and K. S. Jeong, *Tetrahedron Lett.*, 2010, **51**, 4240–4242.

103 J. J. Gassensmith, J. M. Baumes and B. D. Smith, *Chem. Commun.*, 2009, **42**, 6329–6338.

104 J. J. Gassensmith, L. Barr, J. M. Baumes, A. Paek, A. Nguyen and B. D. Smith, *Org. Lett.*, 2008, **10**, 3343–3346.

105 J. J. Gassensmith, S. Matthys, J. J. Lee, A. Wojcik, P. V. Kamat and B. D. Smith, *Chem. Eur. J.*, 2010, **16**, 2916–2921.

106 P. A. Gale and C. Caltagirone, *Coord. Chem. Rev.*, 2018, **354**, 2–27.

107 R. Martínez-Máñez and F. Sancenón, *Chem. Rev.*, 2003, **103**, 4419–4476.

108 T. Gunnlaugsson, A. P. Davis and M. Glynn, *Chem. Commun.*, 2001, **1**, 2556–2557.

109 T. Gunnlaugsson, H. D. P. Ali, M. Glynn, P. E. Kruger, G. M. Hussey, F. M. Pfeffer, C. M. G. Dos Santos and J. Tierney, *J. Fluoresc.*, 2005, **15**, 287–299.

110 P. Sabater, F. Zapata, A. Bastida and A. Caballero, *Org. Biomol. Chem.*, 2020, **18**, 3858–3866.

111 F. Szemes, D. Hesek, Z. Chen, S. W. Dent, M. G. B. Drew, A. J. Goulden, A. R. Graydon, A. Grieve, R. J. Mortimer, T. Wear, J. S. Weightman and P. D. Beer, *Inorg. Chem.*, 1996, **35**, 5868–5879.

112 S. S. R. Namashivaya, A. S. Oshchepkov, H. Ding, S. Förster, V. N. Khrustalev and E. A. Kataev, *Org. Lett.*, 2019, **21**, 8746–8750.

113 T. Gunnlaugsson, M. Glynn, G. M. Tocci (née Hussey), P. E. Kruger and F. M. Pfeffer, *Coord. Chem. Rev.*, 2006, **250**, 3094–3117.

114 D. A. McNaughton, M. Fares, G. Picci, P. A. Gale and C. Caltagirone, *Coord. Chem. Rev.*, 2021, **427**, 213573.

115 H. Miyaji and J. L. Sessler, *Angew. Chem. Int. Ed.*, 2001, **40**, 154–157.

116 H. Miyaji, W. Sato and J. L. Sessler, *Angew. Chem. Int. Ed.*, 2000, **39**, 1777–1780.

117 C. G. Collins, E. M. Peck, P. J. Kramer and B. D. Smith, *Chem. Sci.*, 2013, **4**, 2557–2563.

118 H. A. Klein, H. Kuhn and P. D. Beer, *Chem. Commun.*, 2019, **55**, 9975–9978.

119 G. T. Spence, M. B. Pitak and P. D. Beer, *Chem. A Eur. J.*, 2012, **18**, 7100–7108.

120 T. A. Barendt, A. Docker, I. Marques, V. Félix and P. D. Beer, *Angew. Chem. Int. Ed.*, 2016, **55**, 11069–11076.

121 T. A. Barendt, I. Rašović, M. A. Lebedeva, G. A. Farrow, A. Auty, D. Chekulaev, I. V. Sazanovich, J. A. Weinstein, K. Porfyrakis and P. D. Beer, *J. Am. Chem. Soc.*, 2018, **140**, 1924–1936.

122 P. D. Beer and A. D. Keefe, *J. Organomet. Chem.*, 1989, **375**, C40–C42.

123 R. Hein, P. D. Beer and J. J. Davis, *Chem. Rev.*, 2020, **120**, 1888–1935.

124 J. Y. C. Lim, M. J. Cunningham, J. J. Davis and P. D. Beer, *Chem. Commun.*, 2015, **51**, 14640–14643.

125 K. A. Nielsen, J. O. Jeppesen, E. Levillain and J. Becher, *Angew. Chem. Int. Ed.*, 2003, **42**, 187–191.

126 E. Alonso, A. Labande, L. Raehm, J. M. Kern and D. Astruc, *Comptes Rendus l'Academie des Sci. - Ser. IIc Chem.*, 1999, **2**, 209–213.

127 P. Sokkalingam, S. J. Hong, A. Aydogan, J. L. Sessler and C. H. Lee, *Chem. Eur. J.*, 2013, **19**, 5860–5867.

128 S. Byrne and K. M. Mullen, *RSC Adv.*, 2016, **6**, 33880–33887.

129 Y. Cao, L. Ding, S. Wang, Y. Liu, J. Fan, W. Hu, P. Liu and Y. Fang, *ACS Appl. Mater. Interfaces*, 2014, **6**, 49–56.

130 L. Basabe-Desmonts, J. Beld, R. S. Zimmerman, J. Hernando, P. Mela, M. F. García Parajó, N. F. Van Hulst, A. Van Den Berg, D. N. Reinhoudt and M. Crego-Calama, *J. Am. Chem. Soc.*, 2004, **126**, 7293–7299.

131 R. Wang, *Physiol. Rev.*, 2012, **92**, 791–896.

132 R. Wang, *FASEB J.*, 2002, **16**, 1792–1798.

133 A. Aroca, C. Gotor and L. C. Romero, *Front. Plant Sci.*, 2018, **9**, 1369.

134 D. J. Polhemus and D. J. Lefer, *Circ. Res.*, 2014, **114**, 730–737.

135 J. L. Wallace and R. Wang, *Nat. Rev. Drug Discov.*, 2015, **14**, 329–345.

136 S. Singh and H. Lin, *Microorganisms*, 2015, **3**, 866–889.

137 J. Chen, F.-H. Wu, W.-H. Wang, C.-J. Zheng, G.-H. Lin, X.-J. Dong, J.-X. He, Z.-M. Pei and H.-L. Zheng, *J. Exp. Bot.*, 2011, **62**, 4481–4493.

138 M. Papanatsiou, D. Scuffi, M. R. Blatt and C. García-Mata, *Plant Physiol.*, 2015, **168**, 29–35.

139 A. M. Laureano-Marín, I. Moreno, L. C. Romero and C. Gotor, *Plant Physiol.*, 2016, **171**, 1378–1391.

140 C. Álvarez, I. García, I. Moreno, M. E. Pérez-Pérez, J. L. Crespo, L. C. Romero and C. Gotor, *Plant Cell*, 2012, **24**, 4621–4634.

141 K. Eto, T. Asada, K. Arima, T. Makifuchi and H. Kimura, *Biochem. Biophys. Res. Commun.*, 2002, **293**, 1485–1488.

142 L. P. M. Lamers, L. L. Govers, I. C. J. M. Janssen, J. J. M. Geurts, M. E. W. Van der Welle, M. M. Van Katwijk, T. Van der Heid, J. G. M. Roelofs and A. J. P. Smolders, *Front. Plant Sci.*, 2013, **4**, 1–14.

143 G. Jiang, J. Sun, K. R. Sharma and Z. Yuan, *Curr. Opin. Biotechnol.*, 2015, **33**, 192–197.

144 T. Wang, K. Wu, L. Kan and M. Wu, *Constr. Build. Mater.*, 2020, **247**, 118539.

145 D. S. Hall, M. Behazin, W. Jeffrey Binns and P. G. Keech, *Prog. Mater. Sci.*, 2021, **118**, 100766.

146 P. M. May, D. Batka, G. Hefter, E. Königsberger and D. Rowland, *Chem. Commun.*, 2018, **54**, 1980–1983.

147 Y. Luo, C. Zhu, D. Du and Y. Lin, *Anal. Chim. Acta*, 2019, **1061**, 1–12.

148 B. Peng and M. Xian, *Asian J. Org. Chem.*, 2014, **3**, 914–924.

149 A. R. Lippert, *J. Inorg. Biochem.*, 2014, **133**, 136–142.

150 D. Amilan Jose, R. Sakla, N. Sharma, S. Gadiyaram, R. Kaushik and A. Ghosh, 2020, **5**, 3391.

151 M. D. Hartle, R. J. Hansen, B. W. Tresca, S. S. Prakel, L. N. Zakharov, M. M. Haley, M. D. Pluth and D. W. Johnson, *Angew. Chem. Int. Ed.*, 2016, **55**, 11480–11484.

152 N. Lau, L. N. Zakharov and M. D. Pluth, *Chem. Commun.*, 2018, **54**, 2337–2340.

153 J. Vázquez and V. Sindelar, *Chem. Commun.*, 2018, **54**, 5859–5862.

Chapter 2

Coumarin-based Anion Receptors

2. Coumarin-based Anion Receptors

2.1. Introduction

2.1.1. Coumarin anion sensors

Fluorescent reporter groups incorporated into anion receptor structural frameworks can act as sensors for anions (*see 1.3 Anion Sensing*). Coumarins are a family of well-studied fluorophores that contain a central 1-benzopyran-2-one motif (Figure 2.1).[1] Owing to their high fluorescent quantum yields, tuneable emission wavelengths and their responsiveness to changes in their microenvironments, they have seen wide-spread use in laser dyes, optical brighteners, dispersed fluorescent dyes and as sensors. The majority of coumarin anion sensors reported to date function as irreversible chemodosimeters for nucleophilic anions such as CN^-, F^- and HS^-. Reversible supramolecular coumarin-based anion sensors are rare.

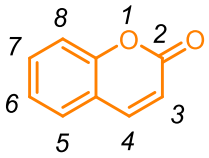


Figure 2.1: *Coumarin — 1-benzopyran-2-one*

A seminal example is Lee's coumarin-strapped calix[4]pyrrole receptor reported in 2005.[2] The system sensed halide anions in 3% H_2O-MeCN via fluorescence PET quenching but required sodium cation coordination to the coumarin carbonyl, to function (Figure 2.2a). More recently, Zappia and co-workers reported a bis-coumarin-urea sensor (Figure 2.2b) that exhibited fluorescence quenching of up to 50% on binding to Cl^-, AcO^- and $HP_2O_7^{3-}$ in CH_3CN.[3] They rationalised the observed quenching was caused by changes to two competing internal processes that influenced the coumarin's fluorescence. Internal charge transfer (ICTr) from the amine at the 7 position, when the fluorophore is planar gives rise to the origin of the fluorescence, whilst twisted intramolecular charge transfers (TICT) from the amine decreases fluorescence.[4] Upon anion binding, the latter becomes dominant and thus induces quenching.

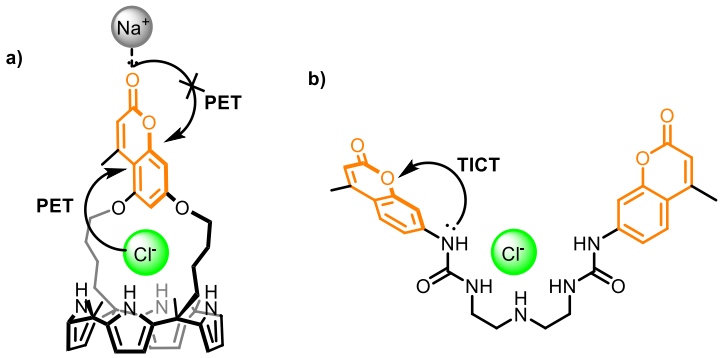


Figure 2.2: a) *Coumarin-1-benzopyran-2-one* ***b)*** *Lee's coumarin-strapped calix[4]pyrolle* ***c)*** *Zappia's bis urea coumarin receptor*

The two examples above highlight the capability of coumarin to act as photo-physical reporter group in supramolecular anion receptors. A host that combines the sensing capabilities of coumarin with the high binding affinities of halogen bonding is unprecedented. Since halogen bonding has repeatedly been shown to outperform hydrogen bonding, particularly in aqueous environments, such as system has much to offer as an anion sensor.

2.1.2. Chapter Objectives

This chapter's objective is to develop novel halogen bonding coumarin-based receptors for sensing anions.

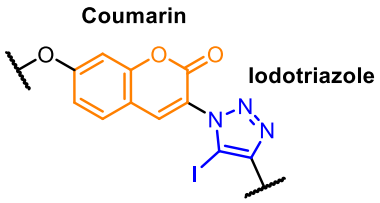


Figure 2.3: *Appended coumarin and iodotriazole, sensing and anion association motif.*

To achieve this, the potent halogen bonding (XB) iodotriazole motif for anion recognition in competitive protic solvent media is directly covalently appended to the coumarin fluorophore reporter group to facilitate anion sensing capability (Figure 2.3).

Specifically, the XB bis-coumarin pyridinium group (Figure 2.4a) featuring two convergent iodotriazoles and a central charged pyridinium motif to enhance anion association, is incorporated into acyclic, macrocyclic and interlocked host structural frameworks. The synthesis of each target receptor system is described, and their anion binding properties investigated by ^{1}H NMR and fluorescence spectroscopic titration experiments.

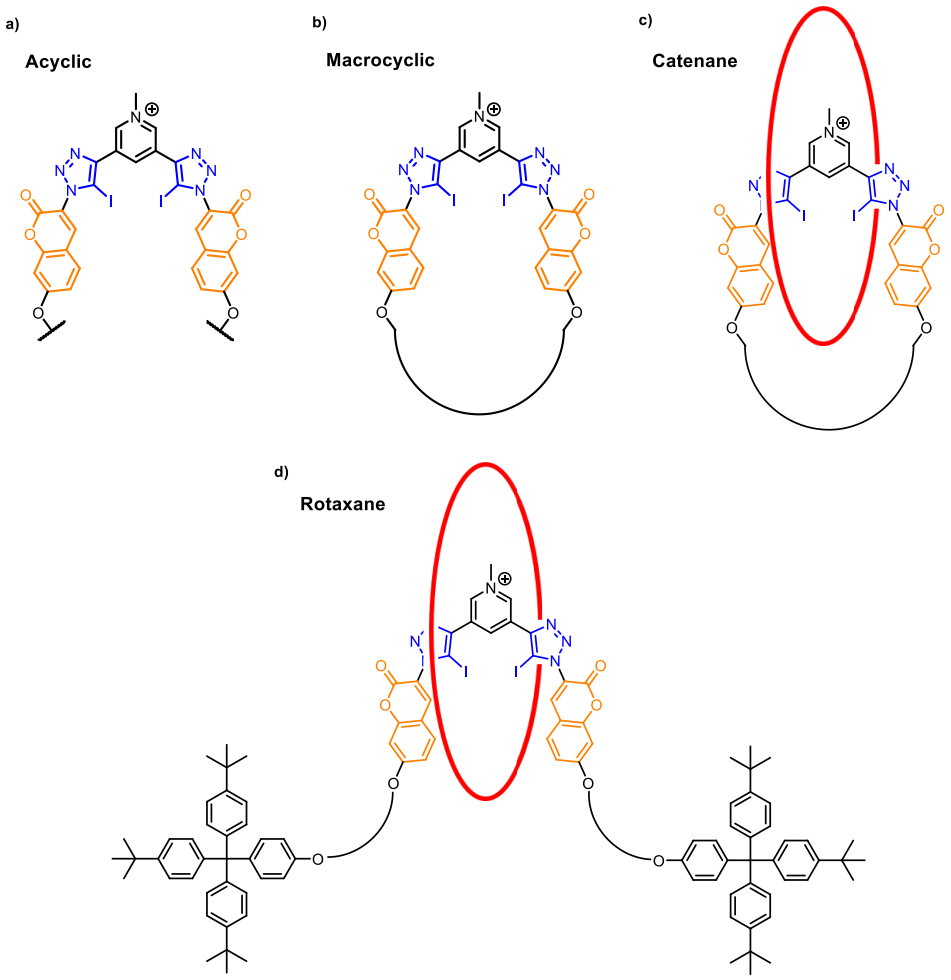


Figure 2.4: *General structures of target XB coumarin anion receptors;* ***a)*** *acyclic receptor* ***b)*** *macrocyclic receptor* ***c)*** *catenane receptor* ***d)*** *rotaxane receptor*

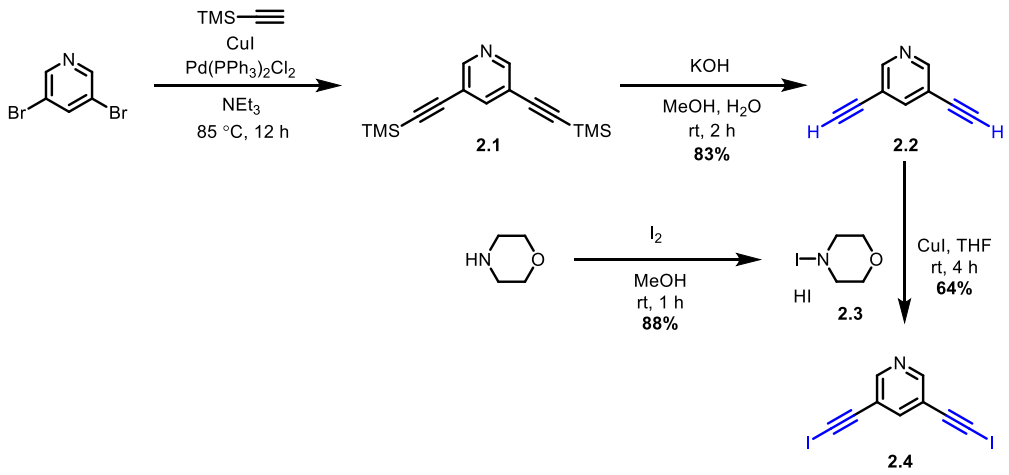
2.2. Acyclic Halogen Bonding Coumarin Receptor

The initial target acyclic halogen bonding receptor (Figure 2.4a) contains the halogen bonding 3,5-bis-iodotriazole pyridinium motif which has previously been shown to bind chloride strongly in acetonitrile and DMSO organic solvent media.[5] This acyclic system would primarily be used to investigate it's potential fluorescence response upon halide binding in organic media, before undertaking further work on the preparation of more complex macrocyclic and interlocked host systems. Because of the extremely hygroscopic nature of the tetra-butyl ammonium (TBA) salt of HS^-,[6] the receptors discussed in this chapter were not tested for sensing this anion unless soluble in aqueous-organic mixtures. Investigations into water

soluble XB coumarin-based receptor analogues for HS^- fluorescence sensing is the subject of the next chapter.

2.2.1. Synthesis

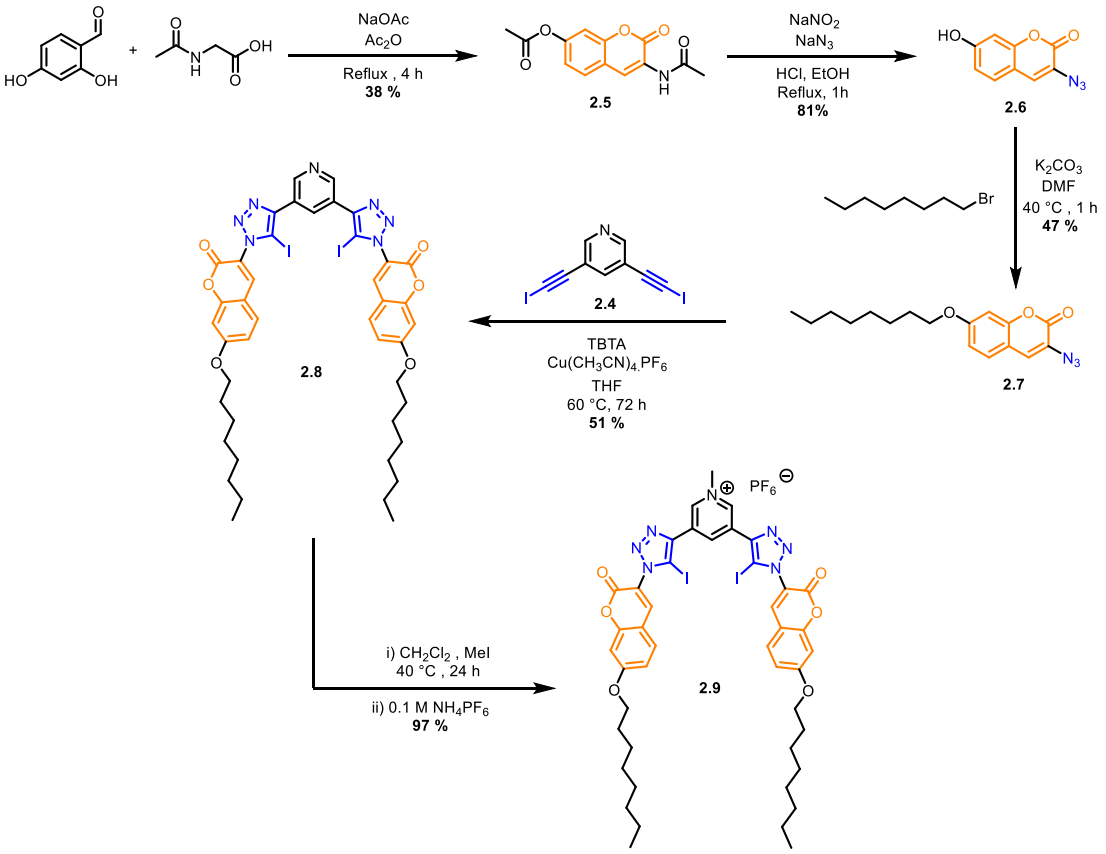
In order to introduce a route to halogen bonding functionality in the form of an iodotriazole motif, 3,5-bis-iodo-alkyne pyridine **2.4** was prepared following literature procedures reported by Beer and co-workers[7] as outlined in Scheme 2.1. Commercially available 3,5-dibromopyridine was reacted with two equivalents of TMS acetylene in the presence of a palladium catalyst *via* a Sonogashira coupling reaction. Subsequent deprotection of crude TMS protected bis-alkyne **2.1** was achieved by stirring with KOH in a MeOH/H_2O mixture, affording bis-alkyne **2.2** in a collective yield of 83%. N-Iodomorpholine hydriodide **2.3** was freshly prepared by reacting morpholine with iodine in MeOH, before being added to bis-alkyne **2.2** in the presence of CuI, to afford bis-iodo alkyne **2.4** in yields as high as 64% (Scheme 2.1).



Scheme 2.1: *Synthesis of bis-iodo-alkyne* ***2.4***

To allow for the introduction of solubilising groups, a coumarin with an alcohol functionality at the 7 position, *trans* to the azide functionality at position 3, was selected. Coumarin derivatives **2.5** and **2.6** were prepared following procedures reported by Xi and co-workers (Scheme 2.2).[8] 2,4 Hydroxybenzaldehyde and N-acetylglycine were refluxed together to afford coumarin **2.5** in up to 38% yield. Successive acetate deprotection and azide substitution were achieved in the presence of HCl and reaction with $NaNO_2$ and NaN_3, affording coumarin azide **2.6** in 81% yield (Scheme 2.2).

Alkylation with octyl bromide in the presence of K_2CO_3 afforded azide **2.7** in a moderate yield of 47%. The low Williamson ether synthesis yield was attributed to partial decomposition of the coumarin azide in the heated basic conditions. A copper(I)-catalysed alkyne-azide cycloaddition click reaction (CuAAC) of bis-alkyne **2.4**, with two equivalents of azide **2.7**, afforded bis-iodotriazole pyridyl-coumarin **2.8** in a 51 % yield. Subsequent methylation with methyl iodide followed by anion exchange to the hexafluorophosphate salt produced the desired XB coumarin octyl-acyclic host system **2.9** in a 97 % yield (Scheme 2.2).



Scheme 2.2: *Synthesis of acyclic receptor* ***2.9***

2.2.2. Anion Binding Studies

2.2.2.1. ^{1}H NMR Titrations

To probe the anion binding properties of acyclic XB receptor **2.9**, ^{1}H NMR titration experiments with TBA halide salts were conducted in the competitive 45/45/10 d_4-MeOD/$CDCl_3$/D_2O solvent mixture. Though the receptor is not soluble in pure water, use of this solvent mixture gives greater insight into the anion recognition capability of the system in aqueous conditions.

Addition of TBABr and TBAI led to significant downfield perturbations of the receptor's internal pyridinium signal *b*, suggesting the halides are bound between the convergent XB iodotriazole donors (Figure 2.5). By contrast, addition of TBACl induced chemical shifts below 0.02 ppm, too small for reliable analysis but suggestive of an interaction. To probe further, fluorescence emission titration experiments, a more sensitive spectroscopic technique, will be used.

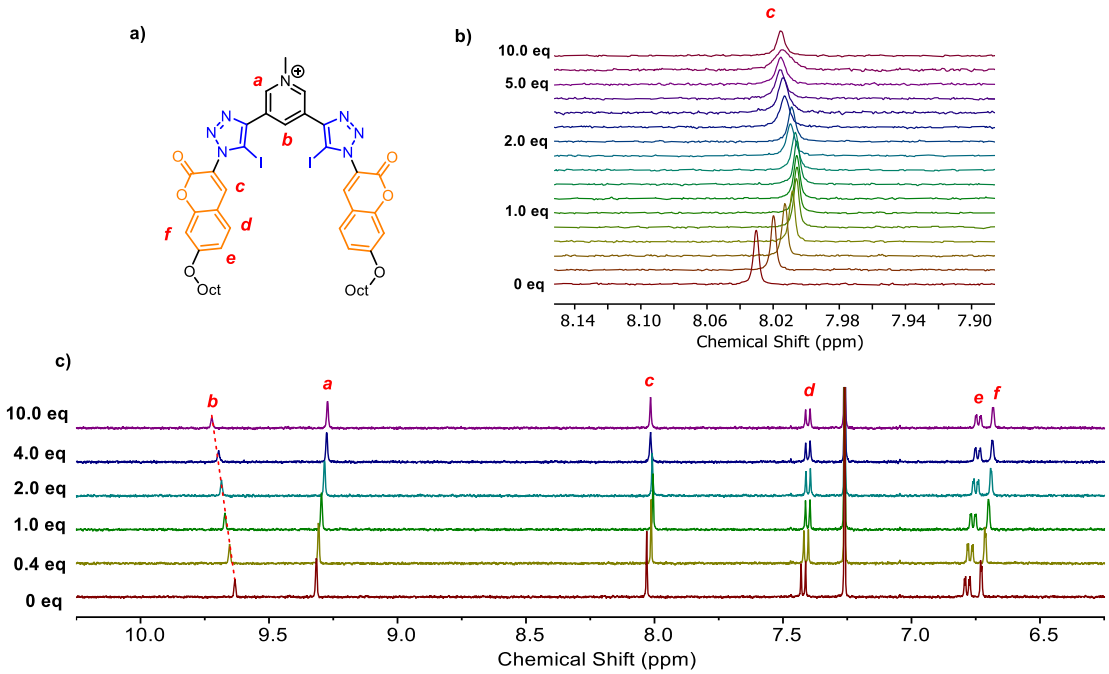
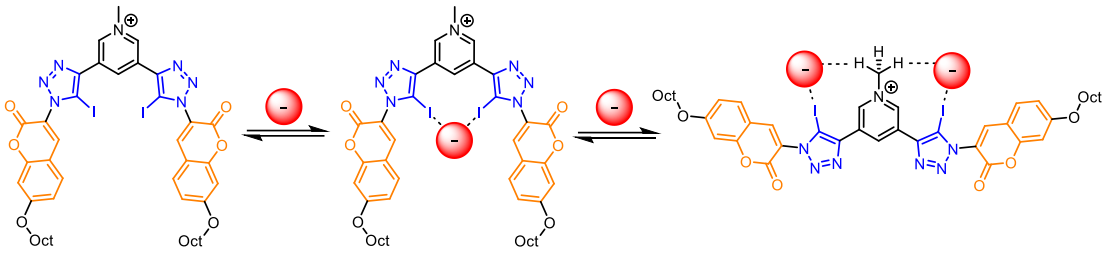


Figure 2.5: *Truncated ^{1}H NMR titration spectra of receptor **2.9** upon addition of 0-10 equivalents of TBAI in 45/45/10 d_4-MeOD/$CDCl_3$/D_2O; ([host] = 1 mM, T = 298 K).* ***a)*** *Receptor **2.9** with proton labels* ***b)*** *Chemical shift of coumarin proton peak c* ***c)*** *^{1}H NMR titration spectra with proton labels.*

Notably, the receptor's coumarin protons *c–f* and also underwent significant perturbations with bromide and iodide addition (Figure 2.5c), indicating involvement in the halide binding event and therefore likely to having an impact on the receptor's fluorescence emission response. This is most significant for proton peak *c* which is closest to the binding site and adjacent to the two convergent halogen bonding units. Interestingly and to a greater extent with the addition of TBAI than TBABr, peaks *a, c,* and the methyl peak, move upfield until 1–2 equivalents are added before shifting downfield upon subsequent additions up to 20. This behaviour is indicative of a 1:2 host-guest binding stoichiometry, suggesting the receptor complexes the two anions in a sequential manner as proposed in Scheme 2.3.



Scheme 2.3: *Proposed binding modes of acyclic XB receptor 2.9*

Internal pyridinium proton *b's* chemical shifts were used to plot binding isotherms (Figure 2.6) and, using nonlinear regression analysis Bindfit v0.5 software,[9,10] to determine the 1:1 host-guest stoichiometric association constants, as shown in Table 2.1. The receptor was found to have a greater association constant for iodide over bromide, exhibiting Hofmeister selectivity for the more hydrophobic, least hydrated halide. Of note is the significant error for the iodide association constant, particularly in contrast to that of bromide, as visualised in the plotted isotherms in Figure 2.6. This iodide isotherm deviation may be indicative of a 1:2 host-guest stoichiometric binding relationship as suggested by the proton shifts of the receptor (Figure 2.5). However, Bindfit analysis of the proton peak shifts using a 1:2 host-guest binding model failed to produce reliable quantitative binding data.

Table 2.1: *Anion association constants for acyclic XB receptor 2.9*

Anion	K_a (M^{-1})
Cl^-	-
Br^-	380 ± 10
I^-	620 ± 100

Anion association constants with errors determined using 1:1 stoichiometric Bindfit analysis of the NMR titration data of receptor **2.9**, monitoring the internal pyridinium peak; 1 mM receptor in 45:45:10 d_4-MeOD:$CDCl_3$:D_2O solution, 298 K. - = limited chemical shifts observed

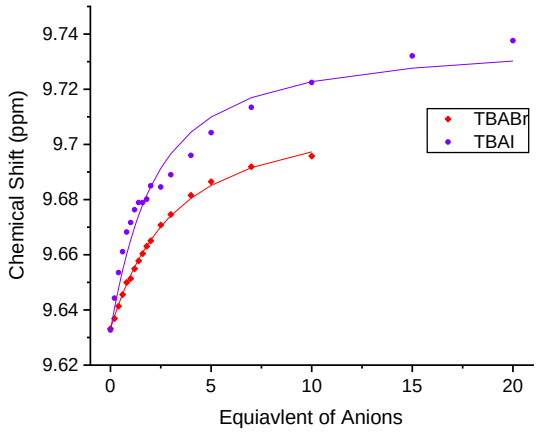


Figure 2.6: *Binding isotherms and 1:1 stoichiometric Bindfit analysis of NMR titration data for receptor* ***2.9****, monitoring internal pyridinium peak upon addition of TBABr and TBAI in 45:45:10 d_4-MeOD:$CDCl_3$:D_2O solution, 298 K.*

2.2.2.2. Fluorescence Titrations

The photophysical properties of receptor **2.9** were investigated using UV-visible absorption and fluorescence emission spectroscopy. Characteristic energies of absorption and emission bands for coumarin were observed in CH_3CN and 45/45/10 $CHCl_3$/MeOH/H_2O (Table 2.2).[1] Two previously reported examples of coumarin compounds (Figure 2.7) and their photophysical properties are included in Table 2.2 for comparison.[11,12]

Table 2.2: *Photophysical data for receptor* ***2.9*** *and literature examples.*

Solvent	$\lambda_{max\ abs}$ / nm	$\lambda_{max\ ems}$ / nm	Stokes Shift / nm
MeCN[a]	339	395	58
45:45:10 $CHCl_3$/MeOH/H_2O[a]	342	406	64
MeCN[b]	342	-	-
DMF[c]	350	426	76

Emission wavelength excited at $\lambda_{max\ abs}$ **[a]** = [10 µM], 298 K; **[b]** Figure 2.7a, [10 µM], 298 K; **[c]** = Figure 2.7b, [1 µM], 298 K.

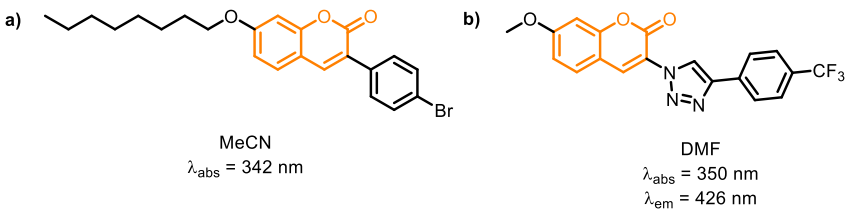


Figure 2.7: *Photophysical properties of similar coumarin derivatives*

The anion binding behaviour of receptor **2.9** was probed by fluorescence titration experiments in CH_3CN and 45/45/10 $CHCl_3$/MeOH/H_2O. Preliminary qualitative fluorescence titrations (λ_{ex} = 339 nm) were performed in MeCN by the addition of up to 175 equivalents of TBACl. Integration of the fluorescence spectra revealed a 60% increase in the intensity of the coumarin fluorescence (Figure 2.8). This notable emission intensity increase is thought to arise from the formation of the receptor-halide anion complex restricting the rotational freedom of the receptor's coumarin motifs, thereby disfavouring nonradiative decay processes. Interestingly, this contrasts with previously reported coumarin anion host-receptors (Figure 2.2), which underwent fluorescence emission quenching.

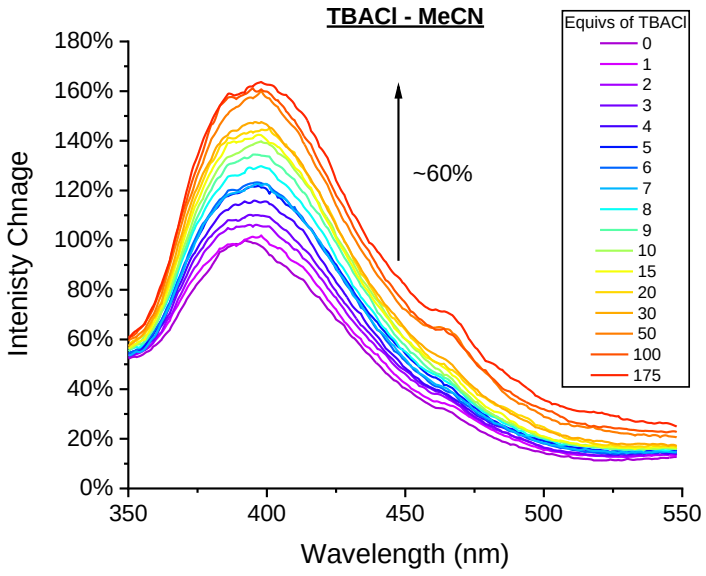


Figure 2.8: *Fluorescence emission intensity change of receptor* ***2.9*** *on addition of TBACl in MeCN; ([host] = 10 μM, 45/45/10 CHCl3/MeOH/H2O, T = 298 K).*

Quantitative fluorescence titration experiments (λ_{ex} = 342 nm) in the competitive aqueous solvent mixture 45/45/10 $CHCl_3$/MeOH/H_2O were undertaken with NaCl, NaBr, NaI and NaHS (Figure 2.9). Upon the addition of anions, an initial increase in the fluorescence intensity was observed. However, after 10–15 equivalents the fluorescence intensity decreased indicating the receptor is binding with 1:2 host-guest stoichiometry at the higher anion concentrations. The decrease in intensity is most notable with the larger halides: bromide and iodide. The quenching can be attributed to a number of factors: a decrease in rigidity caused by the second binding event, photo-induced electron transfer (PET) effects from two, rather than one, associated anions, and heavy atom quenching effects with bromide and iodide.

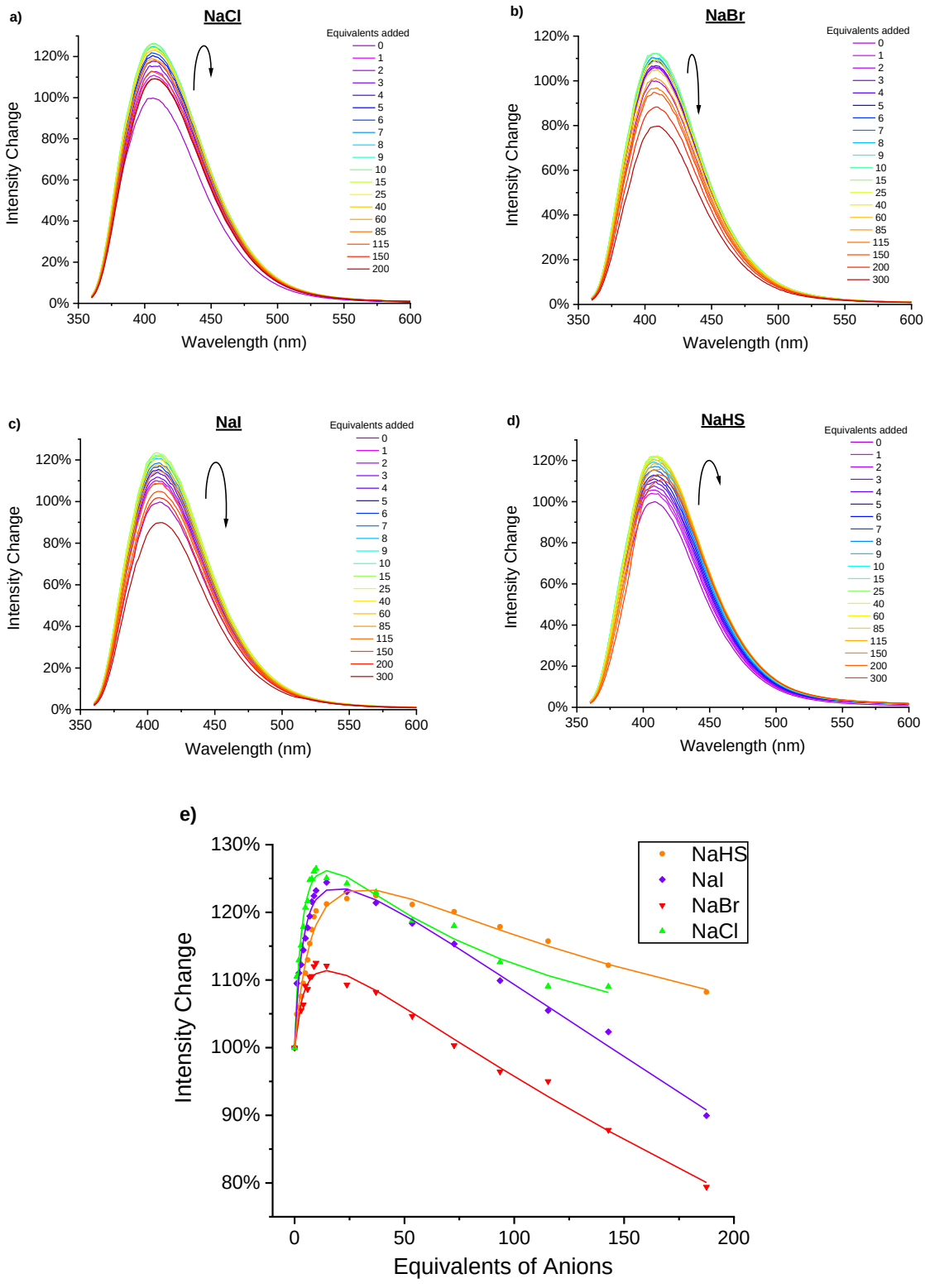


Figure 2.9: *Fluorescence emission intensity changes of receptor* ***2.9*** *upon addition of* ***a)*** *NaCl* ***b)*** *NaBr,* ***c)*** *NaI* ***d)*** *NaHS.* ***e)*** *Binding isotherms and bindfit analysis fit of fluorescence maxima change on addition of anions. ([host] = 10 μM, 45/45/10 $CHCl_3$/MeOH/H_2O, T = 298 K).*

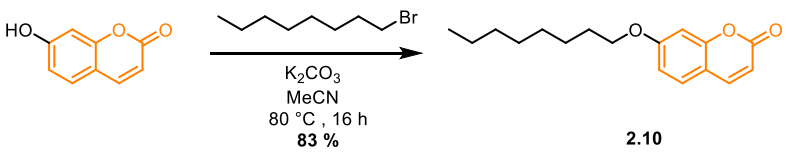
Nonlinear regression analysis of the fluorescence titration data using Bindfit v0.5 software[9,10] determined association constants (Table 2.3). As anticipated, the association constants for the first binding event K_{11} are far larger than for the second K_{12}. This difference can be rationalised on statistical grounds of fewer binding sites and by the significant decrease in favourable electrostatic attraction of the second binding event. The K_{11} association constant magnitudes for all the halides exceed the value for HS^- and display no clear halide preference. Interestingly, the K_{12} values correlate with relative ionic radii size of the anions, with K_{12} being the largest for chloride and iodide the smallest.

Table 2.3: *Receptor **2.9** anion association constants*

Anion	K_{11} (M^{-1})	K_{12} (M^{-1})
NaCl	33000 (4000)	1100 (100)
NaBr	23000 (5000)	150 (10)
NaI	29000 (4000)	30 (1)
NaHS	12000 (1000)	500 (40)

Anion association constants with errors in brackets, determined by Bindfit analysis of fluorescence titration data monitoring the change in emission maxima intensity using a 1:2 host:guest stoichiometric binding model; 10 μM receptor in 45:45:10 MeOH:$CHCl_3$:H_2O solution, 298 K.

To investigate whether the fluorescence response was an artifact of the coumarin motif rather than a XB-anion association event, a coumarin control molecule was synthesised and tested. Using K_2CO_3 as a base, commercially available 7-hydroxy coumarin was reacted with 1-bromooctane in MeCN to afford octyl-coumarin **2.10** in a yield of 83% (**Scheme 2.4**). Fluorescence titration experiments with NaHS and NaCl in 45/45/10 $CHCl_3$/MeOH/H_2O showed no observable change.



Scheme 2.4: *Synthesis of fluorescence test coumarin **2.10***

As the interaction between sodium cations and the coumarin carbonyl group has been previously reported (Figure 2.2a). Quantitative titration experiments of receptor **2.9** in

45/45/10 $CHCl_3$/MeOH/H_2O were conducted with the TBA halides. The same increase of fluorescence followed by a decrease was observed, ruling out any noticeable relationship between the sodium cation and the fluorescence response.

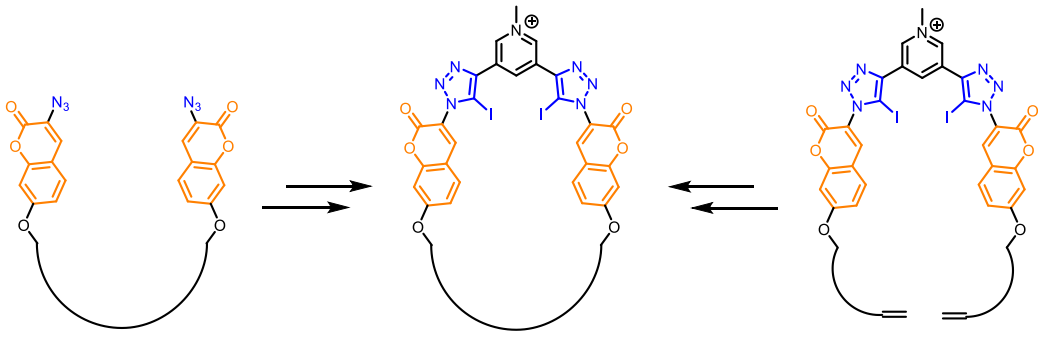
2.2.3. Summary

Acyclic XB coumarin receptor **2.9** was successfully synthesised and found to bind halides and hydrosulfide. Although the binding affinity for HS^- is lower than the halides, these preliminary binding studies provide the first evidence of a XB host-receptor capable of binding and sensing HS^- in a competitive organic-aqueous solvent medium.

2.3. Macrocyclic Halogen Bonding Coumarin Receptors

Macrocyclic receptors benefit from the macrocyclic effect for binding guest species. To further investigate the utility of the coumarin-iodotriazole system and its potential to sense anions, a series of macrocyclic receptors were designed and synthesised.

Two main ring-closing strategies were investigated: one involving a ring-closing copper (I) catalysed azide-alkyne Huisgen cycloaddition (CuAAC) reaction and the other a ring-closing metathesis (RCM) (Scheme 2.5).



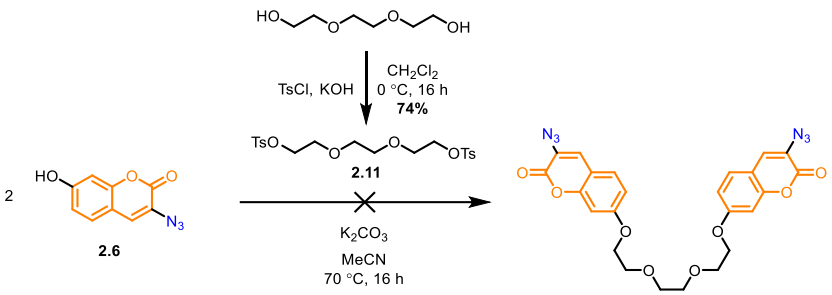
Scheme 2.5: *Two macrocyclization synthetic strategies*

2.3.1. Synthesis

2.3.1.1. Synthesis of a bis-coumarin-azide compound

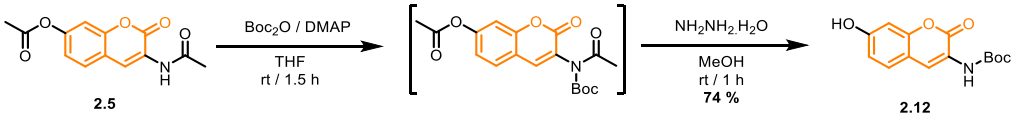
An initial attempt to prepare a bis-coumarin-azide synthon used a Williamson ether reaction approach (Scheme 2.6). Triethylene glycol was stirred with two equivalents of tosyl-chloride in the presence of KOH in CH_2Cl_2 to afford bis-tosylate **2.11** in a yield of 74%. Subsequent

repeated reactions between two equivalents of coumarin **2.6** and bis-tosylate **2.11** in MeCN or DMF in the presence of K_2CO_3 or Cs_2CO_3 at room temperature and with heating were unsuccessful resulting in the decomposition of the starting materials. Similar decomposition issues were observed in the synthesis of coumarin octyl **2.7**, suggesting that coumarin azide **2.6** is unstable under basic conditions.



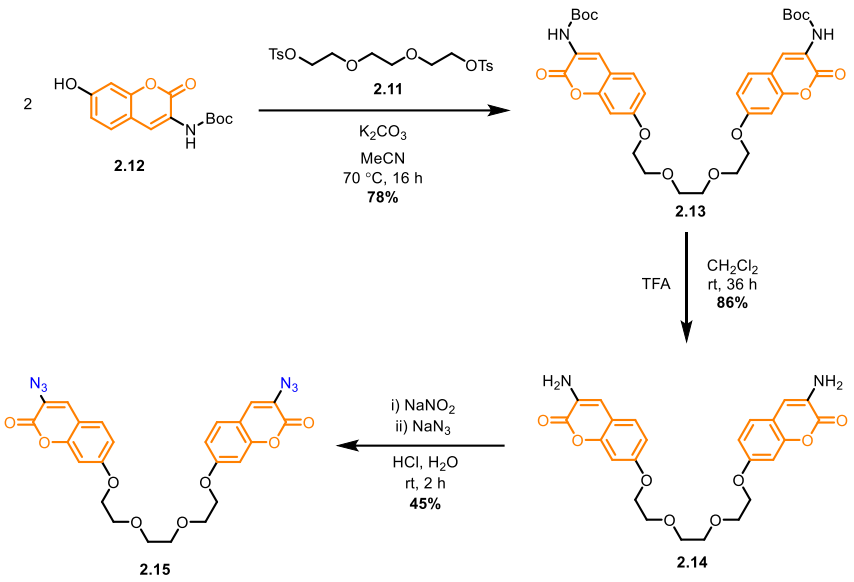
Scheme 2.6: *Attempted synthesis of a coumarin bis-azide*

To circumnavigate the apparent azide-coumarin instability, a Boc-protected coumarin derivative was prepared following procedures reported by Bodwell and co-workers.[13] Coumarin acetyl **2.5** was stirred with Boc_2O and a catalytic amount of DMAP before hydrazine monohydrate in MeOH was slowly added, affording Boc-protected coumarin **2.12** in a 74% yield (Scheme 2.7).



Scheme 2.7: *Synthesis of Boc-protected coumarin derivative*

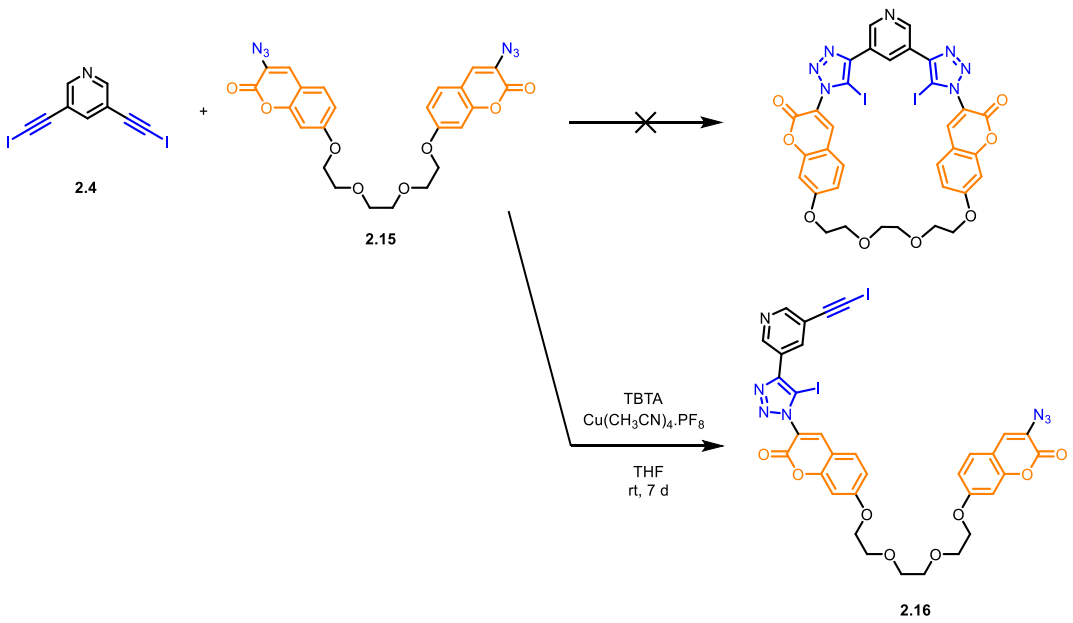
Two equivalents of Boc-protected coumarin **2.12** were reacted with bis-tosylate **2.11** via a Williams-ether synthesis to afford bis-coumarin **2.13** in a 78% yield. Subsequent deprotection to bis-amine **2.14** was achieved by stirring **2.13** with TFA. $NaNO_2$ followed by NaN_3 were added to bis-amine **2.14** in acidic conditions to afford bis-azide coumarin **2.15** in a moderate yield of 45% (Scheme 2.8).



Scheme 2.8: *Synthesis of bis-coumarin azide* ***2.15***

2.3.1.2. Attempted copper (I) catalysed azide-alkyne macrocyclization

To an equimolar mixture of bis-iodo-alkyne **2.4** and bis-azide **2.15** THF at high dilution conditions of 7 mM — to avoid unwanted polymerisation — a catalytic amount of TBTA and $Cu(CH_3CN)_4.PF_6$ was added. Although ESI-MS analysis of the crude reaction mixture revealed over time the emergence of a m/z signal corresponding to the cyclised product, only a mono-click derivative **2.16** of the same molecular mass as the target macrocycle was isolated after column chromatographic purification (Scheme 2.9, Figure 2.10). Repeated macrocyclization attempts at higher concentrations and heating to 50 ˚C were unsuccessful, likely due to conformational restrictions of cyclisation suggesting that the target macrocycle would have significant ring strain.



Scheme 2.9: *Attempted copper catalysed azide-alkyne macrocyclization*

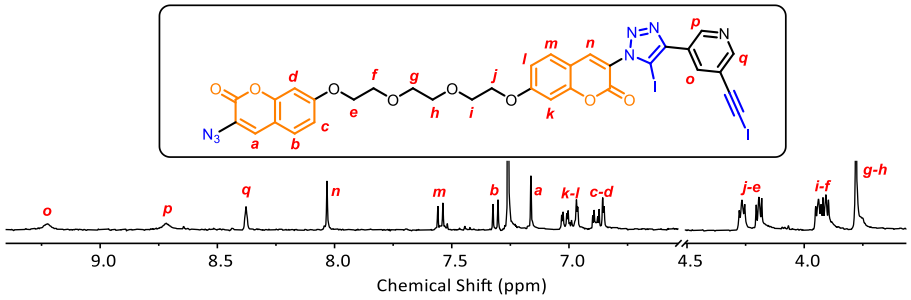
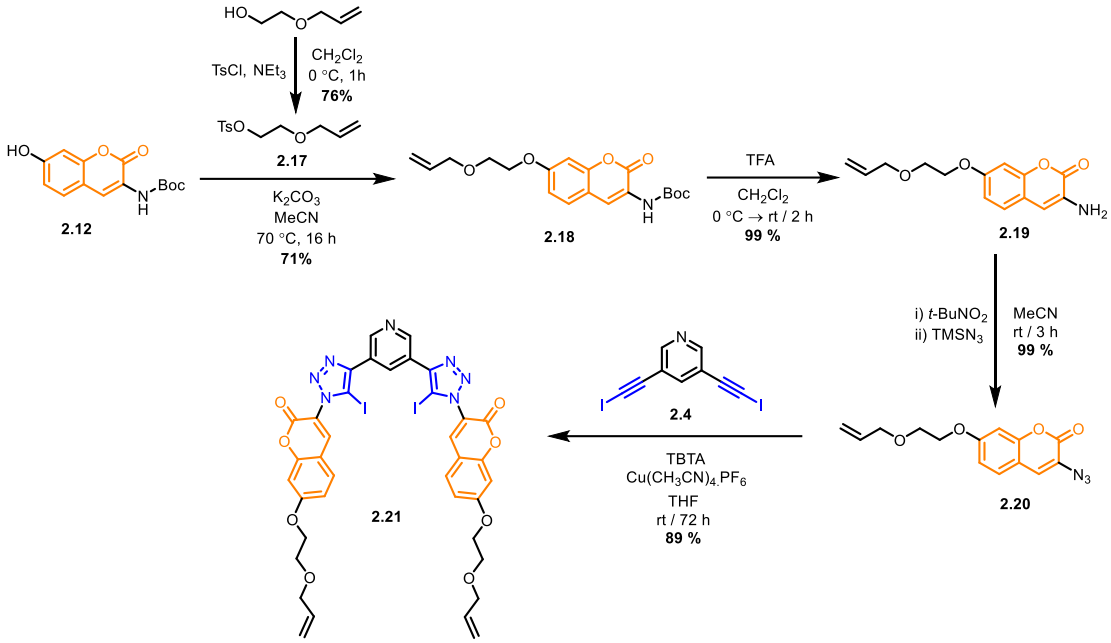


Figure 2.10: *Truncated ^{1}H NMR spectrum of isolated mono-click derivative* ***2.16****; $CDCl_3$, [1 mM], 298 K.*

2.3.1.3. Synthesis of a bis-coumarin-alkene derivative

For the RCM synthetic approach to the target XB coumarin receptor, an appropriate bis-alkene precursor was initially prepared (Scheme 2.10). 2-Allyloxyethanol was reacted with tosyl-chloride in the presence of NEt_3, affording tosylate **2.17** in a 74% yield. Subsequent reaction of tosylate **2.17** with coumarin **2.12** in the presence of K_2CO_3 in dry acetonitrile gave coumarin-alkene **2.18** in an isolated yield of 71%. Boc-coumarin **2.18** was deprotected in quantitative yields by stirring in CH_2Cl_2 with concentrated TFA. Due to the poor solubility of coumarin-amine **2.19** in aqueous solvent media, conversion from the amine to the azide was achieved using an organic solvent procedure reported by Moses *et al.*[14] Coumarin-amine **2.19** was stirred in CH_2Cl_2 before t-$BuNO_2$ and $TMSN_3$ were added in succession, the resultant conversion to azide **2.20** was achieved in quantitative yields. A CuAAC reaction of bis-alkyne

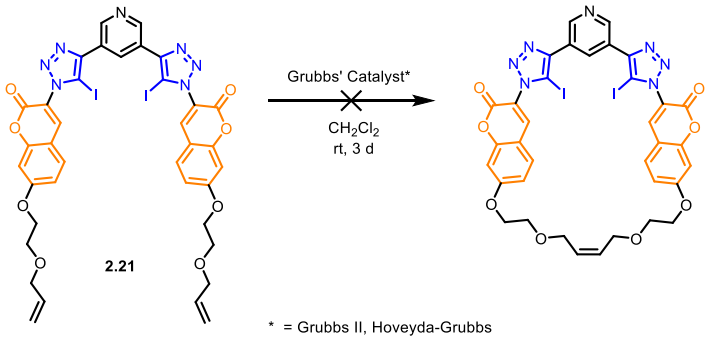
2.4, with two equivalents of azide **2.20**, afforded bis-alkene **2.21** in an 89 % yield (Scheme 2.10).



Scheme 2.10: *Synthesis of bis-alkene* ***2.21***

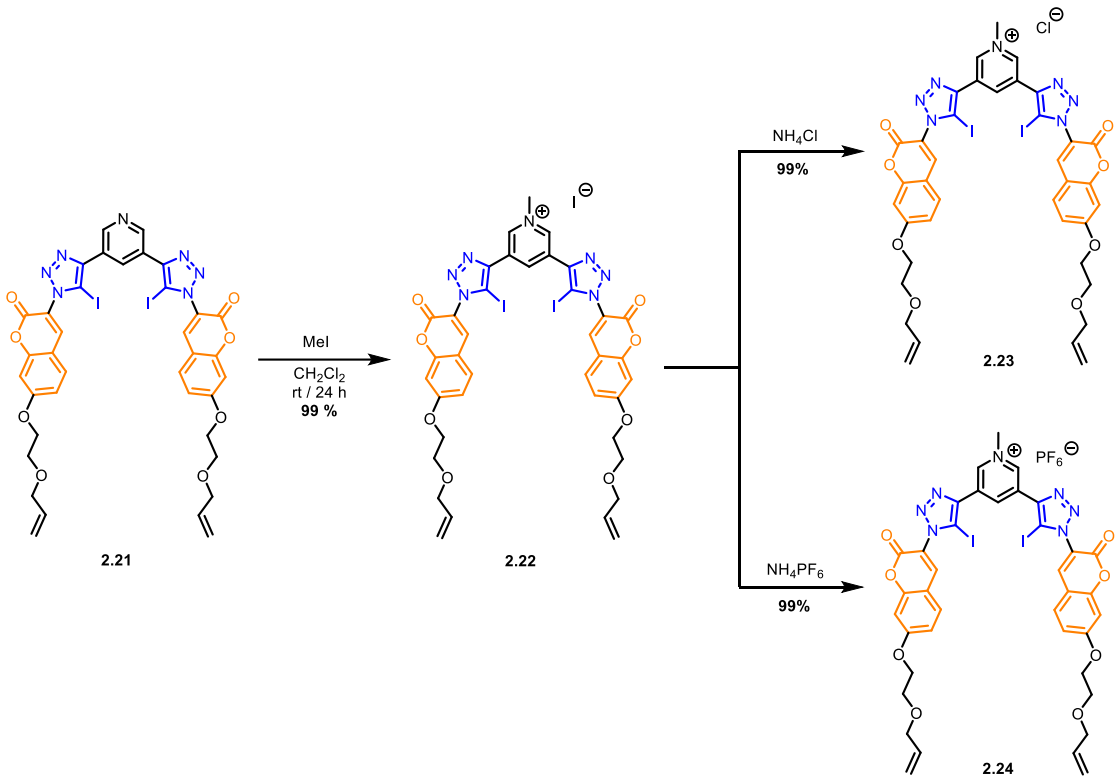
2.3.1.4. Ring-closing metathesis (RCM) reactions

At a high dilution concentration of 7 mM, bis-alkene **2.21** was dissolved in dry CH_2Cl_2 with Grubbs' II and Hoveyda-Grubbs' catalysts (Scheme 2.11). After three days of monitoring by TLC no macrocyclization was observed. This may be a consequence of the pyridyl group of **2.21** inhibiting the reactivity of both catalysts.[15]



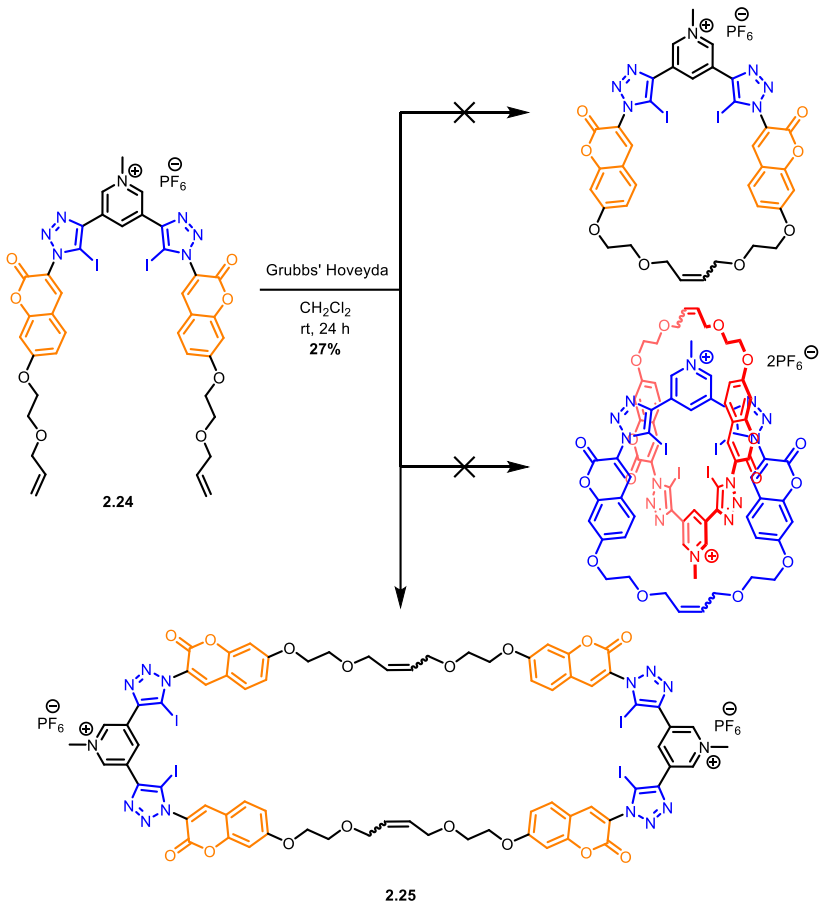
Scheme 2.11: *Attempted RCM of bis-alkene* ***2.21***

To circumvent this, bis-alkene **2.21** was methylated with methyl iodide and exchanged to the chloride salt **2.23** in quantitative yields (Scheme 2.12).



Scheme 2.12: *Methylation and anion exchange of coumarin-bis-alkene*

Bis-alkene pyridinium **2.23** was dissolved in dry CH_2Cl_2 at a concentration of 7 mM. Over a period of 12 hours an equimolar quantity of Hoveyda-Grubbs' catalyst, dissolved in dry CH_2Cl_2, was added. After 24 hours of stirring a product was identified by ES-MS that indicated the formation of a [2+2] macrocycle or [2]catenane, both of which have an identical m/z ration and isotope pattern. However, column chromatographic purification failed to isolate any product, possibly due to the poor solubility of the pyridinium chloride salt **2.23**. To improve solubility in organic media, the iodide salt **2.22** was exchanged to the PF_6^- salt **2.24** in quantitative yields by stirring with NH_4PF_6. Subsequent Hoveyda-Grubbs' catalysed RCM reaction resulted in the isolation of a [2+2] macrocycle or [2]catenane product after preparative thin layer chromatography (PTLC) in a yield of 27%. ^{1}H NMR spectroscopy and HRMS (Figure 2.11) could not elucidate the molecular structure, as both the [2+2] macrocycle and catenane would have similar spectra. By use of tandem mass spectroscopy, the isolated product was identified from the fragmentation patterns as the [2+2] macrocycle (Figure 2.12). The peak at 630.1847 m/z shows a dicationic fragment, suggesting a molecular fragment of around 1260 gmol^{-1}, greater than the mass of a single macrocycle. This type of fragmentation would therefore be impossible for the catenane which would split into its constituent cationic macrocyclic components.



Scheme 2.13: *Synthesis of [2+2] macrocycle* ***2.25***

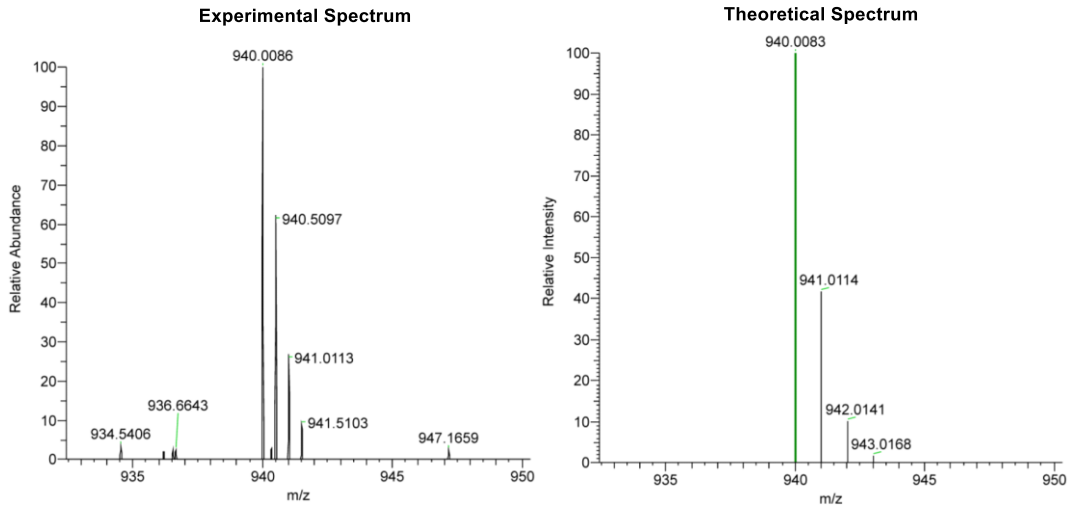


Figure 2.11: *High Resolution Mass spectrometry of [2+2] macrocycle* ***2.25****: experimental and theoretical spectra.*

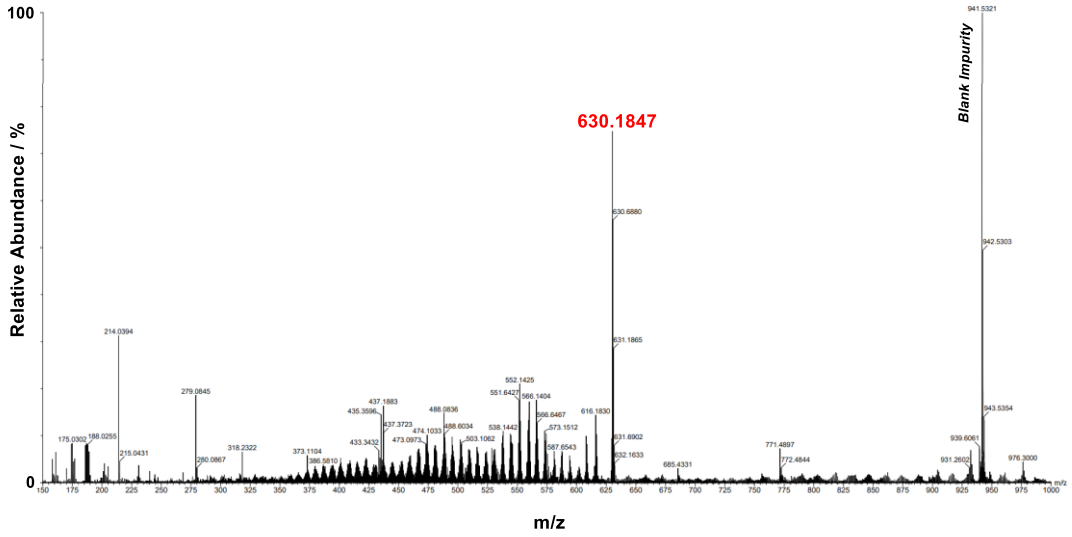


Figure 2.12: *Tandem mass spectrometry (40 V collision energy) of receptor* ***2.25****.*

The synthesis of the large sized [2+2] macrocycle is unexpected and maybe a consequence of poor solubility resulting in its serendipitous precipitation. Interestingly, the macrocycle's ^{1}H NMR spectrum (Figure 2.13) shows the alkene peak *k* as a singlet rather than a mixture of the *cis* and *trans* isomers.

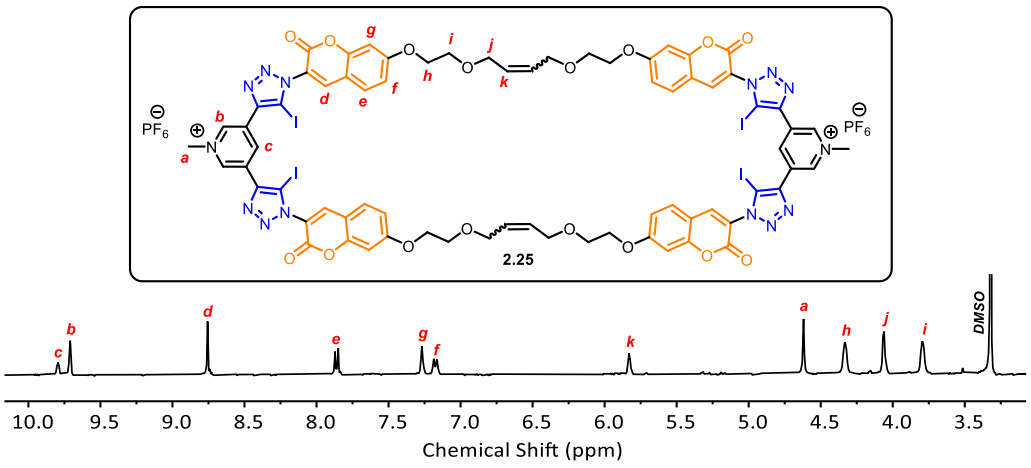


Figure 2.13: *Truncated ^{1}H NMR Spectrum of [2+2] macrocycle* ***2.25*** *with peak assignments; d_6-DMSO, 298 K.*

2.3.2. Anion Binding Studies

Preliminary anion binding studies of [2+2] macrocycle **2.25** were investigated with TBACl using ^{1}H NMR and fluorescence spectroscopy.

2.3.2.1. ^{1}H NMR titrations

Owing to the poor solubility of macrocycle **2.25** in common organic solvents, the ^{1}H NMR titration experiments were conducted in d_6-DMSO at a low concentration of 0.5 mM. On titrating with TBACl, downfield perturbations of the internal pyridinium proton *b* were observed (Figure 2.14).

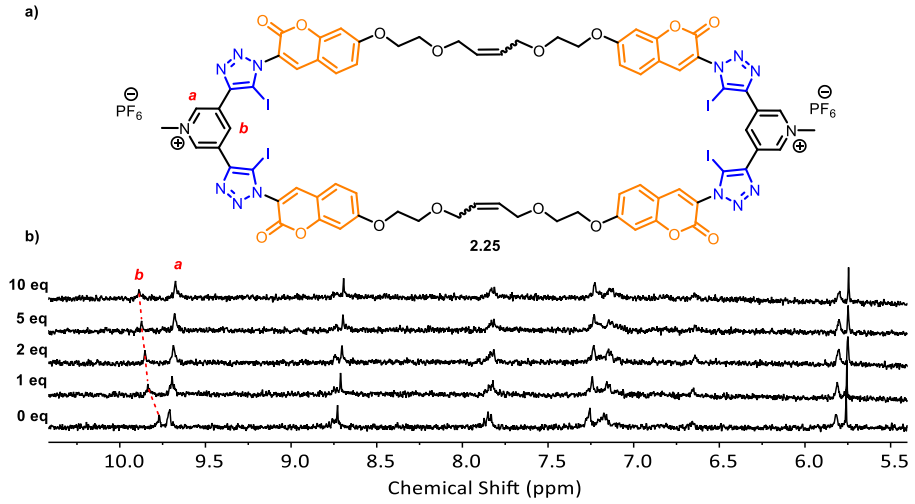


Figure 2.14: *Truncated ^{1}H NMR titration spectra of receptor **2.25** upon addition of 0-10 equivalents of TBACl in d_6-DMSO; ([host] = 0.5 mM, T = 298 K). **a)** Receptor **2.25** with proton labels **b)** ^{1}H NMR titration spectra showing downfield perturbations of proton b.*

Bindfit[9,10] analysis of the binding isotherm titration data monitoring the pyridinium proton *b* was used to determine the 1:2 host-guest stoichiometric association constant (Figure 2.15, Table 2.4). With two separate pyridinium iodotriazole binding sites, the binding of chloride in a 1:2 stoichiometry is expected. Predictably on statistical grounds and electrostatic considerations, K_1 is significantly larger in magnitude than K_2 (Table 2.4).

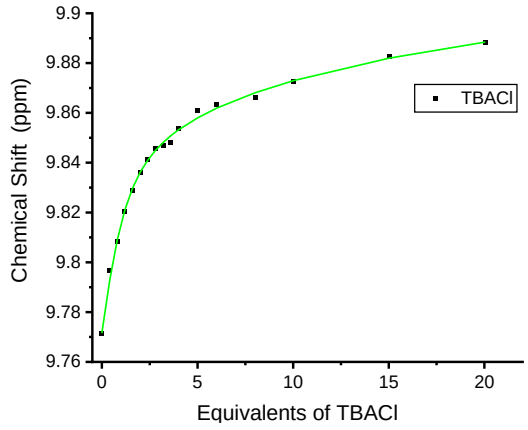


Figure 2.15: *Chloride anion binding isotherm for macrocyclic receptor* ***2.25****; circles represent experimental data and solid lines represent fitted data.*

Table 2.4: *^{1}H NMR anion association constants for [2+2] macrocycle* ***2.25***

Anion	k_{11} (M^{-1})	k_{12} (M^{-1})
Cl^-	4600 ± 550	100 ± 10

Anion association constants with errors determined using 1:2 stoichiometric Bindfit analysis of the ^{1}H NMR titration data of receptor **2.25** monitoring the internal pyridinium peak; 0.5 mM receptor in d_6-DMSO, 298 K.

2.3.2.2. Fluorescence Titrations

The photophysical properties of receptor **2.25** were investigated using UV-visible absorption and fluorescence spectroscopy (Figure 2.16). Characteristic energies of absorption and emission bands for coumarin were observed in CH_3CN (Table 2.5).[1]

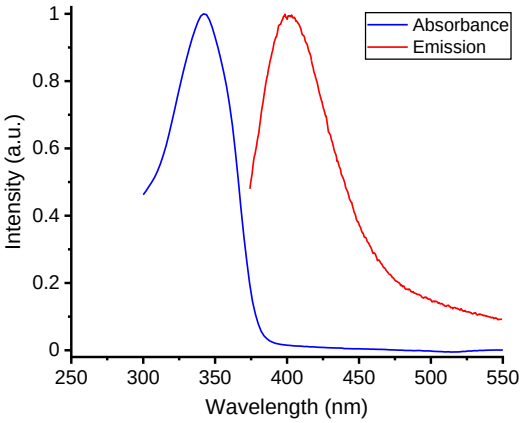


Figure 2.16: *Normalised emission and absorbance spectra for [2+2] macrocycle* ***2.25*** *in CH_3CN*

Table 2.5: *Energies of absorption and emission for receptor* ***2.25*** *in MeCN.*

Absorbance λ_{max} / nm	Emission λ_{max} / nm	Stokes Shift / nm
342	402	60

Emission wavelength excited at $\lambda_{max\ abs}$, CH_3CN, [10 µM], 298 K.

Quantitative fluorescence titration experiments (λ_{ex} = 342 nm) were conducted in CH_3CN to probe the anion binding behaviour of receptor **2.25**. On addition of TBACl, TBABr and TBAI a significant increase in fluorescence intensity was observed (Figure 2.17). This increase was most acute on the addition of TBACl, which saw an increase of up to 125%, whilst TBABr and TBAI induced an increase of around 50–60%.

Bindfit [9,10] was used to determine the association constants (Figure 2.17d, Table 2.6). Unlike the chloride ^{1}H NMR titration result, a 1:1 host-guest stoichiometric binding model was found to give the best fit of titration data, albeit with relatively large errors with the heavier halides. Table 2.6 shows Br^- is bound the strongest followed by I^- and then Cl^-. This may be due to preferred size complementarity of Br^- within the macrocyclic cavity.

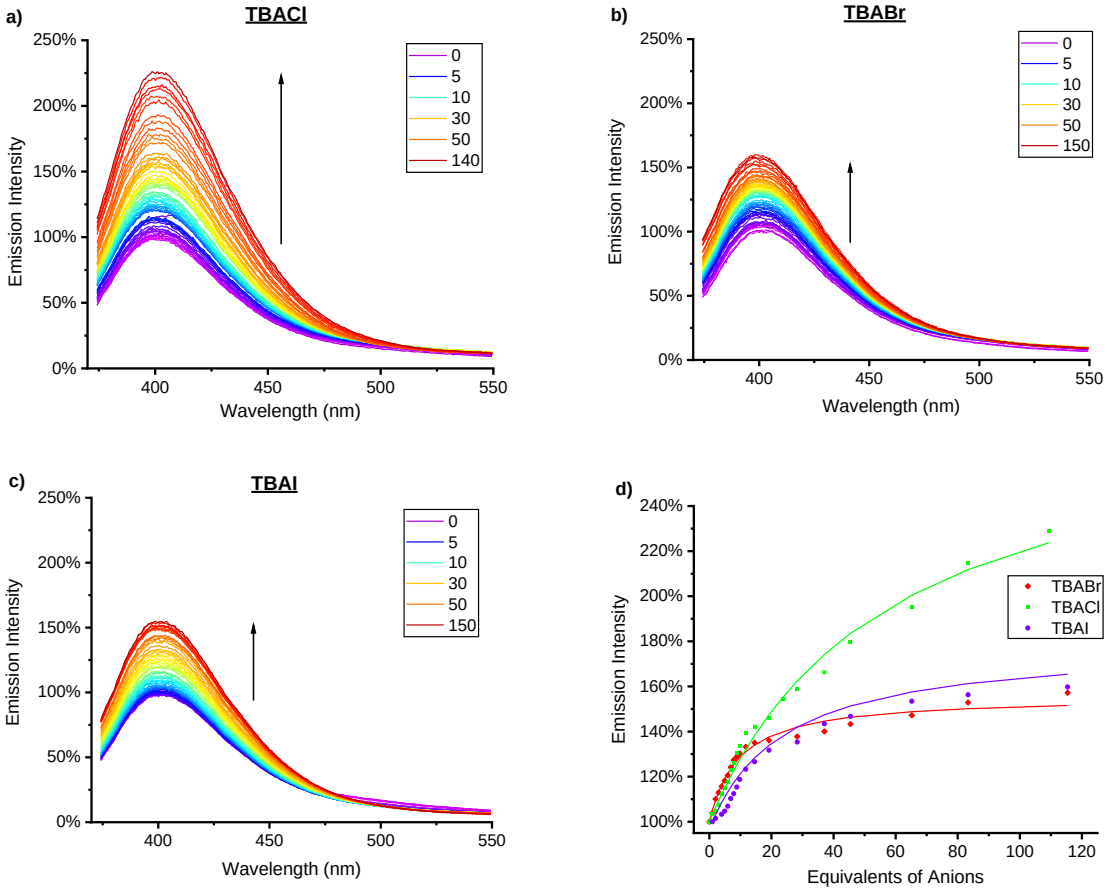


Figure 2.17: *Fluorescence emission intensity changes of receptor 2.25 upon addition of* ***a)*** *TBACl* ***b)*** *TBABr,* ***c)*** *TBAI.* ***e)*** *Binding isotherms and Bindfit analysis of fluorescence maxima change on addition of anions. ([host] = 10 µM, CH_3CN, T = 298 K).*

Table 2.6: *Receptor* ***2.25,*** *halide anion association constants*

Anion	k_{11} (M^{-1})
Cl^-	1800 ± 100
Br^-	11300 ± 1300
I^-	4400 ± 300

Anion association constants with errors determined using 1:1 stoichiometric Bindfit analysis of the fluorescence titration data of receptor **2.25** monitoring the change in emission maxima intensity; 10 μM receptor in CH_3CN, 298 K.

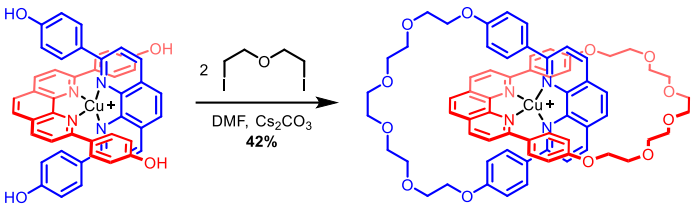
2.3.3. Summary

Two macrocyclization synthetic strategies were explored in the preparation of a target XB coumarin macrocycle. Attempts using CuAAC reactions failed to produce a macrocycle. However, RCM macrocyclization afforded an unexpected [2+2] macrocycle **2.25** capable of binding and sensing halide anions, with selectivity for bromide, via significant enhancements of the macrocycle's coumarins' fluorescence.

2.4. Rotaxane Coumarin Receptors

Rotaxanes are mechanically interlocked molecules whose three-dimensional cavities can be designed to encapsulate charged guest species. In particular, rotaxane and catenane host systems for anions have been demonstrated to exhibit far superior levels of recognition compared to non-interlocked macrocyclic and acyclic receptors due to their ability encapsulate guests and bind with multivalent recognition sites (*see 1.2.4.6. Mechanically Interlocked Hosts*).[16,17]

The construction of rotaxanes and other MIMs requires a template to direct the assembly of precursor components. Cation, anion and neutral template species have all been successfully used for MIM formation.[18,19] Jean-Pierre Sauvage, one of the pioneers in the field, exploited the tetrahedral coordination preference of a Cu(I) template to arrange phenanthroline moieties in an orthogonal fashion for a double cyclisation reaction to produce a [2]catenane (Scheme 2.14).[20]



Scheme 2.14: *Sauvage's copper templated catenation.*

For rotaxane synthesis, the two main exploited methods are 'clipping' and 'stoppering' (Figure 2.18). Stoppering requires the template driven formation of a pseudorotaxane assembly, in which the axle precursor component is threaded through the macrocycle before the bulky stopper groups are appended on either side of the axle thereby preventing dethreading. Clipping involves the template formation of a macrocyclic precursor around an axle component, before a macrocyclization reaction interlocks the components.

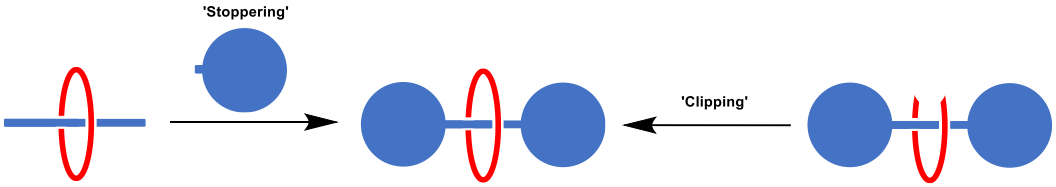
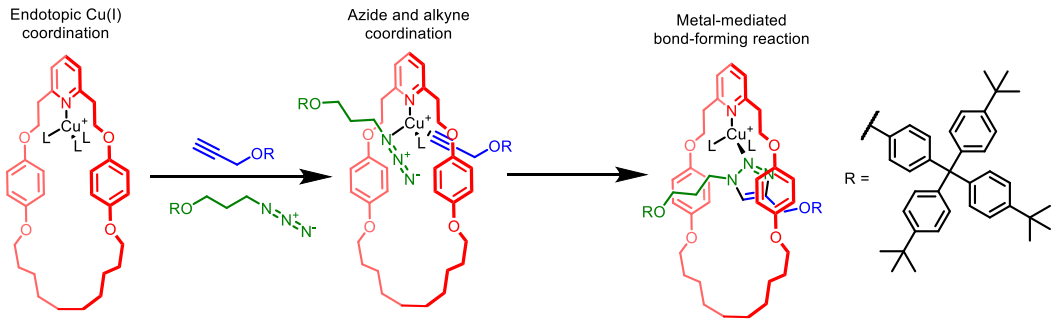


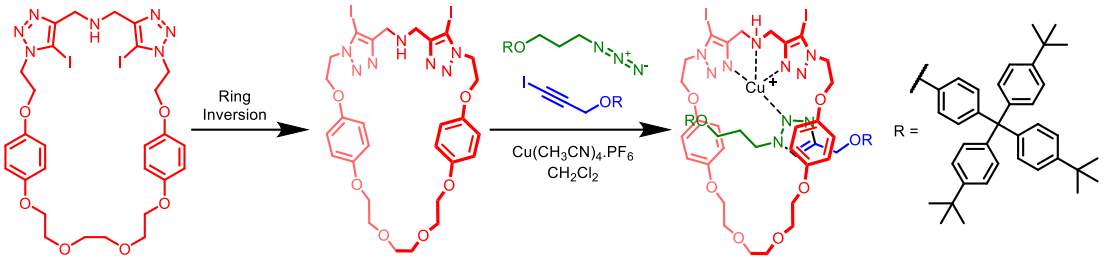
Figure 2.18: *Rotaxane synthesis: Stoppering and Clipping*

Recently, a new method for rotaxane and catenane synthesis has been developed that exploits the catalytic properties of a metal template. Active metal templation (AMT) differs from passive metal templation as the metal used acts as both a catalyst for mechanical bond formation as well as a template.[21] Leigh and co-workers introduced this efficient technique via a CuAAC AMT synthesis of a [2]rotaxane (Scheme 2.15).[22] By chelating the Cu(I) catalyst in an endotopic fashion to a pyridyl containing macrocycle, the metal coordinates alkyne and azide axle precursors in such a way as to favour the CuAAC bond-forming reaction to occur through the cavity of the macrocycle, thereby forming a rotaxane.



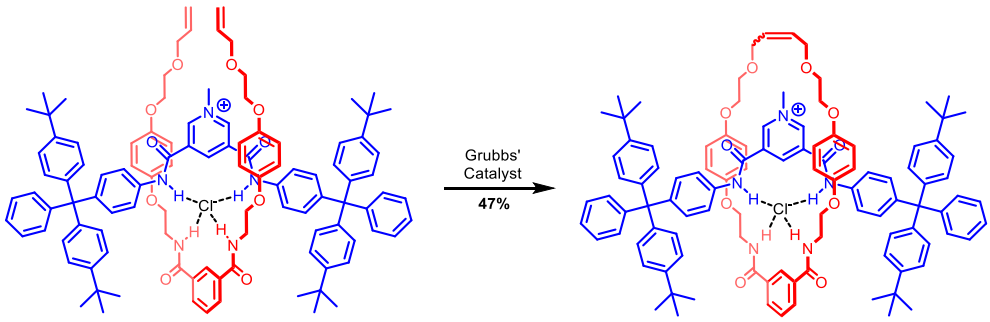
Scheme 2.15: *Leigh's CuAAC AMT rotaxanation.*

Later, Beer and co-workers developed a XB macrocycle that could act both as an anion receptor and, when inverted, could coordinate to copper(I) to undergo AMT rotaxane synthesis (Scheme 2.16).[23]



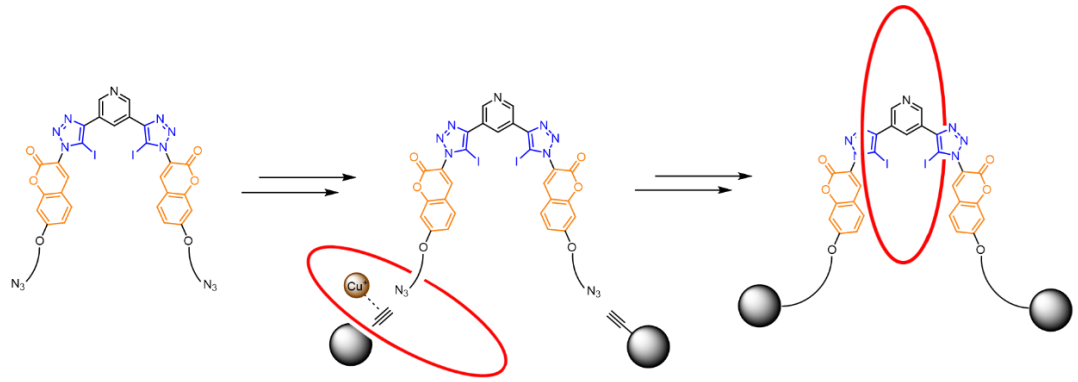
Scheme 2.16: *Beer's inverted anion binding macrocycle capable of CuAAC AMT rotaxanation.*

Beer was also a pioneer in the use of anion-templation methods for the construction of interlocked molecules.[17,24] In the seminal example, a chloride anion template counter-anion of a pyridinium containing axle assembled the macrocyclic precursor around the axle, before a Grubbs' catalysed RCM clipping reaction produced the [2]rotaxane (Scheme 2.17).[25]

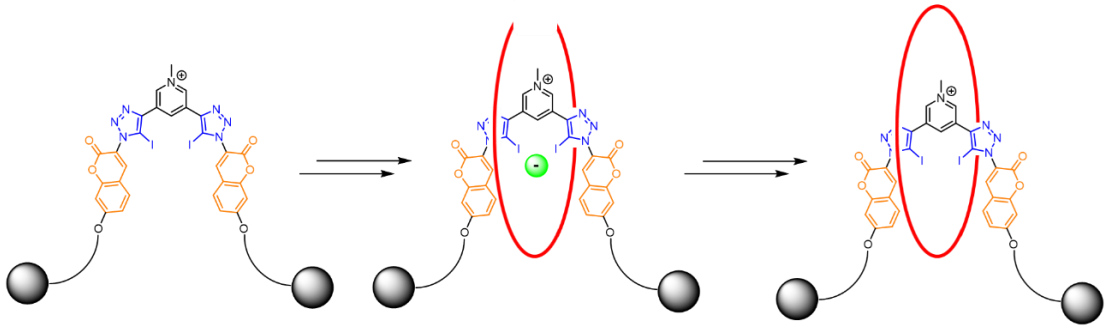


Scheme 2.17: *Beer's chloride templated RCM rotaxanation.*

The objective of this section was to investigate the synthesis of a novel XB rotaxane that contains a coumarin functionalised bis-iodotriazole axle and an anion binding macrocycle component. To achieve this, two synthetic methods were explored. A CuAAC AMT approach utilising a neutral bis-iodotriazole pyridyl axle precursor functionalised with azides (Scheme 2.18), and an anion template strategy using a clipping RCM rotaxanation (Scheme 2.19). Synthetic procedures and characterisation of molecules in the synthesis of neutral rotaxane **2.32** were undertaken by Part II student Adam Beecroft.



Scheme 2.18: *AMT synthesis of target rotaxane*

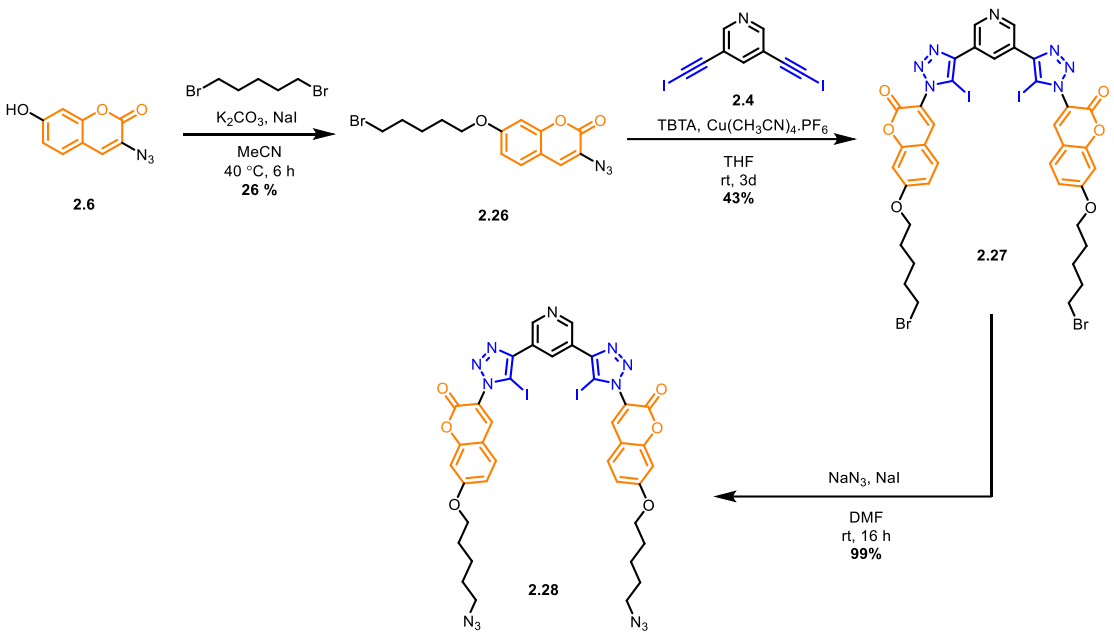


Scheme 2.19: *Anion templated clipping synthesis of target rotaxane.*

2.4.1. Synthesis

2.4.1.1. Synthesis of bis azide axle precursor

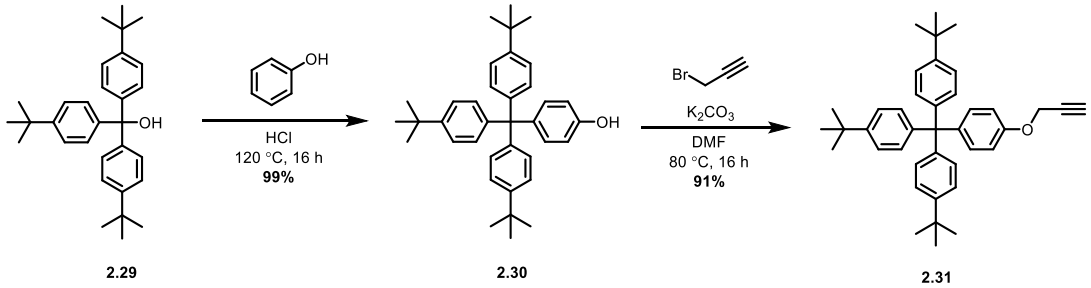
Azide functionalised coumarin **2.6** was reacted with excess 1,5 dibromopentane under basic conditions in acetonitrile to afford, after column chromatographic purification, azide **2.26** in a low yield of 26%. Again, the reactions on the phenolic group of coumarin azide **2.6** proved more challenging than with the Boc protected coumarin **2.12**, giving low yields and complex mixtures of products due to decomposition. Two equivalents of bromo-functionalised coumarin azide **2.26** were reacted with one equivalent of pyridine bis-iodoalkyne **2.4** under CuAAC reaction conditions in THF to give the bis-iodotriazole derivative **2.27** in a 43% yield. Quantitative conversion to the bis-azide axle precursor **2.28** was achieved by stirring with NaN_3 in DMF with no further purification required (Scheme 2.20)



Scheme 2.20: *Synthesis of bis azide axle precursor* ***2.28****.*

2.4.1.3. Stopper synthesis

Terphenyl stopper precursors, **2.30** and **2.31** were synthesised following literature procedures reported by Gibson and co-workers[26] and Leigh and co-workers[27] respectively (Scheme 2.21). Alcohol stopper precursor (*provided by Dr Jane Liew*) **2.29** was reacted with excess phenol in concentrated HCl at 120 ˚C. After 16 h, phenol-stopper **2.30** was isolated by filtration in a quantitative yield. Subsequent S_N2 reaction of **2.30** with propargyl bromide in the presence of K_2CO_3 afforded stopper-alkyne **2.31** in a yield of 91%.

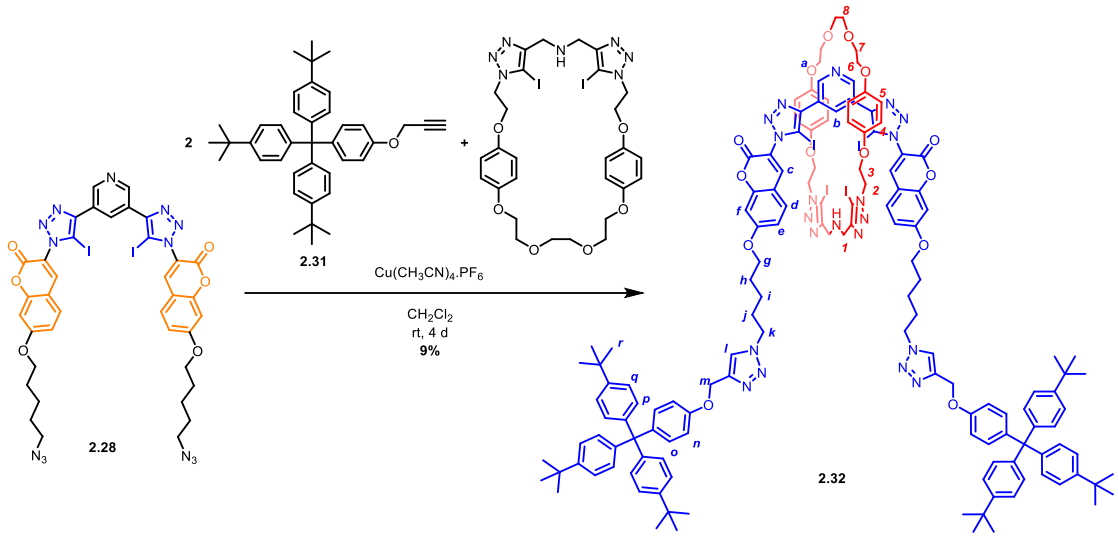


Scheme 2.21: *Synthesis of stopper alkyne* ***2.31***

2.4.1.3. Active metal templation rotaxane synthesis

One equivalent of the XB macrocycle (*provided by Dr Jessica Pancholi*) was stirred in dry CH_2Cl_2 with one equivalent of $Cu(CH_3CN)_4.PF_6$ to achieve endotopic coordination. Six equivalents of stopper alkyne **2.31** and six equivalents of bis azide **2.28** were dissolved in dry CH_2Cl_2 and

added to the reaction mixture. The reaction was left to stir under an inert N_2 atmosphere over 4 days. Purification was achieved using preparative TLC (eluent 5% MeOH in CH_2Cl_2) and rotaxane **2.32** was isolated in a yield of 9%. The poor yield was attributed to difficulties in thin layer chromatographic purification, a significant portion of the axle by-product was also isolated.



Scheme 2.22: *AMT synthesis of rotaxane* ***2.32***

2.4.1.4. Rotaxane 2.32 characterisation

The novel rotaxane **2.32** was characterised by ^{1}H NMR, ^{13}C NMR, ^{1}H-^{1}H ROESY NMR and HRMS. A comparison between the ^{1}H NMR spectra of rotaxane **2.32,** the free axle and the macrocycle (Figure 2.19) provides evidence for formation of the interlocked structure. The rotaxane ^{1}H NMR spectrum reveals significant downfield shifts in the pyridine (*a*, *b*) and coumarin proton peaks (*c*, *d*) of the axle component, the macrocycle component hydroquinone protons (4, 5) move downfield and merge, an indicative sign of rotaxanation reported for this macrocyclic system.[23]

Two dimensional ^{1}H-^{1}H ROESY NMR experiments provided further evidence for the formation of rotaxane **2.32** (Figure 2.20). Through-space interactions were observed between the macrocycle component protons and axle protons; cross peaks between the hydroquinone of the macrocycle and the coumarin peaks of the axle provide evidence for their close proximity and interlocked nature.

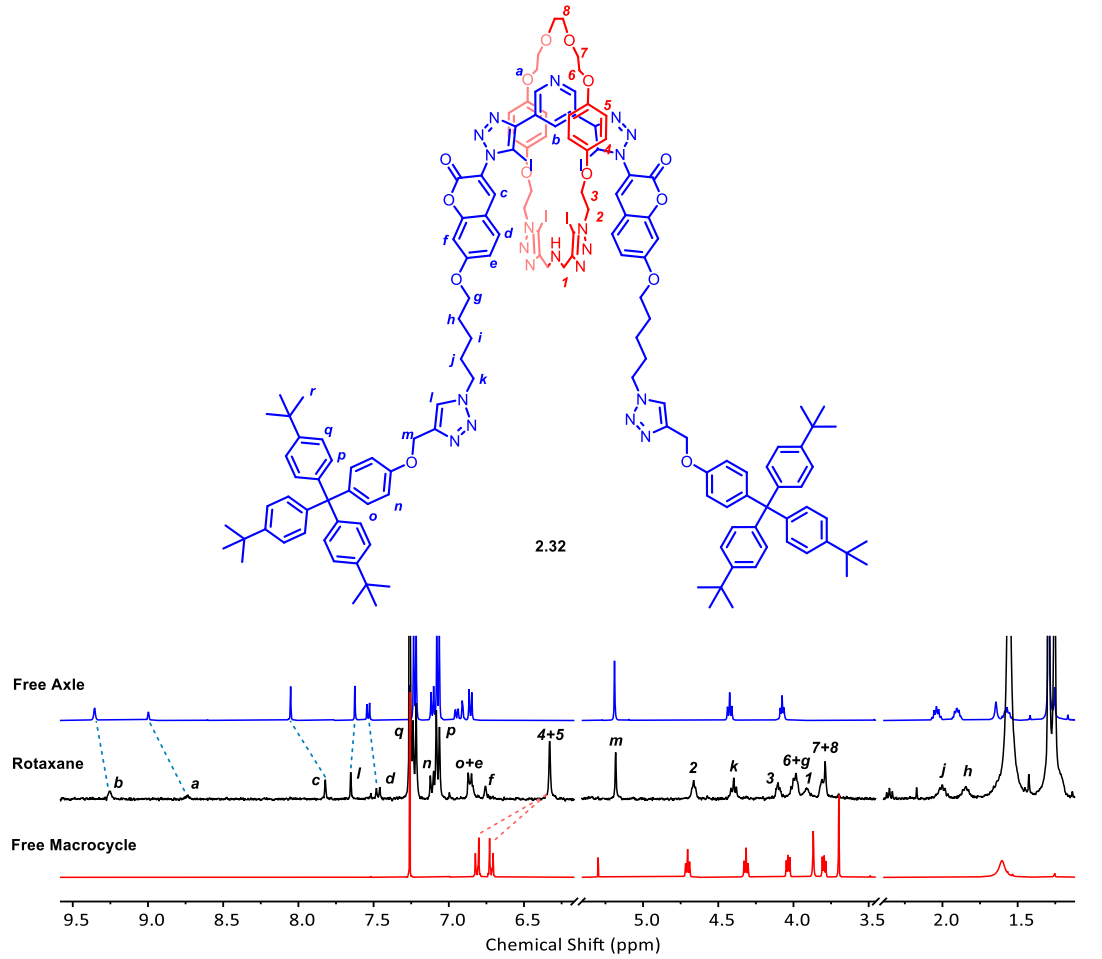


Figure 2.19: *Truncated ^{1}H NMR spectra comparison in $CDCl_3$ between rotaxane* ***2.32****, the free axle and macrocycle.*

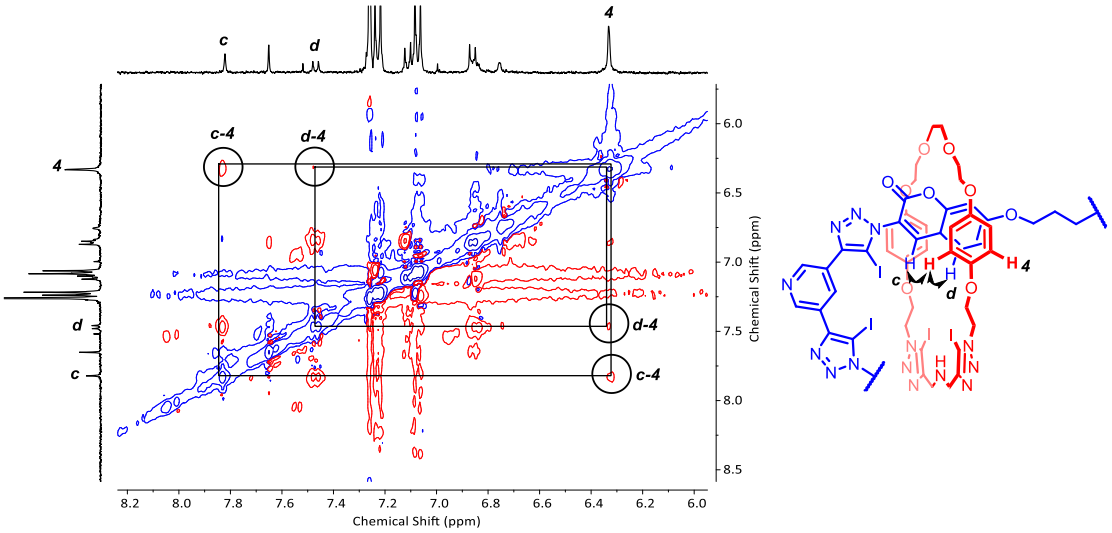


Figure 2.20: *Truncated ^{1}H-^{1}H ROESY NMR of rotaxane 2.32 in $CDCl_3$, highlighting through-space interactions.*

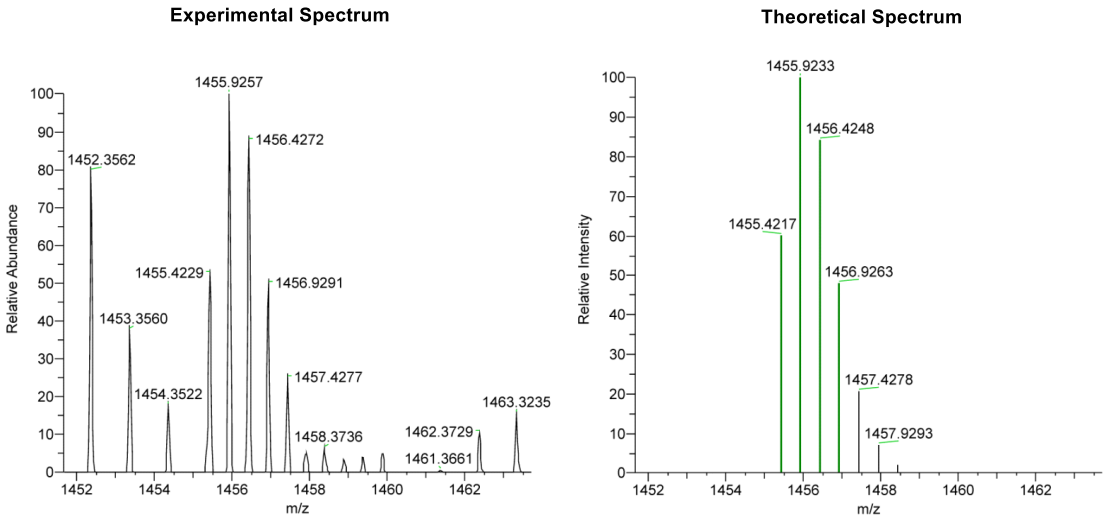


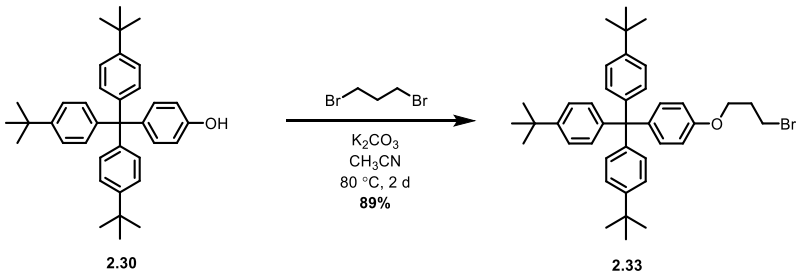
Figure 2.21: *High Resolution Mass spectrometry of rotaxane* ***2.32****: experimental and theoretical spectra; (ESI +ve) m/z=1455.9257 ([M + 2H]$^{2+}$, $C_{145}H_{156}N_{20}O_{14}I_4$, calc=1455.9233)*

Additional evidence for the rotaxanation was provided by HRMS (Figure 2.21), where the dicationic $[M+2H]^{2+}$ rotaxane species was observed.

Due to lack of material and time constraints, anion binding titration studies of rotaxane **2.32** were not undertaken.

2.4.1.5. Synthesis of stopper bromide

Bromo propyl stopper **2.33** was synthesised following a literature procedure reported by Li and co-workers (Scheme 2.23).[28] An excess of 1,3-dibromopropane was added to a solution of phenol stopper **2.30** in the presence of K_2CO_3 and heated to reflux over 2 days in CH_3CN. After an aqueous wash **2.33** was isolated in 89% yield.

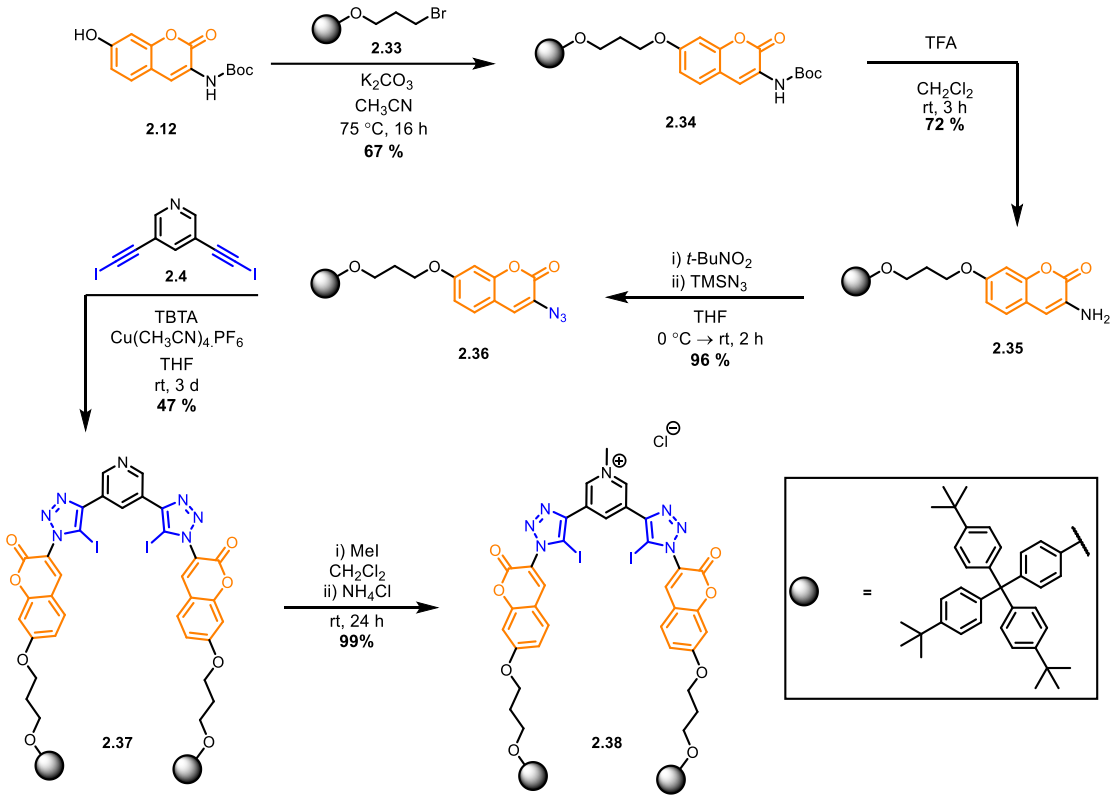


Scheme 2.23: *Synthesis of stopper bromine* ***2.33****.*

2.4.1.6. Synthesis of pyridinium axle

Boc-coumarin **2.12** was reacted with bromo propyl stopper **2.33** in a Williams-ether synthesis affording coumarin stopper **2.34** in a yield of 67%. Boc deprotection of **2.34** to amine **2.35** was

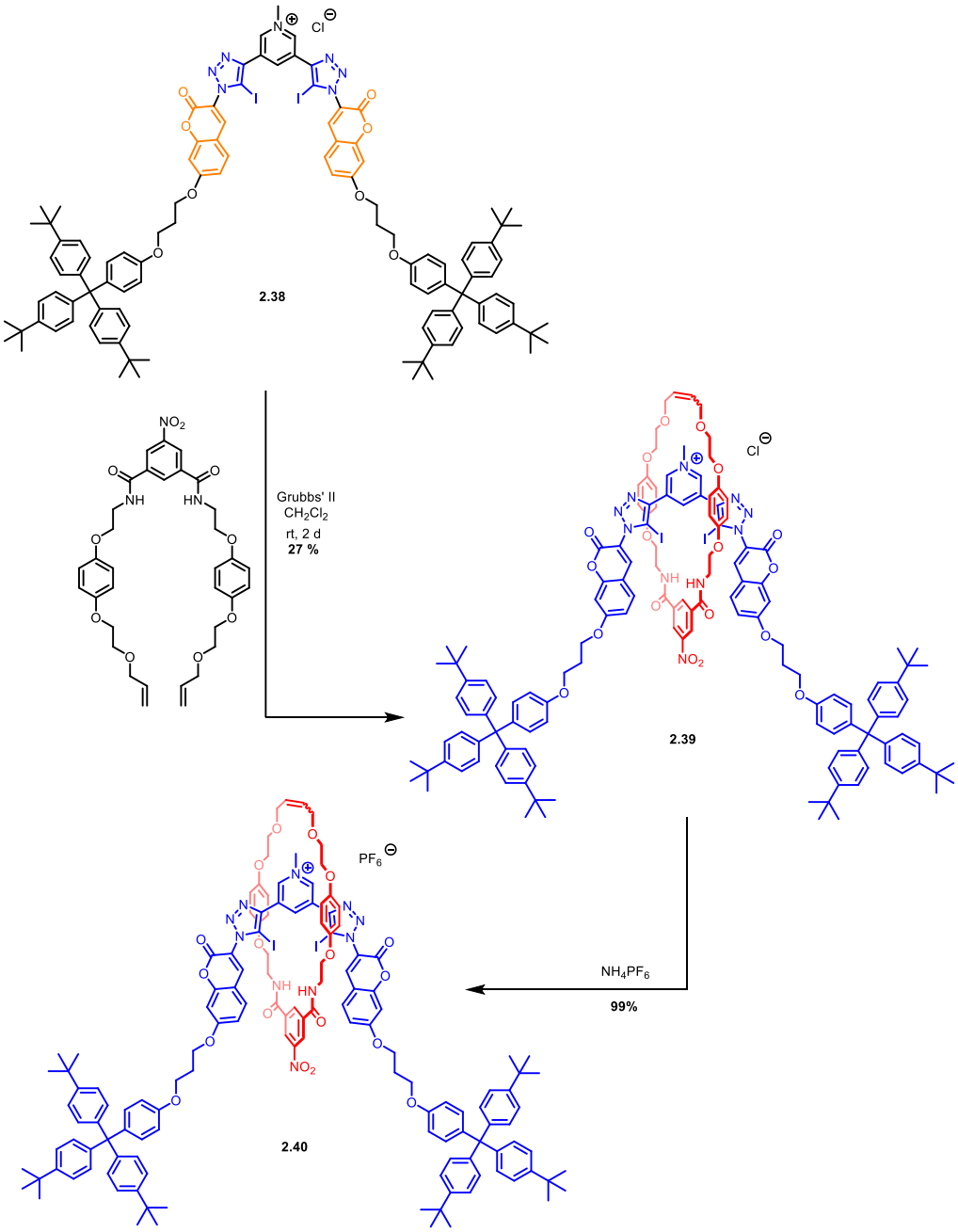
achieved in a 72% yield by stirring in concentrated TFA. At 0 °C, *t*-BuNO$_2$ and TMSN$_3$ were added to a solution of **2.35** in dry THF for a sequential diazotisation and azide substitution step, producing azide **2.36** in a high yield of 96%. Two equivalents of coumarin azide **2.36** were reacted with bis-iodo-alkyne **2.4** in a CuAAC reaction. After stirring for 3 days, coumarin axle **2.37** was isolated in a yield of 47% (Scheme 2.24). Subsequent methylation, by use of methyl iodide, and anion exchange, to the chloride salt, afforded coumarin-axle **2.38** in quantitative yields.



Scheme 2.24: *Synthesis of coumarin-axle* ***2.38****.*

2.4.1.7. Chloride templated ring-closing-metathesis rotaxanation

Methylated axle **2.38** and macrocyclic precursor bis-alkene (*provided by Dr. Harry Klein*) were dissolved in dry degassed CH_2Cl_2 and stirred for 1 h before Grubbs' II catalyst was added. After stirring for 2 days the mixture was purified by PTLC to afford rotaxane **2.39** as a yellow solid in a 27% yield (Scheme 2.25). Rotaxane **2.39** was washed with aqueous NH_4PF_6 and extracted with CH_2Cl_2 to give quantitative yields of rotaxane **2.40** as a yellow powder.



Scheme 2.25: *Chloride templated RCM synthesis of rotaxane* ***2.39*** *and subsequent anion exchange to rotaxane* ***2.40****.*

2.4.1.8. Rotaxane 2.40 characterisation

Rotaxanes **2.39** and **2.40** were fully characterised by ^{1}H NMR, ^{13}C NMR, and HRMS. Due to poor solubility, NMR analysis of rotaxane **2.40** was conducted in 6:4 $CDCl_3$:d_4-MeOD. A comparison of the ^{1}H NMR spectra of rotaxane **2.40**, free axle **2.38**, and the macrocycle provides evidence for the formation of the interlocked structure (Figure 2.22).

The rotaxane ^{1}H NMR spectrum reveals upfield shifts for the axle coumarin peaks *d* and *e* and pyridinium proton signal *b* and *c*, suggesting interaction with the electron rich hydroquinone groups of the macrocycle component. Similarly, hydroquinone peaks *6* and *7* de-symmetrise and move upfield, reflecting the new distinct environments they occupy in the rotaxane.

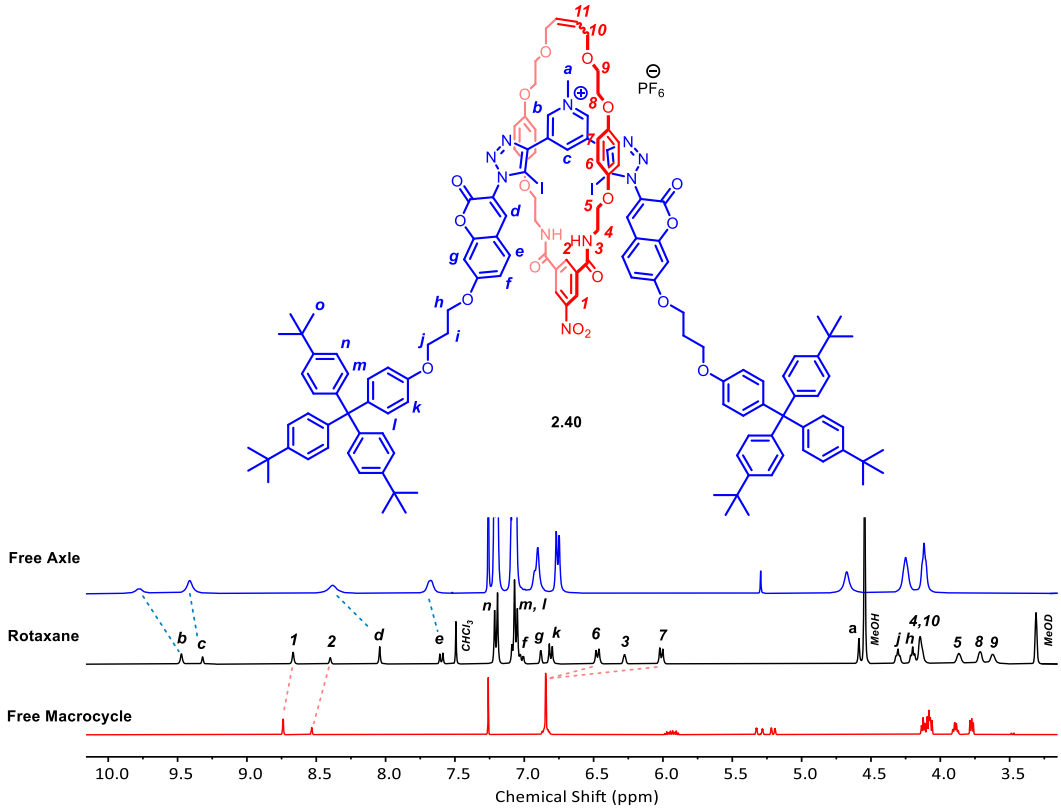


Figure 2.22: *Truncated ^{1}H NMR spectral comparison between rotaxane* ***2.40*** *(6:4 $CDCl_3$:d_4-MeOD), free axle* ***2.38*** *($CDCl_3$) and the macrocycle ($CDCl_3$).*

^{1}H-^{1}H ROESY NMR experiments of rotaxane **2.40** provided further evidence for the formation of the interlocked structure. This can be observed by the through-space interaction between the macrocycle hydroquinone proton *6* and the axle coumarin proton *d* (Figure 2.23), highlighting their interlocked nature.

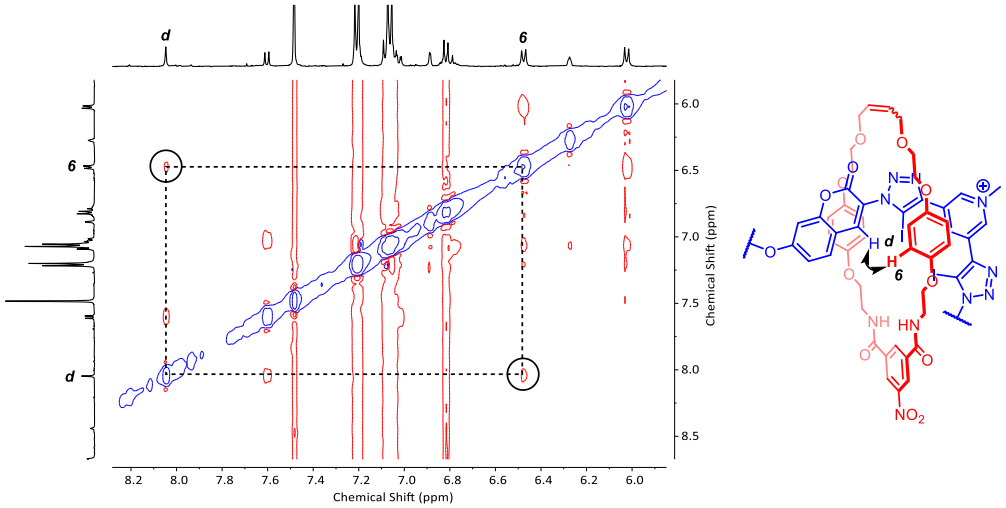


Figure 2.23: *Truncated ^{1}H-^{1}H ROESY NMR of rotaxane* ***2.40*** *in 6:4 $CDCl_3$:d_4-MeOD, highlighting through-space interaction between coumarin peak d and macrocycle hydroquinone peak 6.*

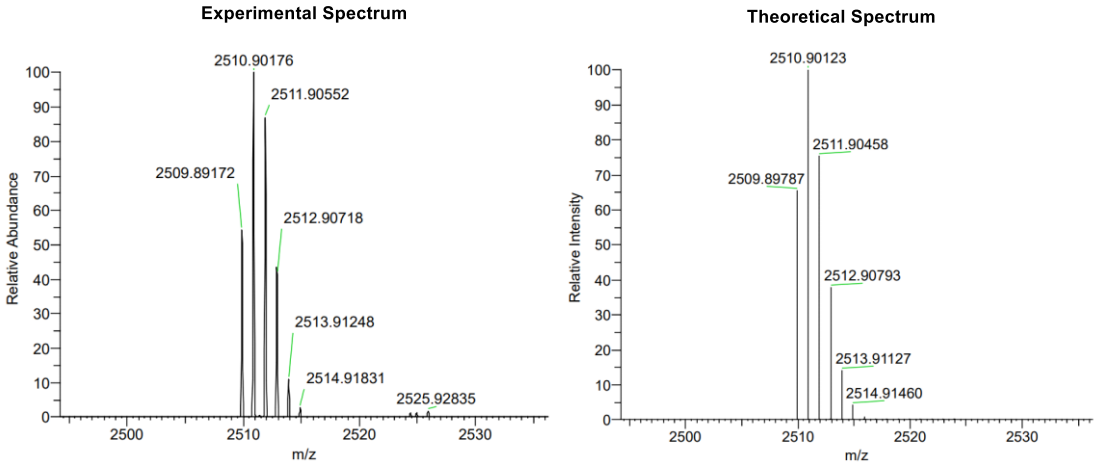


Figure 2.24: *High Resolution Mass spectrometry of rotaxane* ***2.39****: experimental and theoretical spectra HRMS (ESI +ve) m/z= 2509.89160 ($[M - Cl^-]^+$, $C_{140}H_{147}O_{18}N_{10}{}^{127}I_2$, calc= 2509.89787).*

Additional evidence for the rotaxanation was provided by HRMS (Figure 2.24), in which the rotaxane was observed as the $[M]^+$ species.

2.4.2. Anion Binding Studies

2.4.2.1 Fluorescence Titrations

The photophysical characteristics of rotaxane receptor **2.40** were investigated by UV/Vis and fluorescence spectroscopy. Characteristic energies of absorption and emission for the

coumarin chromophore were observed in the 45/45/10 $CHCl_3$/MeOH/H_2O solvent mixture (Figure 2.25, Table 2.27).[1]

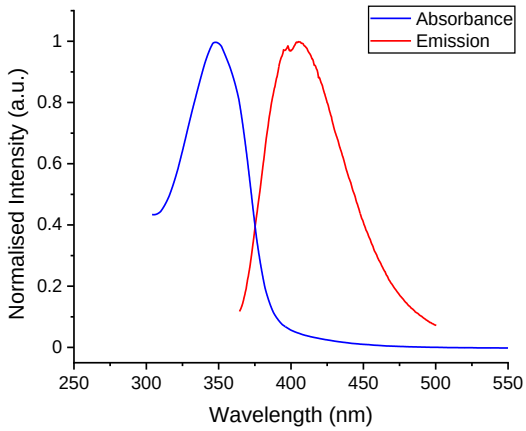


Figure 2.25: *Normalised emission and absorbance spectra for rotaxane* ***2.40.***

Table 2.7: *Energies of absorption and emission for rotaxane* ***2.40*** *in 45/45/10 $CHCl_3$/MeOH/H_2O.*

Absorbance λ_{max} / nm	Emission λ_{max} / nm	Stokes Shift / nm
348	407	59

Emission wavelength excited at $\lambda_{max\ abs}$, [10 μM], 298 K.

The anion binding behaviour of rotaxane receptor **2.40** was probed by fluorescence spectroscopy titration experiments in 45/45/10 $CHCl_3$/MeOH/H_2O. Fluorescence titrations (λ_{ex} = 348 nm) were performed by the addition of NaCl, NaBr, NaI and NaHS. Upon addition of the salts an increase in coumarin fluorescence intensity was observed in all cases. This was greatest for Br^- which induced an increase of 25%, whereas an increase of 20% and 15% were observed for I^- and HS^- respectively (Figure 2.26). As with receptors **2.9** and **2.25** the observed emission intensity increase was attributed to a rigidification of the rotaxane receptor upon anion binding, thereby restricting non-radiative methods of quenching such as vibration and rotation. Notably, on addition of Cl^- the emission intensity initially increased by 10% and then dropped by a further 5% up to 180 equivalents. A similar relationship was observed for acyclic receptor **2.9**, which was found to bind in a 1:2 host:guest stoichiometric ratio. An X-ray crystal structure reported by Beer and co-workers of a rotaxane system using the same macrocyclic component (Scheme 2.17),[25] showed that the cavity is too small to accommodate two anions — suggesting that the second binding event most likely associates on the periphery of the interlocked host. Interestingly and uniquely, on addition of HS^- a red shift in the emission was observed, with the maxima moving from 406 nm to 408 nm. This may be a result of a different binding conformation that accommodates the hydrogen of HS^-.

Nonlinear regression analysis of the fluorescence titration data using Bindfit v0.5 software was used to determine the 1:1 stoichiometric host-guest association constants for Br^-, I^- and

HS^- and the 1:2 stoichiometry host-guest association constants for Cl^- (Table 2.8). Rotaxane **2.40** exhibits a preference for the halides over HS^- which is bound the weakest. Taking into account the relatively large errors, amongst the halides, there is little discrimination between iodide and chloride which are both bound more strongly than bromide.

Surprisingly, the association constant magnitudes are similar to those calculated for acyclic receptor **2.9** (Table 2.3). The enhanced anion recognition properties of rotaxane host systems are well established, which indicates the quantitative anion binding data determined by fluorescence spectroscopy should be treated with caution. Nonetheless, qualitatively, rotaxane **2.40** was able to sense via fluorescence the halides and importantly HS^-.

Table 2.8: *Fluorescence titration anion association constants of receptor* ***2.9***

Anion	K_{11} (M^{-1})	K_{12} (M^{-1})
Cl^-	12500 (1700)	82 (8)
Br^-	10100 (1100)	n/a
I^-	13900 (1700)	n/a
HS^-	7800 (900)	n/a

Anion association constants with errors determined using 1:2 stoichiometric Bindfit analysis of the fluorescence titration data of receptor **2.9** monitoring the change in emission maxima intensity; 10 μM receptor in 45:45:10 MeOH:$CHCl_3$:H_2O solution, 298 K.

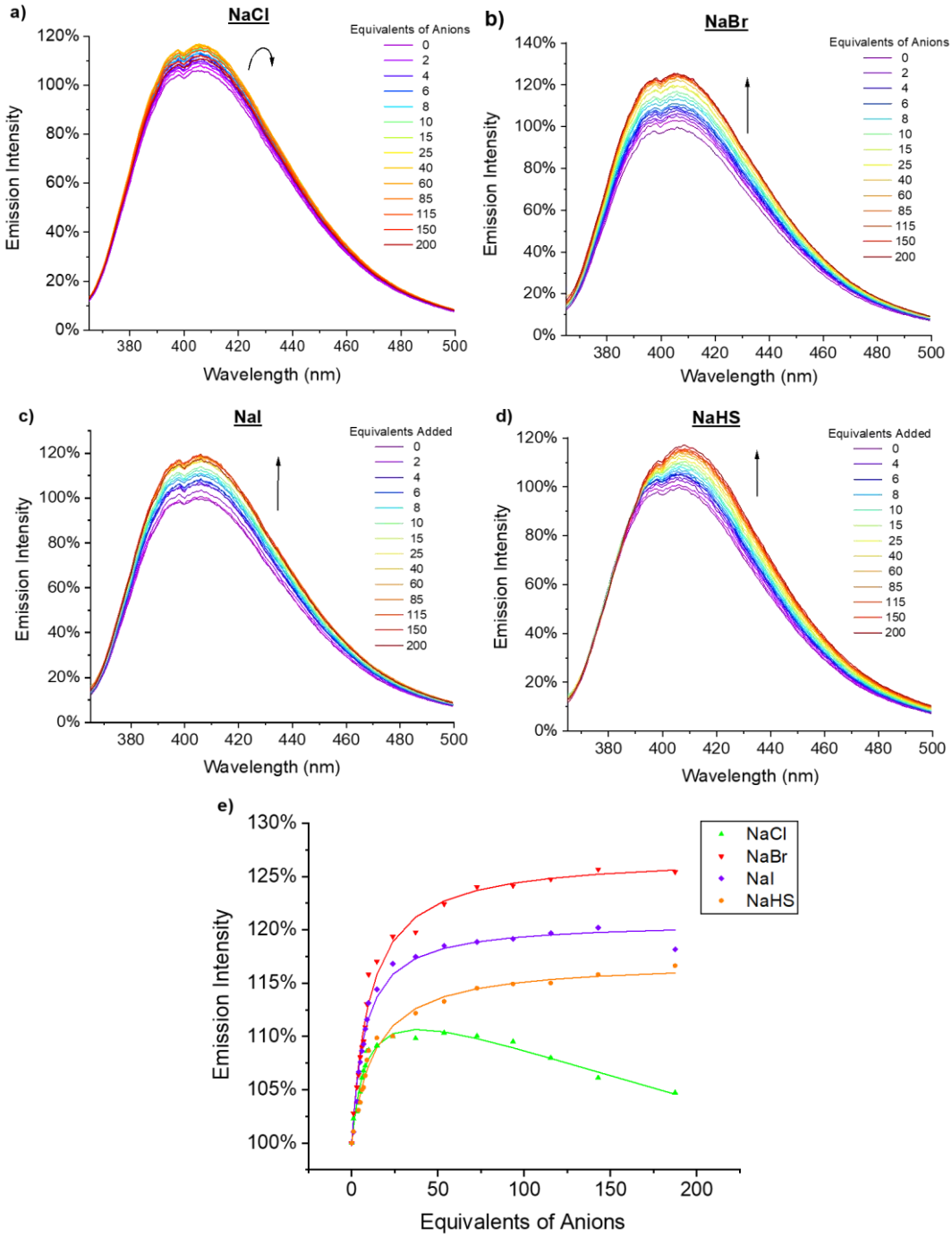


Figure 2.26: *Fluorescence emission intensity changes of receptor* ***2.40*** *upon addition of* ***a)*** *NaCl* ***b)*** *NaBr,* ***c)*** *NaI* ***d)*** *NaHS.* ***e)*** *Binding isotherms and Bindfit analysis of fluorescence emission maxima change on addition of anions. ([host] = 10 μM, 45/45/10 $CHCl_3$/MeOH/H_2O, T = 298 K).*

2.4.3. Summary

Two novel XB rotaxane host systems incorporating coumarin fluorophores and iodotriazoles were synthesised and characterised. Neutral rotaxane **2.32**, was prepared using AMT,

however due to lack of material — owing to the poor yield — anion titration experiments were not conducted. The XB pyridinium rotaxane **2.40** was synthesised using a chloride template approach and was found to display fluorescence sensing behaviour for the halides and HS^- via an emission intensity increase of the coumarin fluorophores.

2.5. Conclusion and Summary

The work described in this chapter has demonstrated the capability of coumarin-XB receptors to recognise and sense anions via notable fluorescence responses of the integrated coumarin reporter groups.

Initial work began with the design and incorporation of two coumarin fluorophores into an acyclic XB receptor, in order to test the reporter motifs capability to sense anions. This acyclic system acted as a proof of principle and was shown to bind and sense, via a coumarin-based fluorescence emission enhancement and quenching, Cl^-, Br^-, I^- and HS^- — being the first XB receptor example for HS^-. Importantly the sensing was observed in competitive aqueous-organic solvent media, showing potential for the functioning of such XB host systems in pure water environments.

Building on the acyclic receptor anion binding results, macrocyclic receptor analogues were designed and synthesised. The preparation of the desired [1+1] macrocyclic systems using RCM and CuAAC ring closing reactions was hampered by poor solubility and ring strain. However, an unexpected [2+2] macrocycle was synthesised via RCM and examined for its capability to sense anions. The receptor was found to bind and sense halides in MeCN via a fluorescence coumarin emission increase. Due to the macrocycle's limited solubility, the receptor's capability to sense HS^- in an organic/aqueous solvent mixture was not tested.

Two novel axle component coumarin containing XB rotaxane systems were synthesised. A neutral rotaxane was prepared via AMT, however due to poor yield and lack of material its capability to sense anions was not investigated. The positively charged pyridinium coumarin axle containing rotaxane was synthesised via a chloride template Grubbs' catalysed RCM clipping reaction in moderate yields. Fluorescence anion binding studies showed emission intensity increases and sensing of Cl^-, Br^-, I^- and HS^-.

Future work will focus on the resynthesis of neutral rotaxane **2.32** and subsequent anion binding titration experiments. ^{1}H NMR anion titration experiments for both rotaxane **2.32** and **2.40** will be conducted and the comparisons between the two examined.

2.6. References

1 D. Cao, Z. Liu, P. Verwilst, S. Koo, P. Jangjili, J. S. Kim and W. Lin, *Chem. Rev.*, 2019, **119**, 10403–10519.

2 H. Miyaji, H. K. Kim, E. K. Sim, C. K. Lee, W. S. Cho, J. L. Sessler and C. H. Lee, *J. Am. Chem. Soc.*, 2005, **127**, 12510–12512.

3 G. Ambrosi, M. Formica, V. Fusi, L. Giorgi, E. MacEdi, G. Piersanti, M. Retini, M. A. Varrese and G. Zappia, *Tetrahedron*, 2012, **68**, 3768–3775.

4 A. K. Satpati, M. Kumbhakar, S. Nath and H. Pal, *Photochem. Photobiol.*, 2009, **85**, 119–129.

5 S. W. Robinson, C. L. Mustoe, N. G. White, A. Brown, A. L. Thompson, P. Kennepohl and P. D. Beer, *J. Am. Chem. Soc.*, 2014, **137**, 499–507.

6 M. D. Hartle, D. J. Meininger, L. N. Zakharov, Z. J. Tonzetich and M. D. Pluth, *Dalt. Trans.*, 2015, **44**, 19782–19785.

7 S. W. Robinson and P. D. Beer, *Org. Biomol. Chem.*, 2017, **15**, 153–159.

8 L. Yi, J. Shi, S. Gao, S. Li, C. Niu and Z. Xi, *Tetrahedron Lett.*, 2009, **50**, 759–762.

9 D. Brynn Hibbert and P. Thordarson, *Chem. Commun.*, 2016, **52**, 12792–12805.

10 BindFit v0.5 | Supramolecular, http://app.supramolecular.org/bindfit/, (accessed 22 June 2021).

11 K. Sivakumar, Fang Xie, B. M. Cash, S. Long, H. N. Barnhill and Q. Wang, *Org. Lett.*, 2004, **6**, 4603–4606.

12 M. Abdallah, A. Hijazi, F. Dumur and J. Lalevée, *Mol. 2020, Vol. 25, Page 2063*, 2020, **25**, 2063.

13 A. A. Kudale, J. Kendall, C. C. Warford, N. D. Wilkins and G. J. Bodwell, *Tetrahedron Lett.*, 2007, **48**, 5077–5080.

14 K. Barral, A. D. Moorhouse and J. E. Moses, *Org. Lett.*, 2007, **9**, 1809–1811.

15 S. J. P'Pool and H. J. Schanz, *J. Am. Chem. Soc.*, 2007, **129**, 14200–14212.

16 M. J. Langton and P. D. Beer, *Acc. Chem. Res.*, 2014, **47**, 1935–1949.

17 K. M. Bąk, K. Porfyrakis, J. J. Davis and P. D. Beer, *Mater. Chem. Front.*, 2020, **4**, 1052–1073.

18 T. J. Hubin and D. H. Busch, *Coord. Chem. Rev.*, 2000, **200**, 5–52.

19 G. T. Spence and P. D. Beer, *Acc. Chem. Res.*, 2013, **46**, 571–586.

20 C. O. Dietrich-Buchecker, J. P. Sauvage and J. P. Kintzinger, *Tetrahedron Lett.*, 1983, **24**, 5095–5098.

21 J. D. Crowley, S. M. Goldup, A. L. Lee, D. A. Leigh and R. T. Mc Burney, *Chem. Soc. Rev.*, 2009, **38**, 1530–1541.

22 V. Aucagne, K. D. Hänni, D. A. Leigh, P. J. Lusby and D. B. Walker, *J. Am. Chem. Soc.*, 2006, **128**, 2186–2187.

23 X. Li, J. Y. C. Lim and P. D. Beer, *Chem. Eur. J.*, 2018, **24**, 17788–17795.

24 G. T. Spence and P. D. Beer, *Acc. Chem. Res.*, 2013, **46**, 571–586.

25 J. A. Wisner, P. D. Beer, M. G. B. Drew and M. R. Sambrook, *J. Am. Chem. Soc.*, 2002, **124**, 12469–12476.

26 H. W. Gibson, S. H. Lee, P. T. Engen, P. Lecavalier, J. Sze, Y. X. Shen and M. Bheda, *J. Org. Chem.*, 1993, **58**, 3748–3756.

27 V. Aucagne, K. D. Hänni, D. A. Leigh, P. J. Lusby and D. B. Walker, *J. Am. Chem. Soc.*, 2006, **128**, 2186–2187.

28 H. Zheng, W. Zhou, J. Lv, X. Yin, Y. Li, H. Liu and Y. Li, *Chem. Eur. J.*, 2009, **15**, 13253–13262.

Chapter 3

Water Soluble Halogen Bonding Receptors for Hydrosulfide

3. Water Soluble Halogen Bonding Receptors for Hydrosulfide

3.1. Introduction

3.1.1. Photo-physical Sensing in Water

While there are many anion receptors that function in organic and organic-aqueous solvent mixtures, those that operate in pure water remain relatively rare in comparison.[1] Indeed, examples capable of sensing in water are even more scarce. The challenges of anion recognition in water, detailed in Chapter 1 (*see 1.2.4.4. Water Soluble Hosts*) include the difficulty of overcoming the significant hydration energy of anions and in the synthesis of water soluble receptor systems.

Kim and co-workers reported a tetra-cationic imidazolium-based cyclophane capable of selectively sensing iodide in water (Figure 3.1a).[2] Size selective binding of iodide between the macrocyclic receptor's two anthracene groups disrupted the anthracene excimer emission band, causing a characteristic fluorescence quenching response.

Puccioni and co-workers appended a chiral (*S*)-BINOL motif with two 1,4,7-triazacyclononane macrocycles (Figure 3.1b).[3] The host was found to display enantiomeric fluorescent sensing selectivity for (*S*,*S*)-tartrate over other chiral dicarboxylates, including (*R*,*R*)-tartrate, in water at physiological pH. The dicarboxylate guests are bound via HB with the gauche disposition of the receptor's two polyammonium macrocycles. The authors propose a proton transfer in the excited state from the BINOL group's OH to the carboxylate guest species is responsible for the observed emission intensity increase.

Beer and co-workers incorporated a luminescent tris-(bipyridine) ruthenium (II) group into the macrocyclic component of a XB axle containing rotaxane (Figure 3.1c) which was shown to bind and sense iodide selectively in aqueous solution. On addition of excess iodide a modest enhancement of the receptor's MLCT emission band of 6% was observed. Conversely, addition of excess iodide to an acyclic ruthenium(II) bipyridyl receptor analogue induced a 10% quenching of the MLCT emission band. It was postulated that of the competing PET and heavy atom quenching, commonly caused by iodide, against the strong rotaxane host-anion guest binding rigidity effects that reduce non-radiative vibrational relaxation pathways, the latter dominates; resulting in a MLCT emission intensity increase of 6%.

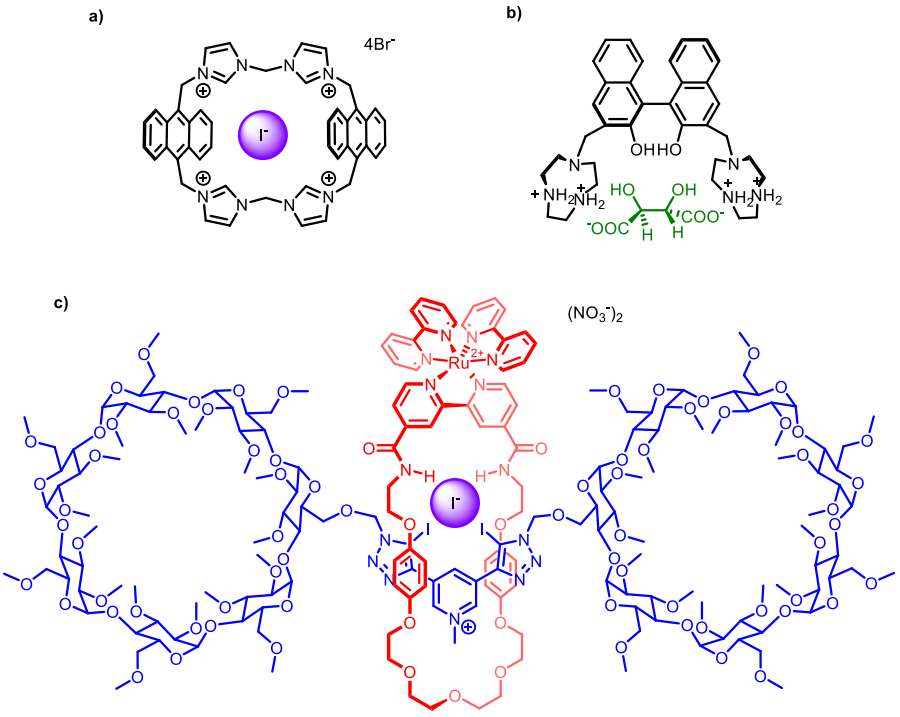


Figure 3.1: *Water soluble host-receptors* ***a)*** *Kim's imidazolium-based cyclophane complexed with iodide* ***b)*** *Puccioni's (S)binol acyclic receptor complexed with (S,S)-tartrate* ***c)*** *Beer's water soluble ruthenium(II) rotaxane complexed with iodide.*

3.1.2. Chapter Objectives

This chapter is concerned with the incorporation of the coumarin iodo-triazole system (Figure 3.2), developed in Chapter 2 into a series of water-soluble XB receptors. These receptors will then be tested for their ability to recognise and sense HS^- in water.

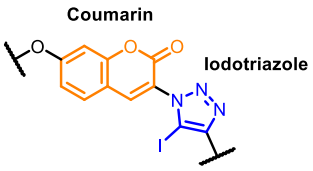


Figure 3.2: *Appended coumarin and iodotriazole, sensing and anion binding motif.*

Two generations of water-soluble XB receptors using different solubilising groups are examined: Generation 1 includes TEG tertiary amine groups (Figure 3.3a) and Generation 2 incorporates benzyl TEG motifs (Figure 3.3b).

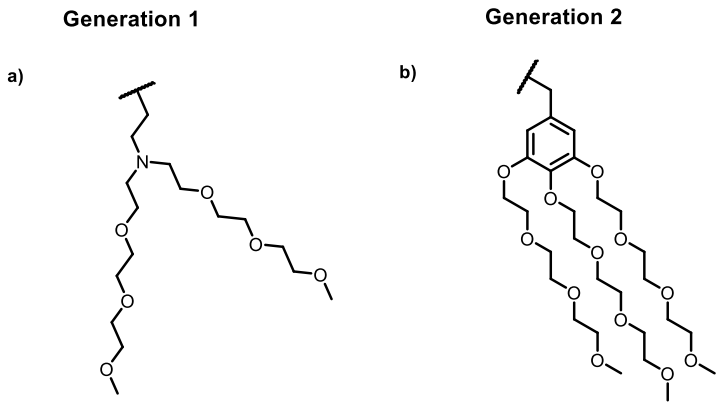


Figure 3.3a: *Two generations of water solubilising groups* ***a)*** *Generation 1, tertiary amine TEG groups* ***b)*** *Generation 2, benzyl TEG groups*

Three central bidentate XB donor frameworks, pyridine, pyridinium and secondary amine will be developed in each generation (Figure 3.4). The 3,5-bis-iodotriazole pyridine motif has been shown to bind anions in organic solvent media. The strength of anion binding can be significantly enhanced via methylation of the pyridine in which charge assisted XB enables anion recognition in aqueous media. As observed in Chapter 2, in combination with coumarin fluorophores, such receptor systems are capable of sensing anions.[4]

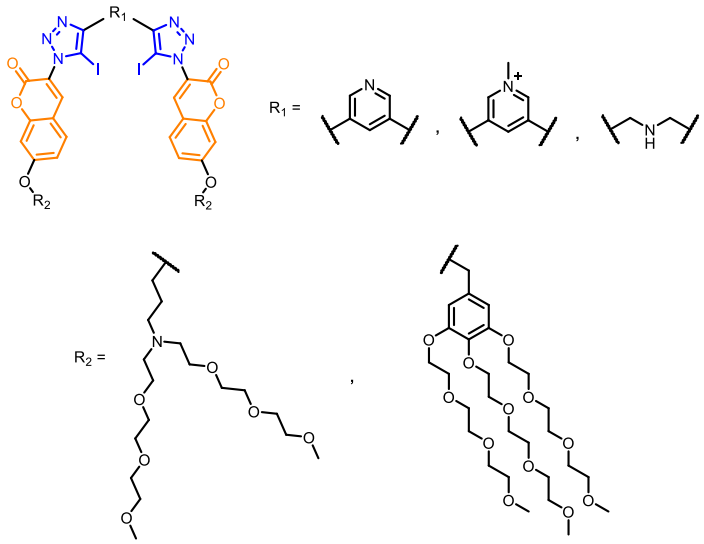


Figure 3.4: *Target water soluble host-receptors*

3.2. Generation 1 Water Soluble XB Receptors

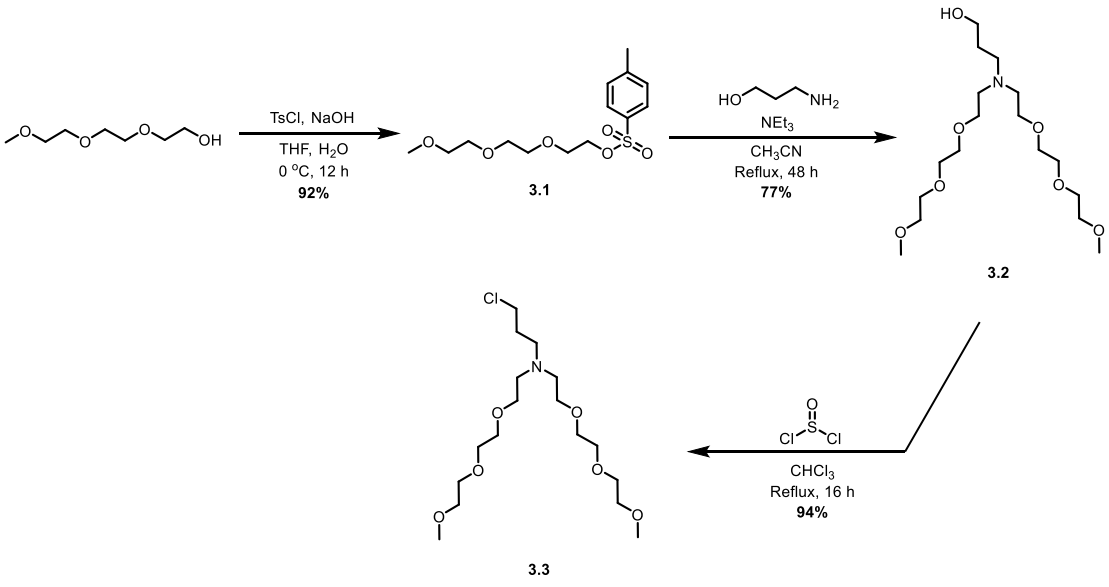
Generation 1 receptor synthesis, characterisation and titration experiments were undertaken by part II student Adam Beecroft under supervision.

3.2.1. Synthesis

Initial work focused on the synthesis of a hydrophilic TEG tertiary amine coumarin azide synthon that could be subsequently reacted with bis-iodoalkynes to form the target acyclic XB receptors..

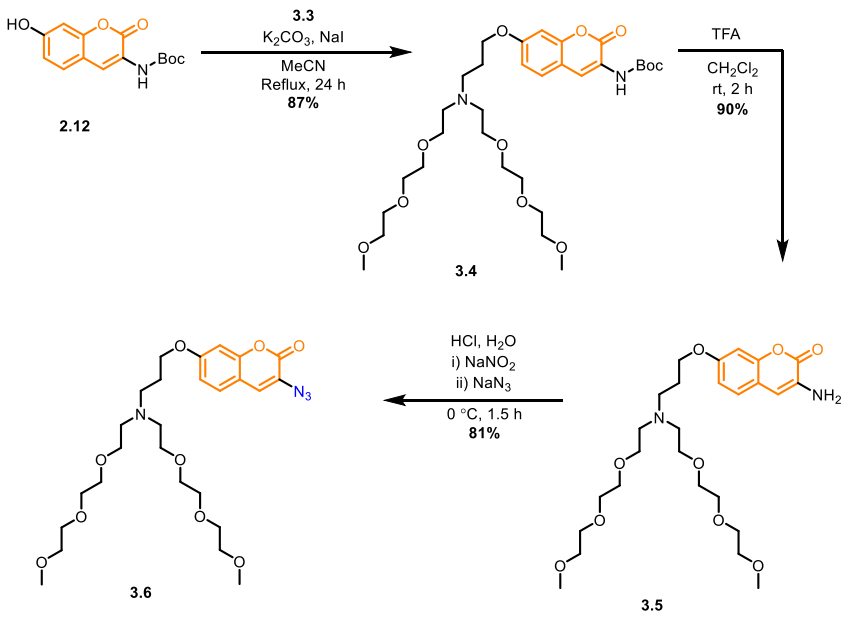
3.2.1.1. Synthesis of TEG tertiary amine coumarin azide

Conversion of triethylene mono methyl ether to tosylate **3.1** was achieved in a 92% yield through a reaction with TsCl in THF under basic conditions.[5] Two equivalents of tosylate **3.1** were subsequently reacted with 3-amino-1-propanol under basic conditions. Purification was achieved via a silica plug affording amine **3.2** in a 77% yield. The hydroxyl group of **3.2** was converted to the corresponding chloro derivative by reaction with thionyl chloride in chloroform, giving amine **3.3** in quantitative yields (Scheme 3.1).



Scheme 3.1: *Synthesis of water soluble chloro-amine synthon* ***3.3***

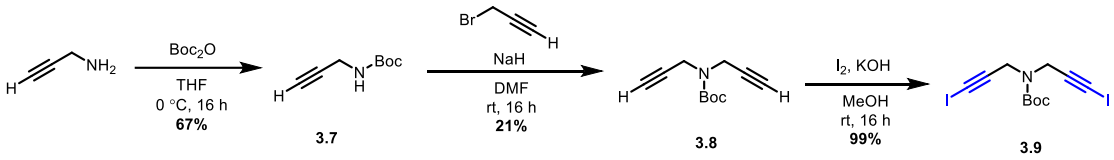
Boc-protected coumarin **2.12** was reacted with chloro derivative **3.3** in acetonitrile under basic conditions, affording coumarin derivative **3.4** in a yield of 87%. Boc-deprotection of **3.4** to amine **3.5** was achieved in a 90 % yield by stirring with TFA in CH_2Cl_2. Conversion of the amine to the azide was achieved by reacting with $NaNO_2$ and NaN_3 in acidic water, affording target TEG tertiary amine coumarin azide **3.6** in 81% yield (Scheme 3.2).



Scheme 3.2: *Synthesis of water soluble coumarin azide* ***3.6***

3.2.1.2. Synthesis of bis-iodoalkyne amine

Bis-iodoalkyne **3.9** was synthesised following a reported procedure by Beer and co-workers (Scheme 3.3).[6] Propargylamine was protected with Boc_2O by stirring in THF, affording **3.7** in a 67% yield. Subsequent S_N2 reaction of **3.7** with NaH and propargyl bromide in DMF gave alkyne **3.8**, in a modest yield of 21% due to difficulty in purification. Quantitative conversion to the bis-iodoalkyne **3.9** was achieved using iodine in methanol under basic conditions (Scheme 3.3).



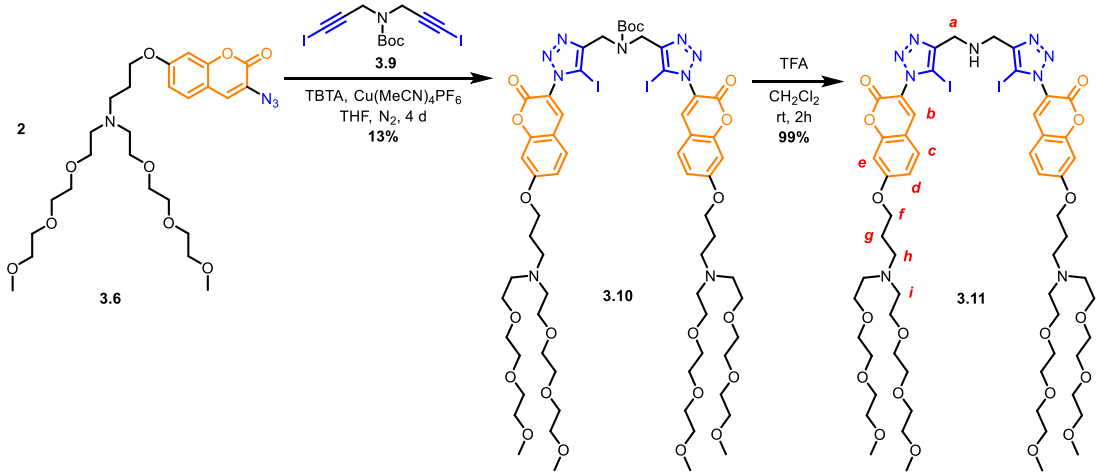
Scheme 3.3: *Synthesis of bis-iodoalkyne* ***3.9***

3.2.1.3. Synthesis of acyclic receptors

Standard CuAAC reactions between appropriate bis-iodoalkynes and TEG tertiary amine coumarin azide **3.6** were used to prepare the first generation XB acyclic receptors.

One equivalent of bis-iodoalkyne **3.9** was stirred with 2.2 equivalents of coumarin azide **3.6** in dry THF solution. A catalytic amount of CuI was added with TBTA and the reaction was left to stir at room temperature under N_2 for 3 days. Purification via preparative TLC afforded Boc-protected receptor **3.10** in a low yield of 13%. The poor yield was attributed to purification difficulties. Subsequent quantitative Boc-deprotection of **3.10** was achieved by stirring with

TFA in CH_2Cl_2, affording secondary amine receptor **3.11** (Scheme 3.4), which was characterised by ^1H NMR (Figure 3.5), ^{13}C NMR and high resolution ESI MS.



Scheme 3.4: *Synthesis of secondary amine receptor* ***3.11***

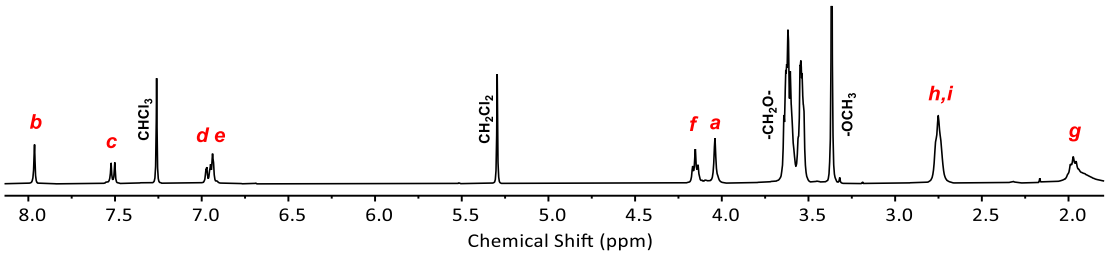
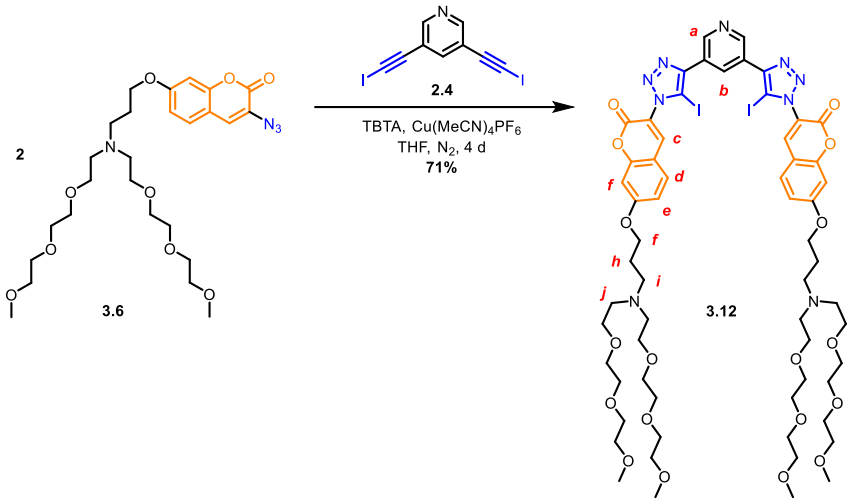


Figure 3.5: *Truncated ^1H NMR spectrum of receptor* ***3.11*** *($CDCl_3$, 298K).*

An analogous CuAAC method was used in the synthesis of receptor **3.12** (Scheme 3.5). The reaction of bis-iodoalkyne **2.4** with 2.2 equivalents of coumarin azide **3.6** in the presence of a CuI and TBTA gave pyridine receptor **3.12** in a yield of 71%, characterised by ^1H NMR (Figure 3.6), ^{13}C NMR and HRMS (Figure 3.7).



Scheme 3.5: *Synthesis of pyridine receptor* ***3.12***

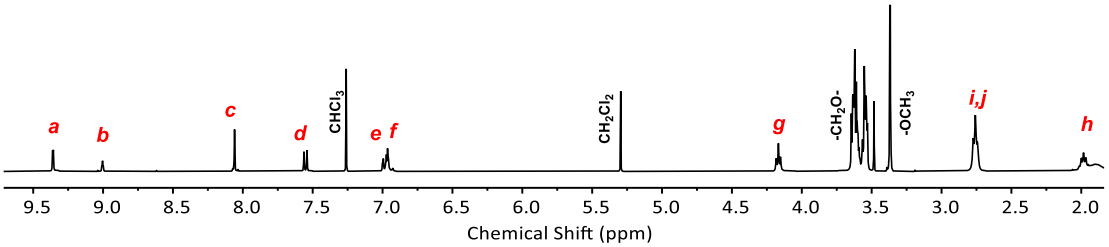


Figure 3.6: *Truncated* ^{1}*H NMR Spectrum of receptor* ***3.12*** *(*$CDCl_3$*, 298 K)*

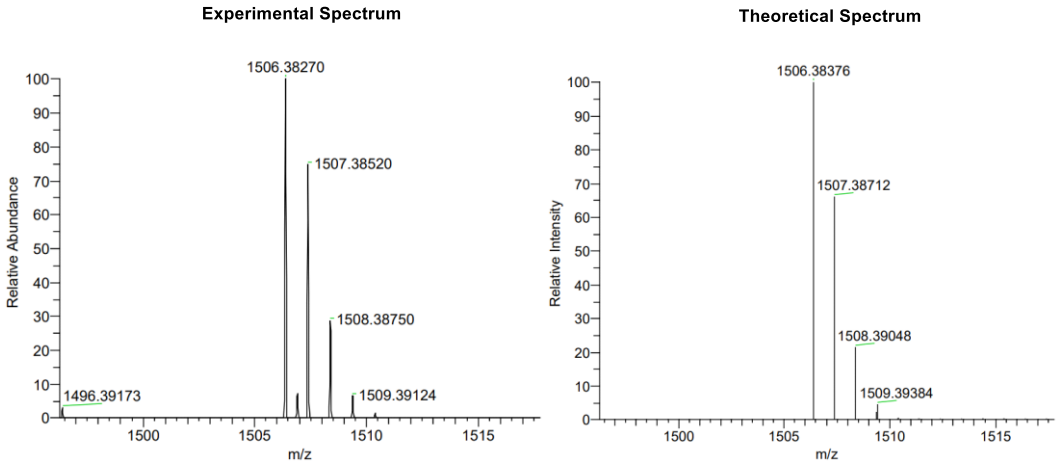
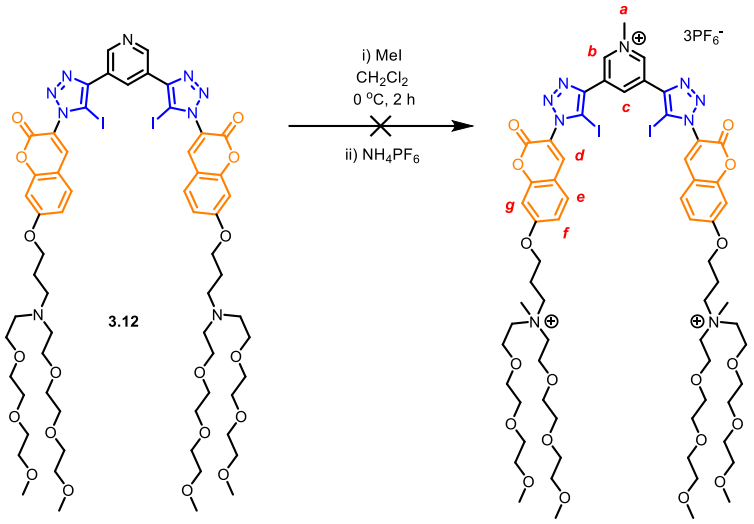


Figure 3.7: *HRMS experimental and theoretical spectrum of receptor* ***3.12,*** *m/z = 1506.38296 ([M + Na]*$^{+}$*,* $C_{61}H_{83}I_2N_9O_{18}Na$*, calc = 1506.38376)*

In an effort to potentially enhance XB binding strength, attempts were made to alkylate neutral pyridyl containing receptor **3.12** by reacting an excess amount of MeI. This would result in a tricationic receptor with quaternary TEG appendages (Scheme 3.6). Stirring **3.12** with excess MeI in CH_2Cl_2 over 2 h gave a crude product whose ^{1}H NMR in d_6-DMSO (Figure 3.8) together with high resolution ESI MS (Figure 3.9) confirmed the formation of the desired

tricationic receptor. However, attempts to purify the crude product via preparative TLC with 10% MeOH in CH_2Cl_2 proved unsuccessful, even after attempted conversion to the PF_6^- salt. This is most likely due to a complex mixture of cationic species which proved impossible to separate via chromatographic techniques.



Scheme 3.6: *Attempted synthesis of pyridinium receptor*

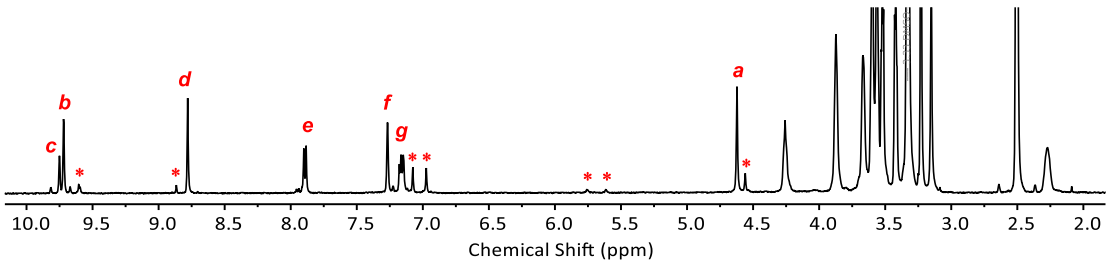


Figure 3.8: *Impure ^{1}H NMR Spectrum of pyridinium receptor (d_6-DMSO, 298 K)*

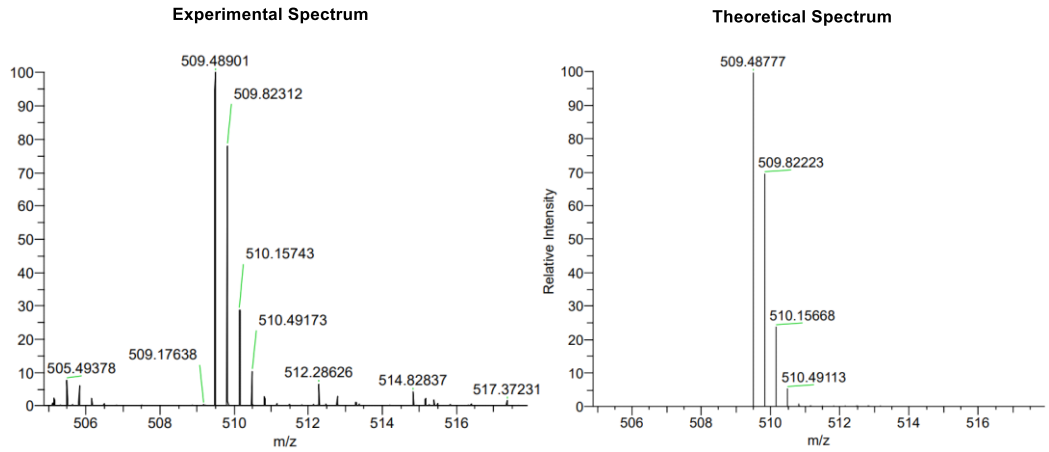


Figure 3.9: *HRMS experimental and theoretical spectrum of pyridinium receptor, m/z = 509.48901 ($[M]^{3+}$, $C_{64}H_{92}I_2N_9O_{18}^{3+}$, calc = 509.48667)*

3.2.2. Anion Binding Studies

3.2.2.1. ^{1}H NMR Titration studies

The anion binding properties of amine receptor **3.11** and pyridine receptor **3.12** were investigated using ^{1}H NMR titration experiments. Chemical shifts of proton signals adjacent to the respective XB binding site were monitored as a function of anion concentration, with the anions being added as their tetrabutylammonium (TBA) salts.

3.2.2.1.1. Preliminary studies in acetone

Preliminary ^{1}H NMR titration studies with TBACl were conducted in acetone-d_6.

Upon addition of chloride to receptor **3.11**, an upfield shift of the adjacent methylene signals *a* (Δδ = −0.12 ppm) was observed (Figure 3.10). Interestingly, the coumarin peaks corresponding to protons *b* and *c* showed significant downfield shifts (Δδ = 0.65 for *b* and Δδ = 0.52 for *c*), suggesting that the halide complexation is occurring within the desired XB cavity and is being assisted by the coumarin C-H protons.

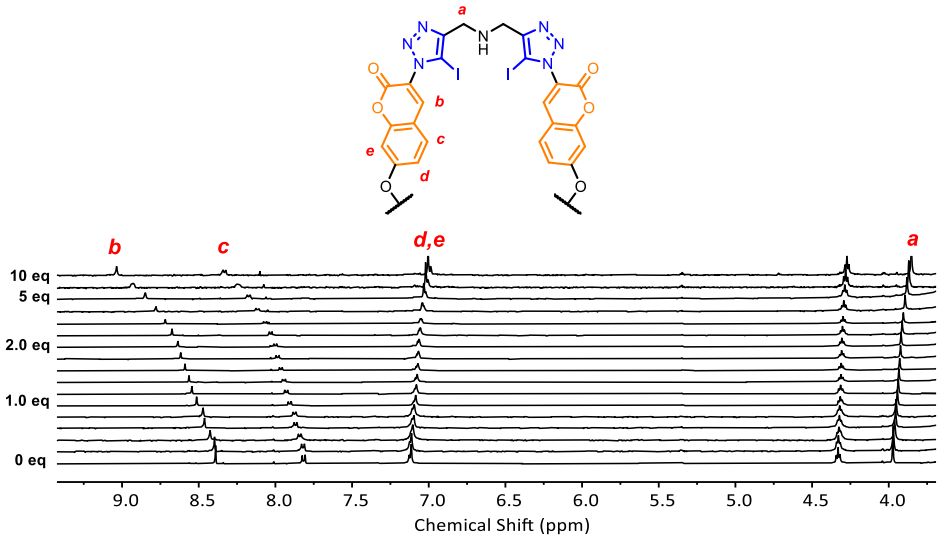


Figure 3.10: *^{1}H NMR titration of receptor **3.11** upon addition of TBACl in acetone-d_6 (1 mM, 298 K)*

An analogous titration with the pyridine receptor **3.12** showed a significant downfield shift of the internal pyridine proton signal *b* (Δδ = 0.42 ppm from 0 to 2.5 equivalents) and a modest upfield shift of the coumarin proton signal *c* (Δδ = -0.02 ppm from 0 to 2.5 equivalents) (Figure 3.11), indicating that the binding of the halide anion was taking place in the vicinity of the XB donors. Further addition of TBACl (>2.5 equivalents) caused no more perturbations, indicating very strong binding of the halide guest in acetone-d_6.

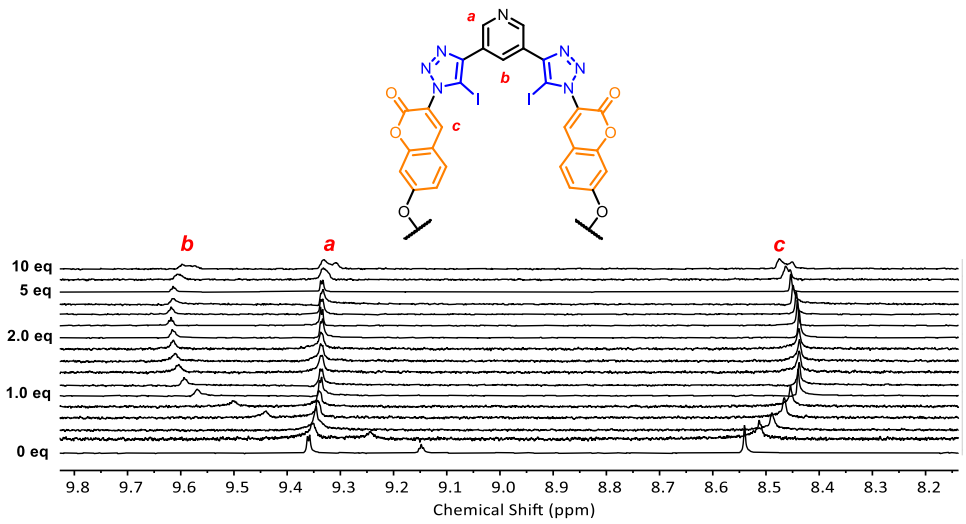


Figure 3.11: *^{1}H NMR titration of receptor* ***3.12*** *upon addition of TBACl in acetone-d_6 (1 mM, 298 K)*

Bindfit[7,8] analysis determined the 1:1 host-guest stoichiometric association constants (Table 3.1).

Table 3.1: *Anion association constants for chloride*

Receptor	K_a (M^{-1})
3.11	119 ± 2
3.12	$>10^5$

Anion association constants with errors determined using Bindfit analysis of the NMR titration data of receptor **3.11** monitoring methylene proton *a* and **3.12** monitoring the internal pyridine proton *b*; 1 mM receptor in acetone-d_6, 298 K.

In spite of the system being neutral, **3.12** forms a strong complex with chloride in acetone, beyond the accuracy limits of ^{1}H NMR spectroscopy. Receptor **3.11,** on the other hand, coordinates relatively weakly to chloride. The stark difference likely originates from the difference in receptor flexibility and preorganisation, where the pyridine system contains a more rigid bidentate iodotriazole structural framework that requires a smaller entropic penalty to complex the halide guest. The amine receptor system has more flexibility around the methylene linked iodotriazoles and therefore a greater entropy loss upon binding.

3.2.2.1.2. Receptor 3.11 ^{1}H NMR Titration Studies in Acetone

Analogous ^{1}H NMR titration experiments with receptor **3.11** and TBA bromide and iodide salts in acetone−d_6 revealed similar receptor proton perturbations to those observed with chloride. In particular an upfield shift of the receptor's methylene proton signals. However, both bromide and iodide induced shifts of a smaller magnitude (Δδ = −0.08ppm, Δδ = −0.02ppm for

10 equivalents respectively). Similarly, the downfield shifts in the coumarin proton environments were less significant for bromide and iodide (Figure 3.13).

Table 3.2 shows the receptor binds bromide and iodide more weakly than chloride, displaying a selectivity bias for the smaller more charge dense and basic halide anion.

Table 3.2: *Anion association constants receptor* ***3.11***

Anion	K_a (M^{-1})
Cl^-	119 ± 2
Br^-	57 ± 0.5
I^-	20 ± 0.2

Anion association constants with errors determined using 1:1 host:guest stoichiometric Bindfit[7,8] analysis of the NMR titration data of receptor **3.11** monitoring the methylene proton a; 1 mM receptor in acetone-d_6, 298 K.

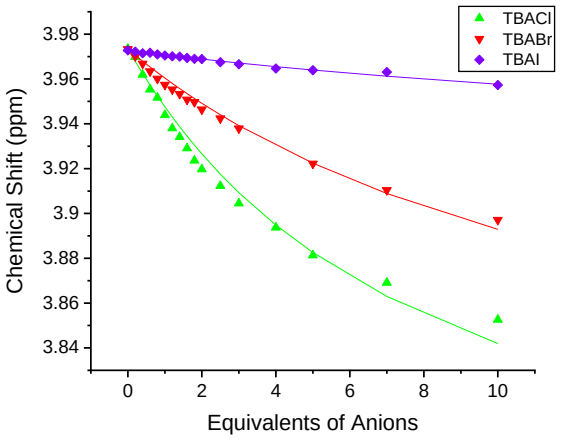


Figure 3.12: *Binding isotherms and 1:1 stoichiometric Bindfit analysis of NMR titration data for receptor* ***3.11****, monitoring internal methylene peak upon addition of TBACl, TBABr and TBAI in acetone-d_6, 298 K.*

3.2.2.1.3. Protonation Studies

With the objective of enhancing anion binding potency, the effect of protonating the secondary amine of receptor **3.11** on anion binding strength was investigated. Initial ^{1}H NMR experiments were performed in acetone-d_6 upon addition of acid HBF_4 (Figure 3.13).

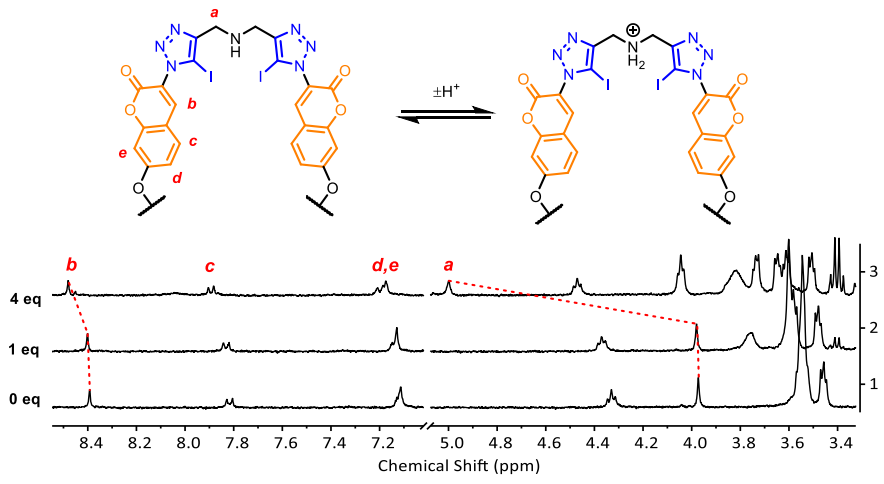


Figure 3.13: *Protonated state of rector* ***3.11*** *and truncated ^{1}H NMR titration spectra upon addition of 0, 1 and 4 equivalents of HBF_4 in acetone-d_6; ([host] = 1 mM, T = 298 K)*

Upon addition of one equivalent of HBF_4 — dissociation into H^+ and non-coordinating BF_4^- — no change was observed for the receptor's methylene protons *a*. The spectral region containing the TEG proton signals did show changes, suggesting initial protonation had occurred at the more basic tertiary amine sites. Further addition of HBF_4 (up to 4 equivalents) resulted in a dramatic downfield shift in the methylene signal *a*, suggesting that protonation of the desired secondary amine had occurred. A slight downfield shift was also seen for the coumarin signal *b* closest to the XB binding site. Subsequent ^{1}H NMR titration experiments with the protonated species and Cl^- and Br^- in acetone-d_6, however, resulted in precipitation, preventing the determination of quantitative binding data.

3.2.2.1.4. Receptor 3.12 ^{1}H NMR Titration Studies in Acetonitrile

In order to determine quantitative association constant data, the halide binding properties of receptor **3.12** were investigated using ^{1}H NMR titration experiments in CD_3CN. As observed in the previous acetone-d_6 titration, addition of chloride in CD_3CN induced significant downfield perturbations of the internal pyridine proton signal b ($\Delta\delta$ = 0.34ppm for 10 equivalents). Accordingly, both bromide and iodide induced downfield shifts but each of a lesser magnitude ($\Delta\delta$ = 0.27ppm and $\Delta\delta$ = 0.17ppm for 10 equivalents respectively).

As expected, the Bindfit determined association constants (Table 3.3, Figure 3.14) show the receptor displaying selectivity for the smaller more charge dense chloride anion.

Table 3.3: *Anion association constants receptor* ***3.12***

Anion	K_a (M^{-1})
Cl^-	1070 ± 30
Br^-	610 ± 10
I^-	470 ± 7

Anion association constants with errors determined using 1:1 stiochiometric Bindfit analysis of the NMR titration data of receptor **3.12** monitoring the methylene peak; 1 mM receptor in CD_3CN, 298 K.

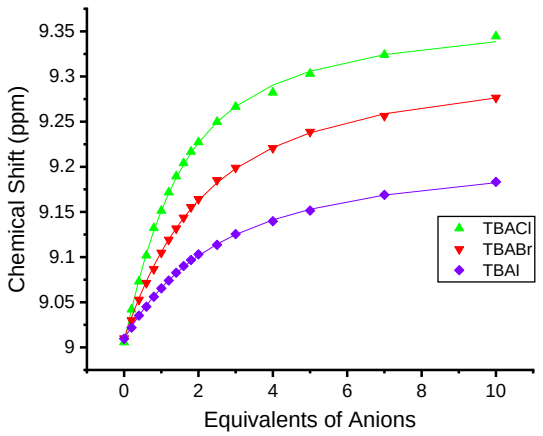


Figure 3.14: *Binding isotherms and 1:1 stoichiometric Bindfit analysis of NMR titration data for receptor* ***3.12****, monitoring internal methylene peak upon addition of TBACl, TBABr and TBAI in d_3-MeCN, 298 K.*

3.2.2.2. Fluorescence Titration Studies

Due to the hydrophilic nature of the TEG substituents both XB receptors **3.11** and **3.12** were found to be soluble in water. Owing to the intrinsic hydrophobic character of the XB iodotriazole binding sites, it was predicted that both receptors had the potential to bind and sense less well solvated hydrophobic anions, such as iodide and HS^-.

Samples were prepared in distilled water at a concentration of 10 µM and the respective receptor's coumarin fluorescent emission band was monitored as a function of anion concentration, with anions added as their sodium salts. Considering that the pK_a of secondary and tertiary amines in aqueous media is typically ca. >10, receptor **3.11** will likely be triply protonated in pure water and is therefore denoted as **3.11H$^+$**.

The photophysical properties of receptors **3.11H$^+$** and **3.12** are shown in Figure 3.16 and Table 3.4. Both receptors exhibit similar characteristic coumarin energies of absorption and emission bands[9] with receptor **3.11H$^+$** being slightly more red shifted. At neutral pH, this likely originates from the cationic protonated secondary amine withdrawing electron density from the iodotriazoles and therefore also the coumarin fluorophores.

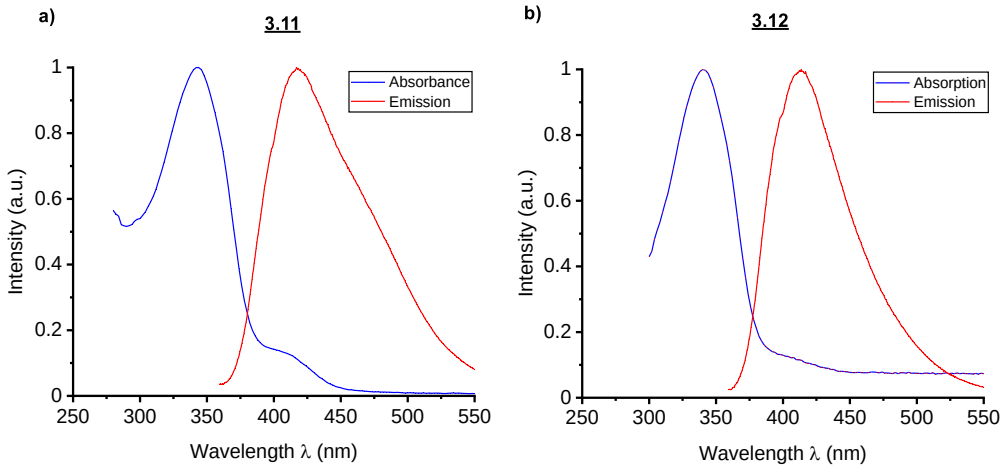


Figure 3.15: *Normalised emission and absorbance spectra for receptors **3.11H$^+$** and **3.12** in H_2O.*

Table 3.4: *Energies of absorption and emission for receptor **3.11H$^+$** and **3.12** in H_2O.*

Receptor	$\lambda_{max\ abs}$ / nm	$\lambda_{max\ ems}$ / nm	Stokes Shift / nm
3.11H$^+$	342	417	75
3.12	340	413	73

Emission wavelength excited at $\lambda_{max\ abs}$, 298K, [10 µM],

3.2.2.2.1. Receptor 3.11 Fluorescence Titration Studies

Following excitation at 342 nm, the receptor's fluorescence emission intensity was monitored upon the addition of NaCl, NaBr, NaI and NaHS.

On addition of bromide, iodide and HS^-, a significant quenching of the receptor's fluorescence emission intensity was observed (Figure 3.16). Remarkably, HS^- induced the greatest quenching effect by a magnitude of up to 67 %, while bromide and iodide induced 23% and 17% respectively. Chloride did not induce any notable change indicative of not being bound in water. Notably, the magnitude of quenching correlates with the smallest charge dense anion — HS^- producing the greatest response, likely due to a PET effect.

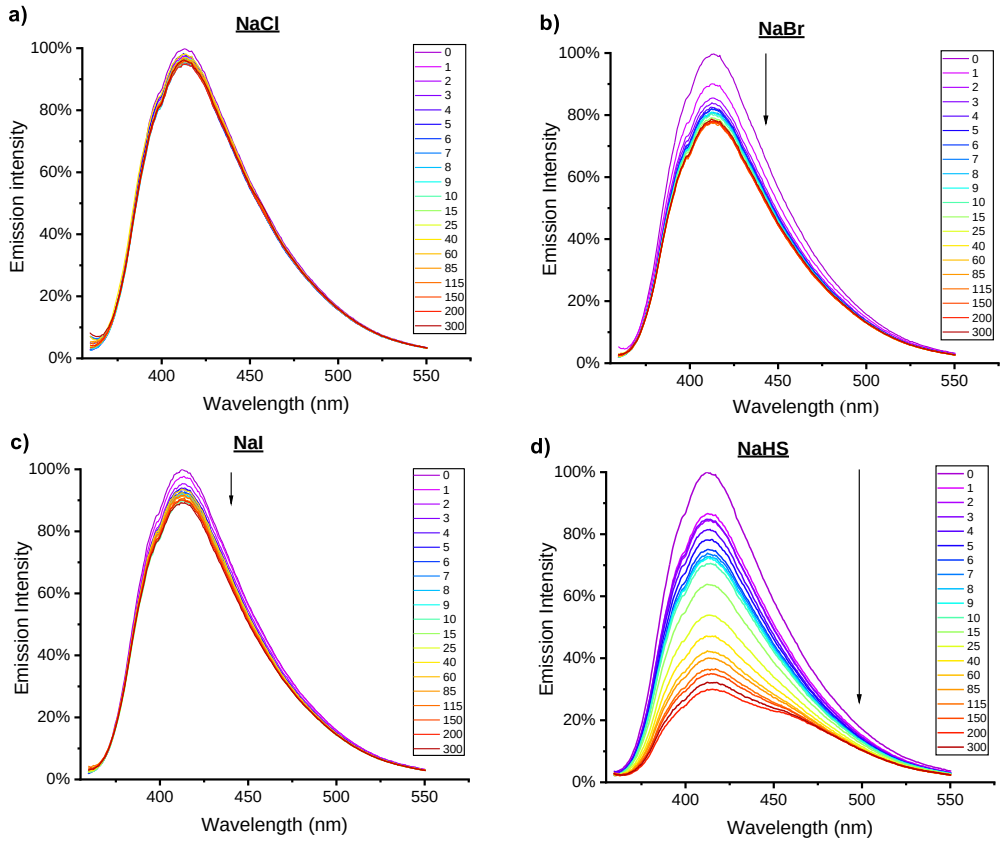


Figure 3.16: *Fluorescence emission intensity changes of receptor* ***3.11H*** $^+$ *upon addition of anions: a) NaCl b) NaBr, c) NaI d) NaHS.*

Monitoring the emission λ_{max}, Bindfit analysis of the intensity changes (Figure 3.18) was used to calculate 1:1 stoichiometric association constants shown in Table 3.5.

Receptor **3.11H**$^+$ exhibits strong binding for the heavier halides Br^- and I^-, while no binding was observed for chloride. The halide association constants follow a Hofmeister bias selectivity trend, $I^- \sim Br^- >> Cl^-$, whereby the binding affinity is greatest for the least hydrated species.

The significant selectivity for HS^- over chloride is of particular interest, as they are similar in relative ionic radii and are commonly found together in the environment. The enthalpy of hydration for the respective anions is reported as ΔH^o_{hyd} = -390 kJ mol^{-1} for chloride and ΔH^o_{hyd} = -330 kJ mol^{-1} for HS^-, suggesting that desolvation and subsequent binding within the receptor's hydrophobic XB binding site would be more favourable for HS^- over Cl^-, as reflected in the experimental data.[10] Efforts to achieve selectivity for HS^- over bromide and iodide in water could be accomplished by use of a water-soluble XB rotaxane host-receptor that could exclude larger anions from binding within the interlocked cavity.

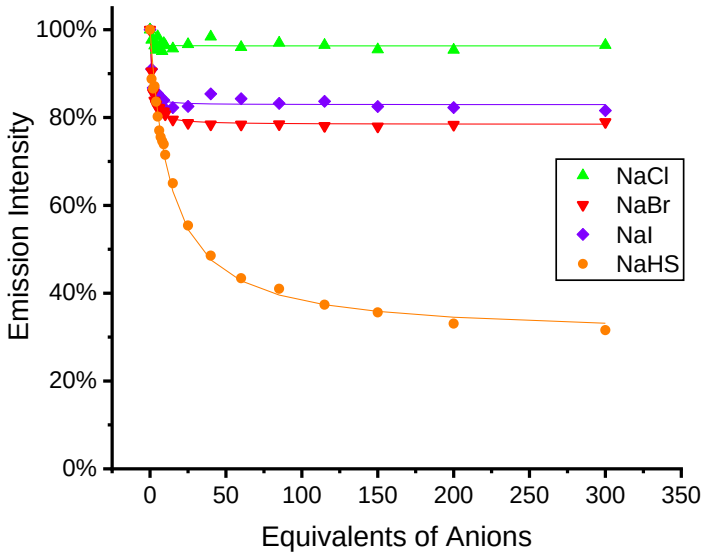


Figure 3.17: *Binding isotherms and Bindfit analysis fit of fluorescence maxima change on addition of anions for receptor* ***3.11H***$^+$*; ([host] = 10 µM, H_2O, T = 298 K).*

Table 3.5: *Fluorescence titration anion association constants of receptor* ***3.11H***$^+$

Anion	k_a (M^{-1})
NaCl	n.b.
NaBr	>10^5
NaI	>10^5
NaHS	7500 ± 660

Anion association constants with errors determined using 1:1 stoichiometric Bindfit analysis of the fluorescence titration data of receptor **3.11H**$^+$ monitoring the change in emission maxima intensity; 10 µM receptor in H_2O, 298 K. (n.b. = no binding observed)

3.2.2.2.2. Receptor 3.12 Fluorescence Titration Studies

Analogous fluorescence titration experiments with **3.12** were hampered with problematic fluctuations in the receptor's emission intensity which prevented any quantitative association constant data from being determined. To investigate this unusual behaviour further preliminary temperature dependent fluorescence studies were conducted at temperatures between 10 ˚C and 50 ˚C in various solvents. The investigation revealed that the receptor's emission intensity was temperature dependent, with higher temperatures leading to reduced emission intensity (Figure 3.18). Additionally, the shape of the emission band exhibited large solvent dependence, concomitant with a hypsochromic shift of 6.5 nm observed in acetonitrile, and shoulders appearing around 475 nm in 1:1 acetonitrile-water containing mixtures, and 380 nm in both pure DMSO and water (Figure 3.19).

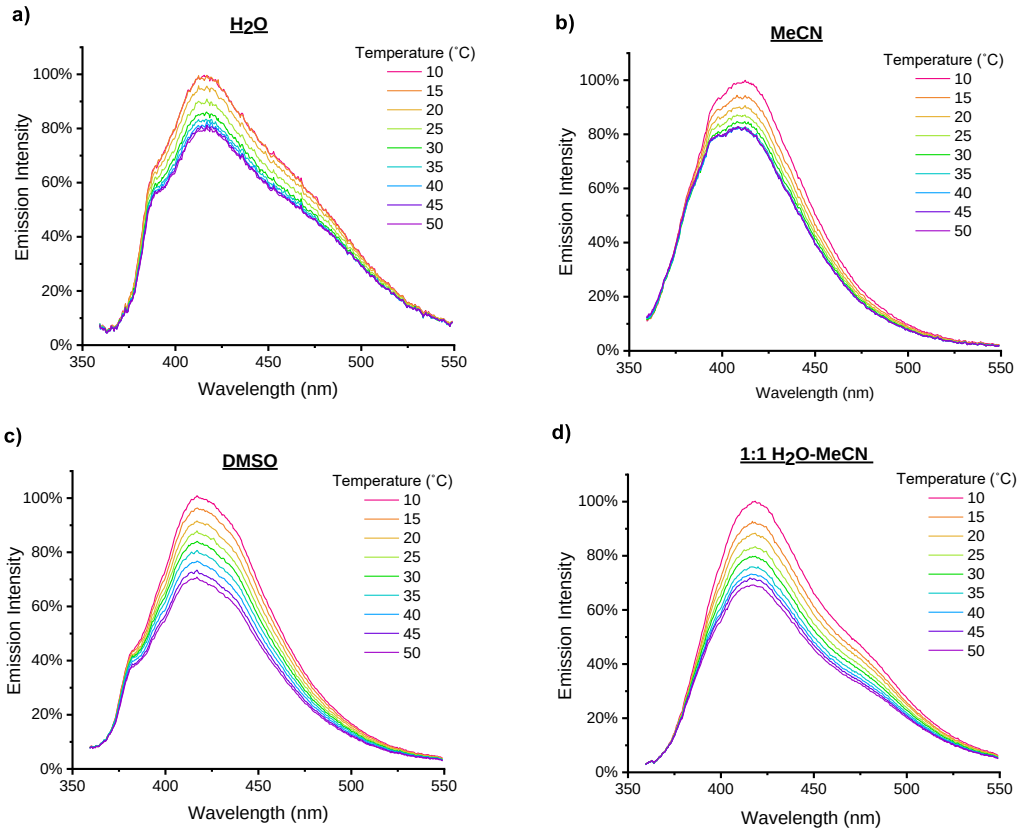


Figure 3.18: *Fluorescence emission intensity changes of receptor* ***3.12*** *with changing temperature in different solvent media: a) H_2O b) MeCN c) DMSO d) 1:1 H_2O-MeCN*

In the acetonitrile-water mixture, this behaviour could be due to aggregation of the receptor. Aggregation induced emission (AIE) arises when the aggregation of an organic fluorophore restricts vibrational and rotational degrees of freedom, limiting relaxation of the excited state via non-radiative processes and increasing the quantum yield of fluorescence.[11] At elevated

temperatures the receptor may become more soluble, have reduced aggregation and therefore a reduction in the emission intensity is observed. Examples of AIE have been reported previously for molecules containing fluorescent coumarin groups.[12,13]

While these preliminary studies provide no conclusive proof for aggregation, based on the hydrophobic nature of the binding site and hydrophilic nature of the PEG chains, it is possible that receptor **3.12** assembles into micelle like structures. Future fluorescence concentration variation studies in aqueous and organic-aqueous solvent mixtures should be undertaken to delineate any receptor aggregation properties.

3.2.3 Summary

Two first generation water soluble XB coumarin containing receptors have been synthesised. The addition of tertiary amine TEG groups introduced water solubility and enabled fluorescence anion titrations studies in water. Owing to the protonation of the central secondary amine, receptor **3.11H$^+$** exhibited significant anion binding for hydrophobic anions. Most importantly, receptor **3.11H$^+$** was able to sense HS^- in water with a characteristic quenching of emission and was selective for HS^- over Cl^-, demonstrating the first example of HS^- chemosensing by a supramolecular receptor in pure water.

3.3. Generation 2 Water Soluble XB Receptors

Although the appendage of tertiary amine TEG groups introduced water solubility to the first generation XB receptors **3.11** and **3.12**, possible aggregation effects noted with the latter receptor negated quantitative anion binding data being obtained. In an effort to overcome this second generation XB receptors containing benzyl TEG motifs were prepared.

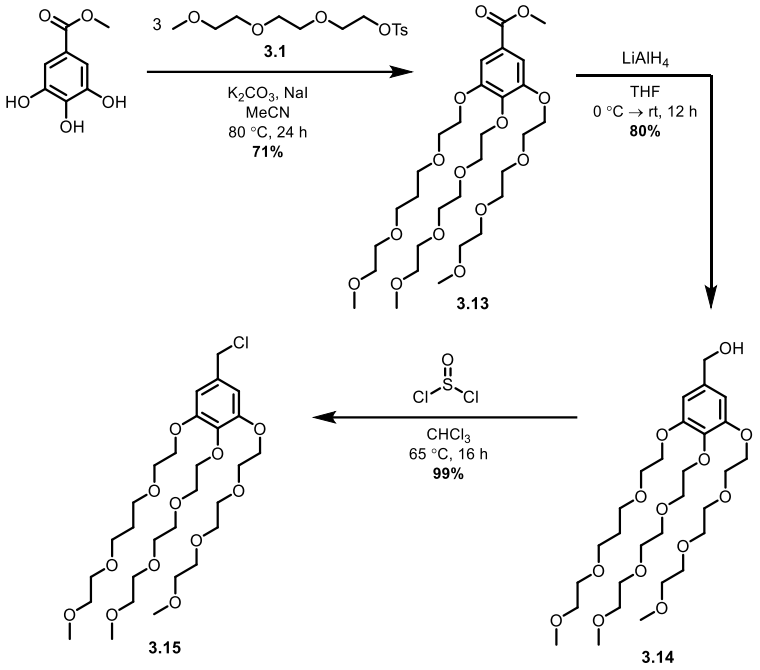
Additionally, to draw comparison between the merits of XB and HB for anion recognition in water and for HS^- in particular, HB analogues of each receptor were also synthesised.

3.3.1. Synthesis

3.3.1.1. Synthesis of benzyl TEG azide

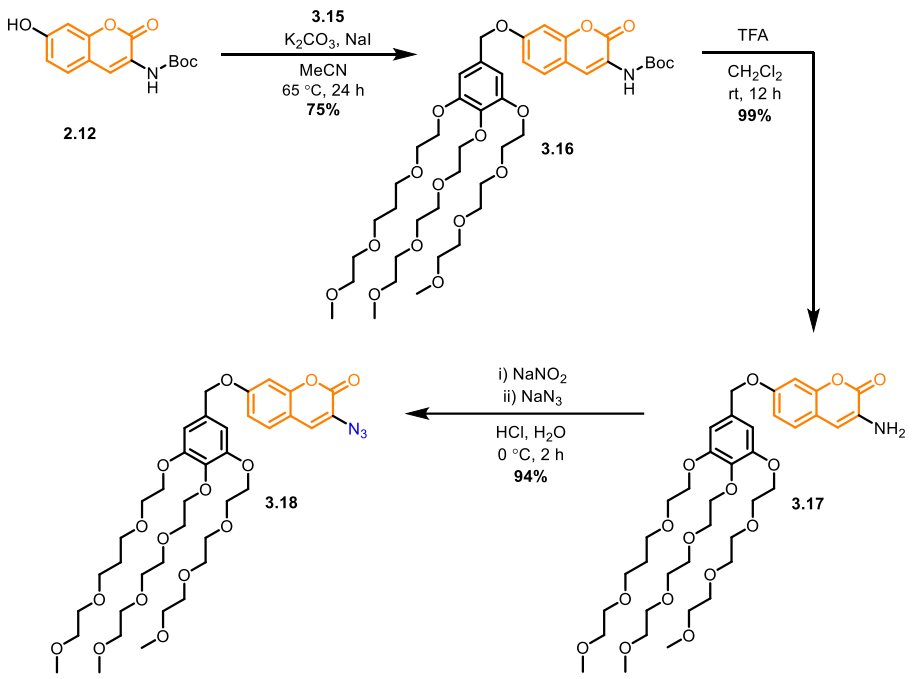
Benzyl TEG group derivatives **3.13**, **3.14** and **3.15** were prepared according to a literature procedure.[14] Methyl 3,4,5-trihydroxybenzoate was stirred with three equivalents of TEG tosylate **3.1** and heated under basic conditions to afford TEG ester **3.13** in a yield of 71%. Subsequent reduction of the ester group was achieved using $LiAlH_4$, producing TEG alcohol

3.14 in an 80% yield. Alcohol **3.14** was converted to the chloro derivative **3.15** in a quantitative yield by stirring and heating with thionyl chloride in chloroform (Scheme 3.7).



Scheme 3.7: *Synthesis of water soluble chloro derivative* ***3.15***

Boc-protected coumarin **2.12** was reacted with chlorobenzyl derivative **3.15** in acetonitrile under basic conditions, affording coumarin **3.16** in a yield of 75%. Boc-deprotection of **3.16** to amine **3.17** was achieved in a quantitative yield by stirring with TFA in CH_2Cl_2. Ensuing conversion of the amine to the azide was achieved by reacting with $NaNO_2$ and NaN_3 in acidic water, affording target water soluble coumarin azide **3.18** in an 94% yield with no purification required (Scheme 3.8).



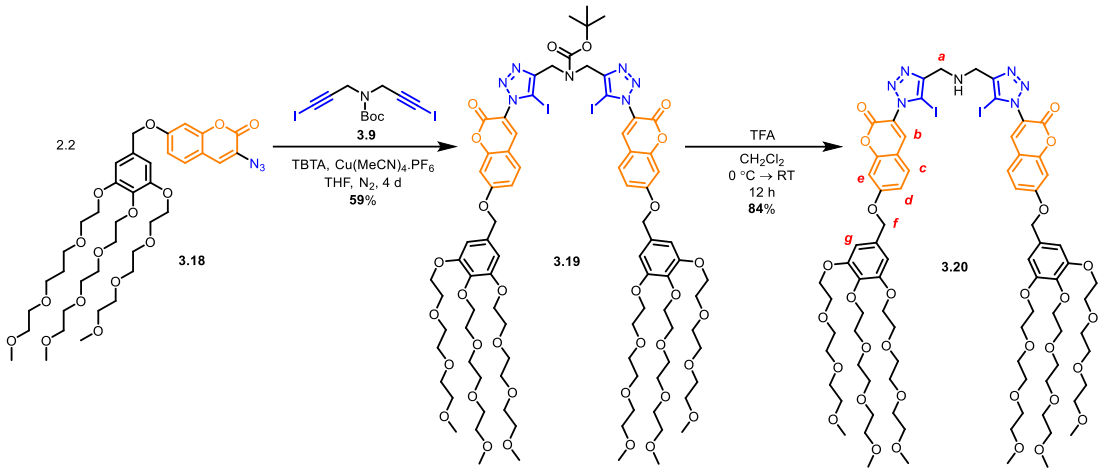
Scheme 3.8: *Synthesis of water soluble coumarin azide* ***3.18***

3.3.1.2. Synthesis of receptors

A series of XB and HB receptors were synthesised via CuAAC reactions using coumarin azide **3.18** and various bis-alkyne synthons.

3.3.1.2.1. Synthesis of secondary amine XB and HB receptors

One equivalent of bis-iodoalkyne **3.9** was stirred with 2.2 equivalents of coumarin azide **3.18**. under CuAAC conditions with TBTA and $Cu(MeCN)_4.PF_6$ in dry THF. The reaction was left to stir at room temperature under N_2 for 4 days and chromatographic purification afforded Boc-protected receptor **3.19** in a yield of 59%. Subsequent deprotection was achieved in a yield of 84% by stirring with TFA in CH_2Cl_2, to give the desired receptor **3.20** (Scheme 3.9), characterised by ^1H NMR (Figure 3.19), ^{13}C NMR and HRMS (Figure 3.20).



Scheme 3.9: *Synthesis of secondary amine XB receptor* ***3.20***

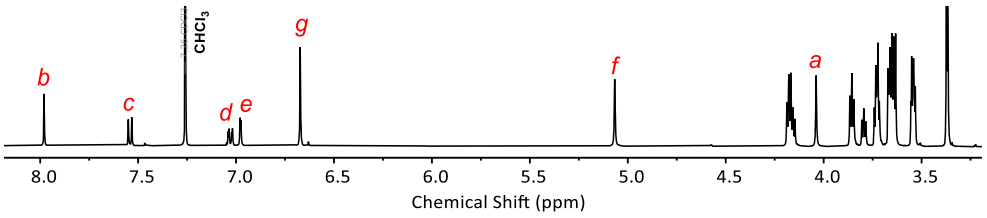


Figure 3.19: *Truncated ^{1}H NMR Spectrum of receptor* ***3.20*** *($CDCl_3$, 298 K)*

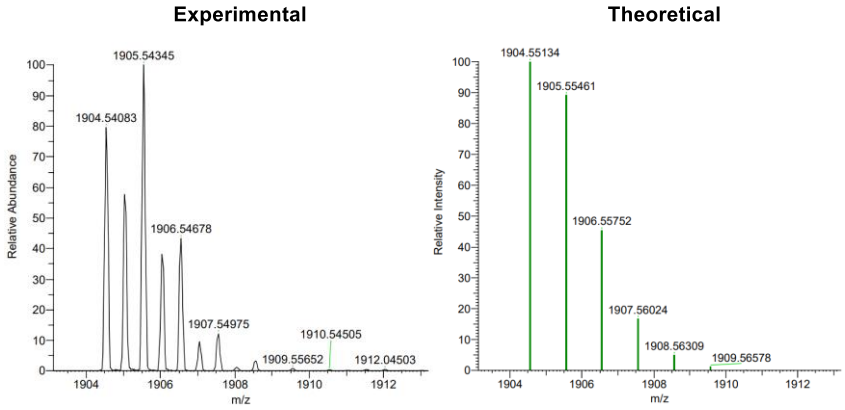
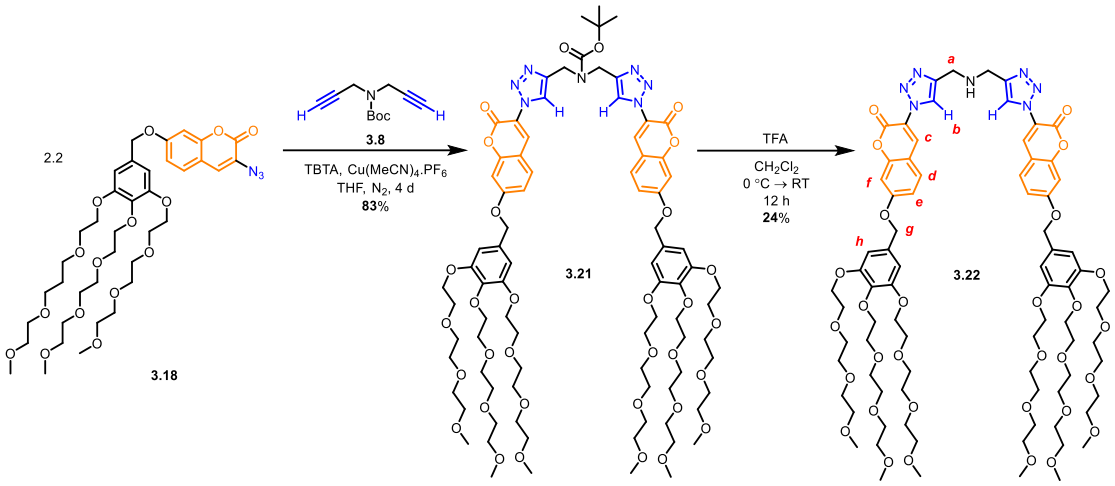


Figure 3.20: *HRMS experimental and theoretical spectrum of receptor* ***3.20,*** *m/z = 1904.55375 ($[M + H]^+$, $C_{80}H_{112}I_2N_7O_{30}$, calc = 1904.54083)*

Analogous reactions were conducted in the synthesis of the HB analogue **3.22** (Scheme 3.10). Bis-protoalkyne **3.8** and 2.2 equivalents of coumarin azide **3.18** were stirred in dry THF with 0.3 equivalents of $Cu(MeCN)_4.PF_6$ and 0.2 equivalents of TBTA. Chromatographic purification gave Boc-protected derivative **3.21** in a yield of 83%. Deprotection of **3.21** with TFA in CH_2Cl_2, afforded **3.22** in a low yield of 24% (Scheme 3.10). The low yield was attributed to difficulty in purification owing to the receptor's high water solubility. HB receptor **3.22** was characterised by ^{1}H NMR (Figure 3.21), ^{13}C NMR and MS (Figure 3.22).



Scheme 3.10: *Synthesis of secondary amine HB receptor* ***3.22***

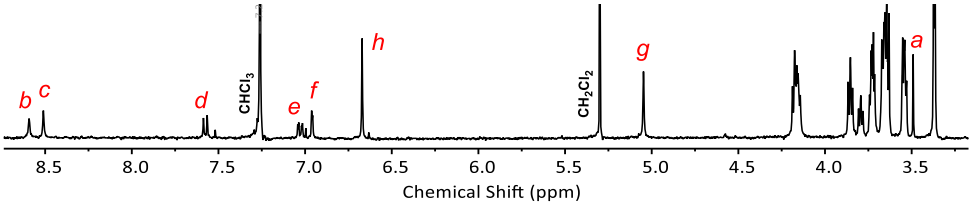


Figure 3.21: *Truncated* ^{1}*H NMR Spectrum of receptor* ***3.22*** *(*$CDCl_3$*, 298 K)*

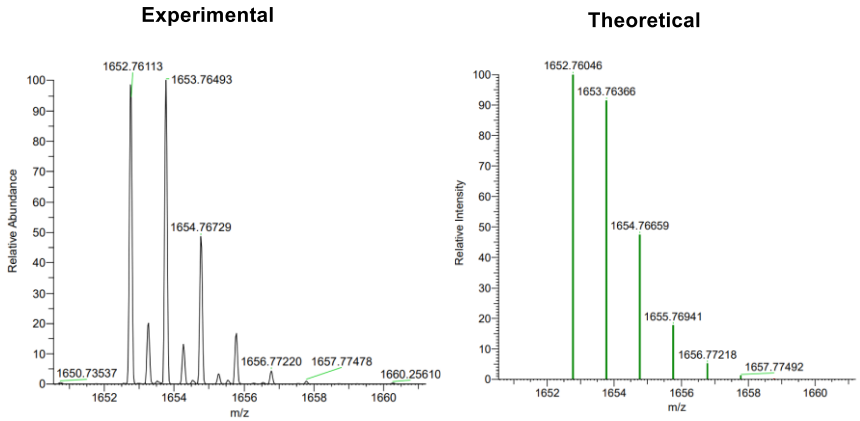
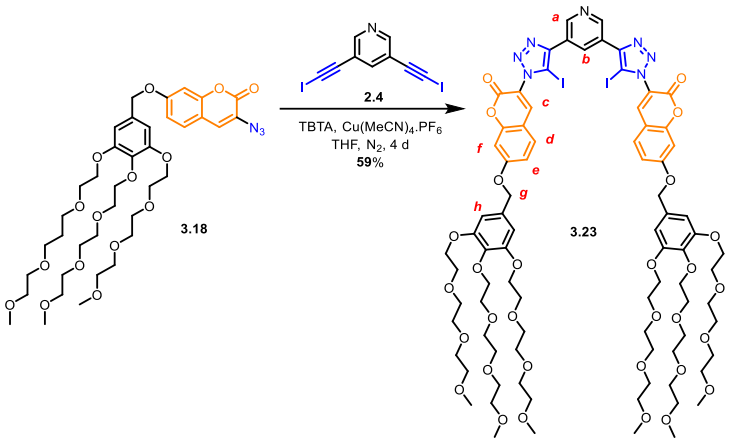


Figure 3.22: *HRMS experimental and theoretical spectrum of receptor* ***3.22,*** *m/z = 1774.79484 ([M + Na]+,* $C_{85}H_{121}N_7O_{32}$*, calc = 1774.79556)*

3.3.1.2.2. Synthesis of XB and HB pyridine receptors

Bis-iodoalkyne **2.4** and 2.2 equivalents of coumarin azide **3.6** were dissolved in dry THF before 0.3 equivalents of $Cu(MeCN)_4.PF_6$ and 0.2 equivalents of TBTA were added, the reaction was left to stir for 4 days under N_2. Purification via PTLC afforded the pyridine receptor **3.23** in a yield of 59% (Scheme 3.11). Receptor **3.23** was characterised by ^{1}H NMR (Figure 3.23), ^{13}C NMR and HRMS (Figure 3.24).



Scheme 3.11: *Synthesis of water soluble XB receptor* ***3.23***

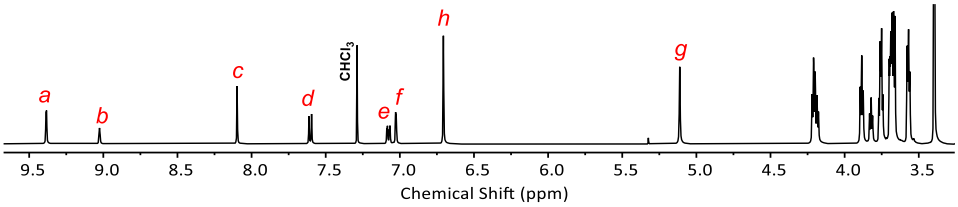


Figure 3.23: *Truncated ^{1}H NMR Spectrum of receptor* ***3.23*** *($CDCl_3$, 298 K)*

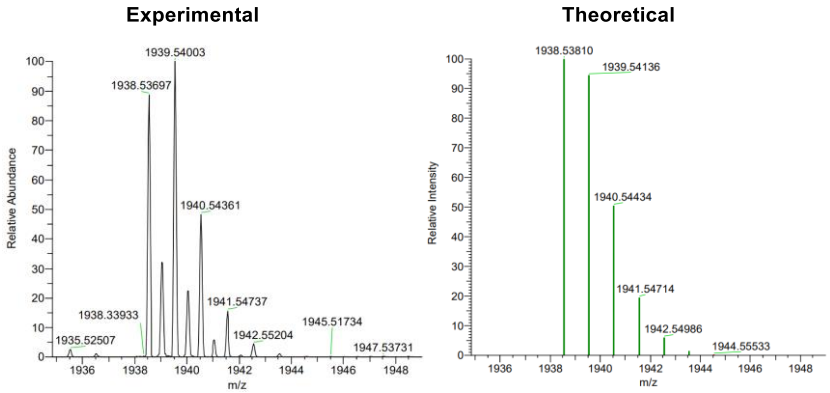
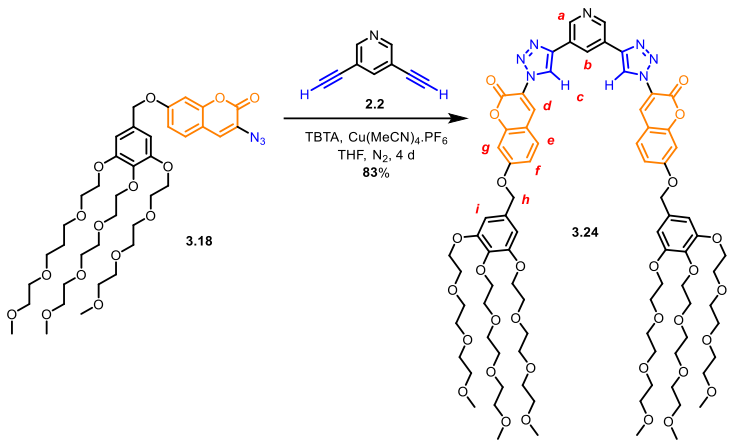


Figure 3.24: *HRMS experimental and theoretical spectrum of receptor* ***3.22,*** *m/z = 1938.53697 ($[M + H]^+$, $C_{83}H_{110}N_7O_{30}I_2$, calc = 1938.53810)*

An analogous CuAAC reaction was used for the synthesis of the HB analogue **3.24** (Scheme 3.12). The receptor's ^{1}H NMR and HRMS are shown in Figure 3.26 and Figure 3.27 respectively.



Scheme 3.12: *Synthesis of water-soluble HB receptor* ***3.24***

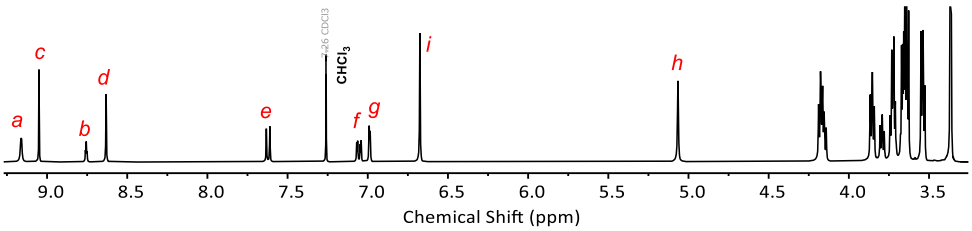


Figure 3.25: *Truncated ^{1}H NMR Spectrum of receptor* ***3.24*** *($CDCl_3$, 298 K)*

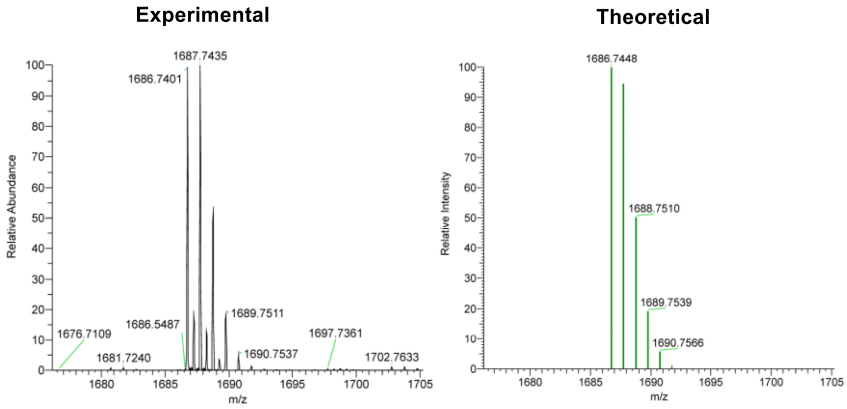
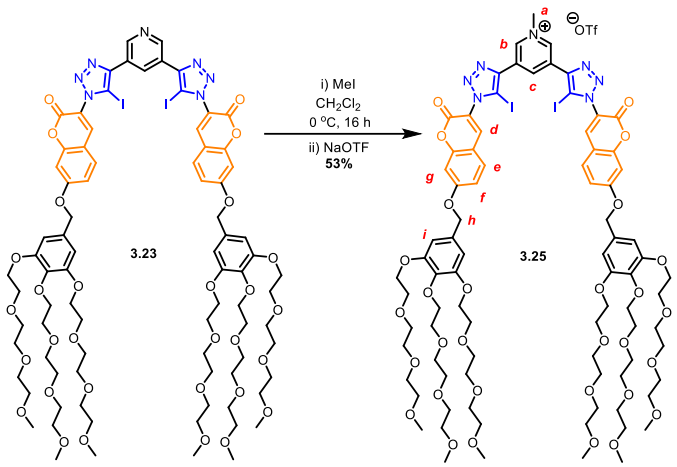


Figure 3.26: *HRMS experimental and theoretical spectrum of receptor* ***3.24,*** *m/z = 1686.7401 ($[M + H]^+$, $C_{83}H_{111}N_7O_{30}$, calc= 1686.7448)*

3.3.1.2.3. Synthesis of XB and HB pyridinium receptors

XB pyridine receptor **3.23** was reacted with excess MeI in CH_2Cl_2 to afford the iodide salt which following anion exchange by passing through an Amberlite (triflate) column gave the pyridinium XB receptor **3.25** as the triflate salt in a yield of 54% (Scheme 3.13). Receptor **3.25** was characterised by ^{1}H NMR (Figure 3.27), ^{13}C NMR and HRMS (Figure 3.28).



Scheme 3.13: *Synthesis of water-soluble XB receptor* ***3.25***

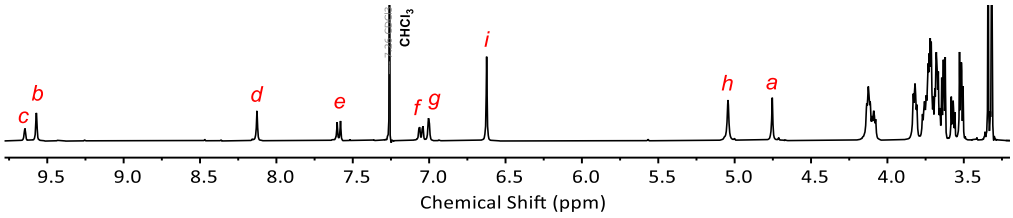


Figure 3.27: *Truncated ^{1}H NMR Spectrum of receptor* ***3.25*** *($CDCl_3$, 298 K)*

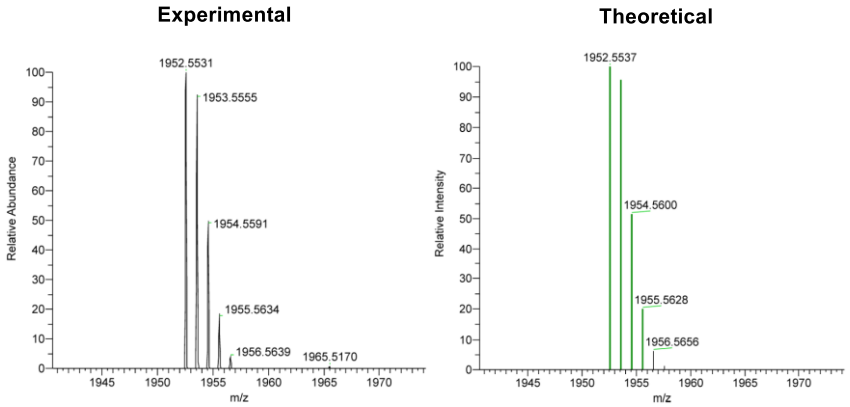
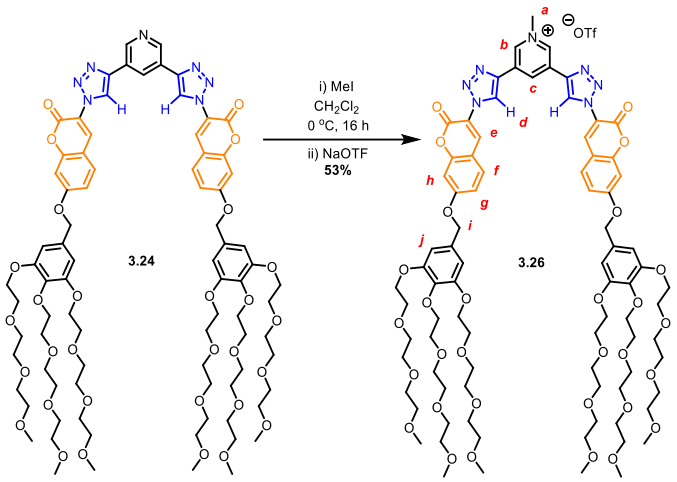


Figure 3.28: *HRMS experimental and theoretical spectrum of receptor* ***3.25,*** *m/z = 1952.5531 ($[M]^+$, $C_{84}H_{112}I_2N_7O_{30}^+$, calc= 1952.5537)*

An analogous procedure was used to prepare the corresponding HB pyridinium receptor **3.26** in a yield of 53% (Scheme 3.1).



Scheme 3.14: *Synthesis of water-soluble HB receptor* ***3.26***

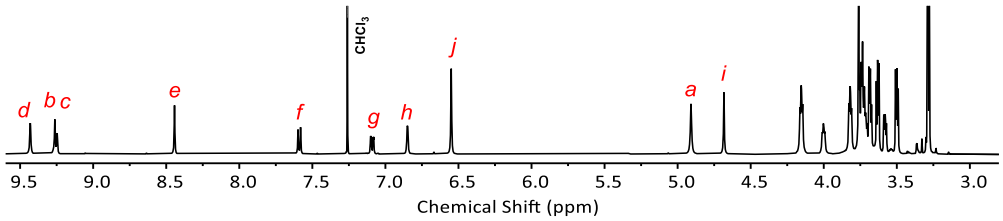


Figure 3.29: *Truncated ^{1}H NMR Spectrum of receptor* ***3.26*** *($CDCl_3$, 298 K)*

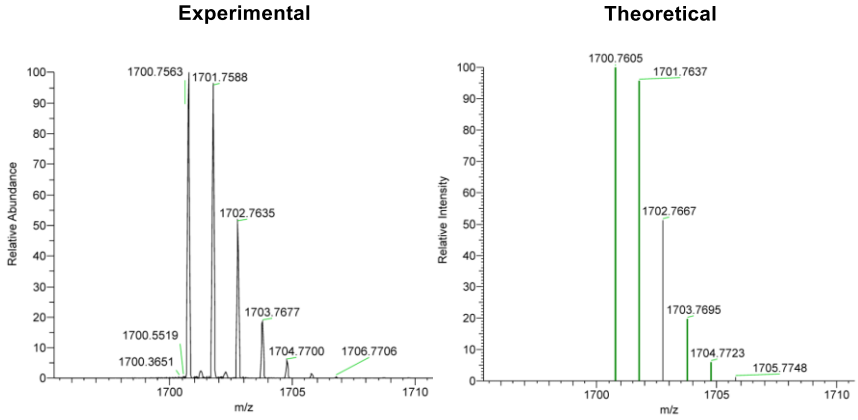


Figure 3.30: *HRMS experimental and theoretical spectrum of receptor* ***3.26,*** *m/z = 1700.7563 ($[M]^+$, $C_{84}H_{114}N_7O_{30}^+$, calc= 1700.7605)*

3.3.2. Anion Binding Studies

The anion binding and sensing properties of the six synthesised receptors (Figure 3.31) in water, were investigated via ^{1}H NMR and fluorescence titration experiments.

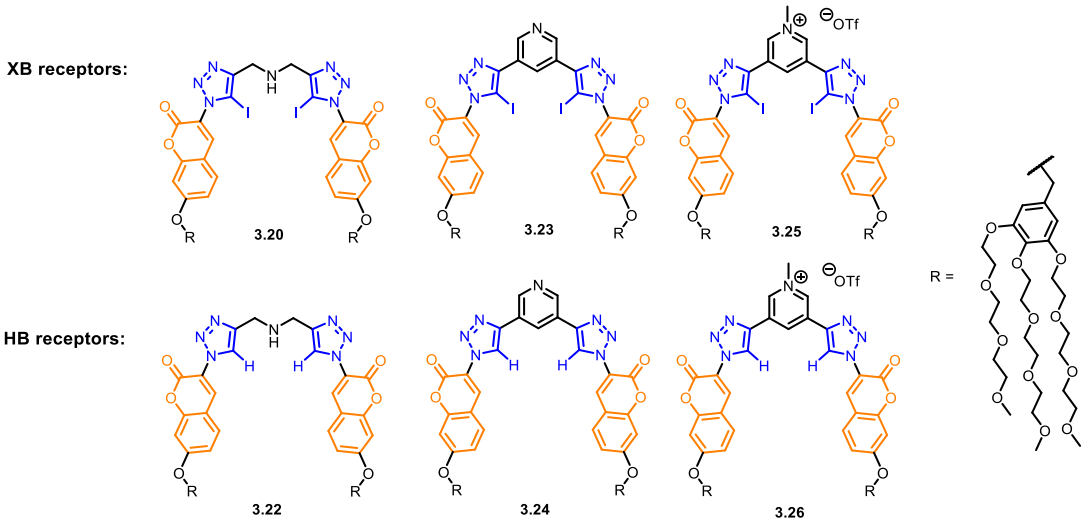


Figure 3.31: *HB and XB receptors* ***3.20****,* ***3.22****,* ***3.23****,* ***3.24****,* ***3.25*** *and* ***3.26****.*

3.3.2.1. ^{1}H NMR Studies

Preliminary ^{1}H NMR titration experiments of XB receptors **3.20**, **3.23** and **3.25** with NaHS were undertaken in D_2O. The addition of NaHS to receptor **3.20** resulted in negligible ($\Delta\delta$ < 0.02ppm) proton peak changes. This may be attributed to the insensitivity of the receptor's methylene and coumarin protons around the XB binding site in the competitive aqueous solvent medium. To further test the anion recognition properties of **3.20** and the central secondary amine in conjunction with the two XB donors, the receptor was dissolved in the organic/aqueous 45:45:10 $CD_3OD/CDCl_3/D_2O$ solvent mixture and protonated with one equivalent of HBF_4. On addition of HBF_4 significant downfield peak shifts were observed. Addition of 10 equivalents of NaI led to significant downfield shifts of the receptor's coumarin proton peaks (Figure 3.32), indicating that the principal binding site is directed by the XB motifs.

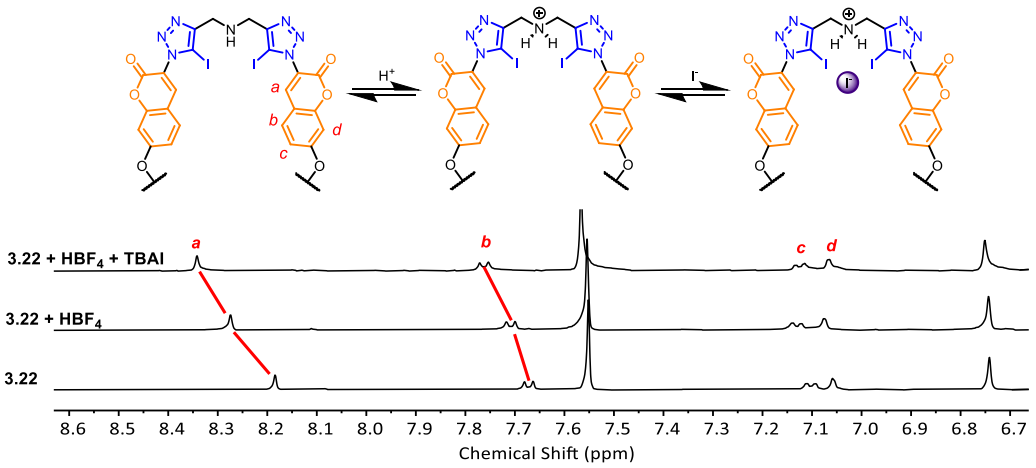
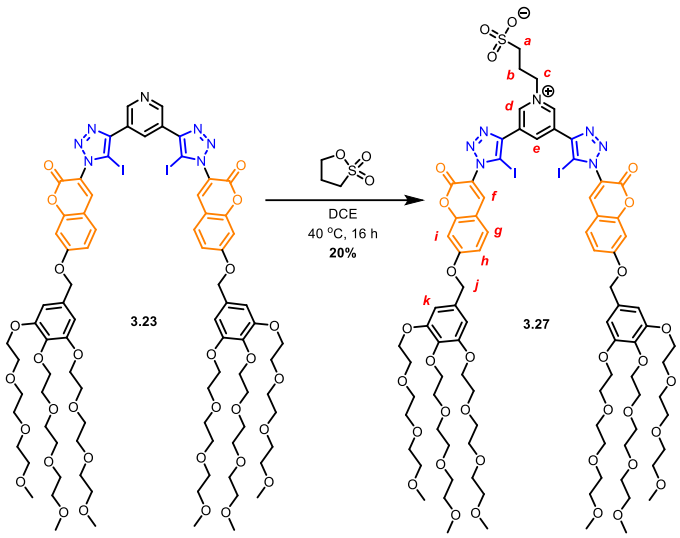


Figure 3.32: *Truncated ^{1}H NMR spectra of receptor **3.22**, receptor **3.22** and 1 equivalent of HBF_4, and receptor **3.22** with 1 equivalent of HBF_4 and 10 equivalents of TBAI.*

Unfortunately, receptors **3.23** and **3.25** were found to be insoluble in D_2O at the desired ^{1}H NMR concentration of 1 mM and at the reduced concentration of 0.5 mM.

As an alternative to D_2O, ^{1}H NMR titration experiments were attempted in d_6-DMSO. However, upon addition of NaHS to d_6-DMSO, prior to the titration with the respective receptor, the solution turned green, suggesting a reaction had taken place. Although HS^- is well-known to be a potent nucleophile, the result was unexpected, as recent chemodosimeter literature reports have claimed the detection of H_2S/HS^- in DMSO.[15] Nonetheless, the reactions of H_2S and HS^- with sulfoxides have been widely reported.[16] Other ^{1}H NMR titration experiments with **3.25** in organic-aqueous mixtures led to precipitation of the receptor upon addition of NaHS.

In an effort to further enhance water solubility, a zwitterionic receptor was synthesised (Scheme 3.15). 1,3-Propane sultone was added to pyridine receptor **3.23** and left to stir in DCE at 40 ˚C for 16 h. The zwitterion **3.27** was isolated via PTLC in a 20% yield and characterised by ^{1}H NMR (Figure 3.33), ^{13}C NMR and HRMS (Figure 3.34).



Scheme 3.15: *Synthesis of zwitterionic receptor* ***3.27***

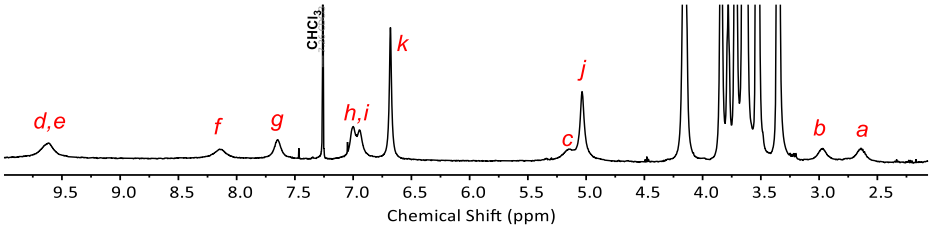


Figure 3.33: *Truncated ^{1}H NMR spectrum of receptor* ***3.27*** *($CDCl_3$, 298 K)*

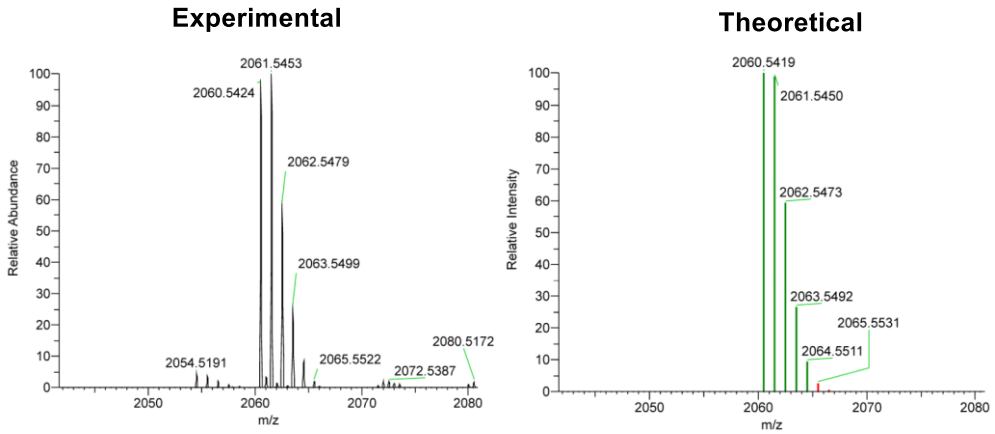


Figure 3.34: *HRMS experimental and theoretical spectrum of receptor* ***3.27,*** *m/z = 2060.5424 ($[M+H]^+$, $C_{86}H_{115}I_2N_7O_{33}S$, calc = 2060.5419)*

Despite it's zwitterionic nature, the receptor was still not soluble enough for ^{1}H NMR titration experiments in D_2O, even at reduced concentrations. To balance the need for complete solubility and the capability to dissolve NaHS, a solvent mixture of 4:2:1 D_2O-CD_4CN-MeOD was chosen. *d_6*-Acetone was not used due to its known reactivity with H_2S.[17] On addition of NaHS to **3.27,** modest perturbations of the receptor's pyridinium protons can be observed

(Figure 3.35). However, after further addition of NaHS, significant broadening and the emergence of new proton signals are seen which suggested receptor decomposition.

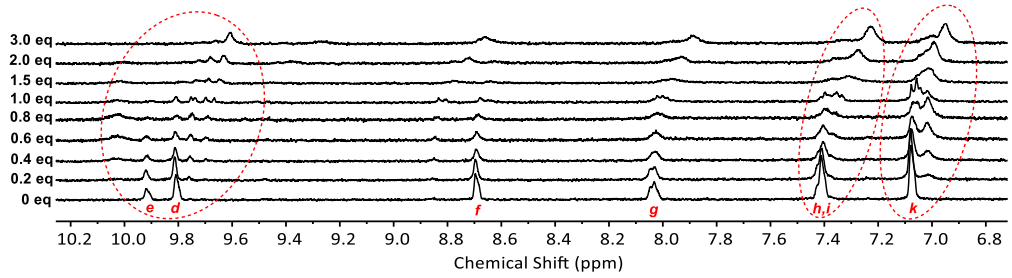


Figure 3.35: *^{1}H NMR titration of receptor **3.27** with NaHS (4:2:1 D_2O-CD_3CN-MeOD, 298 k). Highlighted regions show emergence of new peaks.*

In pure water the nucleophilicity of HS^- is significantly reduced and no evidence of reaction with the receptors has been observed on the spectroscopic timescales. In an aqueous-organic solvent mixture with aprotic solvents however, the nucleophilicity of HS^- is greater due to reduced solvation and stabilisation, enabling HS^- to potentially react with the receptor. The observations with receptor **3.27** highlight the apparent instability of XB donors for HS^- in aqueous-organic solvent media.

3.3.2.2. pK_a determination of secondary amine XB and HB receptors

The pK_a values of secondary amine receptors **3.20** and **3.22** were experimentally determined by monitoring the respective receptor's change in fluorescence emission intensity with pH. Samples were prepared in pure H_2O at a concentration of 10 µM and the pH adjusted to around 3.5 by addition of concentrated HCl. The pH was slowly increased by addition of dilute NaOH and the emission spectra recorded. With both receptors, as the pH increased a decrease in receptor fluorescence intensity was observed (Figure 3.36). This was ascribed to the increasing concentration of secondary amine versus protonated amine ratio to induce PET quenching. Two pK_a values were determined for each receptor (Table 3.6). The lower value was attributed to the pK_a of the triazole groups and the higher to the secondary amine. The value of the iodotriazole pK_a is notably lower than the prototriazole pK_a, 4.07 and 5.91 respectively. This is likely due to the electron withdrawing nature of the iodine substitutent making protonation less favourable. Conversely the XB receptor **3.20** has a higher value for the secondary amine pK_a, 10.29 compared to 9.98, in spite of the iodine's electron withdrawing nature. This suggests that the iodotriazole is stabilising the conjugate acid to a greater extent than the prototriazole. Interactions between protons and the negative equatorial belt of the XB iodine atom have been reported and actively incorporated into

receptor design.[18] The conjugate acid may therefore be stabilised by a hydrogen bond between the amine protons and the iodine (Figure 3.37); which as a result may also enhance XB anion recognition properties.

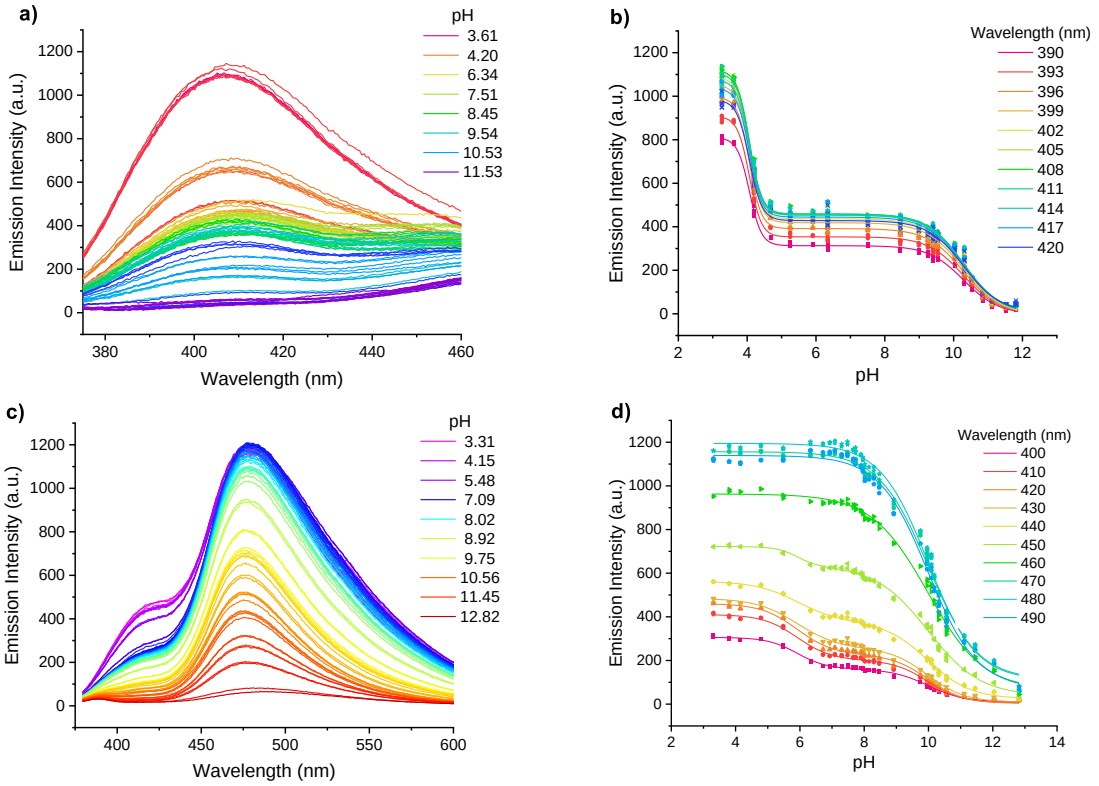


Figure 3.36: *Fluorescence pH titrations: overlaid emission spectra showing intensity decrease with increasing pH* ***a)*** *XB receptor* ***3.20 c)*** *HB receptor* ***3.22****; intensity plotted against pH for varying wavelengths showing a double sigmoidal curve and the equivalence points from which the* pK_a *values were determined* ***b)*** *XB receptor* ***3.20 d)*** *HB receptor* ***3.22****.*

Table 3.6: *Experimentally determined* pK_a *values of receptors* ***3.20*** *and* ***3.22*** *in* H_2O

Receptor	pK_{a1}	pK_{a2}
3.20 (XB)	4.07 ± 0.01	10.29 ± 0.01
3.22 (HB)	5.91 ± 0.07	9.98 ± 0.01

[10 μM], 298K

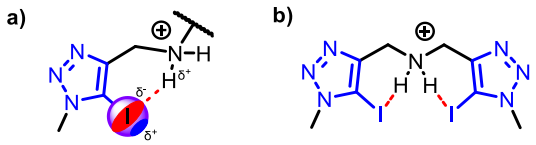


Figure 3.37: *Representation of the intramolecular hydrogen bond between the protonated secondary amine and the negative equatorial belt region of the iodine.*

The experimentally determined pK_a values demonstrate that both receptors will be protonated in aqueous solution and therefore will be denoted as **3.20H**$^+$ and **3.22H**$^+$.

3.3.2.3. Photophysical Studies

The photophysical properties of receptors are shown in Figure 3.38 and Table 3.7. All samples were prepared in pH 7.4 10 mM HEPES aqueous solution at a concentration of 10 µM. As H_2S has a pK_a of 7.0, this pH 7.4 buffer solution was chosen to ensure that HS^- remains the dominant species. In addition, at a pH of 7.4 the solution mimics physiological conditions and gives an insight into the potential functionality of these systems in a biological setting.

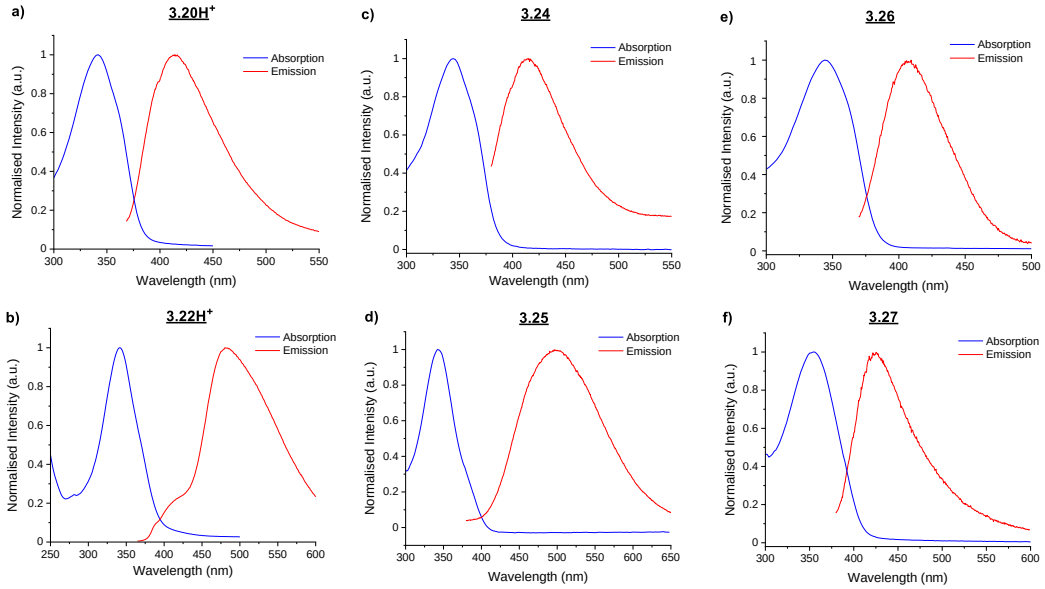


Figure 3.38: *Spectra of absorption and emission for receptors in 10 µM HEPES aqueous solution (pH 7.4, 298 k).*

Table 3.7: *Wavelengths of absorption and emission for receptors in 10 μM HEPES aqueous solution (pH 7.4, 298 k).*

Receptor	$\lambda_{max\ abs}$ / nm	$\lambda_{max\ ems}$ / nm	Stokes Shift / nm
3.20H$^+$ (XB)	342	412	70
3.22H$^+$ (HB)	342	484	142
3.23 (XB)	344	414	70
3.24 (HB)	342	498	156
3.25 (XB)	344	408	64
3.26 (HB)	354	424	70

Emission wavelength excited at $\lambda_{max\ abs}$, [10 μM], 298 K.

Characteristic wavelengths of absorption for coumarin molecules were observed for the receptors in the 10 mM HEPES aqueous solution (Table 3.7). Interestingly, the emission spectra of HB receptors **3.22H$^+$** and **3.24** are significantly more red shifted than their XB analogues. This is in spite of the known influence of electronegative atoms, such as iodine, causing bathochromic shifts in fluorophores.[19] The large extent to which the emission is shifted suggests that the origin of the change is not due to a difference in electronegativity. Looking at the structure of the receptors it may be that there are intramolecular hydrogen bonds occurring between the proto-triazoles and the coumarin carbonyl group (Figure 3.40).[20] In such a case, the internal charge transfer, which is responsible for the fluorescence characteristics, from the oxygen at the 7 position to the coumarin carbonyl will be stabilised, therefore inducing a bathochromic shift and a reduction in the energy transition.[19] Pyridinium HB receptor **3.26**, also capable of forming an intramolecular bond, however, does not display as significant a bathochromic shift, though it does have a greater Stokes shift than the XB analogue. Because of the conjugated cationic charge in receptor **3.26** the dipole moment of the triazole hydrogen is enhanced and therefore has greater interactions with the solvent water. It is likely that the solvent water molecules disrupt the formation of the intramolecular bond, therefore reducing the red shift to the smaller extent which is observed.

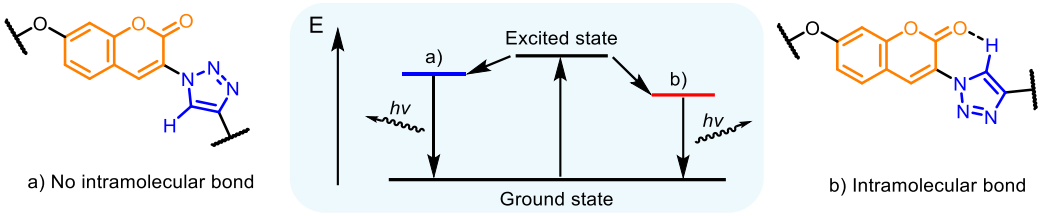


Figure 3.40: *Excitation and emission of a) a non-intramolecular HB conformation and a b) intramolecular HB conformation.*

3.3.2.3.1. XB receptor 3.20H⁺ and HB receptor 3.22H⁺ Fluorescence Titration Studies

The anion sensing properties of receptors **3.20H⁺** and **3.22H⁺** were investigated using fluorescence spectroscopy upon the addition of NaCl, NaBr, NaI and NaHS in pH 7.4 10 mM HEPES aqueous solution.

On addition of up to 30 equivalents of NaI and NaHS to XB receptor **3.20H⁺**, a decrease in fluorescence was observed by up to 10% and 36% respectively (Figure 3.39c, d) — further equivalents of anions added resulted in precipitation of the receptor. Conversely, addition of NaCl and NaBr induced no significant fluorescence intensity diminutions (Figure 3.39a, b). Interestingly, analogous titrations with the HB analogue **3.22H⁺** showed no observable fluorescence intensity changes upon addition of any of the anions (Figure 3.40). This observed contrast between XB and HB highlights the significance of XB for anion recognition and sensing in competitive aqueous solutions. The two anions sensed, iodide and HS^-, are the least well-solvated, showing that the XB receptor is displaying the Hofmeister selectivity bias towards these hydrophobic anions.

These fluorescent sensing observations deviate from those of the generation 1 secondary XB amine receptor **3.11H⁺**, in which bromide was also sensed. Due to the change in water solubilising groups, the generation 2 XB receptor **3.20H⁺** is of lower mono-cationic charge compared to **3.11H⁺**, which is tri-cationic when taking into account the receptor's two protonated tertiary amine solubilising groups. This reduction in electrostatic attraction may be responsible for **3.20H⁺** not sensing bromide.

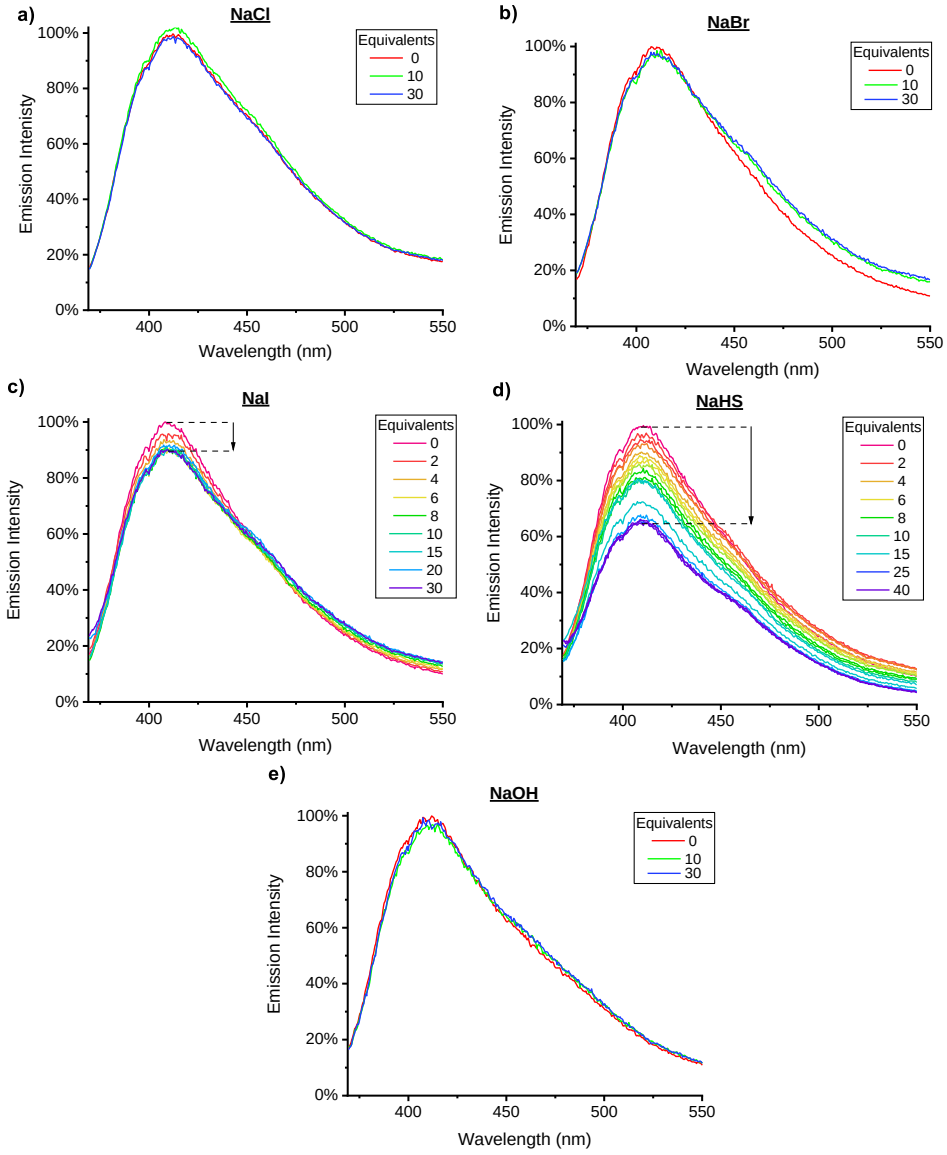


Figure 3.39: *Fluorescence emission intensity changes of receptor* ***3.20H*** $^{+}$ *upon addition of anions:* ***a)*** *NaCl* ***b)*** *NaBr* ***c)*** *NaI* ***d)*** *NaHS* ***e)*** *NaOH (10 mM HEPES aqueous solution, pH 7.4, 298 k).*

As observed in the generation 1 receptor **3.11H**$^{+}$**,** HS^{-} induces a more significant degree of quenching than iodide. Although the titration was conducted in a buffered solution, an increase of the pH could explain the origin of the characteristic intensity change upon addition of basic NaHS. Therefore, to investigate whether changes to the pH were responsible, receptor **3.20H**$^{+}$ was titrated against NaOH (Figure 3.39e). No intensity changes were observed, further supporting the belief that HS^{-} is being sensed via anion recognition.

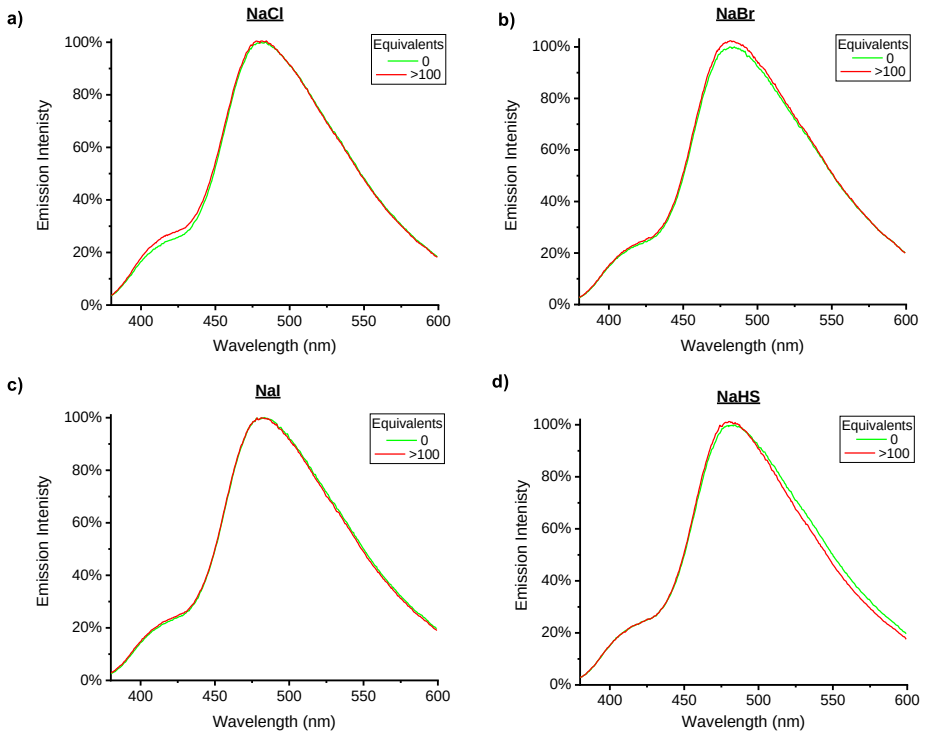


Figure 3.40: *Fluorescence emission intensity changes of receptor* ***3.22H⁺*** *upon addition of anions:* ***a)*** *NaCl* ***b)*** *NaBr* ***c)*** *NaI* ***d)*** *NaHS (10 mM HEPES aqueous solution, pH 7.4, 298 k).*

HB receptor **3.22H⁺** is notably more soluble and did not precipitate out of solution on addition of the sodium salts, while on addition of upwards of 40 equivalents of NaI and NaHS to XB receptor **3.20H⁺** precipitation did occur. This draws into question whether the observed intensity changes may be the result of aggregation-induced quenching, particularly because both iodide and HS^- are hydrophobic anions prone to salting-out effects.[21] In order to investigate the concentration dependence of the fluorescence emission, the intensity was measured at different concentrations (Figure 3.41). The linear relationship observed between concentration and emission intensity shows that, at the starting concentration, there is no aggregation of the receptor.

Association constants for XB receptor **3.20H⁺** were determined using Bindfit (Table 3.8 and Figure 3.42). The association constant for iodide was found to be an order of magnitude greater than that for HS^-. However unlike with the generation 1 XB receptor **3.11H⁺,** the value for iodide is significantly lower which may again, because of the protonated tertiary amine substituents, be attributable to the overall higher charge of **3.11H⁺**. The value for HS^- is also lower than **3.11H⁺** but the difference is not as significant. This reduced difference indicates that the binding of HS^-, in comparison to iodide, is influenced more by XB than electrostatic attraction.

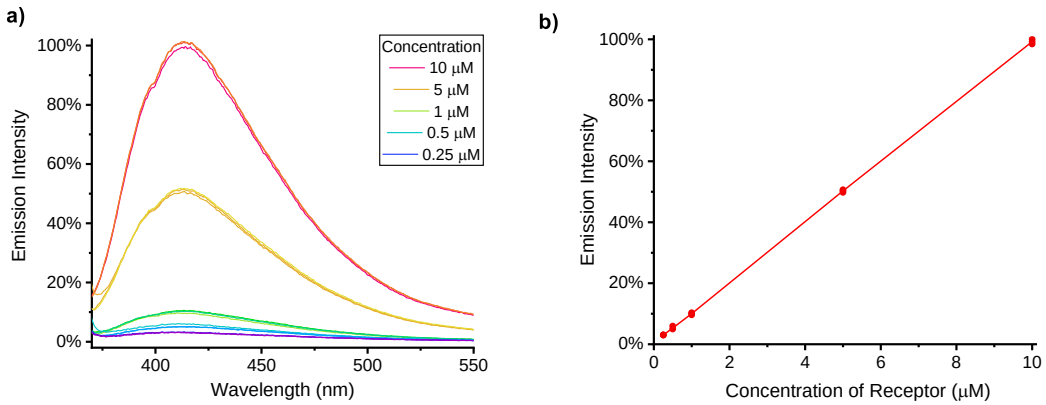


Figure 3.41: *Emission intensity changes with changing concentration of receptor* ***3.22H⁺*** *(10 mM HEPES aqueous solution, pH 7.4, 298 K).*

Table 3.8: *Anion association constants for receptors* ***3.20H⁺*** *and* ***3.22H⁺***

Anion	Association Constants K_a (M^{-1})	
	3.20H⁺	**3.22H⁺**
Cl^-	nb	nb
Br^-	nb	nb
I^-	46000 ± 14000	nb
HS^-	5600 ± 530	nb

Anion association constants with errors determined using 1:1 stiochiometric Bindfit analysis of the fluorescence emission of receptors **3.20H⁺** and **3.22H⁺,** 10 μM receptor in 10 mM HEPES aqueous solution, pH 7.4, 298 K. nb = no binding observed.

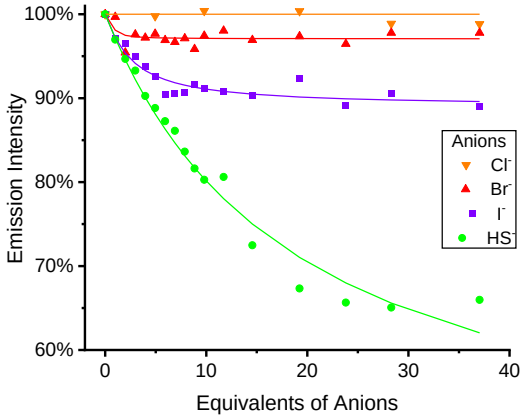


Figure 3.42: *Binding isotherms and 1:1 stoichiometric Bindfit fit of fluorescence emission titration data for receptor* ***3.20H⁺*** *(10 μM) upon addition of NaCl, NaBr, NaI and NaHS in 10 mM HEPES aqueous solution, pH 7.4, 298 K.*

3.3.2.3.2. XB receptor 3.23 and HB receptor 3.24 Fluorescence Titration Studies

Analogous fluorescence spectroscopy titrations were conducted for pyridine receptors XB **3.23** and HB **3.24** with NaCl, NaBr, NaI and NaHS in pH 7.4 10 mM HEPES aqueous solution (Figure 3.43 and Figure 3.44).

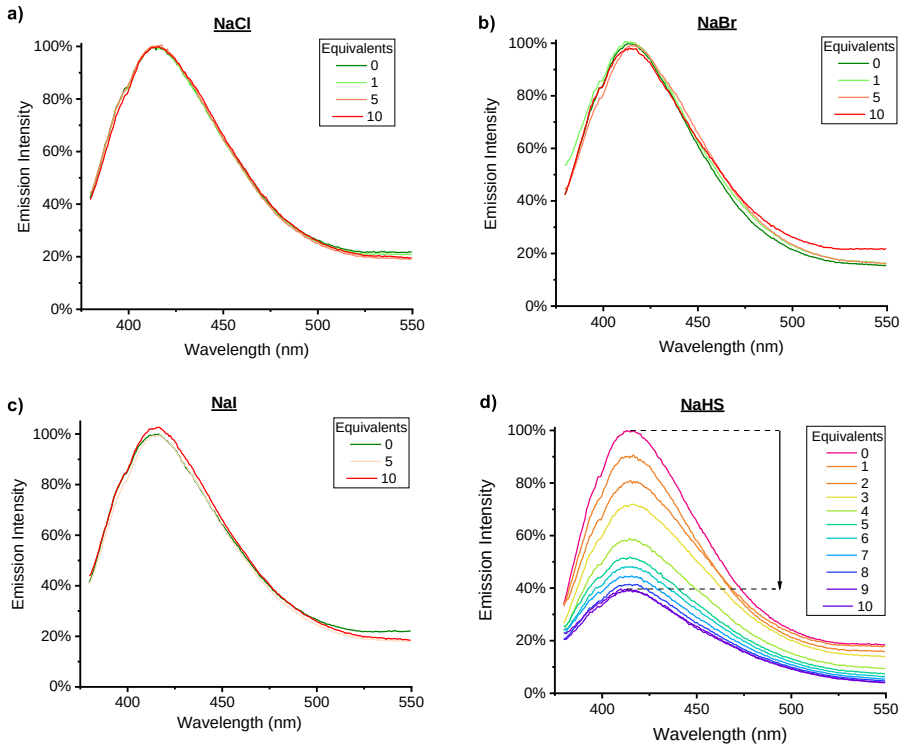


Figure 3.43: *Fluorescence emission intensity changes of receptor* ***3.23*** *upon addition of anions:* ***a)*** *NaCl* ***b)*** *NaBr,* ***c)*** *NaI* ***d)*** *NaHS (10 mM HEPES aqueous solution, pH 7.4, 298 k).*

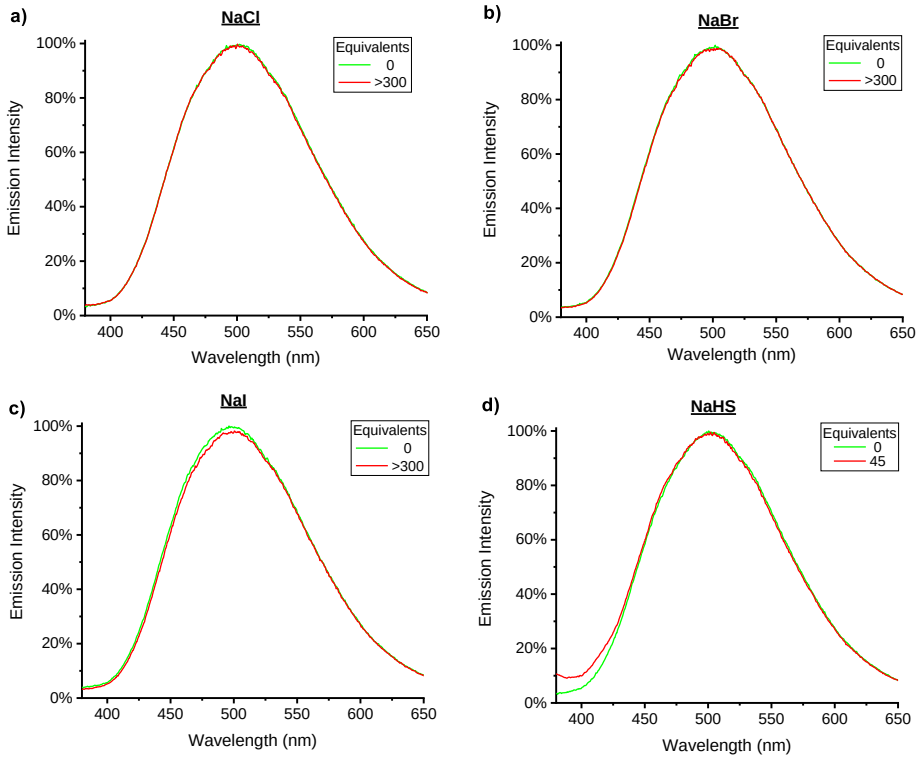


Figure 3.44: *Fluorescence emission intensity changes of receptor* ***3.24*** *upon addition of anions:* ***a)*** *NaCl* ***b)*** *NaBr* ***c)*** *NaI* ***d)*** *NaHS (10 mM HEPES aqueous solution, pH 7.4, 298 k).*

On addition of halides to XB receptor **3.23**, no fluorescence intensity change was observed. In stark contrast, addition of 10 equivalents of NaHS induced quenching by up to 60% (Figure 3.43d) — addition of more than 10 equivalents of sodium salts to **3.23** caused precipitation. Furthermore, HB receptor **3.24** displayed no emission response on addition of any anion (Figure 3.44).

The exclusive selectivity and characteristic quenching for HS^- by XB receptor **3.23** is unprecedented. The development of a XB sensor, selective for HS^- over Cl^- and other anions in water, is the core objective of this research.

Table 3.9: *Anion association constants for receptors **3.23** and **3.24***

Anion	Association Constants K_a (M^{-1})	
	3.23	**3.24**
Cl^-	nb	nb
Br^-	nb	nb
I^-	nb	nb
HS^-	16500 ± 530	nb

Anion association constants with errors determined using 1:1 stoichiometric BindFit analysis of the fluorescence emission of receptors **3.23** and **3.24,** 10 µM receptor in 10 mM HEPES aqueous solution, pH 7.4, 298 K. nb = no binding observed.

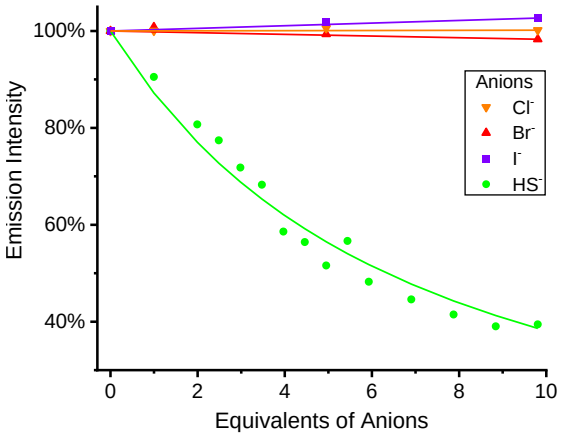


Figure 3.45: *Binding isotherms and 1:1 stoichiometric Bindfit analysis of fluorescence emission titration data for receptor **3.23** (10 µM), upon addition of NaCl, NaBr, NaI and NaHS in 10 mM HEPES aqueous solution, pH 7.4, 298 K.*

It is noteworthy that the association constant for neutral XB **3.23** and HS^- (Table 3.9), determined by Bindfit analysis (Figure 3.45), was found to be an order of magnitude higher than for charged **3.20H$^+$**. This suggests again, the XB component for binding HS^- is more important than electrostatic attraction. In the previous section 3.2.2, the preorganised acyclic XB bis-iodotriazole pyridine motif was shown to be a more potent complexant of anions in organic solvents than the XB secondary amine group.

3.3.2.3.3. XB receptor 3.25 and HB receptor 3.26 Fluorescence Titration Studies

Analogous fluorescence spectroscopy anion titrations were undertaken with cationic pyridinium receptors **3.25** and **3.26** (Figure 3.46 and Figure 3.47).

The addition of 15 equivalents of NaBr, NaI and NaHS to XB receptor **3.25** led to fluorescence intensity quenching of 37%, 19% and 39% respectively (Figure 3.46b, c, d). On the other hand, NaCl induced no observable changes. Interestingly, bathochromic shifts of the emission wavelength maxima of 4 nm for HS^- and 2 nm for Br^- were observed, whereas I^- binding caused no shift (Figure 3.46b, c, d). This may occur due to the anion binding event arranging the receptor in a flat orientation with greater conjugation overlap across the coumarin, iodotriazole and pyridinium motifs, therefore stabilising the internal charge transfer from the coumarins oxygen.

The HB analogue **3.26** was unable to sense Cl^-, Br^- and HS^- but was found to exhibit a fluorescence quenching response of up to 29% with iodide (Figure 3.47c).

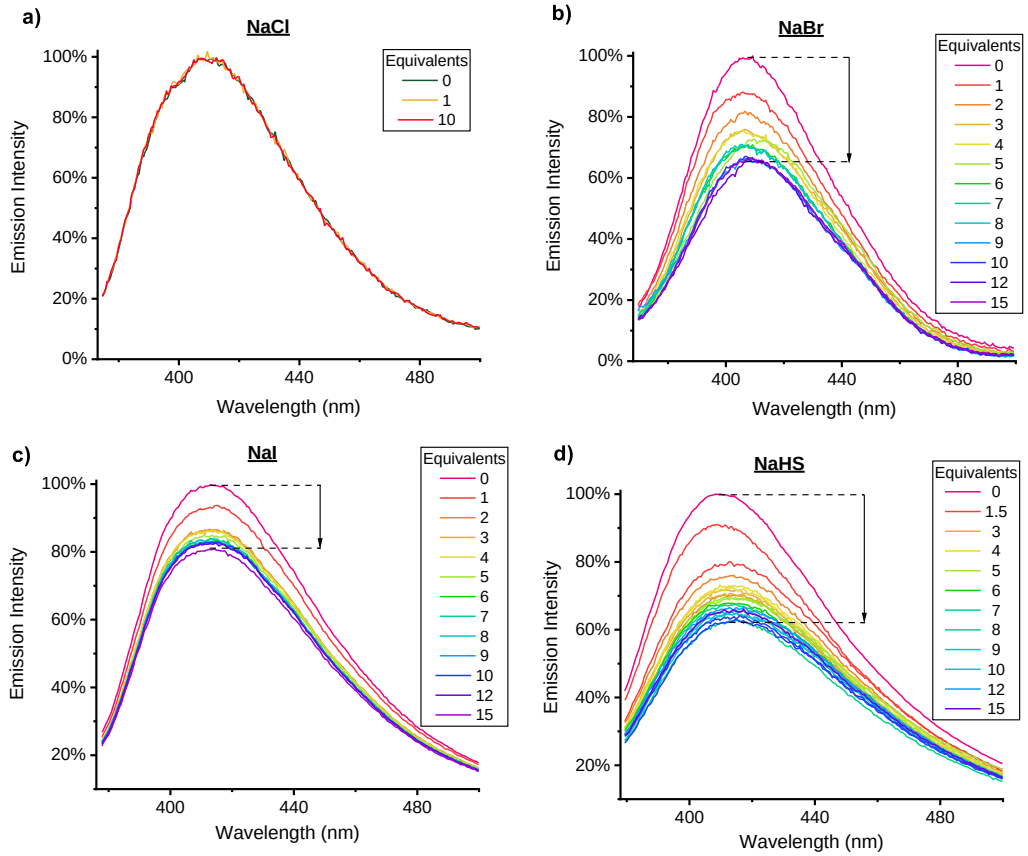


Figure 3.46: *Fluorescence emission intensity changes of receptor **3.25** upon addition of anions:* ***a)*** *NaCl* ***b)*** *NaBr,* ***c)*** *NaI* ***d)*** *NaHS (10 mM HEPES aqueous solution, pH 7.4, 298 k).*

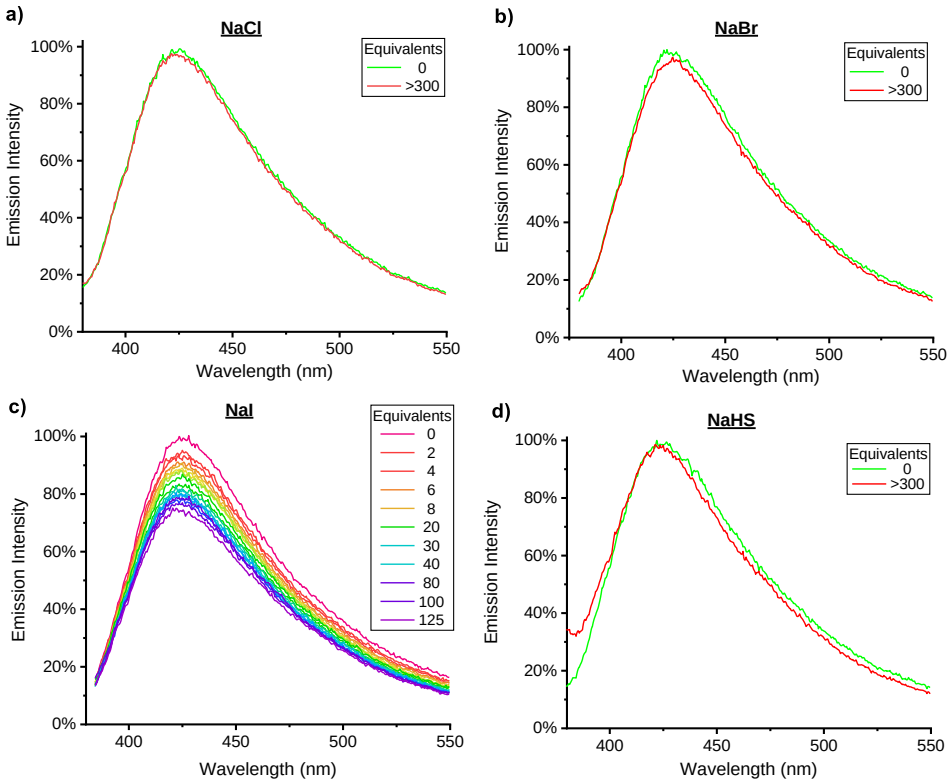


Figure 3.47: *Fluorescence emission intensity changes of receptor* ***3.26*** *upon addition of anions:* ***a)*** *NaCl* ***b)*** *NaBr,* ***c)*** *NaI* ***d)*** *NaHS (10 mM HEPES aqueous solution, pH 7.4, 298 k).*

Association constant values calculated from the isotherm titration data (Figure 3.48) for receptors **3.25** and **3.26** are shown in Table 3.10. The pyridinium component of receptor **3.25**, which introduces additional favourable electrostatic attraction and greater polarisation to the XB iodine donor atoms, is reflected in the increased association constants when compared to neutral pyridine receptor **3.23**. However, the increase in binding strength comes at the expense of a diminished degree of selectivity for HS^-, as **3.25** also binds bromide and iodide strongly. With an association constant for HS^- of over 150,000 M^{-1}, receptor **3.25** exhibits the greatest association constant magnitude for HS^- binding in water of all XB receptors reported to date.

Table 3.10: *Anion association constants for receptors* ***3.25*** *and* ***3.26***

Anion	Association Constants K_a (M^{-1})	
	3.25 (XB)	**3.26 (HB)**
Cl^-	nb	nb
Br^-	60,800 ± 7800	nb
I^-	103,000 ± 24000	6080 ± 550
HS^-	158,000 ± 31000	nb

Anion association constants with errors determined using 1:1 stoichiometric BindFit analysis of the fluorescence emission of receptors **3.25** and **3.26,** 10 µM receptor in 10 mM HEPES aqueous solution, pH 7.4, 298 K. nb = no binding observed.

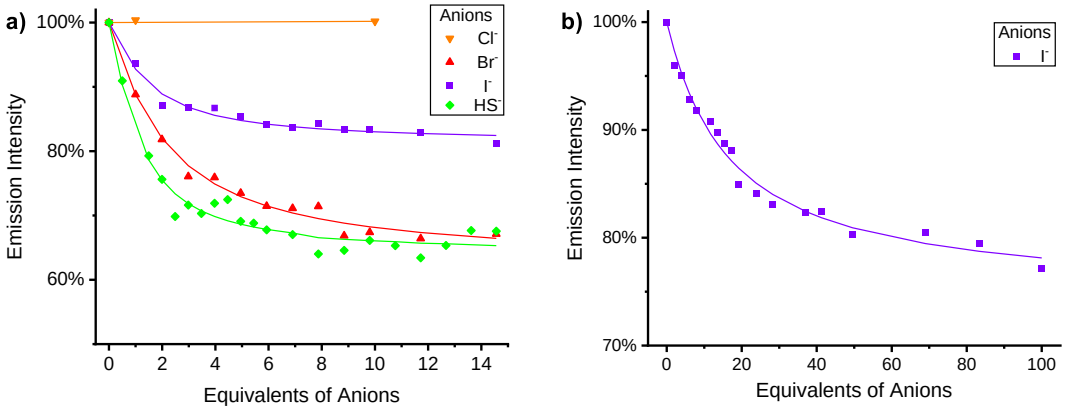


Figure 3.48: *Binding isotherms and 1:1 stoichiometric Bindfit analysis of fluorescence emission titration data in 10 mM HEPES aqueous solution, pH 7.4, 298 K, for* ***a)*** *receptor* ***3.25*** *(10 µM) on addition of NaCl, NaBr, NaI and NaHS* ***b)*** *receptor* ***3.26*** *(10 µM) upon addition of NaI*

3.3.3. Reversibility Studies

One of the key advantages of supramolecular chemosensors over chemodosimeters is their ability to reversibly sense analytes. In order to demonstrate the capability of the generation 2 receptors to sense HS^- in a reversible fashion, a series of reversibility experiments were conducted.

Receptors **3.20H$^+$**, **3.23** and **3.25** were dissolved in H_2O to a concentration of 10 µM, as used in the titration studies. An emission spectrum of each was recorded, before four equivalents of NaHS, dissolved in H_2O, were added. As observed in the titration studies, addition of NaHS led to substantial quenching of the receptors' emission intensities. Following similar reported

procedures,[22,23] an equimolar quantity of $Zn(OTf)_2$ was added to react with HS^- and form ZnS, which precipitated out of solution (Scheme 3.16). The other reaction product triflic acid, remains dissociated in solution and the conjugate base, the triflate anion, is a non-coordinating anion.

$$Zn(OTf)_{2(s)} + HS^-_{(aq)} \rightarrow ZnS_{(s)} + H^+_{(aq)} + 2OTf^-_{(aq)}$$

Scheme 3.16: *Reaction of zinc triflate with hydrosulfide*

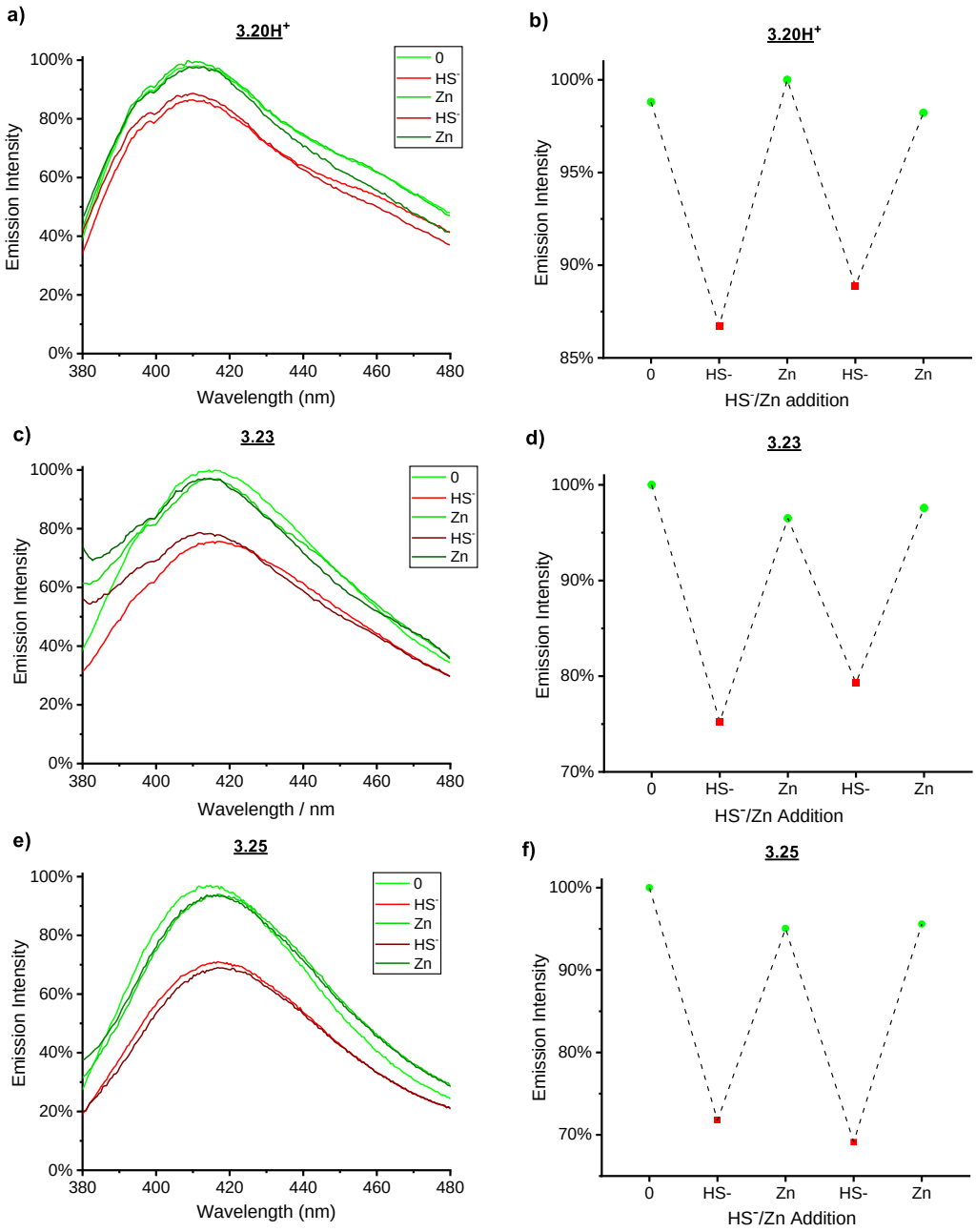


Figure 3.49: *Reversibility studies for receptor **3.20H+**, **3.23** and **3.25**. Showing the repeated cycles of NaHS addition inducing quenching and additions of $ZnOTf_2$ restoring the fluorescence emission.*

After the addition of the zinc salt, and the precipitation of ZnS, the respective receptor emission spectrum returned to near non-quenched levels — demonstrating the reversibility of the sensors (Figure 3.49). Marginal differences in emission intensity were attributed to the free ZnS precipitate and errors in equimolar measurements. Another cycle of adding NaHS and then $Zn(OTf)_2$ was conducted to further test the reversibility.

All receptors were found to be capable of acting as reversible chemosensors for HS^-. This adds further evidence that the characteristic interaction and response observed for HS^- is due to XB binding.

3.3.4. Limit of Detection

The limit of detection (LoD) represents the lowest concentration of an analyte that can be accurately measured with a sensor. The LoD of the XB receptors **3.20H$^+$**, **3.23** and **3.25** for HS^- was determined using the fluorescence titration data, following a reported method using Equation 3.1: Limit of Detection.[24]

Equation 3.1: *Limit of Detection*

$$LoD = \frac{3\sigma}{S}$$

σ = Standard deviation of blank measurement

S = Gradient of initial linear detection plot

The fluorescence spectrum for each receptor was measured five times and a standard deviation of the blank measurements determined. Using the first near linear titration points of each receptor's response to NaHS, a gradient was determined and is graphically demonstrated in Figure 3.50. Using these two values and Equation 3.1, LoDs were calculated and tabulated (Table 3.11).

Table 3.11: *Limits of detection for NaHS*

Host	Limit of Detection (μM)
3.20H$^+$	24.6
3.23	14.3
3.25	6.7

LoD determined using formula 3.1; 10 μM receptor in 10 mM HEPES aqueous solution, pH 7.4, 298 K

As expected, the LoD trend aligns with the association constants, whereby the greater the association the smaller the LoD. All values fall in the low micromolar range, comparable to chemodosimeter probes used for detecting H_2S in aqueous environments and *in vitro* studies.[25]

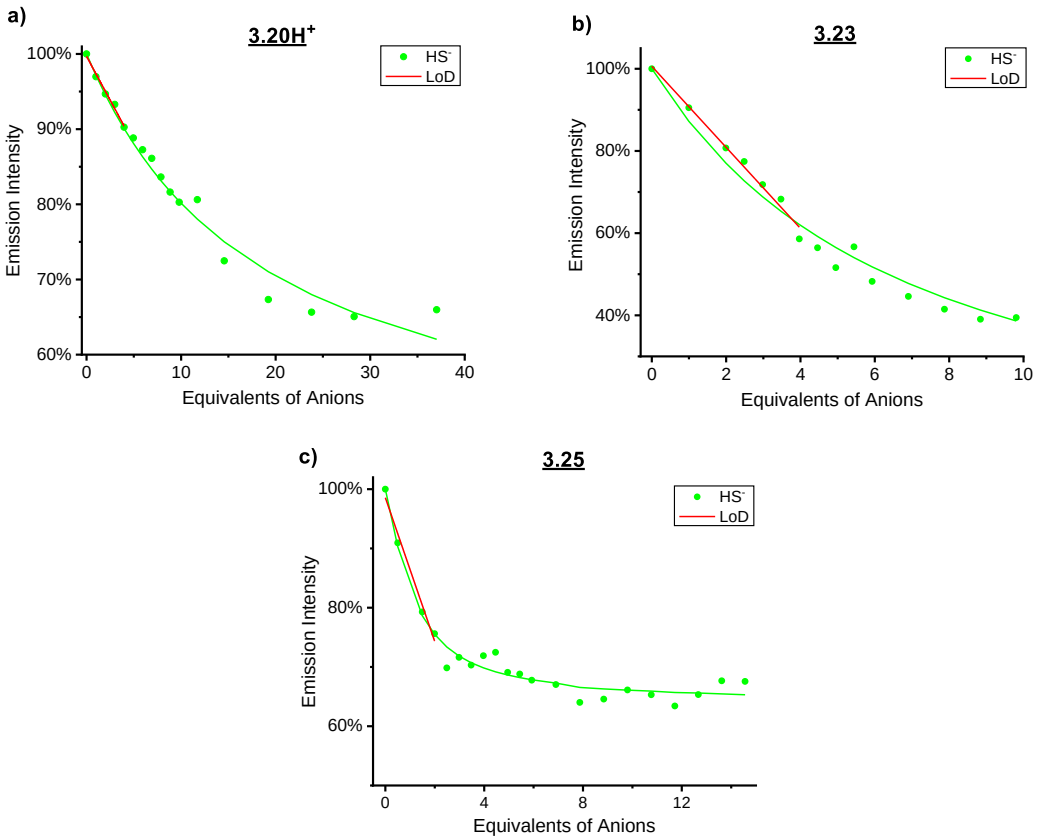


Figure 3.50: *Linear plots of initial NaHS titration data for receptors* ***a) 3.20H$^+$ b) 3.23 c) 3.25***

3.3.5. Molecular Modelling

A series of computational molecular modelling experiments of receptors **3.23** and **3.25** were conducted in collaboration with Dr. Igor Marques and Prof. Vítor Félix (*University of Aveiro, Portugal*) to further investigate the unique XB HS^- interaction.

Using model complexes of receptors **3.23** and **3.25** in which the large benzyl TEG-substitutents were replaced with smaller ethyl groups, affording prototypes **3.23Et** and **3.25Et**, DFT calculations were able to determine the geometric and energetic properties of the XB interactions between HS^- and I^- for each receptor in water. Optimised structures of the HS^- and I^- associations with **3.23Et** and **3.25Et** are presented in Figure 3.51, showing the two iodotriazoles binding in convergence.[26] The XB anion interactions were found to be almost linear, with angles averaging around 171°. Importantly, the I···SH^- distance is markedly shorter than the I···I^- distance, with average values of 3.173±0.032 and 3.580±0.020 Å, respectively. Between the two receptors, charged pyridinium **3.25Et** displayed shorter XB interaction distances by ca. 0.05 Å.

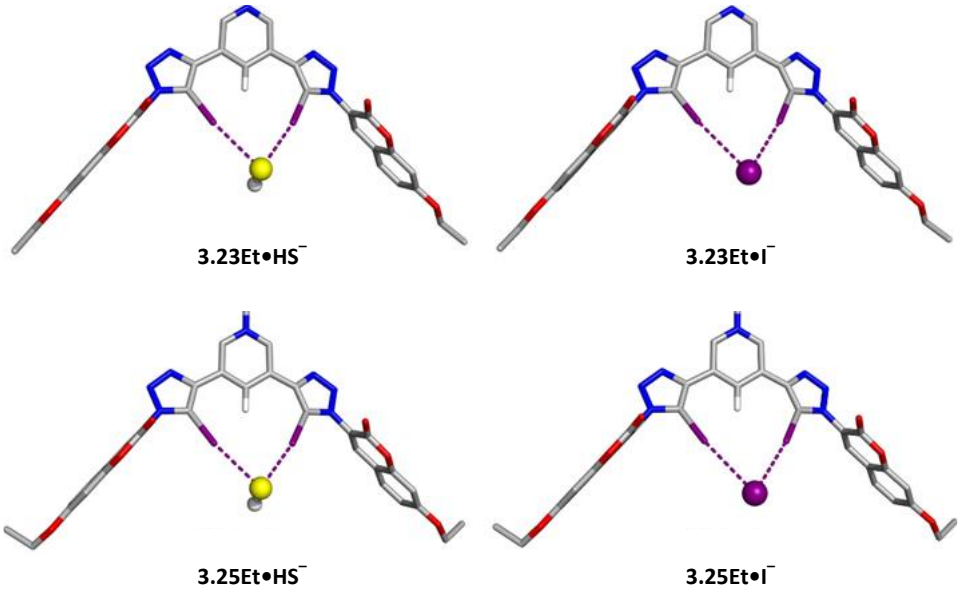


Figure 3.51: *DFT-optimised structures of **3.23Et** and **3.25Et** model receptors halogen-bonded to HS^- and I– anions. The XB interactions are sketched as purple dashed lines.*

The respective binding free energies (ΔG^{SS}) between **3.23Et**, **3.25Et** and I^- and HS^- were found to show an indubitable binding preference of both receptors for HS^-. With **3.23Et** displaying a value of −4.19 kcal mol^{-1} for HS^- and, importantly, an almost negligible value of −0.77 kcal mol^{-1} for iodide, in agreement with the inability of **3.23** to bind iodide in water. As shown

in the experimental association constants, the ΔG^{SS} for pyridinium **3.25Et** was found to be greater than the pyridyl receptor, with values of -8.79 kcal mol^{-1} and -4.18 kcal mol^{-1} for HS^- and I^- respectively.

Within the scope of Quantum Theory of Atoms in Molecules, estimates of the halogen bond energies were calculated. They were able to establish that the XB interactions with iodide were highly electrostatic in nature whilst the interaction with HS^- has a greater degree of covalency.[26]

The XB-based associations between HS^- and I^- and receptors **3.23Et** and **3.25Et** were also investigated by molecular dynamics (MD) simulations in water. During the experiment the XB-anion interactions, surrounded by solvent water molecules, were maintained throughout as shown in Figure 3.52. Notably, the TEG chains were found to exhibit no role on the binding of the anions and specifically did not shield the anions from solvating water molecules. Interestingly, a decrease in the average number of solvating water molecules is observed when compared with the freely solvated anions, particularly for HS^- which for **3.23Et** and **3.25Et** was calculated to decrease from 10.6 to 8.1 and 7.6 respectively (with a 3.5 Å cut-off). This result suggested that the water molecules play an important role in the recognition of both anions.

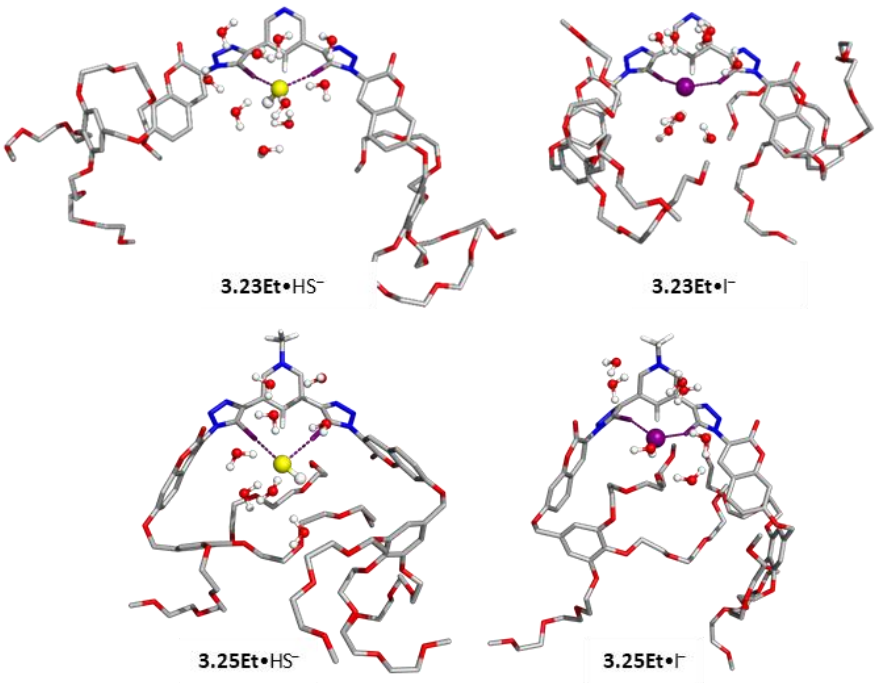


Figure 3.52: *MD simulation snapshot of HS^- and I^- associated with **3.23** and **3.25**, showing the anions enclosed by water molecules and the random orientation of the TEG flexible chains.*

3.3.6. Summary

A series of generation 2 XB coumarin receptors containing water soluble benzyl TEG groups, to enhance solubility whilst remaining unprotonated *in situ*, have been synthesised and tested for their ability to sense halides and HS^-. Analogous HB receptors were also synthesised and tested for comparison. All the XB receptors consistently out-performed the HB analogues, with all but the pyridinium HB receptor **3.26** unable to act as sensors for the halides and HS^-. Amine receptor **3.20H$^+$** was able to sense HS^- but also sensed and bound iodide to a greater extent. Neutral XB pyridine receptor **3.23** exclusively sensed HS^- over the halides; this unique behaviour was attributed to the favourable interaction of XB for HS^-. A XB pyridinium receptor **3.25** displayed enhanced binding for HS^- but with a diminished degree of selectivity as it was also capable of sensing iodide and bromide. Each XB receptor was found to sense HS^- in a reversible chemosensing fashion, displaying similar micromolar LoDs to irreversible chemodosimeter probes. Molecular modelling studies with **3.23** and **3.25** reiterated the unique XB HS^- interaction that was observed in the experimental results, displaying enhanced favourable association free energies for HS^- over I^-, a greater degree of covalency in the HS^- halogen bond, and highlighting the importance of water solvent molecules in the receptors sensing behaviour.

3.4. Conclusions and Future Work

XB anion recognition and reversible chemosensing of HS^- in pure water has been demonstrated for the first time. This was achieved through the integration of coumarin fluorophores into XB bis-iodotriazole pyridine, pyridinium and secondary amine acyclic host structural frameworks, functionalised with hydrophilic triethylene glycol (TEG) substituents. Association constants, emission intensity changes and LoD for each receptor are summarised in Table 3.12.

Remarkably XB receptor **3.23** was found to be capable of exclusively sensing HS^- over the halides in water. In stark contrast, all the HB receptor analogues were incapable of functioning as chemosensors for HS^- in the aqueous buffered solvent conditions. These results advance and highlight the potential of XB based sensor systems for detecting anions in aqueous media and opens the opportunity for a new type of HS^- sensor.

Future work could explore the development of a series of generation 3 XB receptors. These receptors would retain the bis-iodotriazole motifs and incorporate new solubilising groups,

such as carboxylate sodium salts, to ensure greater water solubility for ^{1}H NMR titration studies (Figure 3.53a). Alternatively, the receptors developed could be mounted onto a transparent glass surface for the creation of a set of surface modified sensors for HS^- (Figure 3.53b).

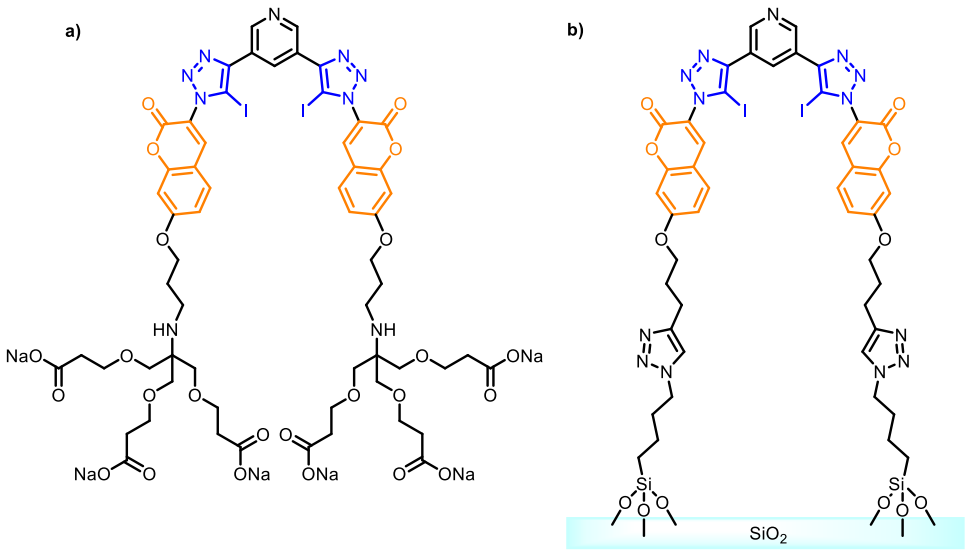


Figure 3.53: *Future work* ***a)*** *Generation 3 receptors with carboxylate solubilising groups* ***b)*** *Surface mounted host-receptor.*

Table 3.12: *Compiled association constants, emission intensity changes and LoDs for receptors.*

Host	Association Constants K_a (M^{-1}) & Emission intensity change				LoD (μM)
	Cl^-	Br^-	I^-	HS^-	
3.11H⁺ (XB)[a]	NB	>10⁵ (-21%)	>10⁵ (-18%)	7500 ± 660 (-63%)	-
3.20H⁺ (XB)[b]	NB	NB	46000 ± 14000 (-10%)	5600 ± 530 (-36%)	24.6
3.22H⁺ (HB)[b]	NB	NB	NB	NB	-
3.23 (XB)[b]	NB	NB	NB	16500 ± 1600 (-60%)	14.3
3.24 (HB)[b]	NB	NB	NB	NB	-
3.25 (XB)[b]	NB	60800 ± 7800 (-37%)	103000 ± 24000 (-19%)	158000 ± 31000 (-39%)	6.7
3.26 (HB)[b]	NB	NB	6080 ± 550 (29%)	NB	-

Anion association constants with errors determined using 1:1 stoichiometric BindFit analysis of the fluorescence emission changes, 10 μM receptor in [a] H_2O [b] 10 mM HEPES aqueous solution, pH 7.4; 298 K. NB = no binding observed.

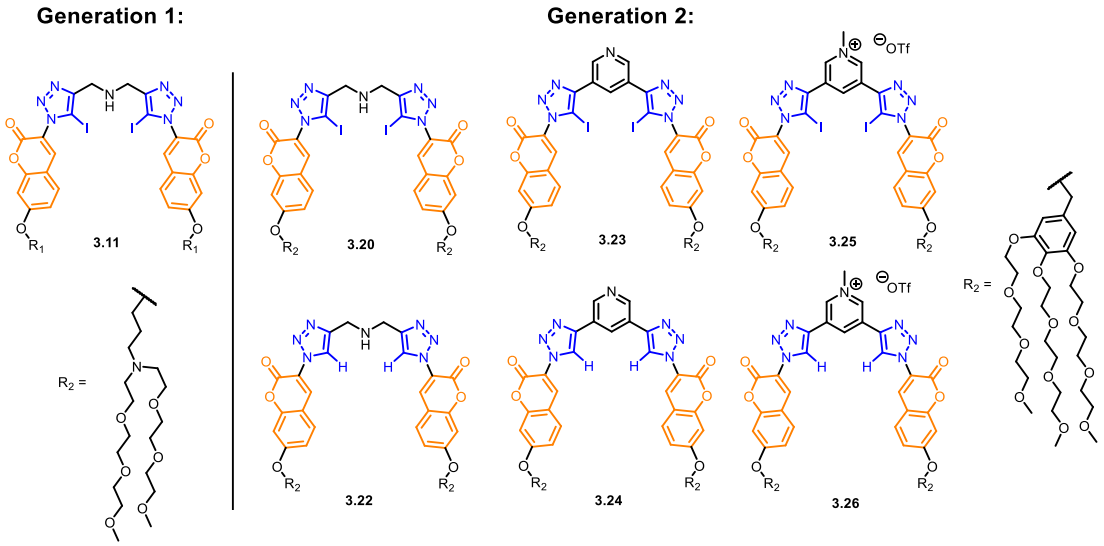


Figure 3.54: *Generation 1 and 2 water soluble receptors.*

3.5. References

1 M. J. Langton, C. J. Serpell and P. D. Beer, *Angew. Chem. Int. Ed.*, 2016, **55**, 1974–1987.

2 N. Ahmed, B. Shirinfar, I. Geronimo and K. S. Kim, *Org. Lett.*, 2011, **13**, 5476–5479.

3 A. Bencini, C. Coluccini, A. Garau, C. Giorgi, V. Lippolis, L. Messori, D. Pasini and S. Puccioni, *Chem. Commun.*, 2012, **48**, 10428–10430.

4 M. J. Langton, S. W. Robinson, I. Marques, V. Félix and P. D. Beer, *Nat. Chem.*, 2014, **6**, 1039–1043.

5 S. H. Jung, J. W. Lee and H. J. Kim, *Supramol. Chem.*, 2016, **28**, 634–639.

6 X. Li, J. Y. C. Lim and P. D. Beer, *Chem. Eur. J.*, 2018, **24**, 17788–17795.

7 OpenDataFit, P. Thordarson, CBNS and UNSW, BindFit v0.5 | Supramolecular, http://app.supramolecular.org/bindfit/, (accessed 2021).

8 D. Brynn Hibbert and P. Thordarson, *Chem. Commun.*, 2016, **52**, 12792–12805.

9 D. Cao, Z. Liu, P. Verwilst, S. Koo, P. Jangjili, J. S. Kim and W. Lin, *Chem. Rev.*, 2019, **119**, 10403–10519.

10 D. W. Smith, *J. Chem. Educ.*, 1977, **54**, 540–542.

11 Y. Hong, J. W. Y. Lam and B. Z. Tang, *Chem. Soc. Rev.*, 2011, **40**, 5361–5388.

12 H. Xiao, K. Chen, D. Cui, N. Jiang, G. Yin, J. Wang and R. Wang, *New J. Chem.*, 2014, **38**, 2386–2393.

13 F. Bu, R. Duan, Y. Xie, Y. Yi, Q. Peng, R. Hu, A. Qin, Z. Zhao and B. Z. Tang, *Angew. Chem. Int. Ed.*, 2015, **54**, 14492–14497.

14 K. C. Elbert, D. Jishkariani, Y. Wu, J. D. Lee, B. Donnio and C. B. Murray, *Chem. Mater.*, 2017, **29**, 8737–8746.

15 M. Strianese, D. Guarnieri, M. Lamberti, A. Landi, A. Peluso and C. Pellecchia, *Inorg. Chem.*, 2020, **59**, 15977–15986.

16 Y. Mehmet and J. B. Hyne, *Am. Chem. Soc. Div. Pet. Chem. Prepr.*, 1974, **19**, 187–197.

17 H. M. van Dort and W. J. Mijs, *Recl. des Trav. Chim. des Pays-Bas*, 1966, **85**, 15–20.

18 M. Morgenthaler, E. Schweizer, A. Hoffmann-Röder, F. Benini, R. E. Martin, G. Jaeschke, B. Wagner, H. Fischer, S. Bendels, D. Zimmerli, J. Schneider, F. Diederich, M. Kansy and K. Müller, *ChemMedChem*, 2007, **2**, 1100–1115.

19 N. A. Kuznetsova and O. L. Kaliya, *Russ. Chem. Rev.*, 1992, **61**, 1243–1267.

20 M. Alkış, D. Pekyılmaz, E. Yalçın, B. Aydıner, Y. Dede and Z. Seferoğlu, *Dye. Pigment.*, 2017, **141**, 493–500.

21 T. Arakawa and S. N. Timasheff, *Biochemistry*, 1984, **23**, 5912–5923.

22 M. D. Hartle, R. J. Hansen, B. W. Tresca, S. S. Prakel, L. N. Zakharov, M. M. Haley, M. D. Pluth and D. W. Johnson, *Angew. Chem. Int. Ed.*, 2016, **55**, 11480–11484.

23 N. Lau, L. N. Zakharov and M. D. Pluth, *Chem. Commun.*, 2018, **54**, 2337–2340.

24 X. Shang, I. Song, G. Y. Jung, W. Choi, H. Ohtsu, J. H. Lee, J. Y. Koo, B. Liu, J. Ahn, M. Kawano, S. K. Kwak and J. H. Oh, *Nat. Commun.*, 2018, **9**, 1–12.

25 X. Wang, L. An, Q. Tian and K. Cui, *RSC Adv.*, 2019, **9**, 33578–33588.

26 E. J. Mitchell, A. J. Beecroft, J. Martin, S. Thompson, I. Marques, V. Félix and P. D. Beer, *Angew. Chem. Int. Ed.*, 2021, **60**, 1–7.

Chapter 4

BODIPY-Based Halogen Bonding Receptors

4. BODIPY-based Halogen Bonding Receptors

4.1. Introduction

BODIPYs (4,4-difluoro-4-bora-3a,4a-diaza-s-indacene, Figure 4.1) are a class of strongly UV-absorbing, fluorescent molecular dyes that display high quantum yields and tuneable emission wavelengths.[1] The photophysical properties of BODIPYs are highly sensitive to their local environments. They remain stable in a range of pH and solvent environments and are robust to chemical and light degradation.[2] Covalent modifications to their molecular structures enable fine tuning of their fluorescence characteristics, enabling their use in a wide variety of applications including biological labelling,[3] electroluminescent devices,[4] tuneable laser dyes,[4] fluorescent switches,[5] solid-state solar concentrators,[6] and fluorophores in sensors.[2,7]

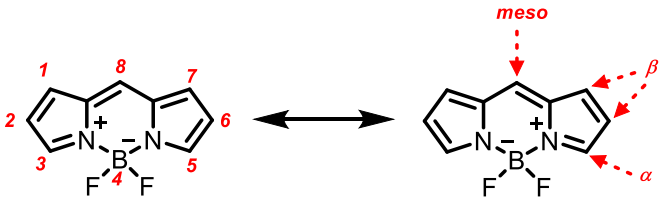


Figure 4.1: *BODIPY's resonance structures and atom labels*

4.1.1. BODIPY receptor systems

Due to its fluorescence sensitivity to the localised environment, BODIPY has been incorporated into a range of sensors. The vast majority of these systems act as chemodosimeter sensors in which they irreversibly react with target analytes.[8] Nonetheless, although uncommon, particularly for anions, supramolecular BODIPY receptor chemosensors for metal cations, in which a cation binding group is covalently attached to a BODIPY fluorophore are known.[9] For example, Burdette and co-workers reported an aza-crown ether *meso*-functionalised BODIPY sensor (Figure 4.2a),[10] which was found to exhibit a 1600-fold enhancement of emission intensity on binding to Pb^{2+} in MeCN, due to the removal of the aza-crown's capability to induce PET quenching effects on the BODIPY fluorophore. An example of a BODIPY anion receptor was described by Shao and co-workers, utilising two appended calix[4]pyrrole derivatives (Figure 4.2b).[11] The receptor system was able to form intramolecular sandwich complexes with anions being bound between the two calix[4]pyrrole macrocycles. At the α-position the π-conjugation was extended and the BODIPYs emission

profile significantly red-shifted, enabling the host to exhibit fluorescence close to the NIR region (703 nm, MeCN). The receptor was found to recognise and sense F^-, AcO^-, $H_2PO_4^-$, Cl^-, and Br^- in MeCN by fluorescence quenching and interestingly exhibited a slight blue shift on binding due to the twisting of the calix[4]pyrroles reducing the π-conjugation.

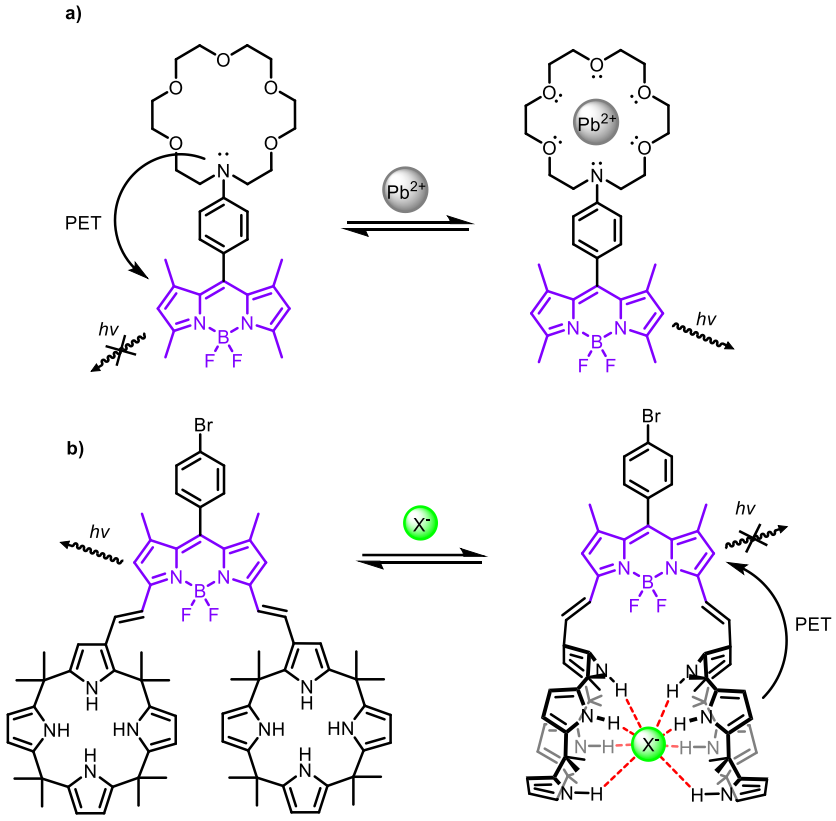


Figure 4.2: *BODIPY host-receptors* ***a)*** *Burdette's lead sensor* ***b)*** *Shao's calix[4]pyrrole anion sensor*

4.1.2. Chapter Objectives

Exploiting XB anion recognition to exclusively influence the optical properties of a BODIPY host system, and therefore act as a chemosensor is unprecedented. This chapter is concerned with the synthesis and anion sensing capabilities of a series of different XB BODIPY receptors. To achieve this, XB iodotriazole motifs, capable of recognising anions, are appended to BODIPY reporter groups in different positions. Three key designs are studied as illustrated in Figure 4.3. Each XB BODIPY receptor system is investigated for its ability to recognise and sense anions via fluorescence spectroscopic titration experiments. The most sensitive chemosensing XB BODIPY design motifs are then incorporated into more complex structural host frameworks to enhance anion binding strength and sensing abilities.

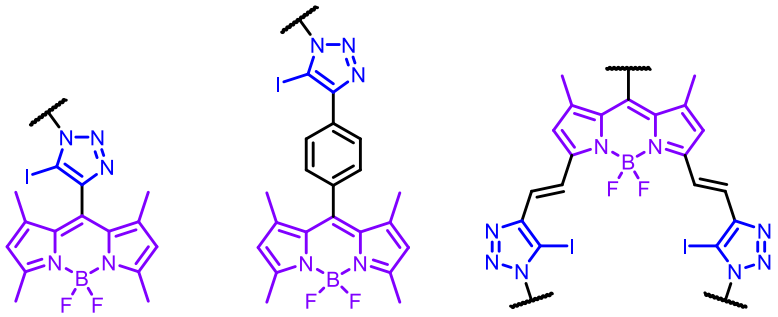


Figure 4.3: *Three proposed XB iodotriazole-BODIPY structures for anion recognition and sensing*

4.2. Iodotriazole BODIPY

In order to maximise the influence of an anion binding event on a BODIPY's fluorescence emission profile, a receptor with the XB iodotriazole covalently bound at the *meso* position was designed (Figure 4.4). For the synthesis two synthetic strategies were apparent: Wenz and co-workers had reported the synthesis of the proto-triazole analogue following a CuAAC reaction of a alkyne at the meso position of a BODIPY.[12] However, due to concerns about the steric bulk of an iodoalkyne at the meso position inhibiting copper coordination, the receptor would be prepared via a condensation of an aldehyde.

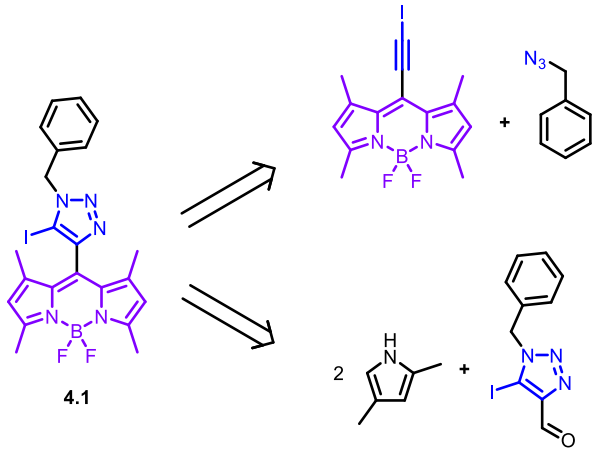
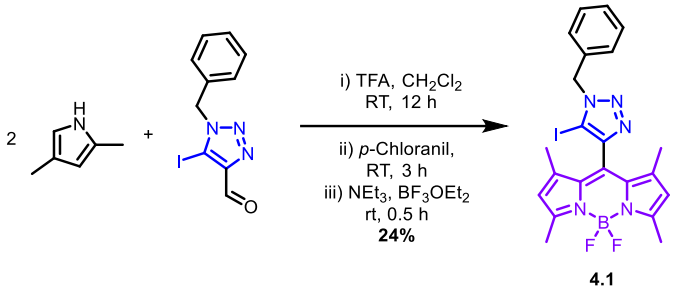


Figure 4.4: *Retrosynthesis of XB BODIPY host-receptor* ***4.1****.*

4.2.1. Mono-Iodotriazole Synthesis

Iodotriazole aldehyde (*provided by Dr Harry Klein*), synthesised via a CuAAC reaction between benzyl azide and propargyl alcohol with $Cu(ClO_4).6H_2O$ and NaI followed by a Swern oxidation, was reacted with two equivalents of 2,4-dimethyl pyrrole in the presence of catalytic quantities of TFA and left to stir for 12 h (Scheme 4.1). *p*-Chloranil was added and the mixture left to stir for 1 h, before NEt_3 and BF_3OEt_2 were subsequently added. The desired product was

purified by column chromatography to afford BODIPY receptor **4.1** as a gold solid in a 24 % yield.



Scheme 4.1: *Synthesis of XB BODIPY Receptor* ***4.1***

4.2.2. Anion Binding Studies

4.2.2.1. ^{1}H NMR Titration Studies

The binding properties of BODIPY receptor **4.1** were initially investigated via ^{1}H NMR titration experiments with TBACl in acetone-d_6.

On addition of TBACl an upfield shift was observed in the methylene benzylic proton *b* and to a lesser degree in BODIPY proton *a* (Figure 4.5), indicating that the chloride anion is being bound in the vicinity of the XB motif. Also the receptor's phenyl proton peaks *c*, *d* and *e,* initially all falling within the same chemical shift range, begin to separate on addition of TBACl.

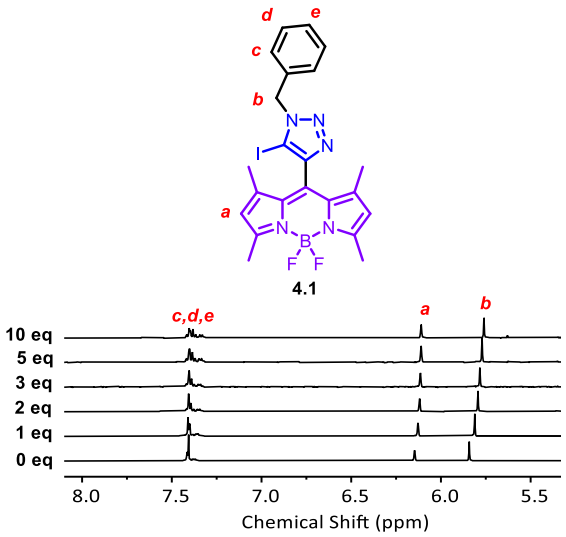


Figure 4.5: *^{1}H NMR titration of receptor* ***4.1*** *upon addition of TBACl in acetone-d_6 (1 mM, 298 K)*

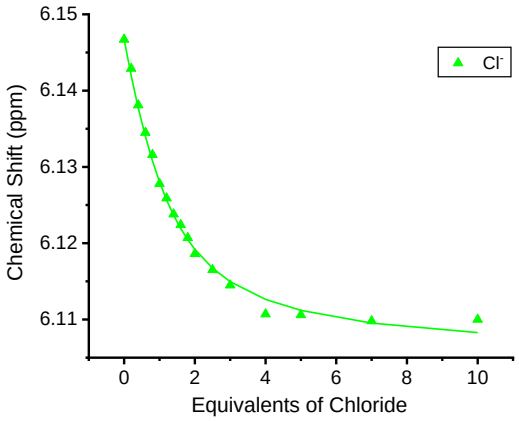


Figure 4.6: *1:1 stoichiometric fit of NMR titration data for receptor* ***4.1****, monitoring alkyl peak b upon addition of TBACl in acetone-d_6, 298 K.*

The chemical shifts of the methylene benzylic proton signals adjacent to the XB binding site were monitored as a function of halide anion concentration (Figure 4.6). From the titration data a 1:1 host-guest stoichiometric association constant of K_a = 1490 ± 100 M^{-1} was determined by Bindfit analysis. For a monodentate XB receptor, it binds chloride relatively strongly in acetone-d_6.

4.2.2.2. Fluorescence Titration Studies

The photophysical characteristics of XB receptor **4.1** were investigated by UV/Vis and fluorescence spectroscopy. Characteristic energies of absorption and emission bands for the BODIPY chromophore were observed in acetone (Figure 4.7) and are shown in Table 4.1, along with a phenyl BODIPY derivative (Figure 4.8) for comparison.[13] Receptor **4.1** exhibits longer absorption and emission wavelengths than the phenyl BODIPY due to the electron withdrawing nature of the XB iodotriazole substituents inducing bathochromic shifts. The receptor was found to have a relatively small Stokes shift of 10 nm with notable absorption-emission overlap.

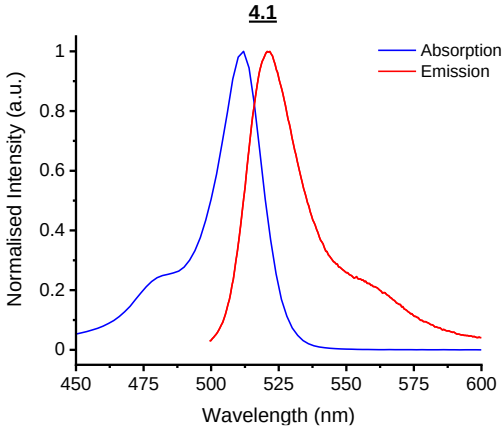
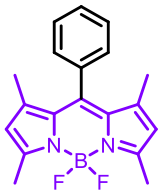


Figure 4.7: *Normalised emission and absorbance spectra for receptor **4.1** in acetone; 1 µM, 298 K.*

Table 4.1: *Energies of absorption and emission for receptor **4.1** in acetone.*

Receptor	λ_{abs} / nm	λ_{ems} / nm	Stokes Shift / nm
4.1[a]	511	521	10
Phenyl BODIPY [b]	498	509	11

[a] λ_{ex} = 480 nm, [1 µM], 298 K; [b] [2 µM], 298 K



Acetone
λ_{abs} = 498 nm
λ_{em} = 509 nm

Figure 4.8: *Photophysical properties of phenyl BODIPY derivative*[13]

The halide anion sensing properties of receptor **4.1** (1 µM) were investigated using fluorescence spectroscopy in acetone. The fluorescence emission intensity, following

excitation at the absorption shoulder (480 nm) to avoid light scattering excitation fluorescence, was monitored upon the addition of TBACl and TBABr.

On addition of TBACl and TBABr a 200% and 100% enhancement of fluorescence intensity was observed respectively (Figure 4.9). This emission enhancement is in stark contrast to previously reported BODIPY anion receptors that have all displayed fluorescence quenching via PET effects on binding anions (Figure 4.2).[11,14,15] Although already in a restricted orthogonal conformation, the significant emission intensity increase observed is thought to arise from the formation of a receptor-halide anion complex further restricting the rotational freedom of the receptor's BODIPY motif, thereby disfavouring nonradiative decay processes (Figure 4.10).

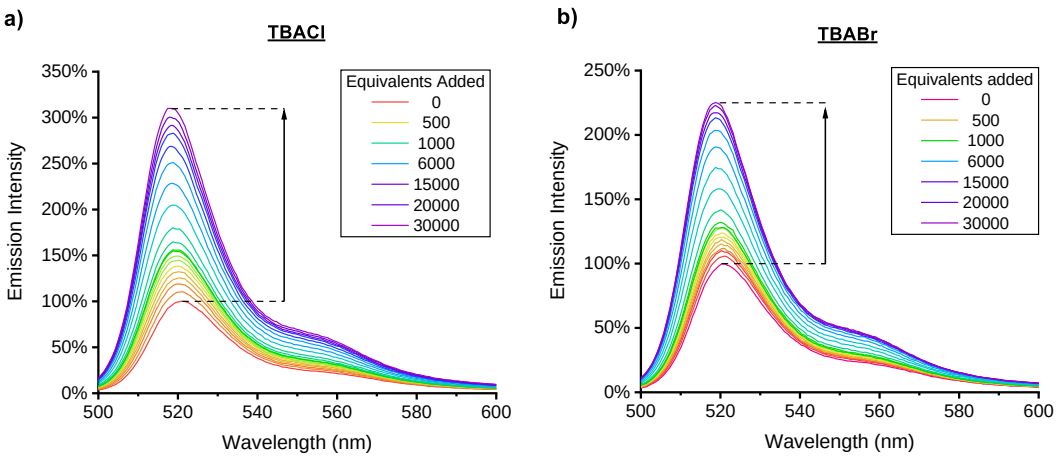


Figure 4.9: *Fluorescence emission intensity changes of receptor **4.1** upon addition of **a)** TBACl **b)** TBABr in acetone, [1 μM], T = 298 K.*

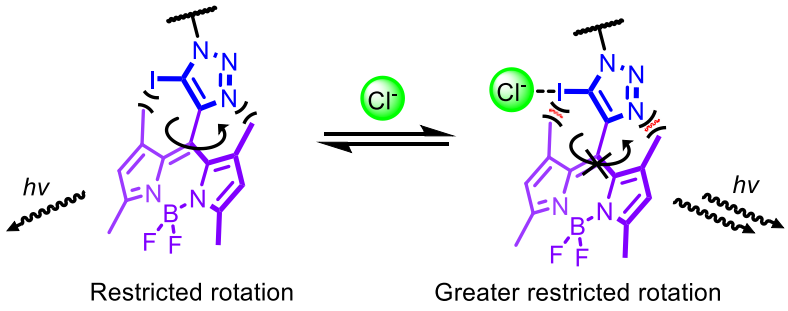


Figure 4.10: *Illustration of the restricted rotation of receptor **4.1** before and after anion complexation*

The emission intensity changes (Figure 4.11) were used to calculate 1:1 host-guest stoichiometric association constants shown in Table 4.2. The receptor was found to have a higher association for chloride than bromide reflecting the known preference for the more charge dense and least well solvated anion. Notably, the association value for chloride is lower

than that determined via ^{1}H NMR titrations. This may be due to using 'wet' acetone in the fluorescence titration experiments.

Table 4.2: *Anion association constants for receptor* ***4.1***

Anion	K_a (M^{-1})
Cl^-	370 ± 20
Br^-	280 ± 10

Anion association constants with errors determined using 1:1 stoichiometric Bindfit analysis of the fluorescence emission intensity following λ_{max} (521 nm); 1 µM receptor in acetone, 298 K.

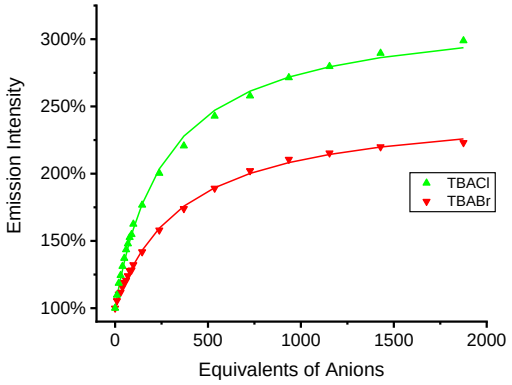


Figure 4.11: *Binding fits of fluorescence maxima change on addition of TBACl and TBABr for receptor* ***4.1****; [host] = 1 µM, acetone, T = 298 K*

4.2.3. Summary

The simple acyclic monodentate XB BODIPY receptor **4.1,** consisting of an appended iodotriazole motif at the BODIPY *meso* position, displays a significant fluorescence emission intensity increase response on binding chloride and bromide anions. This is likely due to receptor-halide anion complex formation restricting the rotational freedom of the receptor's BODIPY fluorophore. XB receptor **4.1** highlights the potential anion recognition and sensing capabilities of this moiety in more complex anion sensor systems.

4.2.4. Bis-Iodotriazole BODIPY

In order to bind anions with greater affinity than receptor **4.1** and to sense anions in more competitive solvent systems, two bis-iodotriazole BODIPY XB receptors were designed and prepared (Figure 4.12). As a proof of principle, the first generation receptor served to evaluate the fluorescence response and enhanced anion binding characteristics of the bidentate XB system, whereas the second generation receptor was used to evaluate the suitability for anion sensing in competitive aqueous solvent media.

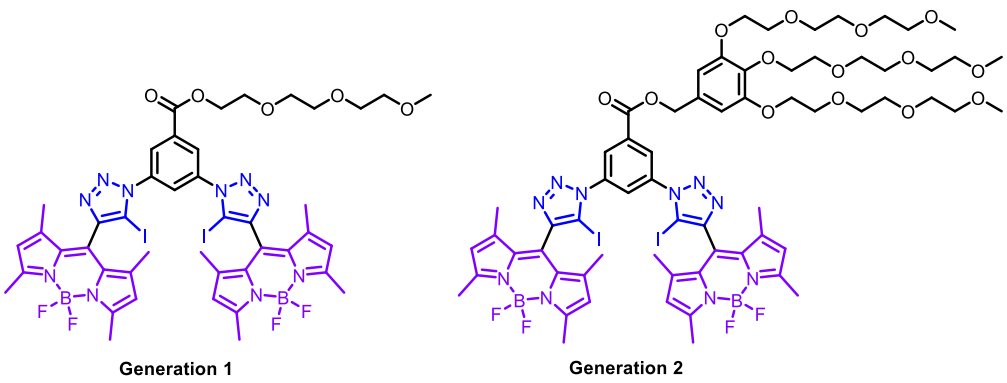


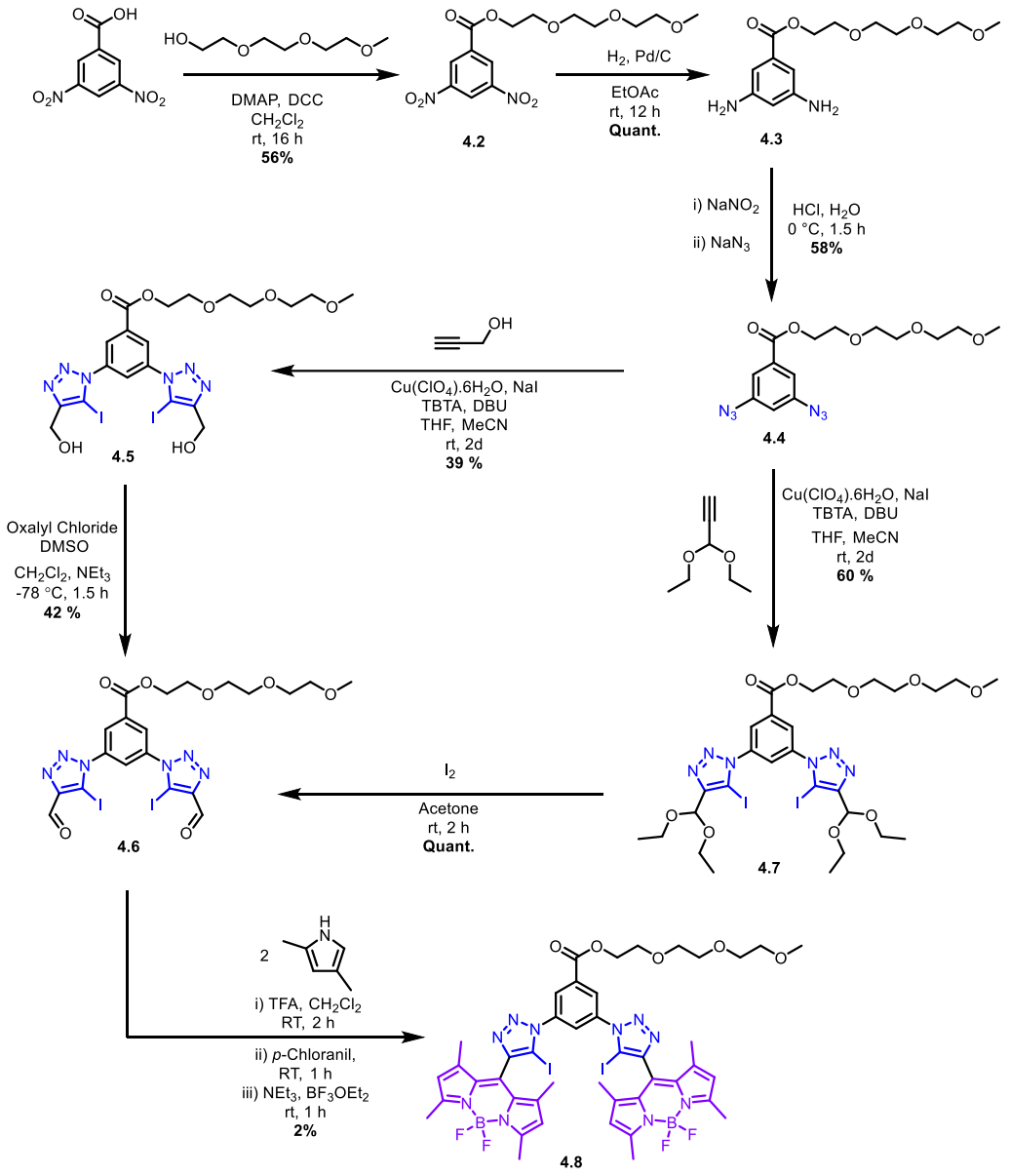
Figure 4.12: *Target bis-iodotriazole BODIPY receptors*

4.2.5. Bis-Iodotriazole BODIPY Generation 1 Synthesis

The multi-step synthesis of generation 1 bis-iodotriazole BODIPY XB receptor **4.8** is shown in Scheme 4.2. Esterification of 3,5 dinitrobenzoic acid with triethylene glycol to afford **4.2** was achieved in a 56% yield. Subsequent reduction of di-nitro **4.2** using H_2 over a palladium carbon catalyst gave di-amine **4.3** in quantitative yields. In acidified water di-amine **4.3** was reacted with $NaNO_2$ and NaN_3 for the formation of di-azide **4.4** in a yield of 58%. Di-azide **4.4** was mixed with 2.1 equivalents of propargyl alcohol in a 'one pot' iodination CuAAC click reaction using NaI, DBU as a base and TBTA to stabilise the copper catalyst. The crude product was purified by column chromatography and afforded di-alcohol **4.5** in a yield of 39% (Scheme 4.2). Conversion to the di-aldehyde **4.6** was achieved through a Swern oxidation. The crude product was purified by column chromatography using a 5% MeOH/CH_2Cl_2 eluent and **4.6** was isolated in a yield of 42%, along with a bis-acetal product obtained following an undesirable side reaction on the column. Deprotection of the acetal to recover aldehyde **4.6** was achieved in quantitative yields using catalytic amounts of I_2 in acetone. To circumvent this undesirable extra step, an alternative route was adopted. Bis-azide **4.4** was reacted with 3,3-diethoxy-1-propyne under the same one-pot iodination-CuAAC reaction conditions. Following column chromatography bis-acetal **4.7** was isolated in a good yield of 60% (Scheme 4.2). Subsequent quantitative deprotection to bis-aldehyde **4.6** was achieved using catalytic amounts I_2 in acetone.

The final synthetic step towards the desired receptor required the ambitious formation of two BODIPY fluorophores. Compound **4.6** was reacted following the procedure detailed in the synthesis of receptor **4.1**. The crude product was purified by column chromatography with a gradient elution of 0–2% MeOH/CH_2Cl_2 to afford XB receptor **4.8** as a red powder in a poor yield of 2% (Scheme 4.2). The low yield was attributed to the number of

side products typically formed during the synthesis of BODIPY and the resultant difficulty in purification.



Scheme 4.2: *Synthesis of BODIPY receptor* ***4.8***

4.2.6. Anion Binding Studies

4.2.6.1. Fluorescence Titration Studies

The photophysical characteristics of XB receptor **4.8** were investigated by UV/Vis and fluorescence spectroscopy. Characteristic energies of absorption and emission for the BODIPY chromophore were observed in acetone (Figure 4.13) and are tabulated in Table 4.3. Receptor

4.8 was found to have a small Stokes shift of 11 nm and excitation for emission titration experiments were undertaken at the lower absorption shoulder wavelength (480 nm).

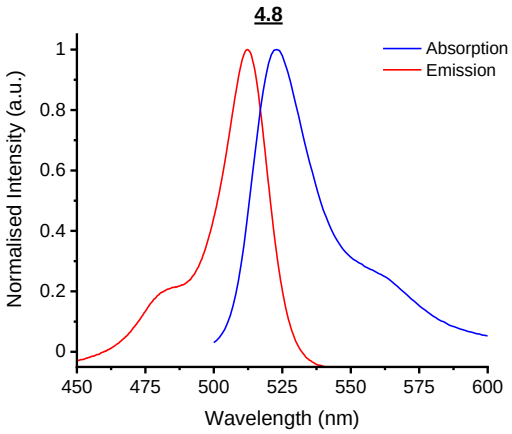


Figure 4.13: *Normalised emission and absorbance spectra for receptor **4.8** in acetone; 1 µM, 298 K.*

Table 4.3: *Energies of absorption and emission for receptor **4.8** in acetone.*

Receptor	λ_{abs} / nm	λ_{ems} / nm	Stokes Shift / nm
4.8	512	523	11

λ_{ex} = 482 nm, [1 µM], 298 K

The anion sensing properties of receptor **4.8** (1 µM) were investigated using fluorescence spectroscopy in acetone.

On addition of TBACl and TBABr a 65% and 80% enhancement of emission intensity was observed respectively (Figure 4.14). As with receptor **4.1**, the increase in intensity was attributed to halide complexation rigidfying the receptor, inhibiting rotational freedoms thereby reducing non-radiative decay processes. However, compared to receptor **4.1**, the percentage emission band increase is appreciably lower, likely due to the steric bulk of the receptor already restricting rotational freedoms.

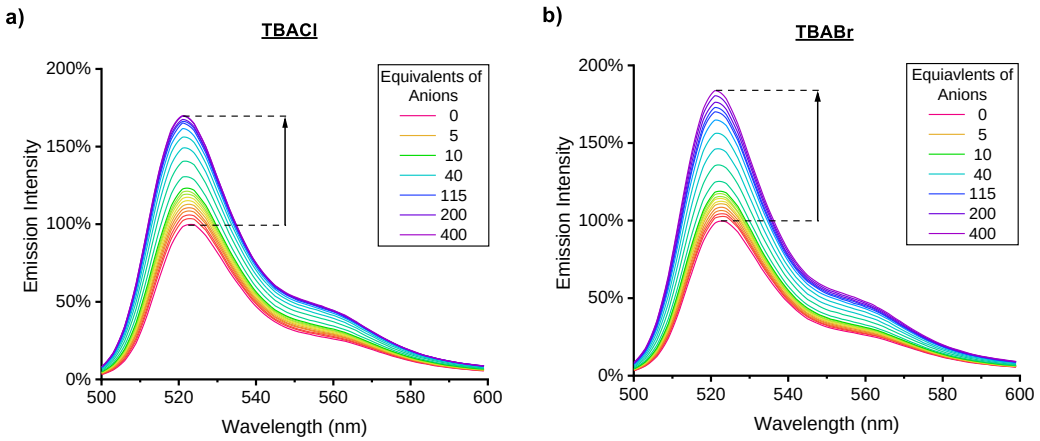


Figure 4.14: *Fluorescence emission intensity changes of receptor **4.8** upon addition of **a)** TBACl **b)** TBABr in acetone, [host] = 1 µM, T = 298 K.*

Association constants determined from the isotherm titration data (Figure 4.15) are reported in Table 4.4. Importantly, both halide association constant values are two orders of magnitude greater than those for the single monodentate iodotriazole receptor **4.1**, highlighting the increased binding strength from using two convergent XB donors.

Table 4.4: *Anion association constants for receptor* ***4.8***

Anion	K_a (M^{-1})
Cl^-	46,400 ± 1300
Br^-	26,200 ± 440

Anion association constants with errors determined using 1:1 stoichiometric Bindfit analysis of the fluorescence emission intensity following λ_{max} (482 nm); 1 µM receptor in acetone, 298 K.

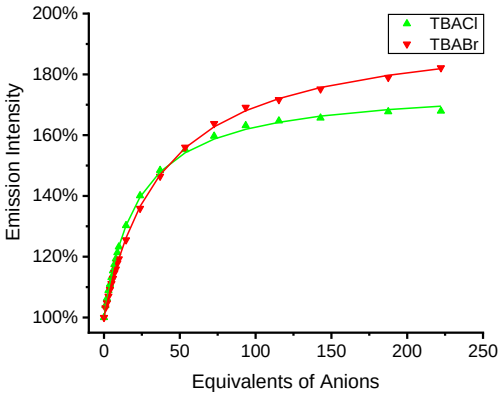
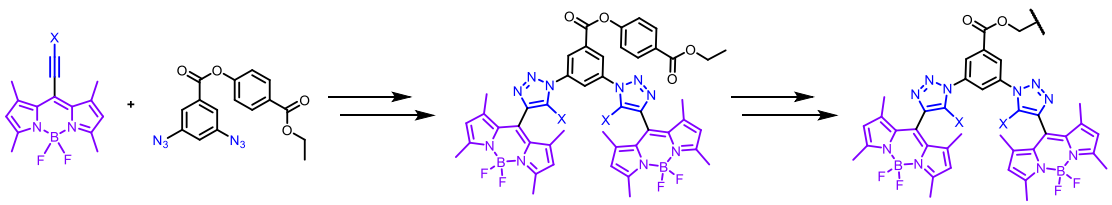


Figure 4.15: *Binding fits of fluorescence maxima change on addition of TBACl and TBABr for receptor* ***4.8****; ([host] = 1 µM, acetone, T = 298 K.*

4.2.7. Bis-Iodotriazole BODIPY Generation 2 Synthesis

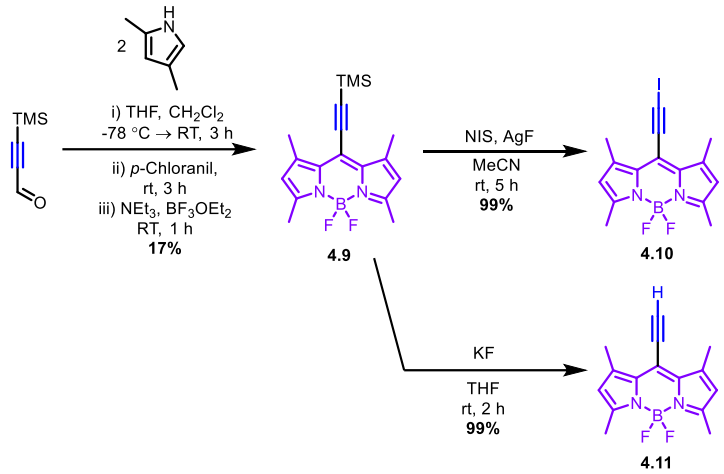
Receptor **4.8** was able to sense and bind both halide anions with significantly greater association than receptor **4.1**. However, due to the extremely low yield of the final synthetic step an alternative synthetic procedure was undertaken (Scheme 4.3) where the iodotriazole-BODIPY motif is introduced through a CuAAC reaction. The final step includes the esterification of an ethyl paraben active ester to allow for a benzylic TEG solubilising group to be appended.



Scheme 4.3: *Generation 2 bis-iodotriazole-BODIPY receptor synthesis*

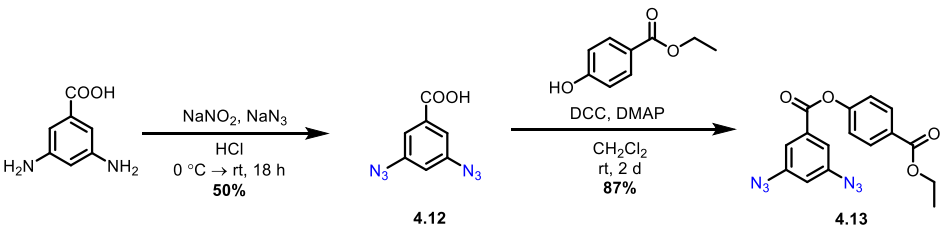
3-(Trimethylsilyl)-2-propynal was reacted with two equivalents of 2,4-dimethyl pyrrole in the presence of catalytic quantities of TFA and left to stir for 3 h. *p*-Chloranil was added and the mixture left to stir for 3 h, before NEt_3 and BF_3OEt_2 were subsequently added. The crude product was purified by column chromatography to give TMS-protected BODIPY alkyne **4.9**

which was isolated in a modest yield of 17%. TMS deprotection and iodination to BODIPY iodo-alkyne **4.10**, was achieved by stirring **4.9** with NIS and AgF in darkness over 5 h, in a quantitative yield. TMS deprotection to **4.11** was achieved in a quantitative yield by stirring with KF in THF over 2 h (Scheme 4.4).



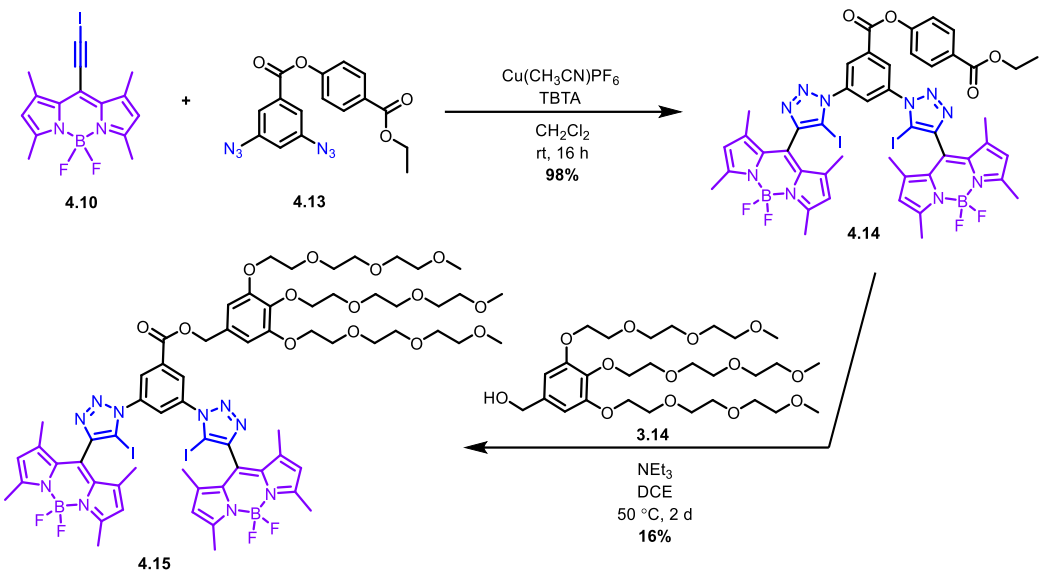
Scheme 4.4: *Synthesis of iodo- and proto-alkyne BODIPYs* ***4.10*** *and* ***4.11***

The synthetic procedures detailed in Schemes 4.5, 4.6 and 4.7 were undertaken by Dr. Robert Hein. Bis-azide **4.12** was synthesised following adapted literature procedures.[16,17] 3,5-Diaminobenzoic acid was dissolved in concentrated HCl and cooled to 0 ˚C before NaN_3 was added and the reaction mixture left to stir overnight. Purification was achieved by column chromatography and bis-azide **4.12** isolated in a yield of 50%. **4.12** was subsequently reacted with ethyl paraben via a Steglich esterification with a DCC coupling reagent and DMAP as a catalyst, affording active ester **4.13** in a yield of 87% (Scheme 4.5).



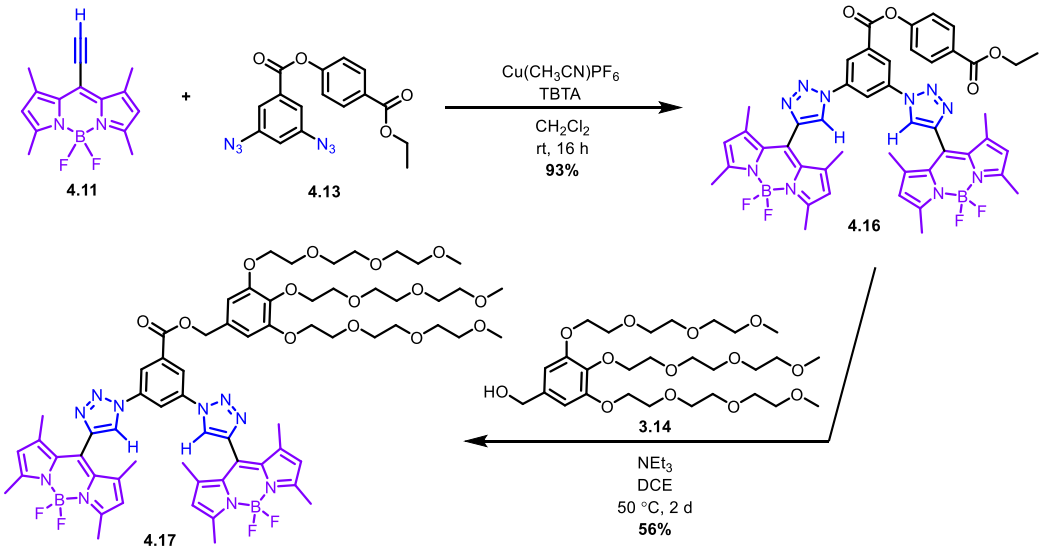
Scheme 4.5: *Synthesis of bis-azide active ester* ***4.13***

Two equivalents of BODIPY iodo-alkyne **4.10** were reacted with one equivalent of active ester bis-azide **4.13** in a CuAAC click reaction using $Cu(CH_3CN)PF_6$ as a catalyst (Scheme 4.6). Following purification via column chromatography, BODIPY active ester **4.14** was isolated in an exceptional yield of 98%. Transesterification was achieved by reacting **4.14** with alcohol **3.14** in DCE with triethylamine as a base, affording receptor **4.15** in a yield of 16% (Scheme 4.6).



Scheme 4.6: *Synthesis of XB BODIPY receptor* ***4.15***

An analogous synthetic route was used for the synthesis of HB BODIPY receptor **4.17** (Scheme 4.7).



Scheme 4.7: *Synthesis of HB BODIPY receptor* ***4.17***

4.2.8. Fluorescence Titration Studies

Fluorescence studies of receptors **4.15** and **4.17** were undertaken by Dr. Robert Hein. Fluorescence anion titration experiments for receptors XB **4.15** and HB **4.17** were conducted in MeCN and 3:7 MeCN-Water.

4.2.8.1. Titration Studies in Acetonitrile

The photophysical properties of receptors **4.15** and **4.17** in MeCN (Figure 4.16) are shown in Table 4.5.

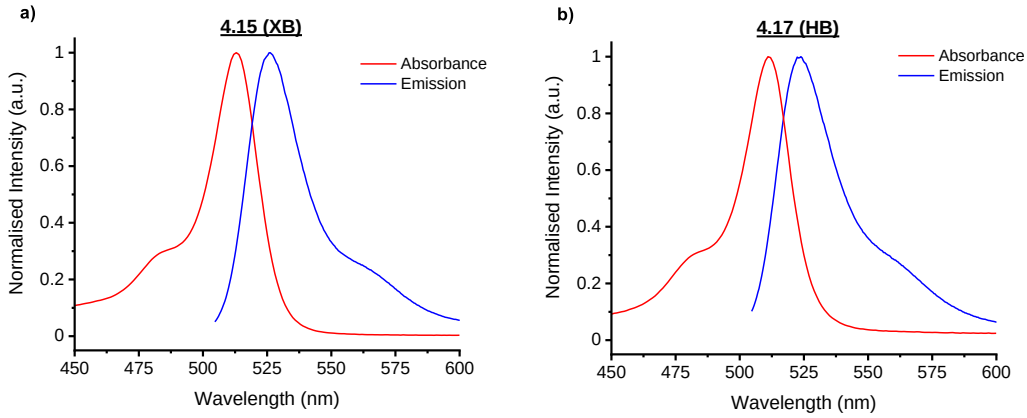


Figure 4.16: *Normalised emission and absorbance spectra for* ***a)*** *XB receptor* ***4.15 b)*** *HB receptor* ***4.17*** *in MeCN; 1 µM, 298 K.*

Table 4.5: *Energies of absorption and emission for XB receptor* ***4.15*** *and HB receptor* ***4.17*** *in MeCN.*

Receptor	$\lambda_{abs,\ max}$ / nm	$\lambda_{ems,\ max}$ / nm	Stokes Shift / nm
4.15 (XB)	513	526	13
4.17 (HB)	511	524	13

λ_{ex} = 480 nm, [1 µM], 298 K

Addition of halides, as TBA salts, to **4.15** in MeCN led to fluorescence intensity increases of 26%, 32% and 5.1% for Cl^-, Br^- and I^- respectively (Figure 4.17a-c). Compared to the titration studies of receptor **4.8** in acetone, the percentage emission increases are notably lower. The HB analogue **4.17** displayed an emission increase for TBACl of 19%, TBABr, 9%, and no response for TBAI (Figure 4.17d-e).

From the fluorescence emission titration data (Figure 4.18), the association constants for both receptors shown in Table 4.6, reveal XB receptor **4.15** displays much stronger halide binding than the HB analogue **4.17**, with both receptors exhibiting the greatest association with bromide. This may be due to preferential size complementarity of the XB bidentate receptors bite angle suiting bromide over chloride and iodide. In comparison to the acetone studies, the association constants are significantly lower in magnitude, owing to the more competitive nature of acetonitrile as a solvent system for anion binding studies.

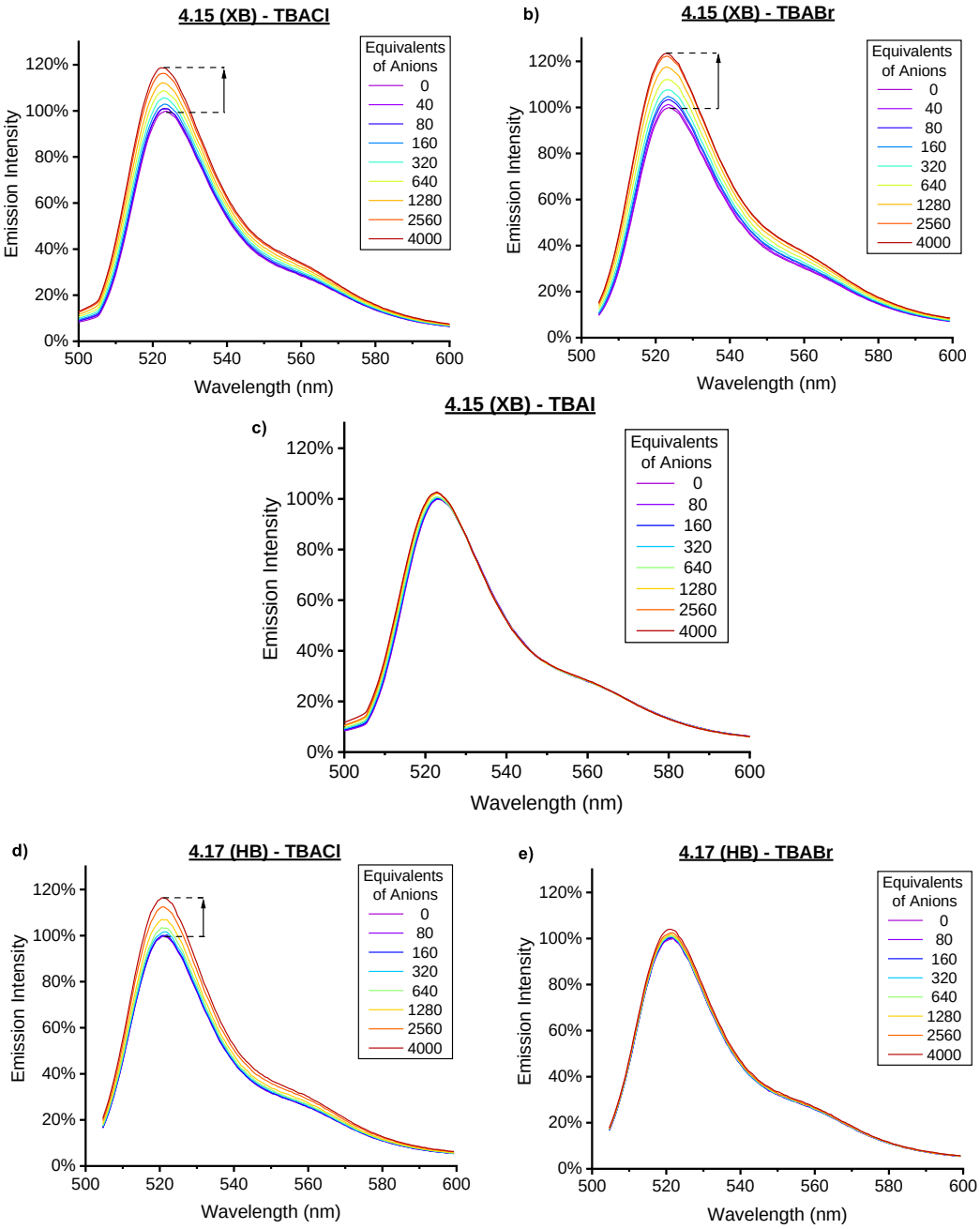


Figure 4.17: *Fluorescence emission intensity changes of XB receptor* ***4.15*** *upon addition of* ***a)*** *TBACl* ***b)*** *TBABr* ***c)*** *TBAI, and HB receptor* ***4.17*** *upon addition of* ***d)*** *TBACl* ***e)*** *TBABr in MeCN; [host] = 1 µM, T = 298 K.*

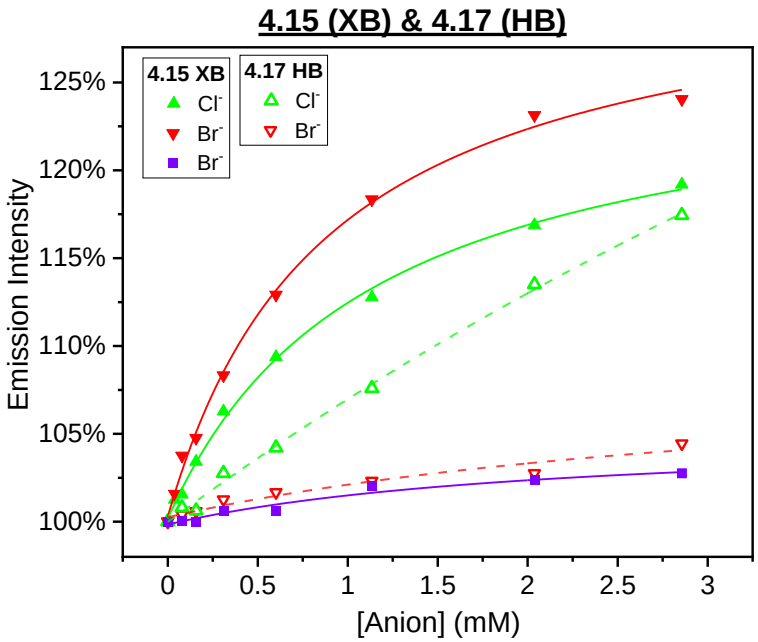


Figure 4.18: *Binding fits of fluorescence maxima change on addition of anions to XB receptor* ***4.15*** *and HB receptor* ***4.17*** *in MeCN; [host] = 1 μM, T = 298 K*

Table 4.6: *Anion association constants for XB receptor* ***4.15*** *and HB receptor* ***4.17***

Anion	Association Constants K_a (M^{-1})	
	4.15 (XB)	**4.17 (HB)**
Cl^-	888 ± 90	79 ± 38
Br^-	1133 ± 126	266 ± 147
I^-	463 ± 308	NB

Anion association constants with errors determined using 1:1 stoichiometric BindFit analysis of the fluorescence emission changes, 1 μM receptor in MeCN; 298 K. NB = no binding observed.

4.2.8.2. Titration Studies in Water-Acetonitrile Mixtures

The anion association properties of XB and HB receptors **4.15** and **4.17** were investigated in mixed aqueous organic-solvent media. Although both receptors contain 3 TEG groups, designed to enhance solubility in aqueous media, each was found to exhibit almost complete quenching in pure water – attributed to aggregation-caused quenching (ACQ).[18] The photo-physical properties of each were investigated in mixtures of MeCN and H_2O to determine a solvent system which combined receptor BODIPY fluorescence with the greatest water content for anion binding studies

The absorbance and emission profiles of receptors **4.15** and **4.17** were investigated in MeCN with increasing aliquots of H_2O. The optical density of both receptors was found to slowly decrease from pure MeCN to 60% H_2O/40% MeCN; an increase of the water ratio is related to a decrease of molar attenuation (extinction) coefficient of the absorption maxima as detailed in the Beer–Lambert law (Equation 4.1).[19]

Equation 4.1: *Beer–Lambert Law*

$$A = \varepsilon c l$$

A = *Absorbance* ε = *Molar attenuation coefficient*

c = *Molar Concentration* l = *Pathlength*

An increased water ratio of >60% resulted in a significant decrease in absorbance and a broadening of the spectra were observed (Figure 4.19 & Figure 4.20). The emergence of two peaks at 510 nm and 530 nm for HB receptor **4.17** has been previously observed in THF-water mixtures and is associated with the intermolecular dimerization assembly of BODIPY derivatives.[19] Interestingly this is not observed in pure water or for XB analogue **4.15** — which, due to the large size of the iodines, may not be able to dimerise as readily. In pure water the receptors are likely aggregated in a variety of conformations resulting in the broad spectra seen for both **4.15** and **4.17**.

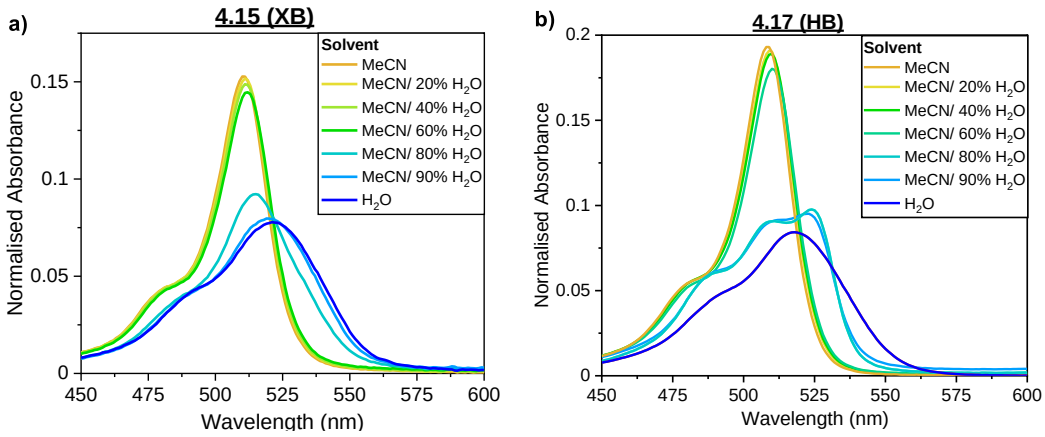


Figure 4.19: *Absorbance spectra of receptors* ***4.15*** *and* ***4.17*** *with changing ratios of H_2O in MeCN*

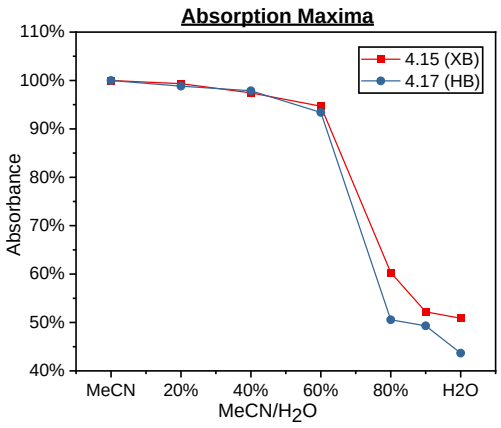


Figure 4.20: *Percentage absorbance maxima of receptors* ***4.15*** *and* ***4.17*** *with changing ratios of H_2O in MeCN*

The association of dimers and aggregation is also observed in the fluorescence emission profiles for each receptor. Increasing the water content from pure MeCN to 70% H_2O 30% MeCN resulted in a fluorescence emission increase for both receptors by over 100%. After exceeding 70% H_2O / 30% MeCN, the emission intensity is significantly quenched due to ACQ (Figure 4.21 & Figure 4.22). This is due to the increasing viscosity of the solvent with an increasing ratio of H_2O,[20] which results in a reduction in the rate of non-radiative decay processes as described in Equation 4.2, often observed when BODIPY is used as a fluorescent rotor group.[21]

Equation 4.2: *Influence of solvent viscosity on non-radiative decay*[21]

$$k_{NR} = \frac{\upsilon}{\eta}\exp\left(-\frac{E_a}{RT}\right)$$

k_{NR} *= Non-radiative rate constants* υ *= Limiting pressure exerted by the rotor* η *= Viscosity*

E_a *= Barrier for internal rotation* R *= Gas constant* T *= Temperature*

To further probe the understanding that both receptors were aggregating in pure water and resulting in ACQ, Triton X-100 (TX) surfactant was added and the fluorescence intensity change monitored (Figure 4.22). The addition of 0.1% TX by volume induced a significant enhancement of fluorescence to above pre-quenching intensities. This indicates that the surfactant had disrupted the aggregation; the enhancement beyond pre-quenched levels may be a result of increased solubility of the receptor due to the solubilising influence of the surfactant molecules.

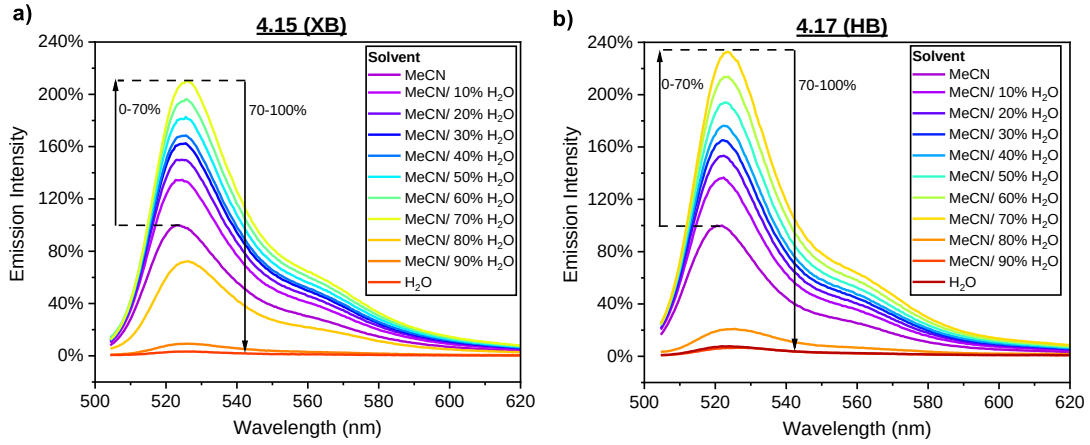


Figure 4.21: *Emission spectra of receptors* ***4.15*** *and* ***4.17*** *with changing ratios of H_2O in MeCN*

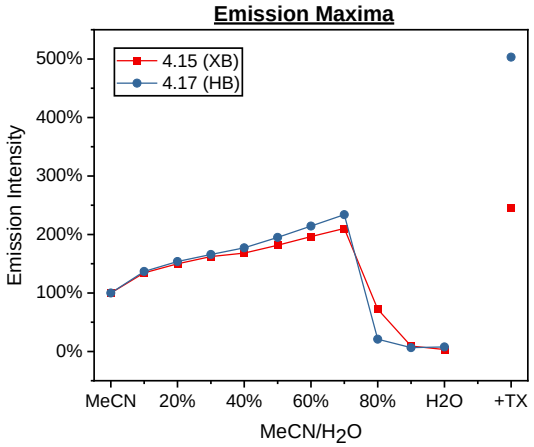


Figure 4.22: *Percentage emission maxima of receptors* ***4.15*** *and* ***4.17*** *with changing ratios of H_2O in MeCN, and addition of TX*

Balancing the need to study the ability of the receptors to act as sensors in aqueous media and the discovery that in pure water there is significant ACQ, the solvent ratio of 70% H_2O / 30% MeCN was used for fluorescence anion titration studies. The photo-physical properties were probed with absorption and fluorescence emission spectroscopy and are plotted and tabulated in Figure 4.23 and Table 4.7. Compared to previous studies in MeCN and acetone the receptors display the greatest Stokes shifts in this solvent mixture due to the increased polarity which stabilises the excited state.

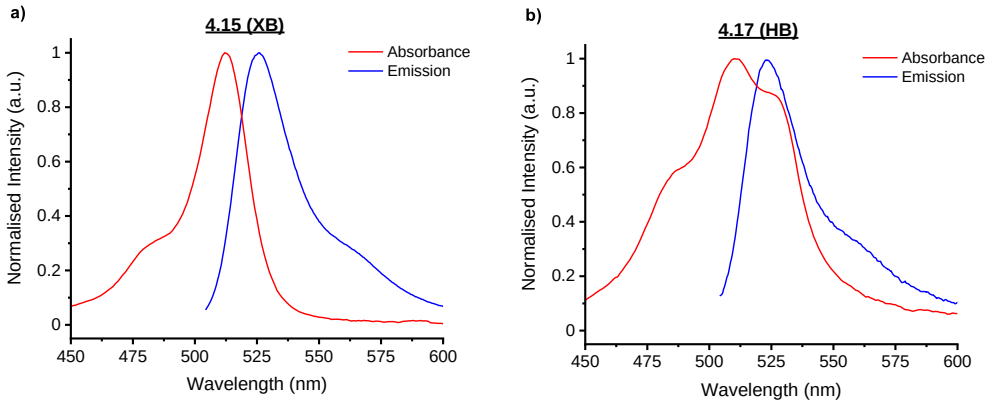


Figure 4.23: *Normalised emission and absorbance spectra for XB receptor* ***4.15*** *and HB receptor* ***4.17*** *in 30% MeCN / 70% H_2O; 1 µM, 298 K.*

Table 4.7: *Wavelengths of absorption and emission for XB receptor* ***4.15*** *and HB receptor* ***4.17*** *in 30% MeCN / 70% H_2O.*

Receptor	$\lambda_{abs,\ max}$ / nm	$\lambda_{ems,\ max}$ / nm	Stokes Shift / nm
XB 4.14	512	526	14
HB 4.17	510	523	13

λ_{ex} = 480 nm, [1 µM], 298 K

Qualitative addition of NaCl, NaBr and $NaClO_4$ to 1 µM solutions of **4.15** and **4.17** in 30% MeCN / 70% H_2O led to no fluorescence response, indicating no binding. However, addition of NaHS, NaSCN and NaI led to fluorescence quenching in both receptors (Figure 4.24) with **4.15** exhibiting 66%, 57% and 50%, and **4.17** displaying 11%, 30% and 40%, respective quenching. Notably, for HS^- the percentage decrease is more significant for XB **4.15** than HB **4.17.**

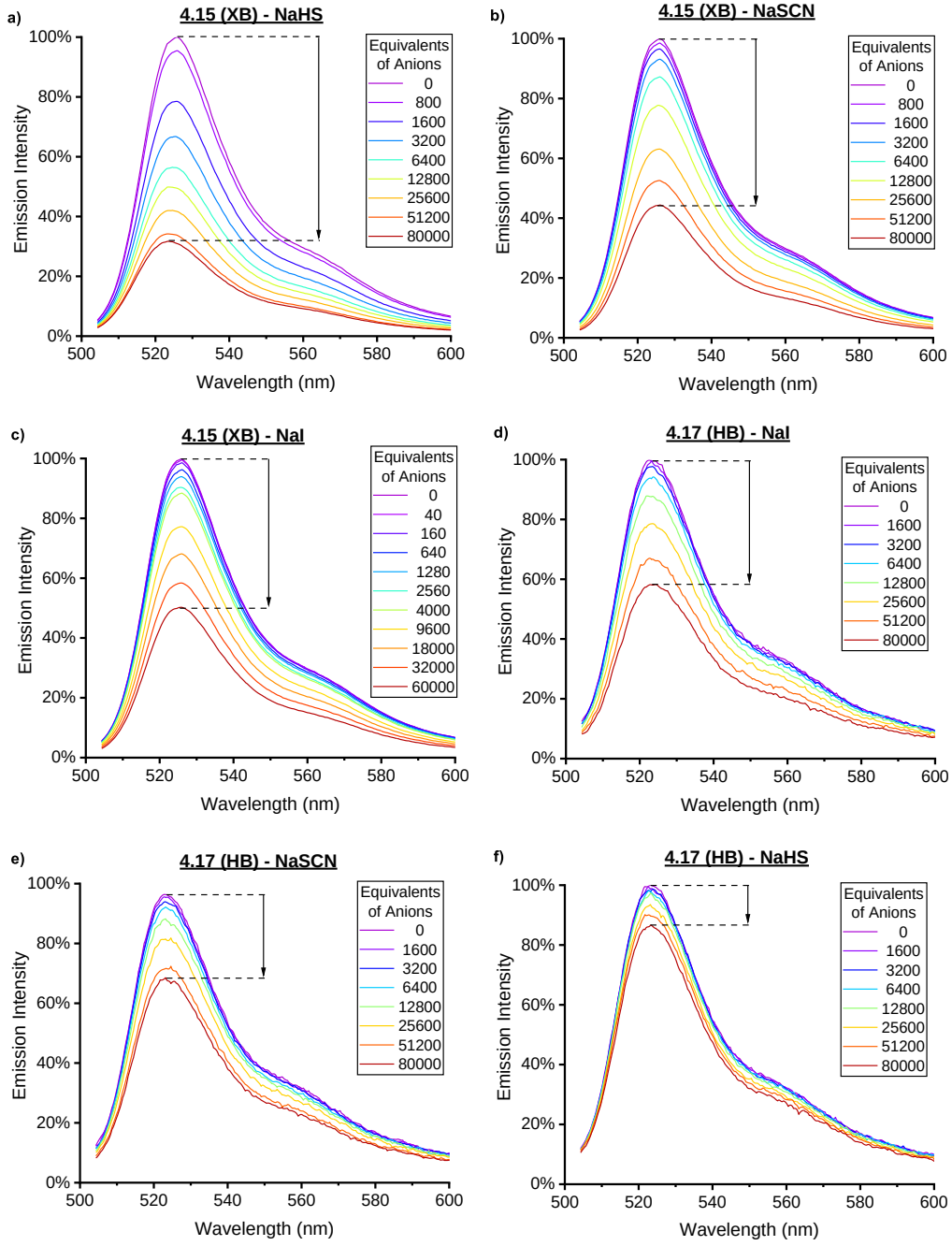


Figure 4.24: *Fluorescence emission intensity changes of XB receptor **4.15** and HB receptor **4.17** upon addition of anions in 30% MeCN / 70% H_2O, [host] = 1 μM, T = 298 K.*

Association constants were determined from the emission titration data (Figure 4.25) using a 1:1 host guest stoichiometric binding model with OriginLab[22] and are shown in Table 4.8. In accordance with the results in MeCN, XB receptor **4.15** displays greater association to the anions than the HB analogue **4.17**. Interestingly, **4.15** shows selectivity for HS^- over both iodide and SCN^-, again highlighting the affinity of XB for HS^- in aqueous media.

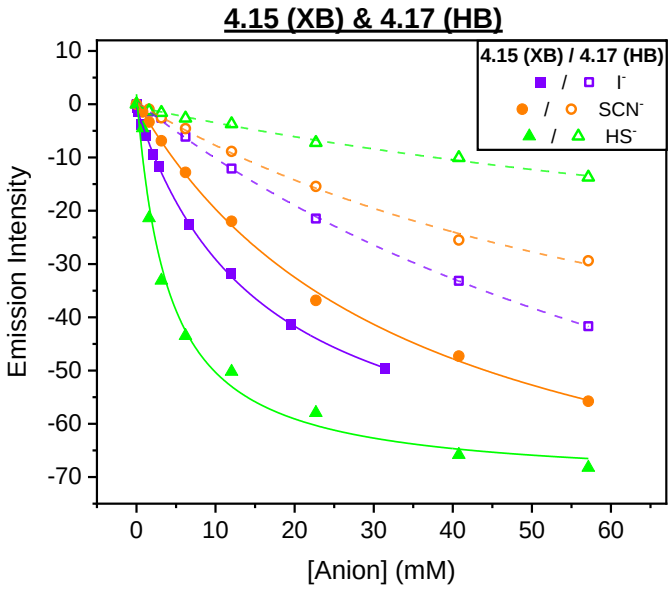


Figure 4.25: *Binding fits of fluorescence maxima change on addition of anions to XB receptor* ***4.15*** *and HB receptor* ***4.17*** *in 30% MeCN / 70% H_2O; [host] = 1 µM, T = 298 K.*

Table 4.8: *Anion association constants for XB receptor* ***4.15*** *and HB receptor* ***4.17***

Anion	Association Constants K_a (M^{-1})	
	4.15 (XB)	**4.17 (HB)**
HS^-	249 ± 48	10 ± 4
SCN^-	29 ± 3	12 ± 3
I^-	63 ± 3	7 ± 1

Anion association constants with errors determined using 1:1 stoichiometric non-linear regression analysis of the fluorescence emission changes, 1 µM receptor in 30% MeCN / 70% H_2O; 298 K.

4.2.9. Summary

An iodotriazole motif appended at the *meso* position of a BODIPY fluorophore was investigated for its ability to recognise and sense anions. Initial results of the monodentate XB iodotriazole receptor **4.1** showed a remarkable fluorescence increase on chloride binding in acetone. A bidentate XB bis-iodotriazole analogue **4.8** displayed similar sensing observations with stronger anion association. A 2nd generation of bis-iodotriazole receptor **4.15**, along with the HB analogue **4.17**, containing three appended TEG groups to enhance solubility in aqueous media were synthesised. Fluorescence anion titration studies in MeCN showed emission intensity increases on binding. In the competitive aqueous-organic solvent mixture, 70% H_2O

/ 30% MeCN, the XB receptor system outperformed the HB analogue in anion binding affinity and sensing capability. Importantly, XB receptor **4.15** was found to be selective for HS^- and represents the first example of a XB BODIPY receptor capable of sensing HS^- in aqueous solvent media.

4.3. BODIPY Rotaxanes

Rotaxane host systems are well understood to harbour enhanced anion binding capabilities due to their ability to encapsulate guests (*See Section 1.2.4.5*). Incorporation of fluorescence reporter groups into rotaxanes can enable the system to optically report binding events. Due to the BODIPY fluorophore's desirable photophysical properties and synthetic versatility, it is well suited as a reporter group in MIM design.

In addition, owing to a BODIPY derivative's relatively large size, it has seen use as a combined stopper and optical reporter group in rotaxane systems.[23–27] This was demonstrated by Lin and co-workers, who developed a multi-stimuli-responsive BODIPY rotaxane system capable of optically reporting acid/base changes and sensing anions (Figure 4.26).[23,27] On deprotonation of the central amine, the macrocyclic component translocated from the axle ammonium to the triazolium station, resulting in a quenching of emission intensity. In addition, they found that the rotaxane selectively sensed $H_2PO_4^-$ in MeCN over other anions including F^-, Cl^- and CN^-. However, the free axle exhibited similar selectivity, suggesting that the selectivity was not due to the interlocked nature of the rotaxane system.

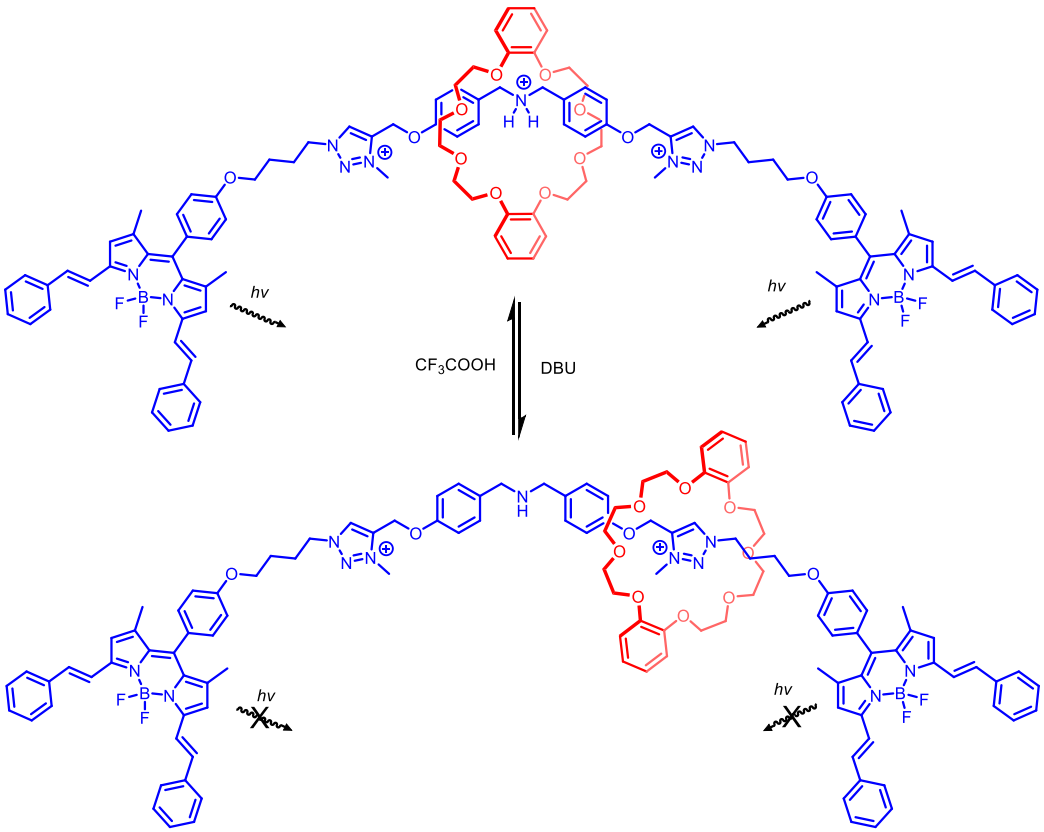


Figure 4.26: *Lin's multi-stimuli-responsive BODIPY rotaxane undergoing deprotonation.*

In 2010, Stoddart and co-workers demonstrated an electrochemically switchable bistable [2]rotaxane that uses a BODIPY reporter group. In the starting redox state, the cyclobis(paraquat-p-phenylene) macrocycle occupies the central TTF station, allowing the BODIPY group to freely rotate unhindered and exhibit low fluorescence. Upon oxidation to the TTF^{2+} cation in toluene, the macrocyclic component was found to translocate towards the BODIPY (Figure 4.27), restricting the BODIPY's rotational freedoms, reducing non-radiative decay processes and resulting in a 3-fold fluorescence enhancement.

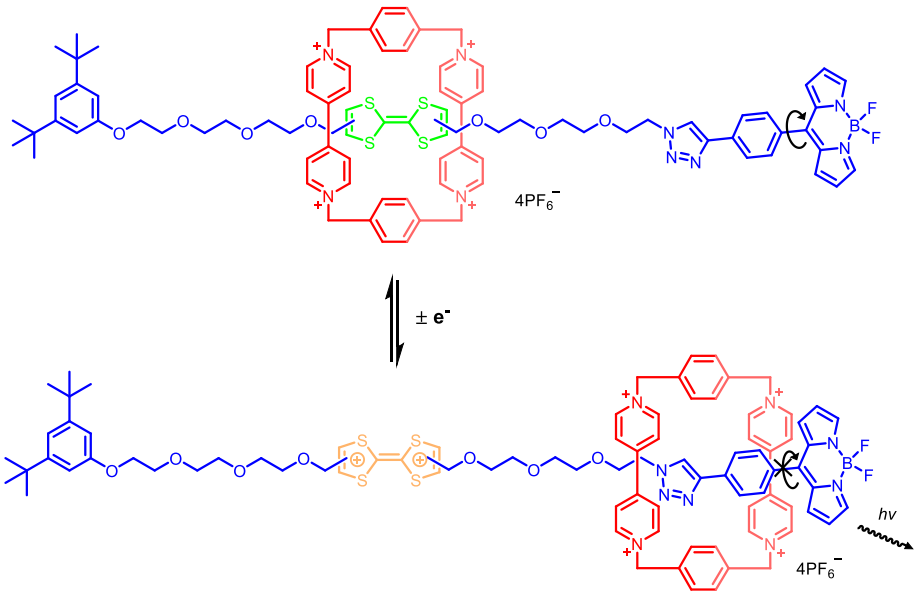


Figure 4.27: *Stoddart's electrochemically switchable BODIPY containing bistable [2]rotaxane undergoing oxidation.*

Following the precedent of using BODIPY as both a stopper as well as a reporter group, a BODIPY containing [2]rotaxane for anion sensing was designed (Figure 4.28). Rotaxanation would be achieved via AMT CuAAC reactions.

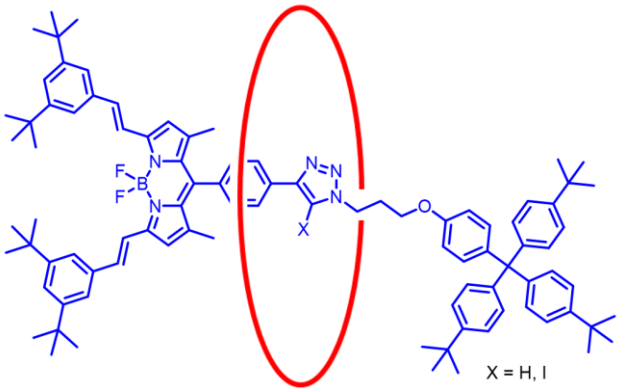


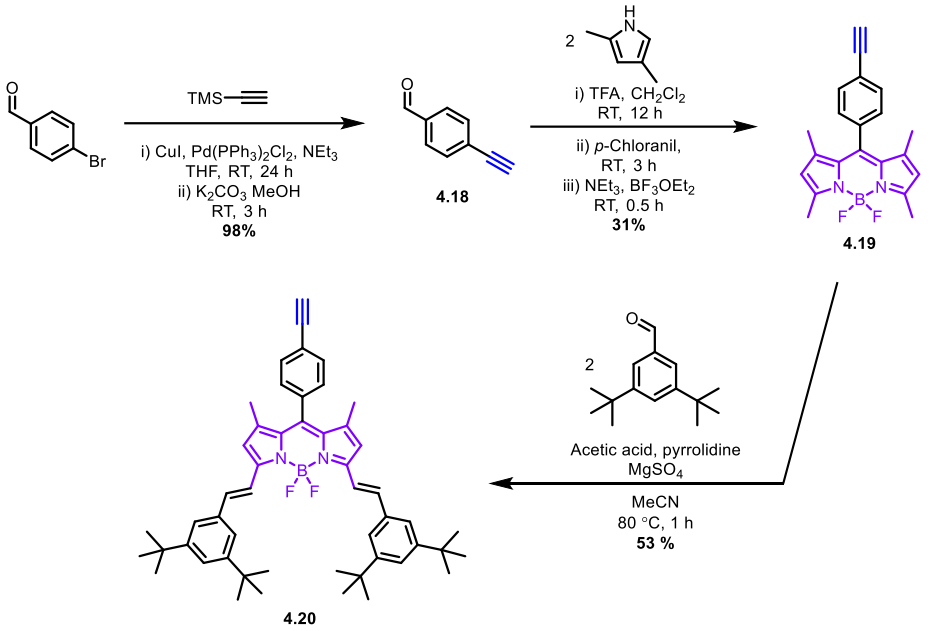
Figure 4.28: *Proposed BODIPY containing rotaxane*

4.3.1. BODIPY Stopper Synthesis

The alkyne functionalised BODIPY stopper **4.20** was prepared according to Scheme 4.8. 4-Bromobenzaldehyde was reacted with trimethylsilylacetylene, via a Sonogashira reaction using a palladium catalyst. Subsequent deprotection of the TMS group was achieved by stirring with K_2CO_3 in MeOH, to afford benzaldehyde **4.18** in a combined yield of 98%.[28] Benzaldehyde **4.18** was reacted with two equivalents of 2,4 dimethyl pyrrole in the presence of a catalytic amount of TFA before *p*-chloranil was added as an oxidant. The dipyrromethene

intermediate was subsequently reacted with BF_3OEt_2 in the presence of NEt_3, affording BODIPY alkyne **4.19** in a moderate 31% yield (Scheme 4.8).

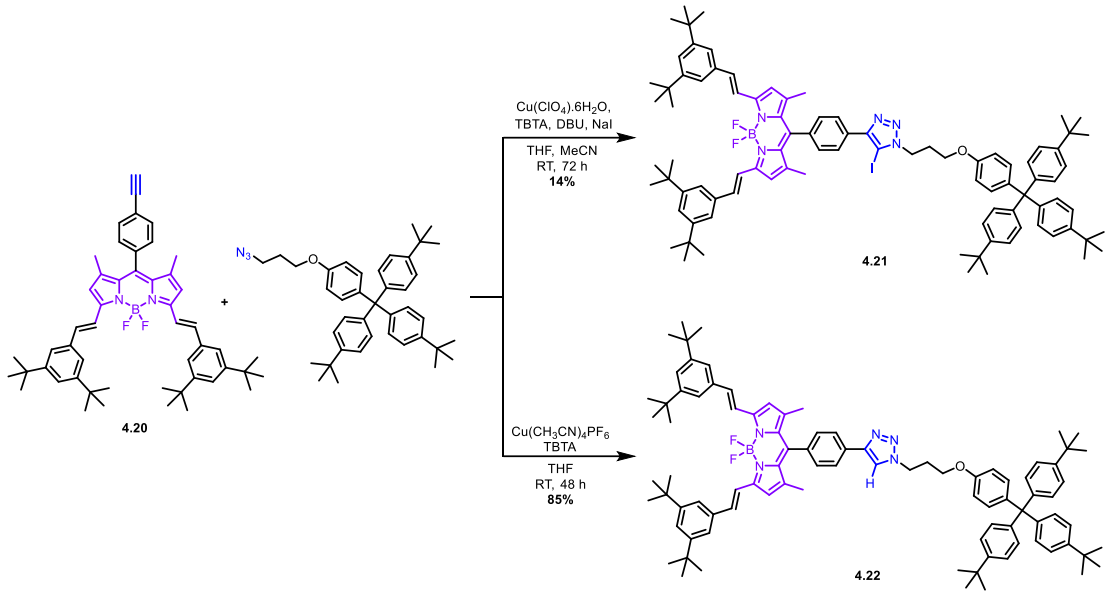
BODIPY alkyne **4.19** was reacted with two equivalents of 3,5-di-tert-butylbenzaldehyde via a Knoevenagel condensation, in the presence of 10 equivalents of pyrrolidine and acetic acid. To ensure dry conditions, excess $MgSO_4$ was added and the reaction was left to stir at 80 ˚C for 1 h. Purification was achieved by column chromatography to afford BODIPY-stopper-alkyne **4.20** in a yield of 53 % (Scheme 4.8).



Scheme 4.8: *Synthesis of BODIPY-stopper-alkyne*

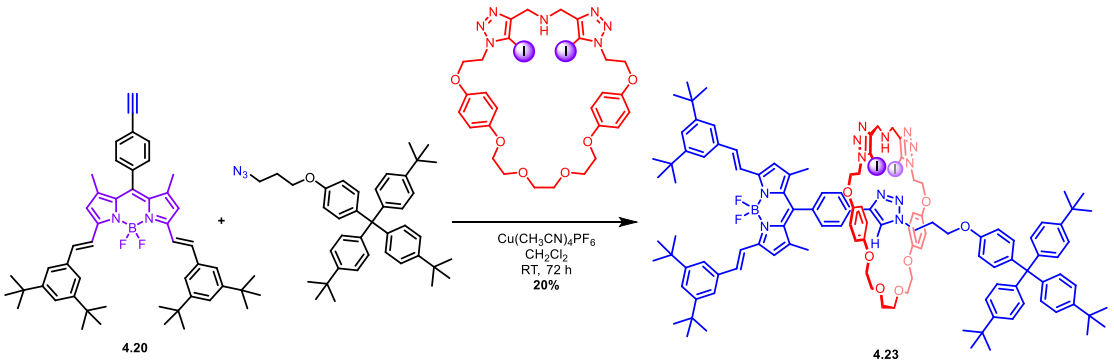
4.3.2. Axle and Rotaxane Synthesis

BODIPY-stopper-alkyne **4.20** was reacted with one equivalent of the stopper azide (*provided by Dr. Klein*) in a combined CuAAC click and iodination reaction using a $Cu(ClO_4)$ catalyst, with TBTA, DBU and NaI. XB axle **4.21** was purified and isolated in a modest yield of 14 % (Scheme 4.9). The HB analogue was synthesised by reacting BODIPY-stopper-alkyne **4.20** with one equivalent of stopper azide in a CuAAC click reaction using a $Cu(CH_3CN)_4PF_6$ catalyst, affording HB axle **4.22** in a yield of 85% (Scheme 4.9).



Scheme 4.9: *Synthesis of XB and HB BODIPY axles* ***4.21*** *and* ***4.22***

One equivalent of the XB macrocycle (*provided by Dr Xiaoxiong Li*) was stirred in dry CH_2Cl_2 with one equivalent of $Cu(CH_3CN)_4.PF_6$ to achieve endotopic coordination. Four equivalents of BODIPY-stopper alkyne **4.20** and stopper azide were subsequently added and the reaction left to stir for 72 h in darkness and under an N_2 atmosphere. The crude mixture was washed with EDTA solution to remove the copper catalyst and purification was achieved using preparative TLC (eluent CH_2Cl_2), affording rotaxane **4.23** in a yield of 20% (Scheme 4.10).



Scheme 4.10: *AMT synthesis of BODIPY rotaxane 4.23.*

4.3.2.1. Rotaxane Characterization

Novel rotaxane **4.23** was characterised by ^{1}H NMR, ^{13}C NMR, ^{1}H-^{1}H ROESY NMR and HRMS. A comparison between the ^{1}H NMR spectra of rotaxane **4.23**, free axle **4.22** and the macrocycle (Figure 4.29) provides evidence for formation of the interlocked structure. The rotaxane ^{1}H NMR spectrum reveals significant downfield shifts in the alkyl axle (*k, l, m*), suggesting shielding by the electron rich hydroquinone macrocycle moieties.

Two dimensional ^{1}H-^{1}H ROESY NMR experiments provided further evidence for the formation of rotaxane **4.23** (Figure 4.30). Through-space interactions were observed between the macrocycle component protons and axle protons; cross peaks between the hydroquinone of the macrocycle (5, 6) and the proto-triazole and aryl peaks of the axle provide evidence for their close proximity and interlocked nature.

Additional evidence for the rotaxanation was provided by HRMS (Figure 4.31), where rotaxane **4.23** was observed as a cationic $[M+H]^{+}$ species.

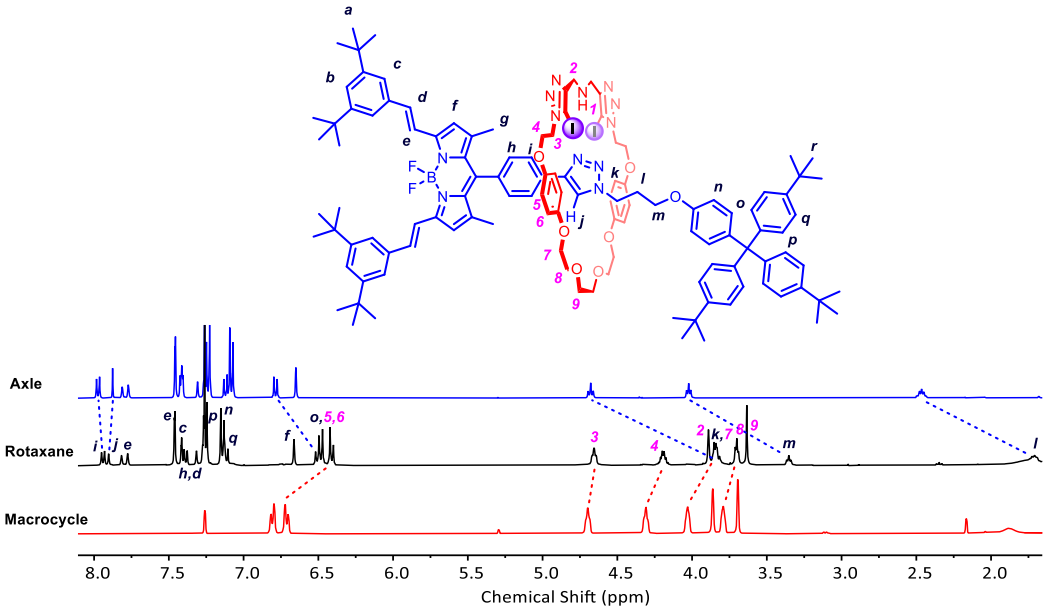


Figure 4.29: *Truncated ^{1}H NMR spectral comparison in $CDCl_3$ between rotaxane **4.23**, HB axle **4.22** and the free macrocycle.*

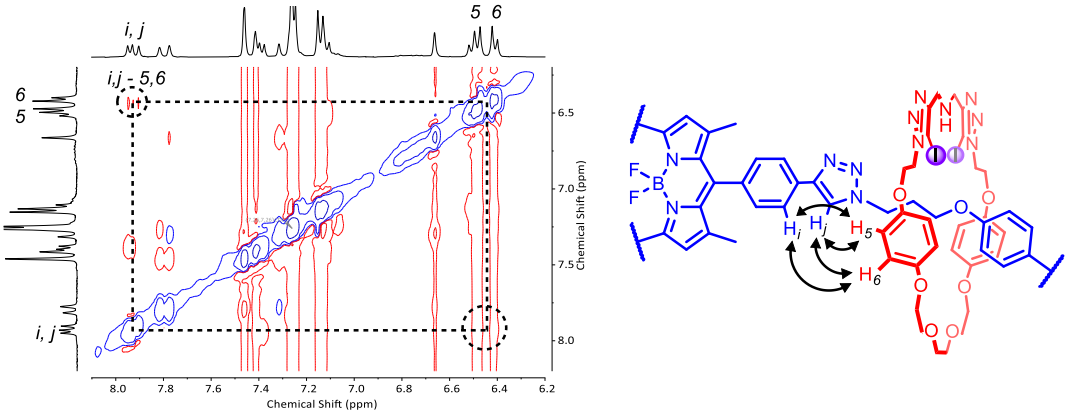


Figure 4.30: *Truncated ^{1}H-^{1}H ROESY NMR of rotaxane **4.23** in $CDCl_3$, highlighting through-space interactions.*

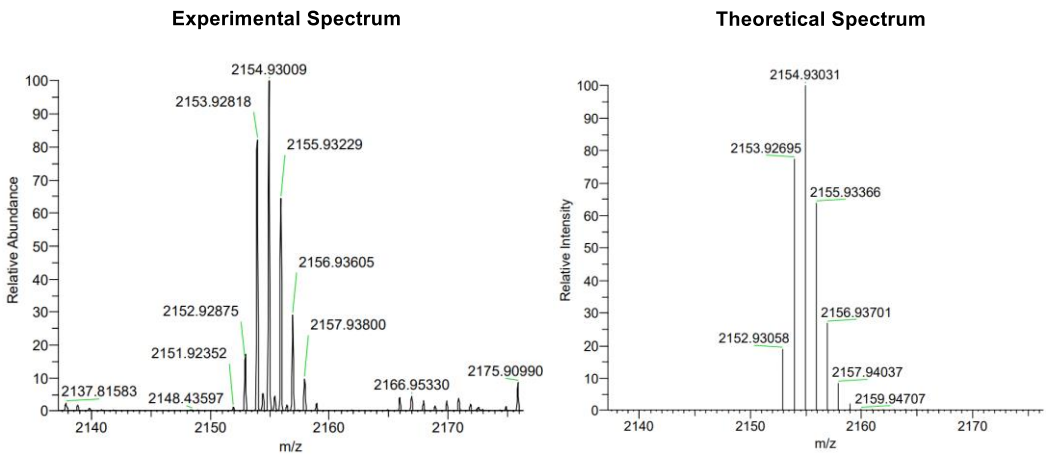


Figure 4.31: *HRMS experimental and theoretical spectrum of rotaxane* ***4.23****, m/z = 2152.92871 ([M+H]⁺, $C_{119}H_{142}O_7N_{12}{}^{10}BF_2{}^{127}I_2$, calc = 2152.93058)*

4.3.3. Rotaxane and Axle Anion Binding Studies

4.3.3.1. ^{1}H NMR Chloride Anion Titration Studies

The anion binding properties of XB axle **4.21**, HB axle **4.22**, and rotaxane **4.23** were investigated by ^{1}H NMR titration experiments in d_6-acetone with TBACl. Chemical shifts of proton signals adjacent to the respective XB binding site for **4.21** or involving the proto-triazole for **4.22** and **4.23** were monitored as a function of halide anion concentration.

On addition of 10 equivalents of TBACl to XB axle **4.21** downfield shifts in the aryl peak *i* (Δδ = 0.10 ppm) were observed, indicating that the binding event is being directed by the XB iodotriazole (Figure 4.32a). For HB axle **4.22,** analogous experiments induced downfield shifts in the proto-triazole peak *j* (Δδ = 0.12 ppm) (Figure 4.32b), indicating binding to chloride.

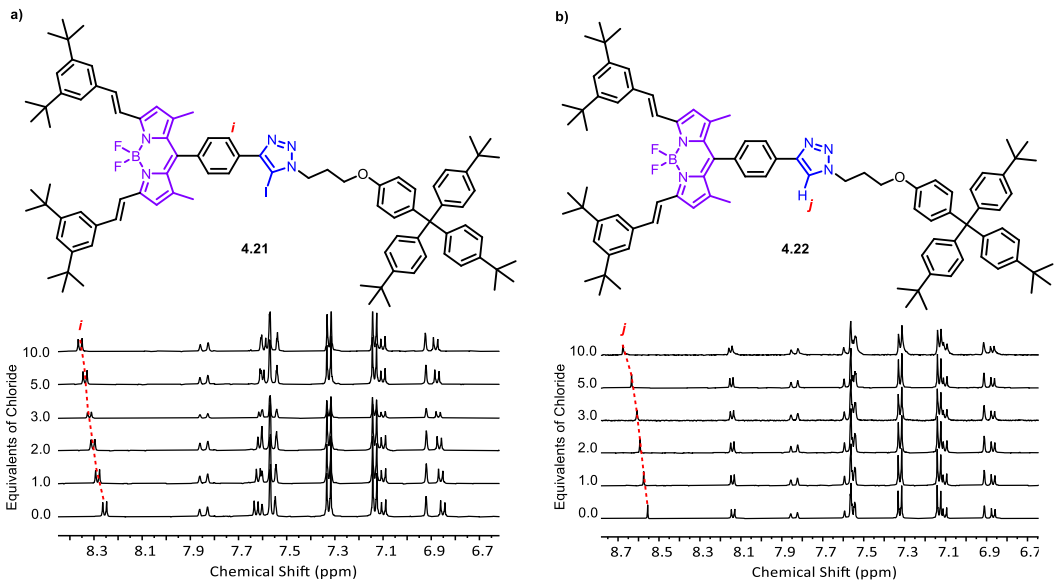


Figure 4.32: *^{1}H NMR titrations of **a)** XB axle **4.21** and **b)** HB axle **4.22** on addition of TBACl in acetone-d_6 (1 mM, 298 K).*

On addition of up to 10 equivalents of TBACl to rotaxane **4.23**, a downfield shift of the proto-triazole signal *J* (Δδ = 0.73 ppm) was observed (Figure 4.33). Interestingly, the hydroquinone peaks corresponding to protons *5* and *6* showed convergence and symmetrisation, suggesting that the halide complexation is occurring within the rotaxane cavity. Similarly, the macrocycle alkyl peaks *3* and *4*, converge and then split apart after 1.0 equivalents of TBACl, with peak *3* shifting upfield and *4* downfield (Figure 4.33).

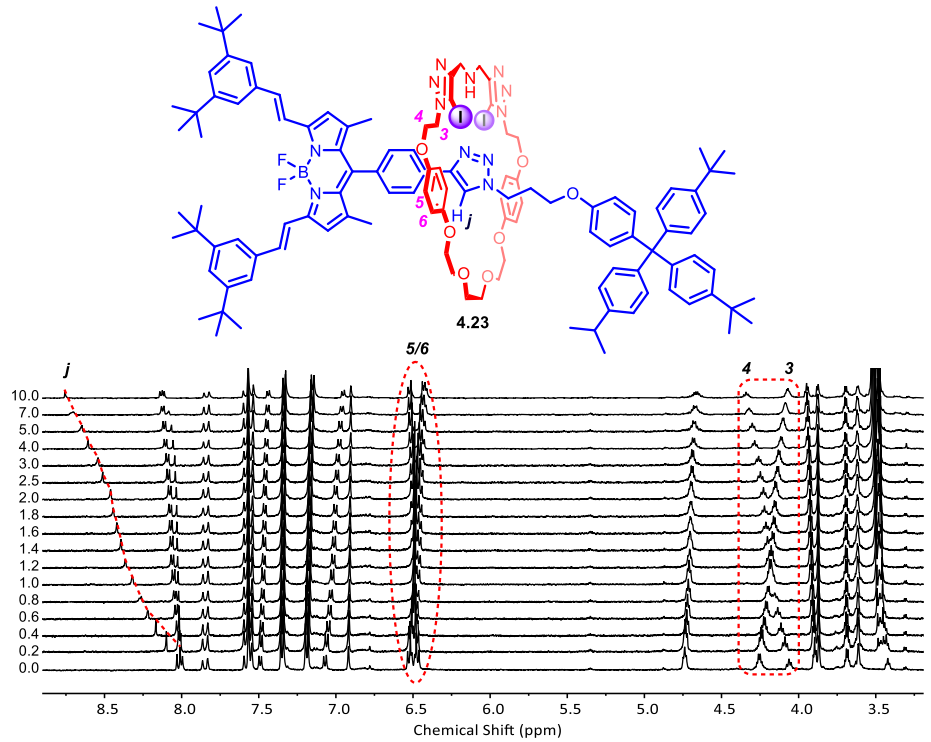


Figure 4.33: *^{1}H NMR titration of rotaxane **4.23** on addition of TBACl in acetone-d_6 (1 mM, 298 K).*

1:1 Host-guest stoichiometric association constants of axles **4.21**, **4.22** and rotaxane **4.23** for chloride in d_6-acetone were determined (Table 4.9, Figure 4.6). As anticipated, the association constant of the XB axle **4.21** is greater than that of the HB analogue **4.22**. Similarly, rotaxane **4.23** was found to have a greater association constant than both axles, displaying a tenfold increase over the HB axle and a 2-fold over the XB analogue — attributed to the multivalent binding within the cavity. However, the determined associaton constant of 790 M^{-1} falls far short of what would be expected from a rotaxane system, particularly in a less competitive solvent such as acetone. This may be due to steric restrictions within the cavity preventing the two iodotriazoles from cooperatively coordinating to chloride. Alternatively, it could be due to an energetic penalty of translocating the macrocycle into a new conformation, as observed by Smith and co-workers with their squaraine rotaxane (*see section 1.2.4.5. Mechanically Interlocked Anion Hosts, Figure 1.24*).

Table 4.9: *^{1}H NMR titration anion association constants of receptor **4.21**, **4.22** and **4.23** in d_6-acetone; 10 mM, 298 K.*

Receptor	K_a / M^{-1}
XB Axle 4.21	340 ± 10
HB Axle 4.22	65 ± 1
Rotaxane 4.23	790 ± 30

Values of K_a determined using Bindfit by monitoring shifts in peaks with the addition of anions; a host-guest 1:1 stoichiometric binding model was used; errors (±) in parentheses; [host] = 1 mM, d_6-acetone, T = 298 K.

4.3.3.2. Rotaxane Decomposition

Further ^{1}H NMR titration experiments with other anions could not be conducted as rotaxane **4.23** was found to have decomposed over time, in spite having been stored in a sub-freezing, dark environment under N_2. ^{1}H NMR analysis and comparison of the decomposed product to the pure rotaxane, axle and macrocycle indicated that the mechanical bond has been broken amongst other forms of decomposition. Specifically, the emergence of a free axle proton and of macrocycle proton signals point towards a rotaxane de-threading process (Figure 4.34). Due to the flexible nature of the macrocycle and the ability of the BODIPY stopper to rotate, this may tentatively be rationalised as depicted in Figure 4.35.

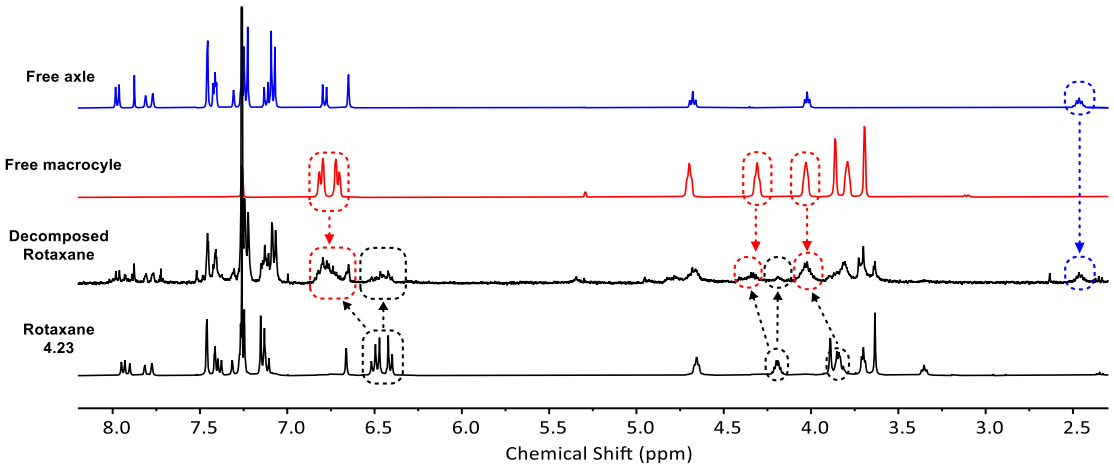


Figure 4.34: *Truncated ^{1}H NMR spectral comparison in $CDCl_3$ between rotaxane **4.23**, HB axle **4.2** , the free macrocycle and the decomposed rotaxane.*

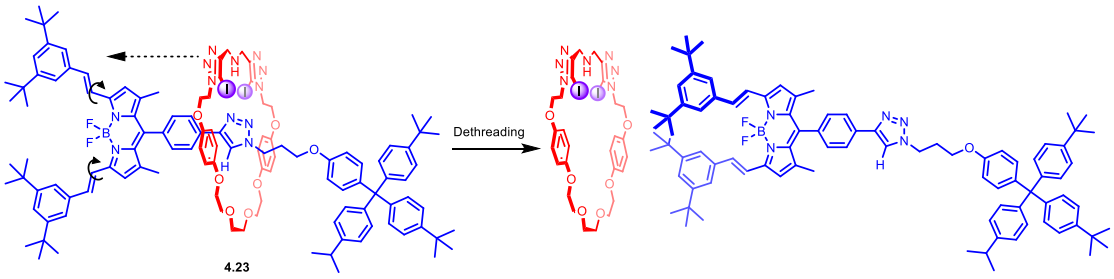


Figure 4.35: *Proposed de-threading process of rotaxane* ***4.23***

4.3.3.3. XB Axle 4.21 and HB Axle 4.22 Fluorescence Titration Studies

The photophysical properties of axles **4.21**, **4.22**, were investigated with absorption and fluorescence spectroscopy (Figure 4.10). Interestingly, due to the 3,5-di-tert-butyl aryl groups conjugated directly to the BODIPY, the wavelengths of absorption and emission are significantly red shifted when compared to phenyl BODIPY (Table 4.1). On account of the small Stokes shift, each system was excited at the lower absorption shoulder wavelength (588 nm).

Table 4.10: *Energies of absorption and emission for receptor* ***4.21*** *and* ***4.22*** *in acetone, 298 K.*

Receptor	$\lambda_{abs,\ max}$ / nm	$\lambda_{ems,\ max}$ / nm	Stokes Shift / nm
XB Axle 4.21	629	642	13
HB Axle 4.22	628	639	11

λ_{ex} = 588 nm, [1 µM], 298 K

The chloride anion sensing properties of axles **4.21**, **4.22** at 1 µM were investigated using fluorescence spectroscopy in acetone. The fluorescence emission intensity was monitored on the addition of TBACl. Surprisingly, in spite of the binding observed in ^{1}H NMR titration studies and the known sensitivity of BODIPY to changes in their localised environments, neither receptor displayed any emission intensity changes. This was attributed to the lack of conjugation and electronic communication between the triazole binding site and the BODIPY due to the orthogonal connectivity between the BODIPY and aryl group (Figure 4.36).

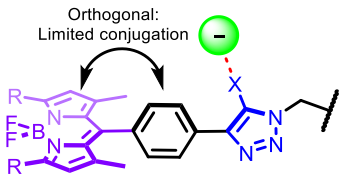


Figure 4.36: *Orthogonal nature of meso positioned aryl group to BODIPY*

4.3.4. Summary

A BODIPY stopper system was synthesised and incorporated into a rotaxane system and two axle receptors. ^{1}H NMR chloride anion titration experiments showed enhanced binding in the rotaxane system in acetone. However, the rotaxane underwent decomposition as a result of de-threading, demonstrating that the BODIPY stopper was not of sufficient size for larger flexible macrocycles.

4.4. BODIPY-Porphyrin Rotaxanes

4.4.1. Introduction to Porphyrin Receptors

Porphyrins are a set of heterocyclic macrocyclic molecules. Zinc (II) metalloporphyrins (Figure 4.37) have photophysical and redox properties that are highly sensitive to their local environments. Consequently, they are prime candidates to function as signal transducers in supramolecular host systems. Taking advantage of the Lewis acidic metal centre through judicious design, porphyrin moieties have been incorporated into various anion receptor structural frameworks.

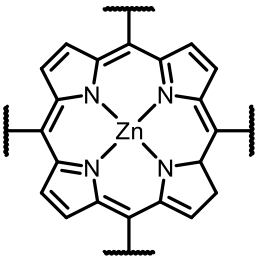


Figure 4.37: *Zinc Porphyrin*

By incorporating two porphyrin moieties, Jang and co-workers were able to significantly enhance the anion affinity of their bis-indole molecular tweezer.[29] On binding, the tweezer adopted a *cis* conformation and, due to favourable π–π interactions between the porphyrins, displayed enhanced binding to chloride in THF ($K_a = 4.93 \times 10^4$ M^{-1}) compared to the analogue without porphyrins (2.28×10^3 M^{-1}) (Figure 4.38).

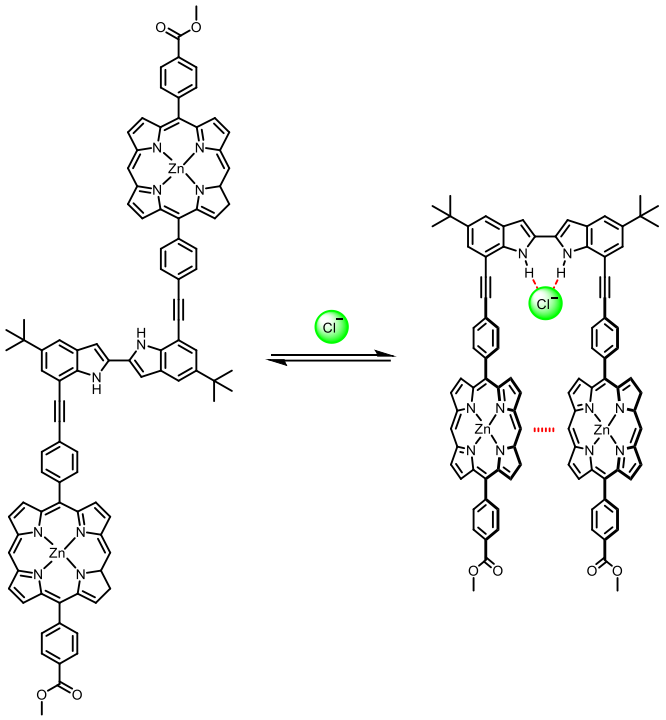


Figure 4.38: *Jang's porphyrin containing biindole molecular tweezer.*

Jang and co-workers later reported a tetraphenyl zinc–porphyrin that contained four proto-triazole groups at the ortho-position of each meso-phenyl substituent (Figure 4.39a).[30] The receptor was found to be capable of recognising chloride (K_a = 22,200 M^{-1}) bromide (K_a = 409 M^{-1}) and iodide (K_a = 12 M^{-1}) in d_6-DMSO. Each halide anion was also found to induce a characteristic bathochromic shift in the receptor's porphyrin Soret absorbance band. The capability to encapsulate anions with porphyrin cages was reported by Li and co-workers.[31] The group synthesised a 'smart' porphyrin cage, via four CuAAC click reactions, that was capable of selectively encapsulating between the metal centres and sensing azide via a bathochromic shift in Soret absorbance and a visible colour change, in d_6-acetone (Figure 4.39b).

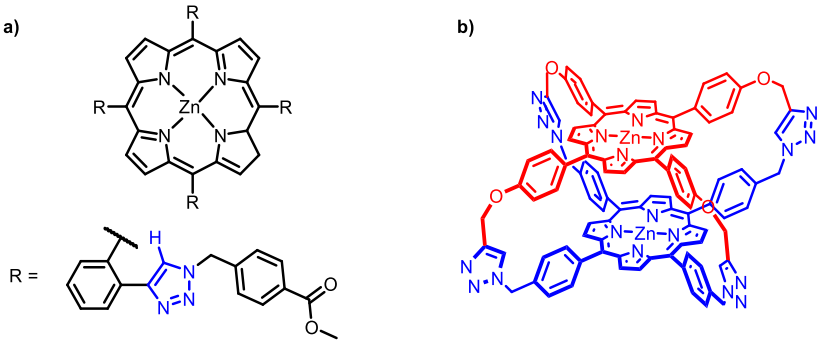


Figure 4.39: *Porphyrin anion host-receptors* ***a)*** *Jang's tetra proto-triazole host* ***b)*** *Li's smart porphyrin cage capable of recognizing azide anions*

Macrocyclic strapped porphyrins have been reported to function as anion receptors.[32] However, their incorporation into rotaxane host systems remains uncommon.[33,31] Other porphyrin containing MIM anion receptors also remain relatively rare, in spite of their desirable photophysical and electrochemical properties.[34]

The development of a BODIPY-porphyrin rotaxane, which could act as a dual optical and electrochemical sensor for anions, is unprecedented. In collaboration with fellow graduate Richard Tse, a novel set of BODIPY-porphyrin [2]rotaxanes were developed and their anion binding and sensing properties investigated. The basic rotaxane design structure shown in Figure 4.40 includes a BODIPY stopper axle component and a XB strapped zinc(II) metalloporphyrin macrocycle. Macrocycle component XB and axle HB triazole anion binding interactions were anticipated to act as communication channel for relaying binding events to the BODIPY and porphyrin photo- and redox-active reporter groups.

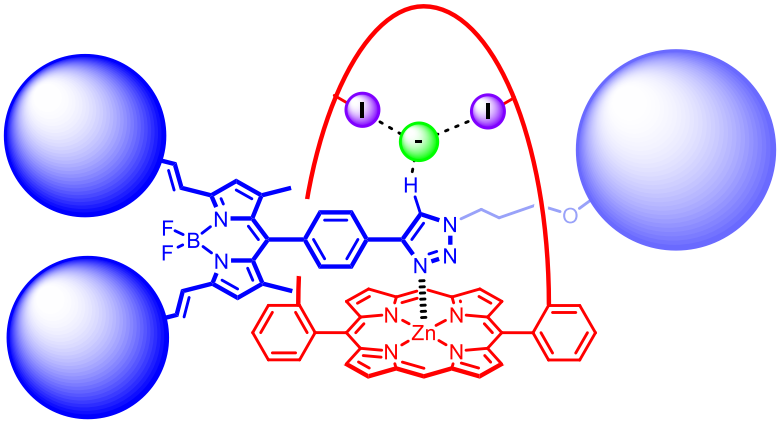


Figure 4.40: *Design of BODIPY-porphyrin [2]rotaxane*

The work in this section was conducted in collaboration with Richard Tse; all rotaxanation synthetic steps, rotaxane characterisation and titration studies were undertaken by Richard Tse.

4.4.2. BODIPY Phenyl Spacer Rotaxane Synthesis & Characterisation

To achieve the synthesis of the neutral porphyrin-BODIPY [2]rotaxanes, an AMT strategy, as described in Section 2.4, was followed. A general scheme is illustrated in Figure 4.41 in which a BODIPY stopper alkyne and a stopper azide are brought together by a copper(I) cation catalyst which is chelated to the strapped porphyrin macrocycle.

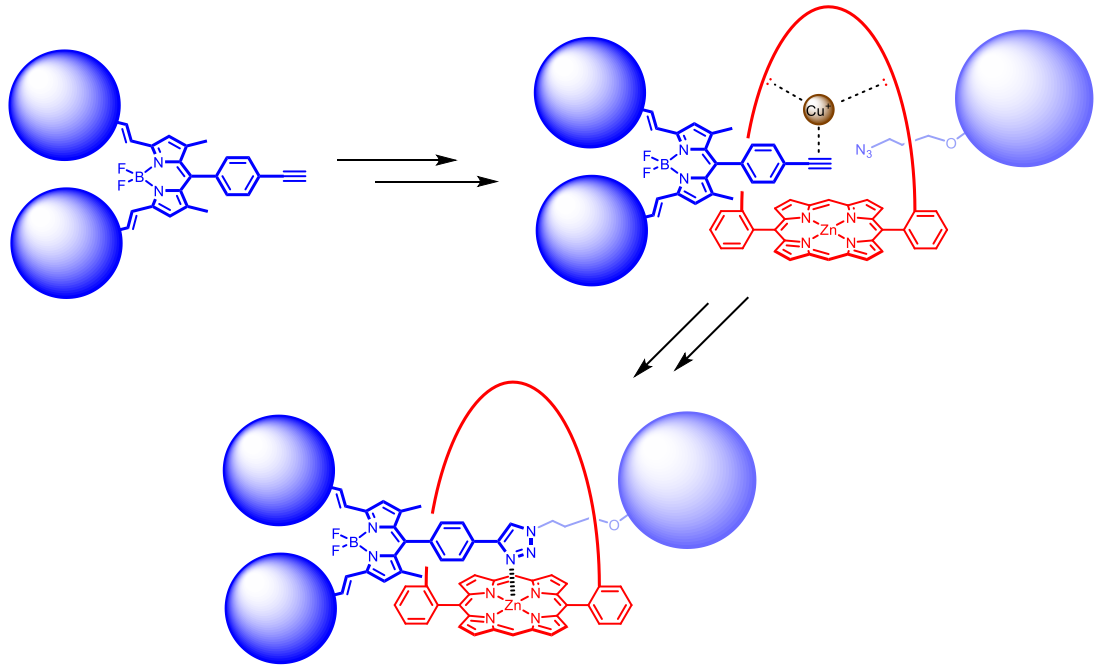
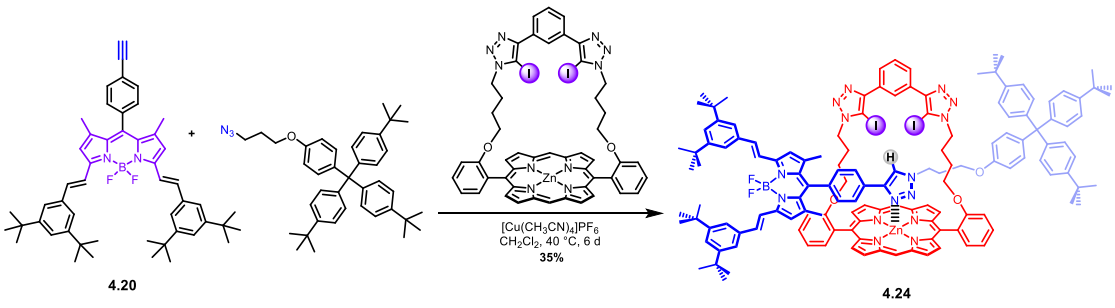


Figure 4.41: *AMT synthesis of target porphyrin-BODIPY [2]rotaxane*

One equivalent of the strapped porphyrin (*provided by Richard Tse*) and one equivalent of $[Cu(CH_3CN)_4]PF_6$ were dissolved in dry, degassed CH_2Cl_2 and left to stir at room temperature under N_2 for 15 minutes to achieve endotopic copper(I) coordination. Five equivalents of the stopper azide and BODIPY stopper **4.20** were subsequently added, and the reaction mixture stirred at 40°C in darkness for six days. The crude reaction mixture was washed with basic aqueous EDTA solution and purification was achieved via preparative TLC to afford the desired [2]rotaxane **4.24** as a blue powder in a yield of 35% (Scheme 4.11).



Scheme 4.11: *Synthesis of BODIPY-porphyrin rotaxane* ***4.24***

Novel [2]rotaxane **4.24** was characterised by ^{1}H NMR (Figure 4.42 & Figure 4.43), ^{13}C NMR, ^{1}H-^{1}H ROESY NMR and HRMS (Figure 4.44). Analysis of the ^{1}H NMR spectrum provides evidence for the formation of the interlocked structure. Most notable are the appearance of new aromatic proton signals corresponding to the desymmetrization of porphyrin protons, *l*, *m* and *n* in the interlocked structure (Figure 4.43). Axle aryl peaks *8* and *9* show significant

upfield shifts indicating substantial shielding from proximity to the aromatic porphyrin component (Figure 4.42 & Figure 4.43).

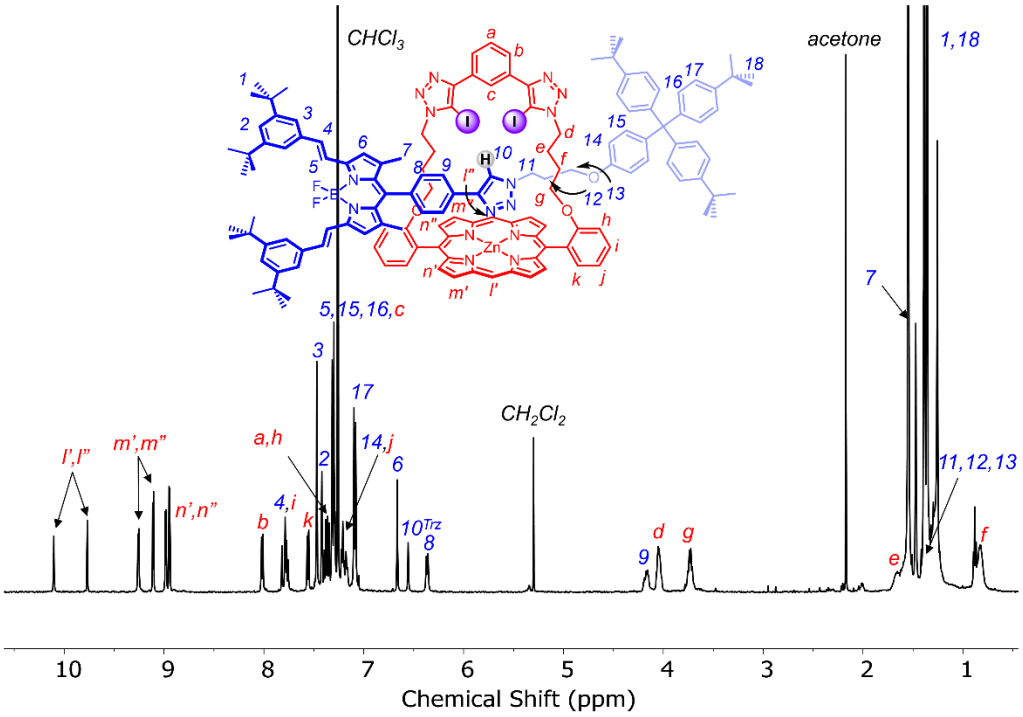


Figure 4.42: *^{1}H NMR spectrum of rotaxane **4.24** with proton assignments; $CDCl_3$, 298 K.*

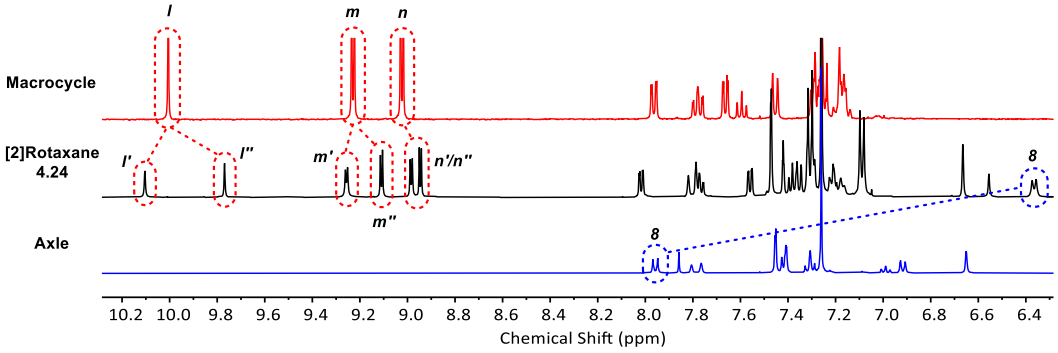


Figure 4.43: *Truncated stacked ^{1}H NMR spectra of the free strapped porphyrin macrocycle, [2]rotaxane **4.24** and the free axle; $CDCl_3$, 298 K.*

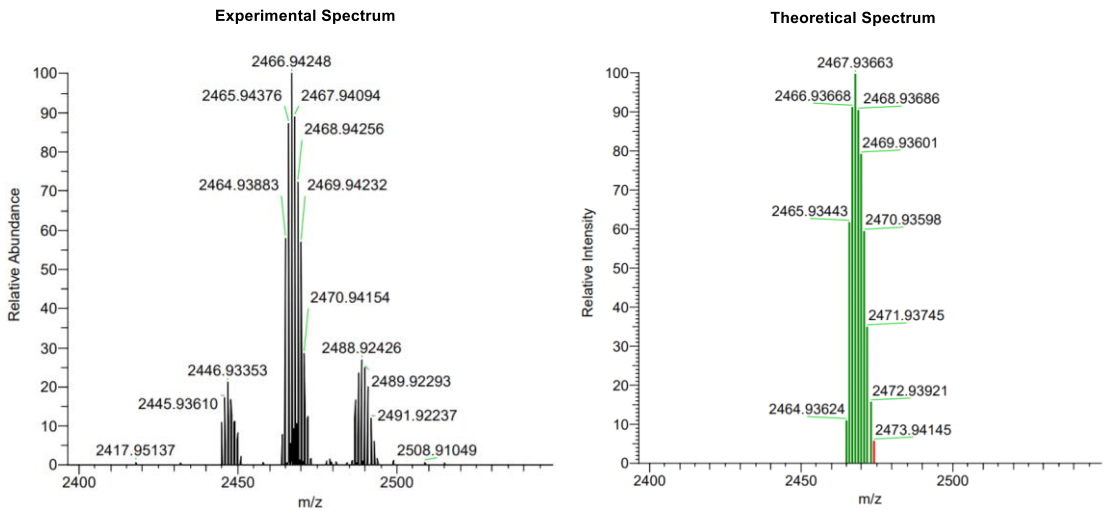


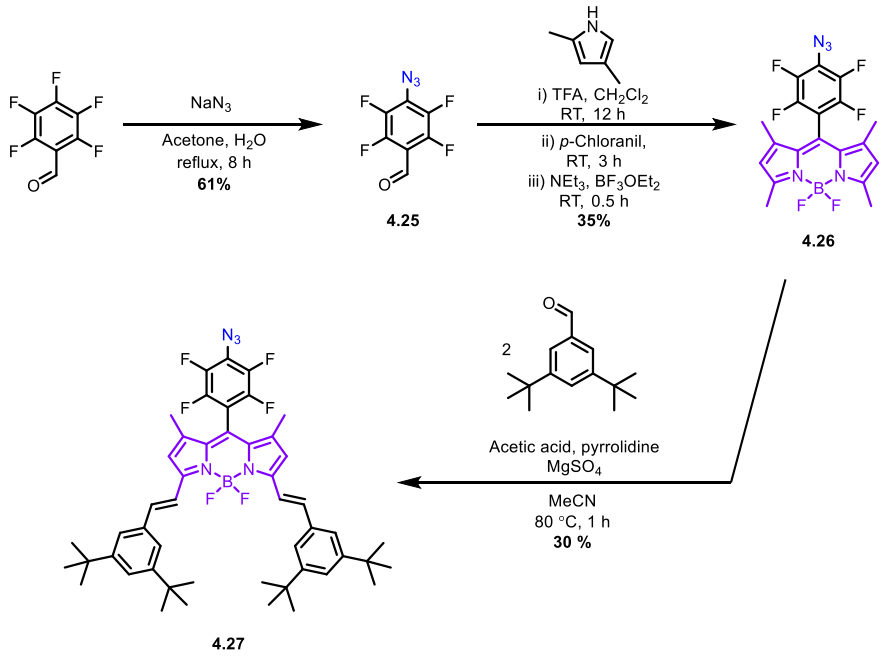
Figure 4.44: *HRMS experimental and theoretical spectrum of [2]rotaxane* ***4.24****, m/z = 2466.94248 ([M+H]$^+$, $C_{141}H_{148}O_3N_{15}BF_2I_2Zn$, calc = 2466.93668.)*

4.4.3. BODIPY Perfluoroaryl Spacer Rotaxane Synthesis & Characterisation

Due to the high electronegativity and inductive electron-withdrawing nature of fluorine, perfluorinated aryl group substituents are known to polarise and enhance the anion binding affinity of, in particular, triazole HB and XB donor motifs.[35] For this reason a second BODIPY-perfluoroaryl axle containing porphyrin [2]rotaxane was prepared.

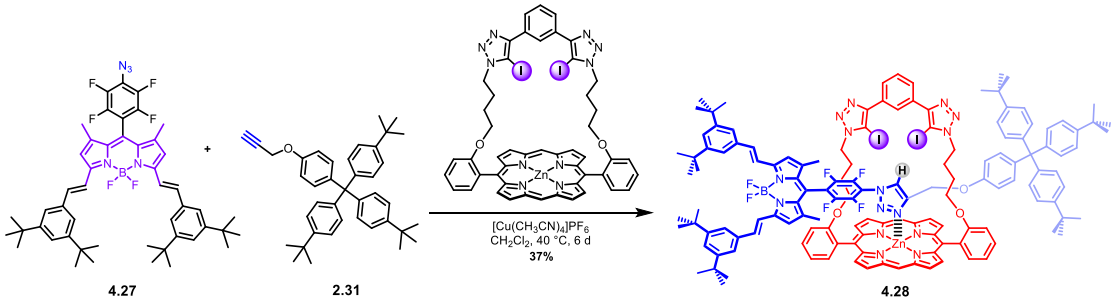
Nucleophilic aromatic substitution of pentafluorobenzaldehyde to azide **4.25** was achieved in a yield of 61% by reacting with NaN_3 in a refluxing water-acetone mixture.[36] The azide **4.25** was subsequently reacted with two equivalents of 2,4-dimethyl pyrrole in the presence of catalytic quantities of TFA and left to stir for 12 h. *p*-Chloranil was added as an oxidant and the mixture left to stir for 3 h, before NEt_3 and BF_3OEt_2 were added in succession. Purification was achieved by column chromatography and BODIPY **4.26** was isolated in a yield of 35% as a red powder (Scheme 4.12).

BODIPY **4.26** was reacted with two equivalents of 3,5-di-tert-butylbenzaldehyde via a Knoevenagel condensation, in the presence of 10 equivalents of pyrrolidine and acetic acid. Excess $MgSO_4$ was added as a drying agent and the reaction was left to stir at 80 ˚C for 1 h. y Column chromatography purification afforded BODIPY-stopper-azide **4.26** in a yield of 30 % as a blue powder (Scheme 4.12).



Scheme 4.12: *Synthesis of perfluoro BODIPY stopper* ***4.27***

An analogous AMT synthetic procedure to that used in the preparation of rotaxane **4.24** was used for [2]rotaxane **4.28.** One equivalent of the XB strapped porphyrin (*provided by Richard Tse*) and one equivalent of $[Cu(CH_3CN)_4]PF_6$ were dissolved in dry, degassed CH_2Cl_2 and left to stir at room temperature under N_2 for 15 minutes. Five equivalents of stopper alkyne **2.31** and BODIPY-azide **4.27** were subsequently added, and the reaction mixture was stirred at 40°C in darkness for six days. After washing with with basic aqueous EDTA solution and preparative TLC purification, the desired [2]rotaxane **4.28** was isolated in 37% yield (Scheme 4.13).



Scheme 4.13: *Synthesis of perfluoro BODIPY-porphyrin rotaxane* ***4.28***

Perfluoroaryl [2]rotaxane **4.28** was characterised by ^{1}H NMR (Figure 4.45 & Figure 4.46), ^{13}C NMR, ^{1}H-^{1}H ROESY NMR and HRMS (Figure 4.47). As with [2]rotaxane **4.24**, the porphyrin proton environments *l*, *m* and *n* desymmetrized (Figure 4.45) showing the macrocycles involvement in a conformationally locked MIM. Axle aryl peaks *10* and *11* show significant upfield shifts and broadening indicating substantial shielding from proximity to the aromatic

porphyrin component (Figure 4.45 & Figure 4.46). This is in contrast to [2]rotaxane **4.24** which shows the aryl peaks adjacent to the BODIPY shifting up-field, suggesting that the two rotaxanes adopt notably different conformations.

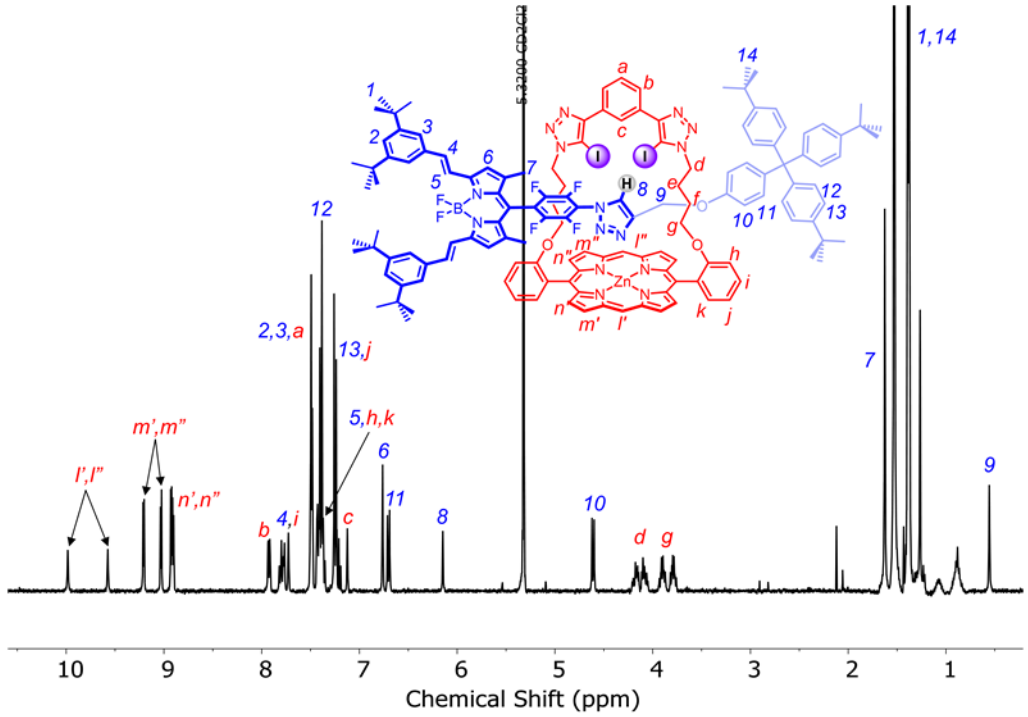


Figure 4.45: *^{1}H NMR spectrum of rotaxane **4.28** with proton assignments; $CDCl_3$, 298 K.*

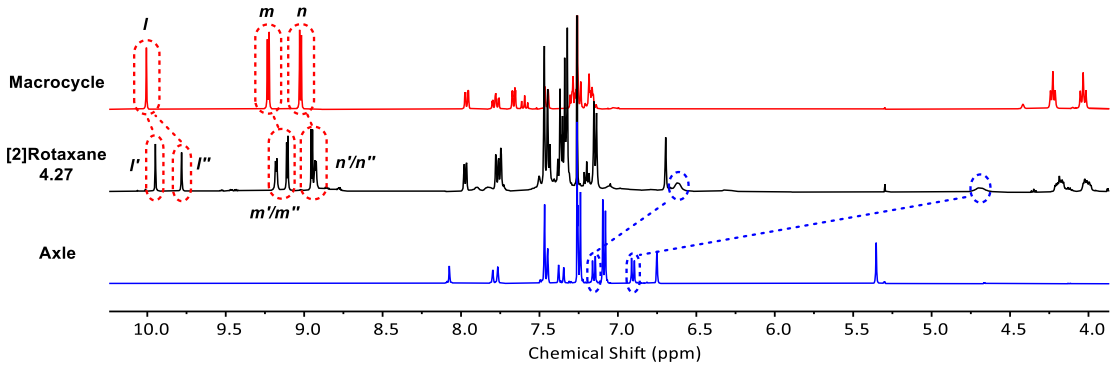


Figure 4.46: *Truncated stacked ^{1}H NMR spectra of the free strapped porphyrin macrocycle, [2]rotaxane **4.28** and the free axle; $CDCl_3$, 298 K.*

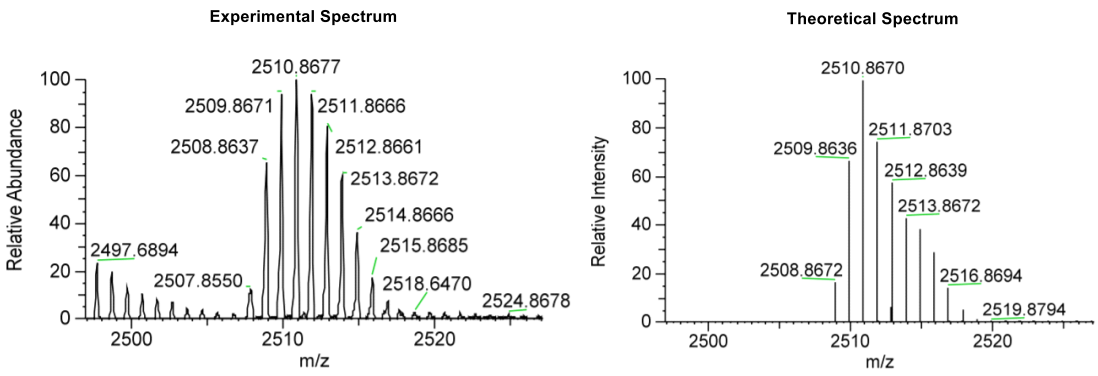


Figure 4.47: *HRMS experimental and theoretical spectrum of rotaxane* ***4.28,*** *m/z = 2510.8677, ($[M+H]^+$ $C_{139}H_{140}BF_6I_2N_{15}O_3Zn$ calc = 2510.8670).*

4.4.4. Anion Binding Studies

4.4.4.1. Fluorescence Titrations

The photophysical properties of [2]rotaxanes **4.24** and **4.27** (Figure 4.48 & Table 4.11) reveal characteristic energies of absorption and emission bands for BODIPY. The emission peak and absorption band of **4.27** are notably higher than **4.24** due to the presence of the electron-withdrawing perfluoroaryl group appended to the BODIPY core.

Table 4.11: *Energies of absorption and emission for [2]rotaxanes* ***4.24*** *and* ***4.27*** *in acetone.*

Receptor	$\lambda_{abs,\ max}$ / nm	$\lambda_{ems,\ max}$ / nm	Stokes Shift / nm
4.24[a]	629	639	10
4.27[b]	653	666	13

[1 μM], 298 K, [a] λ_{ex} = 575 nm; [b] λ_{ex} = 595 nm

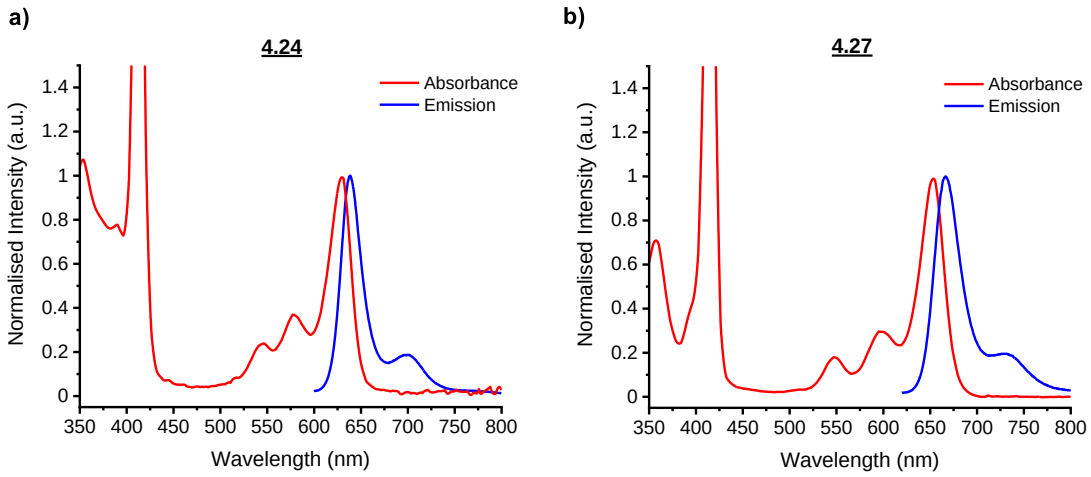


Figure 4.48: *Normalised emission and absorbance spectra for [2]rotaxane receptors* ***a) 4.24*** *and* ***b) 4.27*** *in acetone; 1 µM, 298 K.*

During the anion fluorescence titration experiments in acetone, addition of chloride, bromide, iodide, acetate and sulfate to each rotaxane led to fluorescence quenching (Figure 4.49 & Figure 4.50). The magnitude of quenching was greatest for oxyanions OAc^- and SO_4^- over the halides, and notably perfluoroaryl receptor **4.27** exhibited stronger quenching than **4.24** (Table 4.12).

Table 4.12: *Magnitudes of fluorescence emission quenching for rotaxanes* ***4.24*** *and* ***4.27*** *on addition of up to 500 equivalents of anions in acetone.*

	Magnitude of quenching	
Anion	**4.24 / %**	**4.27 / %**
Cl^-	37	50
Br^-	22	54
I^-	–[a]	45
OAc^-	69	78
SO_4^-	58	86

All anions added as their TBA salts; [1 µM], 298 K; [a] No reliable emission data could be obtained.

Analogous fluorescence titration experiments with axles **4.21** and **4.22** demonstrated that the BODIPY-stopper-aryl-triazole receptor motifs are incapable of functioning as anion sensors when not part of the porphyrin-BODIPY [2]rotaxane.

By monitoring the change in BODIPY emission as a function of anion concentration, anion association constants for **4.24** and **4.27** for a range of anions were determined by global fitting fluorescence titration data using OriginLab and are summarised in Table 4.13. For the halides, both receptors displayed a strong preference for chloride over bromide in acetone. This can be rationalised based on anion basicity, with chloride bearing higher charge density. Importantly, the substitution of the aryl motif in **4.24** to a perfluoroaryl group in **4.27** led to an 8- and 15-fold increase in the binding of chloride and bromide respectively (Table 4.13) — attributable to the inductive electron-withdrawing effect making the proto-triazole proton more acidic and a stronger HB donor. Because of this, the anion binding affinity of rotaxane receptor **4.27** is consistently higher than **4.24**. Both rotaxane receptors show the highest association to the oxyanions and particularly acetate. Despite structural rigidification induced by the axle triazole coordinating to the zinc metalloporphyrin, the strong affinity to the oxyanions suggests a degree of flexibility in the receptors to allow binding to these bulkier guests.

Analogous fluorescence titrations were also conducted in the more competitive 2% H_2O/acetone solvent mixture. While no fluorescence emission perturbations were observed on addition of anions in **4.24**, perfluoroaryl [2]rotaxane **4.27** displayed significant quenching for both chloride and bromide (Figure 4.51), showing greater selectivity for the smaller anion (Table 4.13).

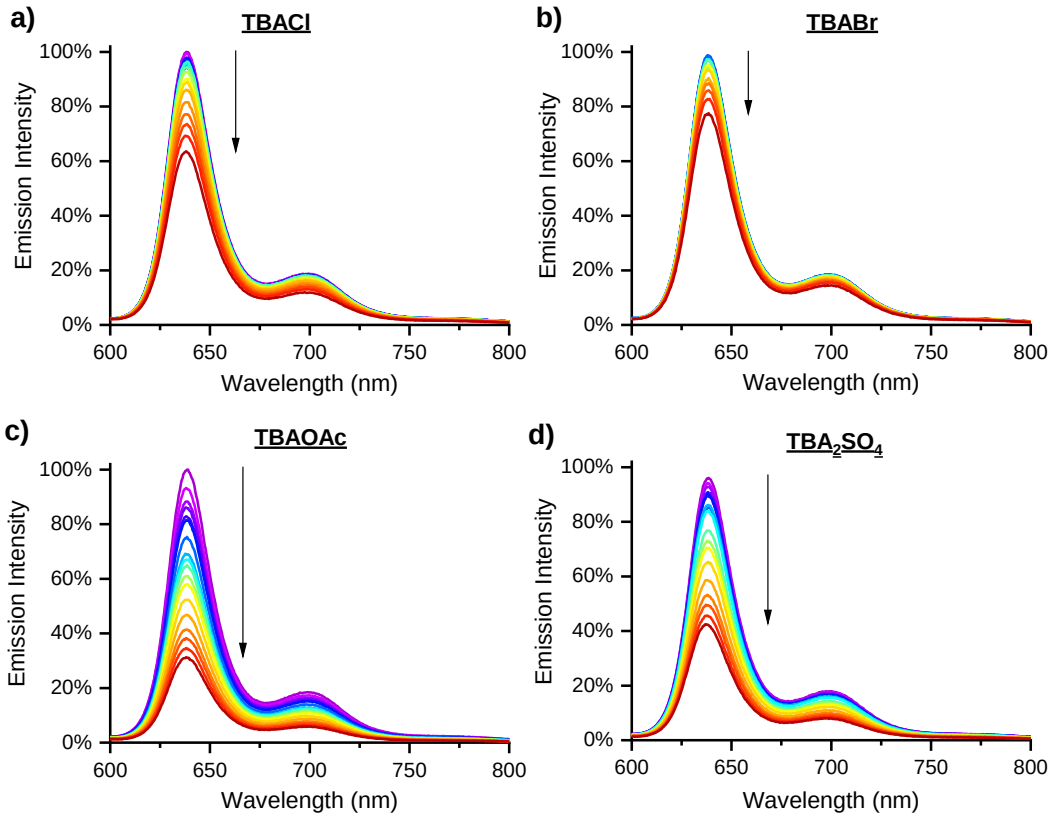


Figure 4.49: *Fluorescence titration spectra of* ***4.24*** *upon addition of 500 equivalents of* ***a)*** *TBACl,* ***b)*** *TBABr,* ***c)*** *TBAOAc and* ***e)*** *TBA_2SO_4; [****4.24****] = 1 µM, λ_{ex} = 575 nm, 298 K, acetone.*

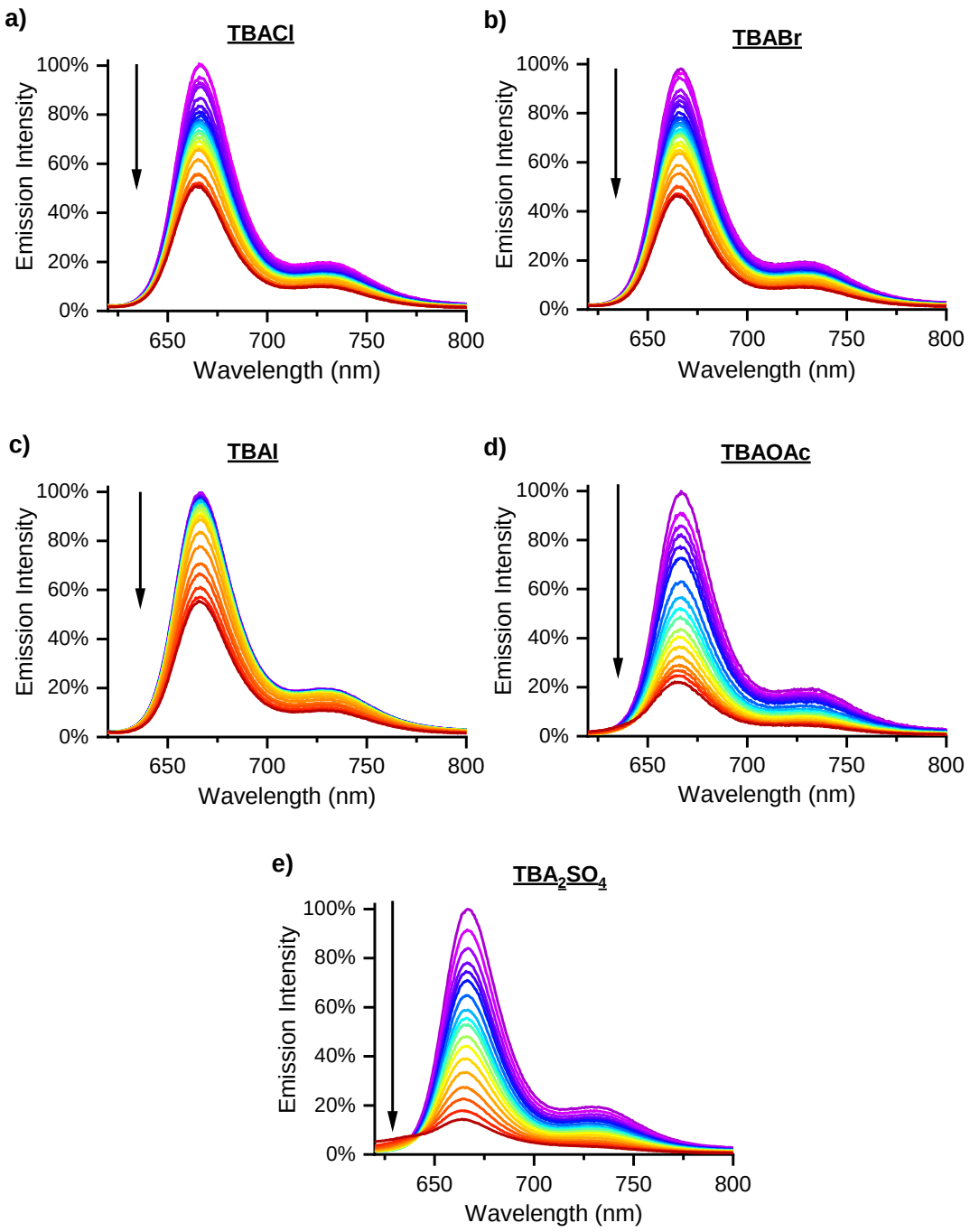


Figure 4.50: *Fluorescence titration spectra of* ***4.27*** *upon addition of 500 equivalents of* ***a)*** *TBACl,* ***b)*** *TBABr,* ***c)*** *TBAI,* ***d)*** *TBAOAc and* ***e)*** *TBA_2SO_4; [****4.27****] = 1 μM, λ_{ex} = 595 nm, 298 K, acetone.*

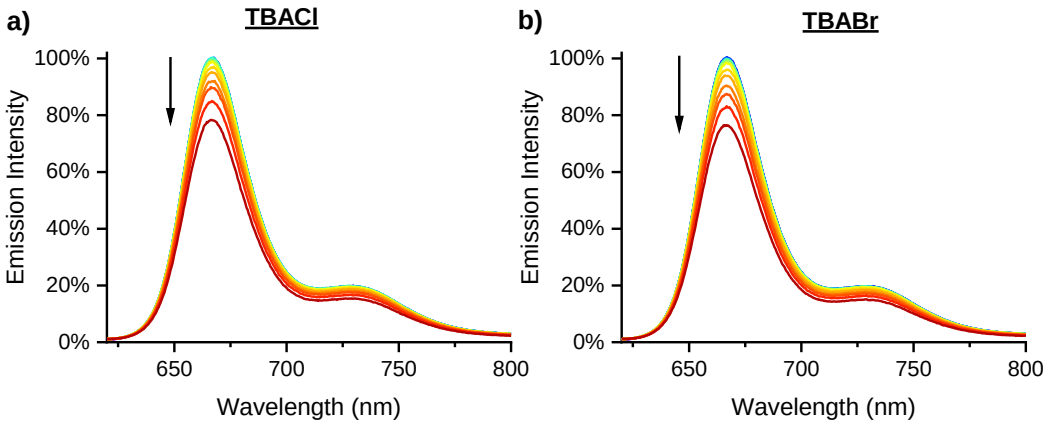


Figure 4.51: *Fluorescence titration spectra of* ***4.27*** *upon addition of 500 equivalents of* ***a)*** *TBACl,* ***b)*** *TBABr; [****4.27****] = 1 µM, λ_{ex} = 595 nm, 298 K, 2% H_2O/acetone.*

Table 4.13: *Fluorescence titration anion association constants of receptor* ***4.24*** *and* ***4.27*** *in acetone and 2% H_2O/Acetone; 1 µM, 298 K.*

	Association Constants K_a (M^{-1})			
	Acetone		**2% H_2O/Acetone**	
Anion	**4.24**	**4.27**	**4.24**	**4.27**
Cl^-	5440	44900	NB	1090
Br^-	2280	35200	NB	650
I^-	–[a]	4820	NB	NB
OAc^-	29940	58310	NB	NB
SO_4^{2-}	13820	39220	NB	NB

Anion association constants determined using 1:1 stoichiometric host-guest global fitting analysis of the fluorescence emission changes in OriginLab, errors (±) are all <10% and omitted. All anions added as their TBA salts; [1 µM], 298
NB = No binding observed, [a] No reliable association constants could be obtained.

4.4.5. Summary

Two novel BODIPY-porphyrin rotaxanes have been synthesised and tested for their ability to recognise and act as optical sensors for anions. Each were found to display sensing behaviour by fluorescence quenching of the BODIPY fluorophore, with the perfluoroaryl containing [2]rotaxane **4.27** showing a greater magnitude of quenching and affinity to anions.

4.5. Conjugated XB BODIPY Receptor

Anion sensors that have fluorescence emission wavelengths in the infra-red region (>780 nm) are highly desirable due to their ability to relay information through visibly opaque substrates. Extension of a BODIPY's π-conjugation can tune the emission profile close to the near-infra-red (NIR).[1] A synthetically accessible route to extend the conjugation of BODIPY is via a Knoevenagel reaction, as used in the synthesis of BODIPY stoppers **4.20** and **4.27**. By appending electron donating moieties to a BODIPY with a nitro aryl at the *meso* position, Cooke and co-workers demonstrated a BODIPY system capable of fluorescence emission close to the NIR at 721 nm (Figure 4.52).[37] Incorporation of iodotriazole XB donor motifs as part of an extended π conjugation offers a route to anion sensing capabilities at longer fluorescence emission wavelengths.

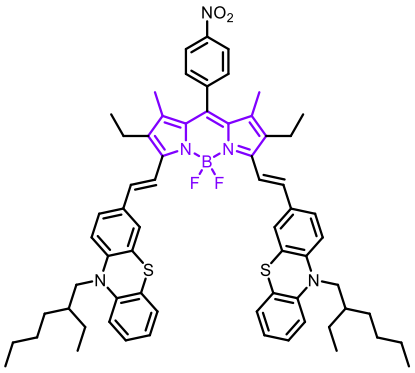
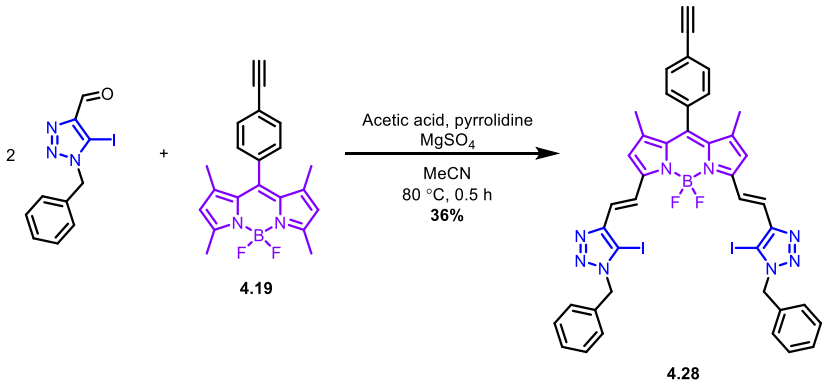


Figure 4.52: *Cooke's NIR BODIPY*

4.5.1. Synthesis



Scheme 4.14: *Knoevenagel synthesis of BODIPY receptor 4.28*

BODIPY-alkyne **4.19** was reacted with five equivalents of iodotriazole-aldehyde (*provided by Dr Harry Klein*) via a Knoevenagel condensation, in the presence of 10 equivalents of pyrrolidine and acetic acid. Excess $MgSO_4$ was added as a drying agent and the reaction was

left to stir at 80 ˚C for 0.5 h. Purification was achieved by column chromatography to afford receptor **4.28** in a yield of 36 % as a blue powder (Scheme 4.14).

4.5.2. Preliminary Anion Binding Studies

4.5.2.1. ^{1}H NMR titrations

Preliminary halide binding investigations of BODIPY receptor **4.28** were initially undertaken using ^{1}H NMR titration experiments in acetone-d_6.

On addition of TBACl and TBABr a modest upfield shift was observed in methylene proton *4* (Figure 4.53), indicating binding at the XB donor sites. Alkene proton *5* initially underwent a downfield shift and then from 5 equivalents onwards was perturbed upfield suggesting a binding stoichiometry of greater than 1:1. Alkene proton *6*, likely to be involved in binding, shifted downfield after one equivalent of halide and became indistinguishable from aromatic proton signals *1*, *2* and *3*. Due to the low magnitude of proton peak shifts, the ^{1}H NMR binding data association constants were not calculated.

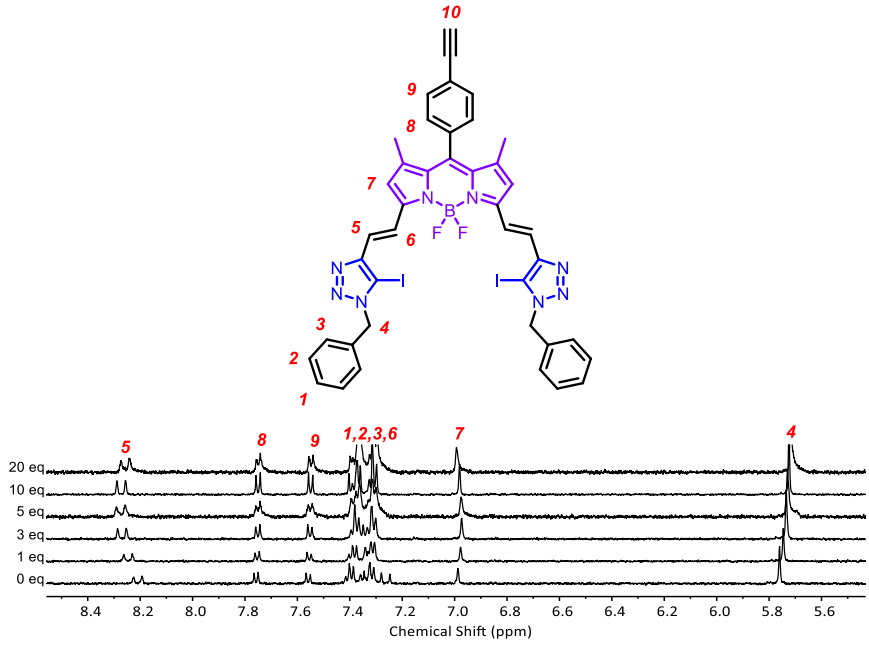


Figure 4.53: *^{1}H NMR titration of receptor 4.28 upon addition of TBACl in acetone-d_6 (1 mM, 298 K).*

4.5.2.2. Fluorescence Titrations

The photophysical properties of **4.28** (Figure 4.54) are shown in Table 4.14. Due to the extension of the conjugated network from the Knoevenagel reaction, both the absorption and emission profiles are significantly red shifted in comparison to other BODIPYs systems. Notably, the receptor's BODIPY emission max of 633 nm is approaching the NIR region.

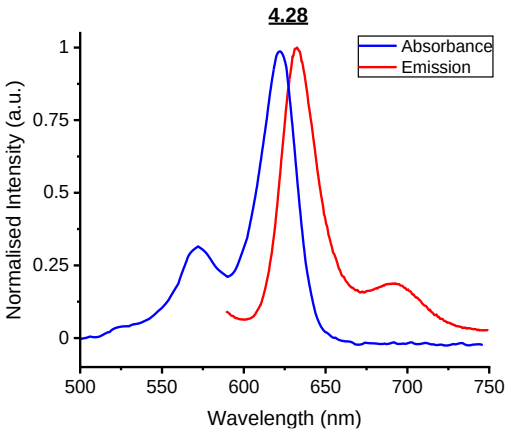


Figure 4.54: *Normalised emission and absorbance spectra for receptor* ***4.28*** *in acetone; [1 µM], 298 K.*

Table 4.14: *Energies of maximum absorption and emission for receptor* ***4.28*** *in acetone.*

Receptor	λ_{abs} / nm	λ_{ems} / nm	Stokes Shift / nm
4.28	622	633	11

[1 µM], 298 K, λ_{ex} = 572 nm

Addition of TBACl, TBABr and TBAI led to an initial increase in fluorescence intensity before substantial quenching of up to 30%, 25% and 48% respectively (Figure 4.55). This behaviour suggests a binding stoichiometry greater than 1:1 host-guest. Furthermore, each anion induced a red shift in the fluorescence emission spectra, with chloride inducing the greatest of 11 nm, bromide 7 nm and iodide the least with 4 nm. Hypochromic shifts have been previously reported in similar systems.[11] In this case, the red shift may be a result of an increase in conjugation occurring when binding.

Due to the unusual emission intensity changes (Figure 4.56) no reliable association constants could be determined using 1:1 or 1:2 stoichiometric host:guest binding models, suggesting a more complex binding relationship between receptor **4.28** and anion guests.

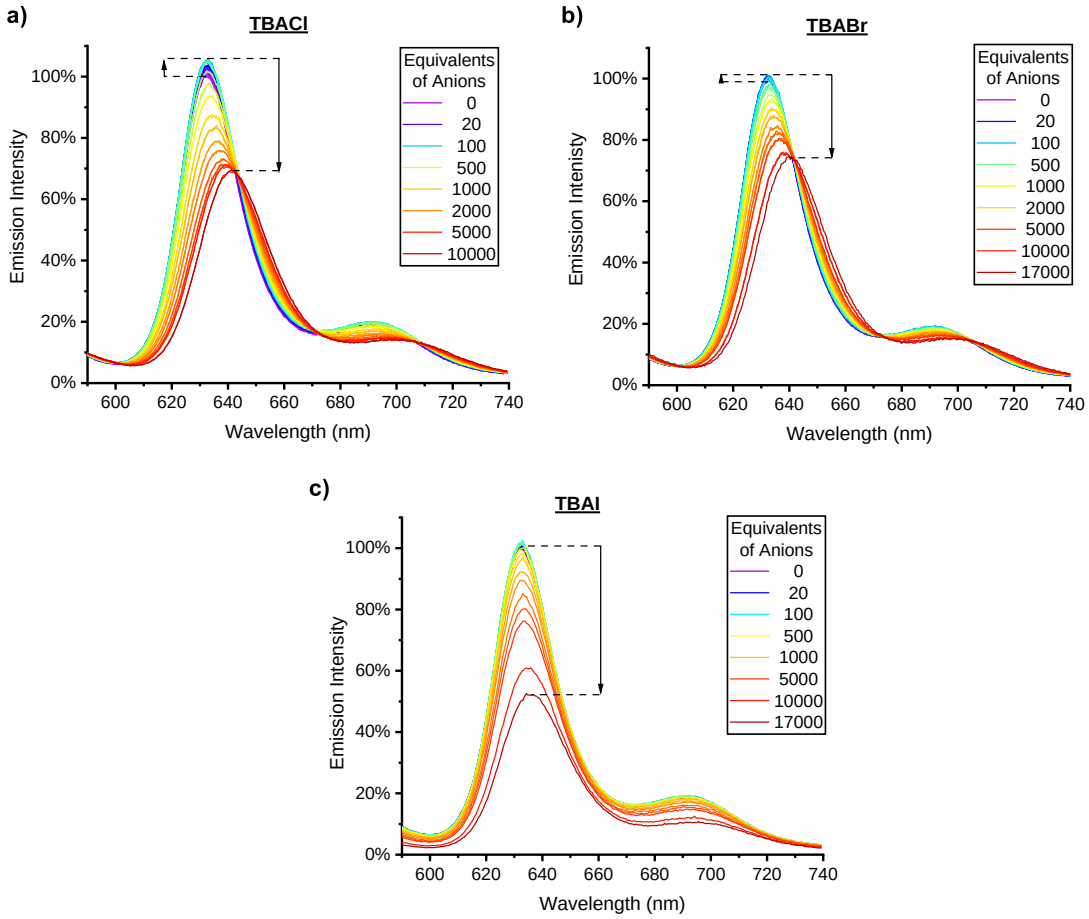


Figure 4.55: *Fluorescence emission intensity changes of receptor* ***4.28*** *on addition of* ***a)*** *TBACl* ***b)*** *TBABr* ***c)*** *TBAI; acetone, [1 µM], T = 298 K.*

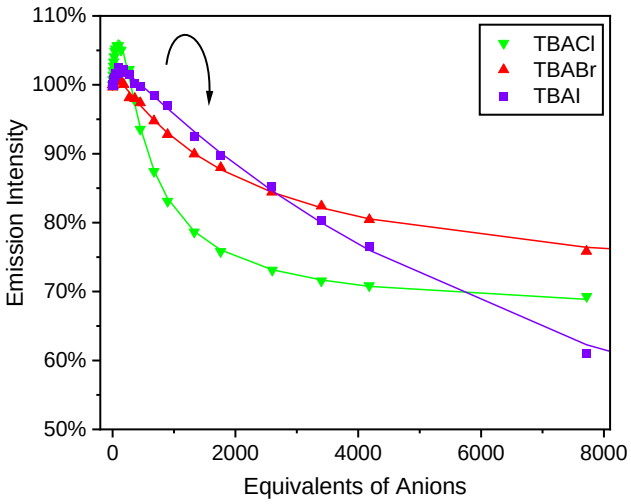


Figure 4.56: *Emission maxima data points and 1:2 stoichiometric fits on addition of TBACl, TBABr and TBAI to receptor* ***4.28****; [1 µM], acetone, 298 K*

4.5.3. Summary

A novel bis-iodotriazole BODIPY receptor **4.28** was synthesised via a Knoevenagel condensation. Preliminary ^{1}H NMR titration studies show that the receptor is capable of recognising chloride and bromide in acetone. Likewise, preliminary fluorescence titrations showed that the receptor was also capable of sensing halides via an initial enhancement in BODIPY emission intensity followed by quenching. Interestingly each halide anion induced a bathochromic shift in the emission wavelength.

4.6. Conclusions and Future Work

A series of BODIPY XB receptor motifs have been developed and tested for their ability to recognise and sense anions in solution. XB donor motif functionalisation at the BODIPY *meso* position showed promising anion sensing behaviour, with **4.15** being capable of sensing anions in 70% H_2O / 30% MeCN, with selectivity for HS^-. Notably the XB hosts outperform the HB analogues, particularly for HS^-, highlighting the unique affinity of XB for HS^-. Future work will focus on the development of water-soluble BODIPY receptors that will tested for their ability to sense HS^- and other anions in pure water. To achieve this, the PEG solubilising groups will be substituted for sodium carboxylate salts to enhance water solubility (Figure 4.57).

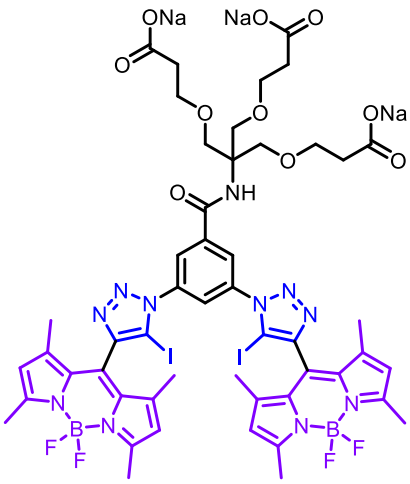


Figure 4.57: *Proposed water soluble BODIPY receptor*

Initial efforts to incorporate BODIPY as an axle component into a [2]rotaxane structure were unsuccessful due to the flexibility of the macrocycle leading to dethreading. Subsequent use of a more ridged porphyrin macrocyclic component led to the development of a pair of host-receptors capable of sensing anions via an increase in fluorescence intensity. Notably the perfluorinated aryl analogue was able to function in 2% water-acetone, sensing both chloride and bromide. Future efforts will focus on the enhancement of solubility in aqueous media by

the introduction of solubilising groups into the BODIPY axle component as shown in Figure 4.58.

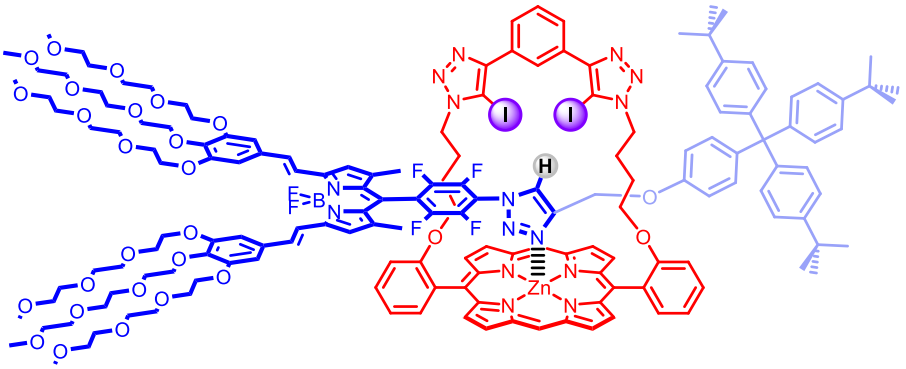


Figure 4.58: *Increased solubility porphyrin-BODIPY [2]rotaxane*

Finally, two iodotriazole motifs were appended to a BODIPY via a Knoevenagel reaction. The XB receptor was found to sense halide anions via an initial increase and subsequent decrease in BODIPY fluorescence intensity upon increasing anion concentration, concomitant with a bathochromic shift of the emission λ_{max}. To further investigate the potential of this system to sense anions, an additional pair of convergent iodotriazoles could be incorporated by functionalisation of the BODIPY boron (Figure 4.59).[38] With an increased number of convergent XB donor-motifs, the system stands to display high levels of anion association. Additionally, solubilising TEG groups could be added to enhance solubility in both aqueous and organic solvent media.

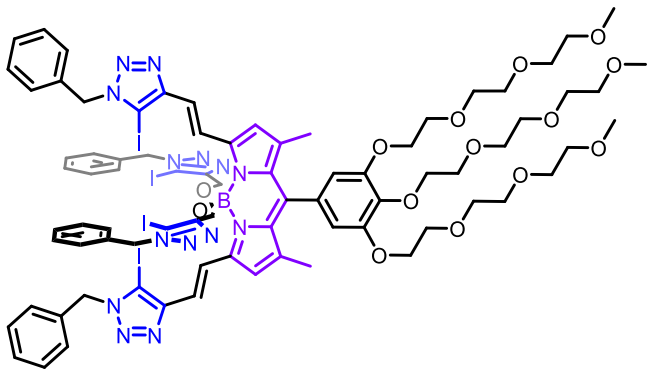


Figure 4.59: *Proposed BODIPY receptor with four convergent iodotriazole XB motifs and solubilising PEG groups*

4.7. References

1 A. Loudet and K. Burgess, *Chem. Rev.*, 2007, **107**, 4891–4932.

2 N. Boens, V. Leen and W. Dehaen, *Chem. Soc. Rev.*, 2012, **41**, 1130–1172.

3 Y. Ni and J. Wu, *Org. Biomol. Chem.*, 2014, **12**, 3774–3791.

4 B. M. Squeo, V. G. Gregoriou, A. Avgeropoulos, S. Baysec, S. Allard, U. Scherf and C. L. Chochos, *Prog. Polym. Sci.*, 2017, **71**, 26–52.

5 J. Zhao, K. Xu, W. Yang, Z. Wang and F. Zhong, *Chem. Soc. Rev.*, 2015, **44**, 8904–8939.

6 A. C. Benniston and G. Copley, *Phys. Chem. Chem. Phys.*, 2009, **11**, 4124–4131.

7 T. Kowada, H. Maeda and K. Kikuchi, *Chem. Soc. Rev.*, 2015, **44**, 4953–4972.

8 S. Dixit and N. Agarwal, *J. Photochem. Photobiol. A Chem.*, 2017, **343**, 66–71.

9 E. V. Antina, N. A. Bumagina, A. I. V'yugin and A. V. Solomonov, *Dye. Pigment.*, 2017, **136**, 368–381.

10 H. W. Mbatia, D. P. Kennedy, C. E. Camire, C. D. Incarvito and S. C. Burdette, *Eur. J. Inorg. Chem.*, 2010, **32**, 5069–5078.

11 Y. Lv, J. Xu, Y. Guo and S. Shao, *Chem. Pap.*, 2011, **65**, 553–558.

12 M. Albrecht, A. Lippach, M. P. Exner, J. Jerbi, M. Springborg, N. Budisa and G. Wenz, *Org. Biomol. Chem.*, 2015, **13**, 6728–6736.

13 J. Jiménez, R. Prieto-Montero, B. L. Maroto, F. Moreno, M. J. Ortiz, A. Oliden-Sánchez, I. López-Arbeloa, V. Martínez-Martínez and S. de la Moya, *Chem. Eur. J.*, 2020, **26**, 601–605.

14 Y. Lv, J. Xu, Y. Guo and S. Shao, *J. Incl. Phenom. Macrocycl. Chem.*, 2012, **72**, 95–101.

15 R. Gotor, A. M. Costero, P. Gaviña, S. Gil and M. Parra, in *European Journal of Organic Chemistry*, John Wiley & Sons, Ltd, 2013, vol. 2013, pp. 1515–1520.

16 A. T. Zill and S. C. Zimmerman, *Isr. J. Chem.*, 2009, **49**, 71–78.

17 L. H. Xie and M. P. Suh, *Chem. Eur. J.*, 2013, **19**, 11590–11597.

18 D. Tleugabulova, Z. Zhang and J. D. Brennan, *J. Phys. Chem. B*, 2002, **106**, 13133–13138.

19 Y. Tokoro, A. Nagai and Y. Chujo, *Tetrahedron Lett.*, 2010, **51**, 3451–3454.

20 J. W. Thompson, T. J. Kaiser and J. W. Jorgenson, *J. Chromatogr. A*, 2006, **1134**, 201–209.

21 E. Bahaidarah, A. Harriman, P. Stachelek, S. Rihn, E. Heyer and R. Ziessel, *Photochem. Photobiol. Sci.*, 2014, **13**, 1397–1401.

22 Origin(Pro), 2021, OriginLab Corporation.

23 R. Arumugaperumal, V. Srinivasadesikan, M. V. Ramakrishnam Raju, M. C. Lin, T. Shukla, R. Singh and H. C. Lin, *ACS Appl. Mater. Interfaces*, 2015, **7**, 26491–26503.

24 Y. Wu, M. Frasconi, W. G. Liu, R. M. Young, W. A. Goddard, M. R. Wasielewski and J. F. Stoddart, *J. Am. Chem. Soc.*, 2020, **142**, 11835–11846.

25 N. Yesilgul, O. Seven, R. Guliyev and E. U. Akkaya, *J. Org. Chem.*, 2018, **83**, 13228–13232.

26 N. Sun, X. Xiao, W. Li and J. Jiang, *Adv. Sci.*, 2015, **2**, 1500082

27 R. Arumugaperumal, P. Venkatesan, T. Shukla, P. Raghunath, R. Singh, S. P. Wu, M. C. Lin and H. C. Lin, *Sensors Actuators, B Chem.*, 2018, **270**, 382–395.

28 X. Wang, V. Ervithayasuporn, Y. Zhang and Y. Kawakami, *Chem. Commun.*, 2011, **47**, 1282–1284.

29 C. H. Lee, H. Yoon and W. D. Jang, *Chem. Eur. J.*, 2009, **15**, 9972–9976.

30 C. H. Lee, S. Lee, H. Yoon and W. D. Jang, *Chem. Eur. J.*, 2011, **17**, 13898–13903.

31 J. Zhang, Y. Li, W. Yang, S. W. Lai, C. Zhou, H. Liu, C. M. Che and Y. Li, *Chem. Commun.*, 2012, **48**, 3602–3604.

32 A. Brown, M. J. Langton, N. L. Kilah, A. L. Thompson and P. D. Beer, *Chem. Eur. J.*, 2015, **21**, 17664–17675.

33 M. J. Gunter, S. M. Farquhar and K. M. Mullen, *New J. Chem.*, 2004, **28**, 1443–1449.

34 A. Brown and P. D. Beer, *Dalt. Trans.*, 2012, **41**, 118–129.

35 T. Bunchuay, A. Docker, A. J. Martinez-Martinez and P. D. Beer, *Angew. Chem. Int. Ed.*, 2019, **58**, 13823–13827.

36 J. F. W. Keana and S. X. Cai, *J. Org. Chem.*, 2002, **55**, 3640–3647.

37 J. Marques Dos Santos, L. K. Jagadamma, N. M. Latif, A. Ruseckas, I. D. W. Samuel and G. Cooke, *RSC Adv.*, 2019, **9**, 15410–15423.

38 A. L. Nguyen, P. Bobadova-Parvanova, M. Hopfinger, F. R. Fronczek, K. M. Smith and M. G. H. Vicente, *Inorg. Chem.*, 2015, **54**, 3228–3236.

Chapter 5

Conclusions

5.1. Conclusions

The work described in this thesis was focused on the preparation and study of fluorescent iodotriazole containing host molecules designed to exploit halogen bonding for the selective molecular recognition and sensing of hydrosulfide in aqueous media.

Chapter Two described the design and synthesis of a coumarin fluorophore-iodotriazole motif that was incorporated into acyclic, macrocyclic and rotaxane anion receptor structural frameworks. An initial acyclic receptor, utilising two convergent XB donor iodotriazoles and a central pyridinium motif, was found to be capable of recognising and sensing halides in organic solvent media. Most notably, the receptor was also capable of sensing HS^- and halides in organic-aqueous solvent media (45:45:10 MeOH:$CHCl_3$:H_2O) via fluorescence quenching of the receptor's coumarin emission band. With the aim of improving anion binding affinity, a series of macrocyclic receptors were designed. Unexpectedly, a large [2+2] macrocycle was synthesised and shown to sense halides in organic solvent media. Two [2]rotaxane host systems were synthesised: the first via an AMT azide-alkyne Huisgen cycloaddition and the second via an anion template RCM rotaxanation. Due to lack of material resulting from low yield, the first rotaxane was not investigated for its ability to recognise and sense anions. The second rotaxane was demonstrated to sense halides and HS^- in organic-aqueous solvent media. In summary, the research findings in this chapter highlighted the capability of the coumarin-iodotriazole motif to function as an efficient fluorescence transducing reporter group for anion sensing.

Chapter Three expanded upon the observations of Chapter two with the incorporation of the coumarin-iodotriazole motif into two generations of XB bidentate water-soluble acyclic receptors that contained secondary amine, pyridine and pyridinium central core structural groups. Employing tertiary amine solubilising groups, the first generation of secondary amine receptors demonstrated halides and HS^- fluorescence sensing in pure water. Notably, the protonated amine receptor displayed a characteristic fluorescence intensity quenching for HS^- of up to 63%. The second generation XB bidentate receptors replaced the water solubilising tertiary amine groups for benzyl PEG groups. Importantly, these XB receptors were found to consistently outperform their HB receptor analogues, sensing HS^- in aqueous HEPES buffer solution. Remarkably, the neutral 3,5-bis-coumarin-iodotraizole pyridine receptor was found to be exclusively selective for HS^- over the halides, exhibiting fluorescence intensity quenching of up to 60%. Reversibility studies demonstrated the unprecedented reversible chemosensing of each receptor for HS^- and computational modelling corroborated the experimental results,

highlighting the selective affinity of XB for HS^- recognition. These observations serve to demonstrate the selective affinity of halogen bonding donor motifs for HS^- in aqueous solvent media, paving the way for a generation of HS^- chemosensors.

Chapter Four initially investigated the synthesis and fluorescence anion sensing capabilities of various mono- and bidentate XB BODIPY acyclic receptors. A simple monodentate XB acyclic host with an iodotriazole motif appended to the *meso* position of a BODIPY fluorophore notably displayed fluorescence intensity increases by over 200% and 100% when recognising chloride and bromide in acetone. The design was expanded upon with the synthesis of two generations of acyclic bis-iodotriazole-BODIPY systems; the first generation acting as a proof of principle to evaluate the fluorescence response and enhanced anion binding characteristics of the bidentate XB system, the second to evaluate the suitability for anion sensing in competitive aqueous solvent media. The first generation demonstrated enhanced binding affinity to the halides in acetonitrile but suffered from poor synthetic yields. The second generation, with appended benzyl TEG motifs to enhance water solubility, were able to function in 70% water 30% acetonitrile and importantly were found to sense HS^-, I^- and NCS^- via BODIPY fluorescence quenching. HB analogues were found to have both lower binding affinity to anions and relayed less significant fluorescence changes.

A BODIPY alkyne stopper motif was synthesised and incorporated into a [2]rotaxane synthesised via a AMT azide-alkyne Huisgen cycloaddition. ^{1}H NMR titration studies showed binding to chloride in acetone but due to decomposition, the rotaxane could not be tested for its fluorescence sensing behaviour. The same BODIPY alkyne stopper and a perfluorinated aryl linked analogue were successfully incorporated into two [2]rotaxanes with strapped-porphyrin macrocycle components. Each were found capable of sensing halides and oxyanions in acetone, with the perfluorinated aryl BODIPY axle containing rotaxane analogue capable of functioning in 2% H_2O-acetone for both chloride and bromide. Finally, an acyclic XB BODIPY receptor with two vinyl group appended iodotriazole motifs was synthesised via a Knoevenagel reaction. Preliminary fluorescence sensing studies in acetone revealed an increase followed by a decrease in emission intensity upon addition of halides. Interestingly, the halides also induced a bathochromic shift in the emission spectra.

To summarise, the results described in this thesis have demonstrated the functionality and efficacy of halogen bonding fluorescent host systems to sense anions in solution and, most importantly, overcome the formidable challenges of selective HS^- anion recognition and sensing in aqueous-organic solvent mixtures and pure water.

Chapter 6

Experimental

6. Experimental

6.1. General Information

All solvents and reagents were purchased from commercial suppliers and used as received unless otherwise stated. Dry organic solvents were degassed with nitrogen and then dehydrated by passing through an MBraun MPSP-800 column and used immediately. Deionised water was obtained through a micro filter using a Milli-Qr Millipore machine. Triethylamine was distilled from potassium hydroxide and stored over the same base prior to usage. TBTA (tris(benzyltriazolemethyl)amine) was synthesised as described[1] and stored under ambient conditions. The various Grubbs catalysts (Grubbs II, Hoveyda-Grubbs, Stewart-Grubbs) and $[Cu(CH_3CN)_4]PF_6$ were stored in vacuum desiccators containing P_2O_5 powder. Ratios of solvent mixtures are reported by volume. Brine refers to a saturated aqueous solution of NaCl, aqueous ammonia ($NH_4OH_{(aq)}$) refers to an approximately 10% solution of NH_3 in water, EDTA solution refers to a 0.02 M EDTA, 1% NH_3, aqueous, and petroleum ether refers to the fraction of petrol boiling between 40-60°C. Thin layer chromatography (TLC) analysis was performed using Merck silica Kieselgel 60 F254 0.25 mm, with spots visualised under UV light (254 nm) and/ or staining with $KMnO_4$ solution (only for silica TLC). Column chromatography was performed using silica gel (particle size 40-63 uM) under a positive N_2 head pressure, and preparatory TLC on 20 x 20 cm glass plates with 1 mm silica thickness. Amberlite® anion exchange columns were packed using IRA-400 resin beads containing styrene/divinylbenzene gel with quaternary ammonium matrix active groups (Cl^- salt), and prepared/preloaded by washing the beads sequentially with water and 1M NaOH (aq) till the eluent becomes colourless, water, 10% aqueous NH_4X (X = anion of interest), water and finally the organic solvent mixture (containing water) used for anion exchange.

Safety note: Organic azides, NaN_3, $TBAN_3$, and 1,2,3-triazole used throughout this thesis are potentially explosive and should be handled with care and in small quantities. In particular, direct heating under reduced pressure should be avoided, and especially for reactions containing NaN_3 and chlorinated solvents (i.e. CH_2Cl_2, $CHCl_3$ and DCE) should be avoided even for reaction work-ups due to their potential for forming highly explosive poly-azidomethanes.[2,3] In addition, NaN_3 should be cautiously used in the presence of acids due to formation of highly toxic $HN_{3(g)}$.[4] If this is unavoidable, the reaction should be performed strictly in the fume hood.

6.1.1. Instruments

NMR spectra were recorded on Bruker AVIII HD Nanobay 400 MHz, Bruker AVIIIHD 500 MHz and Bruker AVIIIHD 500 MHz (with ^{13}C cryoprobe) spectrometers. Chemical shifts are quoted in parts per million (ppm) relative to the residual solvent peak with signal splittings denoted as singlet (s), doublet (d), triplet (t), quartet (quart.), quintet (quint.), septet (sep.) and multiplet (m); with broad peaks being denoted with (br). Low resolution electrospray ionisation mass spectrometry (ESI-MS) was performed using the Waters Micromass LCT for characterisation of compounds previously reported in the literature, and high resolution ESI-MS (HRMS) was recorded using Bruker microTOF spectrometer for novel compounds. Absorption spectra were recorded on a Horiba Duetta™ spectrofluorometer whilst fluorescence spectra were recorded on a Horiba Fluorolog®-3 spectrophotometer or a Horiba Duetta™ spectrofluorometer using a quartz cuvette with path length of 1 cm.

6.2. Solution Titration Protocols

6.2.1. Tetrabutylammonium (TBA) Salts for Titration

Commercially available tetrabutylammonium (TBA) salts were used as purchased, where salts were dried on the high-vacuum and stored in vacuum desiccators at room temperature with P_2O_5 or silica bead desiccant.

6.2.2. ^{1}H NMR Titrations

^{1}H NMR titration experiments were performed on a Bruker AVIIIHD 500 MHz spectrometer. In a typical experiment, a solution of the appropriate tetrabutylammonium (TBA) salt was added to 0.5 mL of a 1.0 or 0.5 mM solution of the receptor molecule at the pre-set temperature (298 K if not stated). Both TBA salt and receptor were dissolved in the same solvent. TBA was chosen as the counter-cation due to its non-coordinating nature. At least 17 data points are obtained for each titration to ensure a good fit to the appropriate host-guest binding models.

The values of the observed chemical shift and concentration of anion were entered into BindFit[5,6] or OriginLab for every titration point. From initial estimates made of the binding constants and limiting chemical shifts, these parameters were refined using non-linear least-squares analyses to obtain the best fit between empirical and calculated chemical shifts based on a host-guest 1:1 or 1:2 binding stoichiometry (or otherwise stated). In all cases, convergence of the best fit values of the binding constants and their errors were obtained.

Prior to each titration and after each anion addition, the temperature of the solution in the NMR tube was allowed to equilibrate before ^{1}H NMR spectra was recorded. In graphical binding isotherms, empirical data points are represented by the filled or hollow points, while continuous lines represent the calculated binding curves.

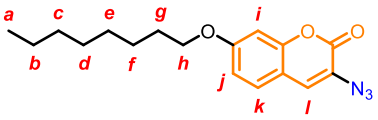
6.2.3. Fluorescence Titrations

Fluorescence titration experiments were performed on a Horiba Fluorolog®-3 spectrophotometer. In a typical experiment, a solution of the appropriate tetrabutylammonium (TBA) or sodium was added to 1.0 mL of a known concentration solution of the receptor molecule. TBA and sodium salts were dissolved in the same receptor solution to keep host concentration constant throughout the titration. In a typical experiment, an aliquot of the anion solution was added to the receptor solution in the cuvette and thoroughly mixed by upturning the cuvette several times or by stirrer bar stirring before any spectra were recorded. Temperatures were maintained at 298 K to within a margin of ± 0.5 K. Association constants were calculated from the optical titration data by non-linear global fitting analysis using Bindfit software.[5,6]

6.3. Synthesis from Chapter 2

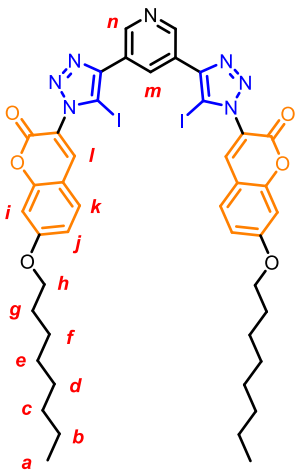
The synthesis of compounds **2.1**,[7] **2.2**,[7] **2.3**,[7] **2.4**,[7] **2.5**,[8] **2.6**,[8] **2.10**,[9] **2.11**,[10] **2.12**,[11] **2.17**,[12] **2.29**,[13] **2.30**,[13] **2.31**,[14] and **2.33**[15] have been described previously.

Octyl Coumarin Azide 2.7



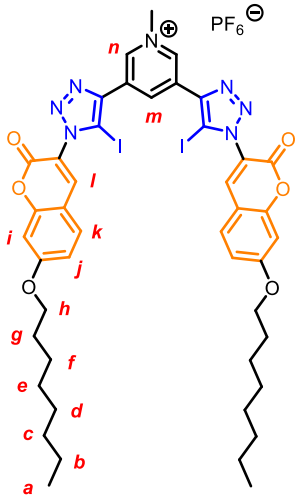
To a solution of 1-bromo-octane (42 µL, 0.244 mmol, 1.5 eq) and coumarin azide **2.6** (33 mg, 0.162 mmol, 1 eq) in DMF (3 mL), potassium carbonate (34 mg, 0.244 mmol, 1.5 eq) was added under an N_2 atmosphere. The mixture was left to stir at 40 °C for 1 h. The DMF was then removed *in vacuo* and the residue then dissolved in CH_2Cl_2 (20 mL), filtered, dried with $MgSO_4$ and had the solvent removed *in vacuo*. The crude product was purified via column chromatography (eluent: CH_2Cl_2) to afford to the product as a yellow oil (24 mg, 47%). **^{1}H NMR** (500 MHz, CD_3Cl) δ 7.30 (d, *J* = 8.6 Hz, 1H, H_k), 7.16 (s, 1H, H_l), 6.85 (dd, *J* = 8.6, 2.4 Hz, 1H, H_j), 6.82 (d, *J* = 2.4 Hz, 1H, H_j), 4.00 (t, *J* = 6.6 Hz, 2H, H_h), 1.85 – 1.76 (m, 2H, H_g), 1.51 – 1.41 (m, 2H, H_f), 1.39 – 1.25 (m, 8H, $H_{e,d,c,b}$), 0.89 (t, *J* = 6.8 Hz, 3H, H_a). **^{13}C NMR** (126 MHz, CD_3Cl) δ 161.55, 157.94, 153.19, 128.17, 126.64, 123.25, 113.86, 112.55, 101.30, 68.88, 31.93, 29.44, 29.35, 29.12, 26.10, 22.80, 14.24. **HRMS –** *unable to obtain due to decomposition*

Pyridine Bis-Octyl-Coumarin-Iodotriazole 2.8



Octyl coumarin azide **2.7** (30 mg, 0.095 mmol, 2 eq), bis-iodo alkyne pyridine **2.4** (18 mg, 0.048, 1 eq), TBTA (5.3 mg, 0.01 mmol, 0.2 eq) and $Cu(CH_3CN)_4.PF_6$ were dissolved in dry THF and stirred at 60 °C for 72 h. After this period the solvent was removed *in vacuo* and the residue dissolved in $CHCl_3$ (20 mL) and washed with aqueous 0.1 M EDTA solution dissolved in 1 M NH_4OH (3 x 10 mL) and H_2O (2 x 10 mL). The organic phase was then dried over $MgSO_4$ and concentrated *in vacuo*. The crude product was purified by column chromatography (eluent: $MeOH/CH_2Cl_2$ 4:96 *v/v*) yielding an off white solid (24 mg, 51 %): **^{1}H NMR** (500 MHz, $CDCl_3$) δ 9.33 (s, 2H, H_n), 8.98 (s, 1H, H_m), 8.07 (s, 2H, H_l), 7.55 (d, *J* = 8.7 Hz, 2H, H_k), 6.97 (dd, *J* = 8.7, 2.4 Hz, 2H, H_j), 6.92 (d, *J* = 2.4 Hz, 2H, H_i), 4.08 (t, *J* = 6.6 Hz, 2H, H_h), 1.88 – 1.80 (m, 2H, H_g), 1.51 – 1.44 (m, 2H, H_f), 1.41 – 1.23 (m, 8H, $H_{e,d,c,b}$), 0.89 (t, *J* = 6.7 Hz, 3H, H_a); **^{13}C NMR** (126 MHz, $CDCl_3$) δ 164.5, 156.5, 156.4, 148.3, 147.3, 143.0, 132.8, 130.4, 125.9, 120.2, 114.5, 110.9, 101.5, 80.8, 69.2, 31.8, 29.3, 29.2, 28.9, 25.9, 22.7, 14.1. **HRMS** (ESI +ve) m/z= 1010.15912 ($[M + H]^+$, $C_{43}H_{46}O_6N_7{}^{127}I_2$, calc= 1010.15934)

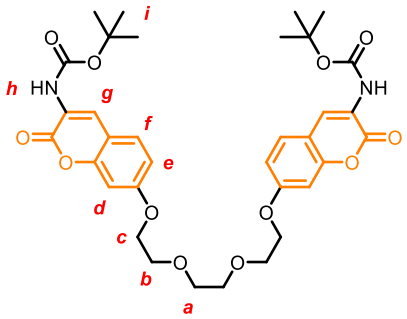
Pyridinium Bis-Octyl-Coumarin-Iodotriazole 2.9



MeI (0.01 mL, >10 eq) was added to a solution of the pyridine coumarin system (10 mg, 0.01 mmol, 1 eq) in dry CH_2Cl_2 and left to stir for 24 h under a N_2 atmosphere and at 40 °C. After this period the solvent and excess MeI were removed *in vacuo* and the residue dissolved in $CHCl_3$ (10 mL) and washed with aqueous 0.1 M NH_4PF_6 solution (8 x 6 mL) and H_2O (2 x 6 mL). The combined organic phases were dried over $MgSO_4$ and concentrated *in vacuo*. The crude product was purified *via* column chromatography (eluent: $MeOH/CH_2Cl_2$ 7:93 *v/v*) to yield a yellow solid (11.2 mg, 97 %): **^{1}H NMR** (500 MHz, $CDCl_3$) δ 9.55 (s, 1H, H_m), 9.28 (s, 2H, H_n), 8.13 (s, 2H, H_l), 7.59 (d, *J* = 8.7 Hz, 2H, H_k), 6.88 (d, *J* = 8.7 Hz, 2H, H_j), 6.78 (s, 2H, H_i), 4.53 (s, 3H,

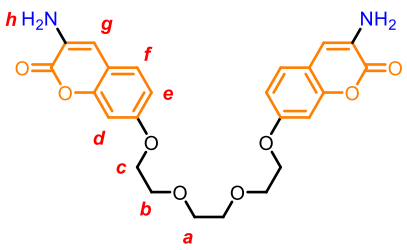
H_o), 4.00 (d, *J* = 6.8 Hz, 4H, H_h), 1.82 – 1.75 (m, 4H, H_g), 1.47 – 1.40 (m, 4H, H_f), 1.37 – 1.24 (m, 16H), 0.88 (t, *J* = 6.7 Hz, 6H); **^{13}C NMR** (126 MHz, $CDCl_3$) δ 164.74, 156.91, 156.37, 144.58, 143.05, 142.07, 131.36, 119.19, 114.55, 111.04, 101.49, 69.30, 50.11, 31.95, 29.84, 29.49, 29.35, 29.09, 26.08, 22.79, 14.25, 1.16; **HRMS** (ESI +ve) m/z= 1024.17478 ($[M + H]^+$, $C_{44}H_{48}O_6N_7{}^{127}I_2$, calc= 1024.17499).

Bis Boc-Coumarin 2.13



Bis-tosylate **2.11** (300 mg, 0.65 mmol) was added to a mixture of coumarin **2.12** (500 mg, 1.80 mmol) and K_2CO_3 (375 mg, 2.71 mmol) in dry MeCN (10 mL) and left to stir at 70 °C for 16 h. The solvent was then removed *in vacuo* and the crude residue dissolved in $CHCl_3$ (20 mL). The solution was washed with water (3 x 20 mL), brine (20 mL), dried over $MgSO_4$, filtered and had the solvents removed *in vacuo*. The crude was then purified by silica column chromatography (eluent: MeOH:CH_2Cl_2 4:96 *v/v* to yield an off-white powder (342 mg, 0.51 mmol, 78 %). **^{1}H NMR** (400 MHz, $CDCl_3$); δ 8.20 (s, 2H, H_h), 7.31 (d, *J* = 8.7 Hz, 2H, H_f), 7.26 (s, 2H, H_g), 6.86 (dd, *J* = 8.6, 2.4 Hz, 2H, H_e), 6.80 (d, *J* = 2.4 Hz, 2H, H_d), 4.16 – 4.12 (m, 4H, H_c), 3.84 – 3.80 (m, 4H, H_b), 3.74 (s, 4H, H_a), 1.51 (s, 18H, H_i); **^{13}C NMR** (126 MHz, $CDCl_3$); δ 159.90, 158.85, 152.59, 150.84, 128.07, 122.23, 121.18, 113.48, 113.45, 101.45, 81.47, 70.95, 69.59, 67.97, 28.24; **HRMS** (ESI +ve) m/z= 669.26538 ($[M + H]^+$, $C_{34}H_{41}O_{12}N_2$, calc= 669.26540).

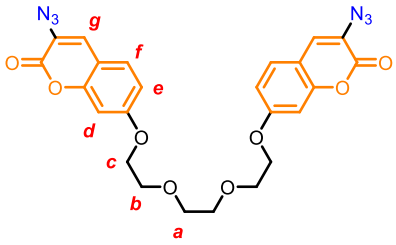
Bis Coumarin-Amine 2.14



Bis Boc-coumarin **2.13** (200 mg, 0.30 mmol) was dissolved in CH_2Cl_2 (3.5 mL) and cooled to 0 °C using an ice bath before TFA (3.0 mL) was slowly added. The mixture was left to heat to

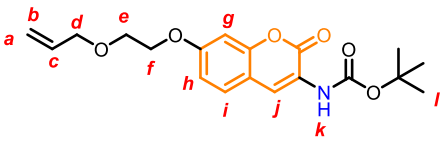
RT over 36 h. $NaHCO_3$ was then added till the solution became neutral and a precipitate had formed. The solution was filtered and the precipitate washed with cold water and CH_2Cl_2 to yield an off white solid requiring no further purification (120 mg, 0.25 mmol, 85 %). **^{1}H NMR** (500 MHz, DMSO-d_6) δ 7.32 (d, J = 8.6 Hz, 2H, H_f), 6.91 (d, J = 2.4 Hz, 2H, H_d), 6.84 (dd, J = 8.6, 2.5 Hz, 2H, H_e), 6.71 (s, 2H, H_g), 5.36 (s, 4H, H_h), 4.14 – 4.08 (m, 4H, H_c), 3.78 – 3.72 (m, 4H, H_b), 3.61 (s, 4H, H_a); **^{13}C NMR** (126 MHz, DMSO-d_6) δ 159.36, 157.37, 149.53, 131.45, 126.10, 115.37, 113.04, 109.50, 101.48, 70.39, 69.32, 68.07; **HRMS** (ESI +ve) m/z= 469.16055 ([M + H]$^+$, $C_{24}H_{25}O_8N_2$, calc= 469.16054).

Bis Coumarin Azide 2.15



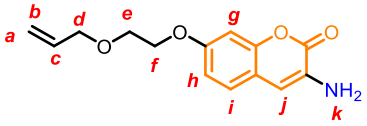
Bis coumarin-amine **2.14** (60 mg, 0.13 mmol, 1 eq) was dissolved in conc. HCl (5 mL), water (2 mL) and then sonicated. $NaNO_2$ (32 mg, 0.46 mmol, 3.6 eq) dissolved in water (1 ml) was added, followed by the slow addition of NaN_3 (33 mg, 0.51 mmol, 4 eq). The mixture was left to stir at rt for 2 h. The solution was filtered and the precipitate collected and washed with cold water. The solid was then purified by silica column chromatography (eluent: MeOH:CH_2Cl_2 4:96 *v/v*) to yield an orange powder (30 mg, 0.058 mmol, 45 %). **^{1}H NMR** (500 MHz, $CDCl_3$); δ 7.30 (d, J = 8.7 Hz, 2H, H_H), 7.15 (s, 2H, H_J), 6.87 (dd, J = 8.7, 2.4 Hz, 2H, H_G), 6.82 (d, J = 2.4 Hz, 2H, H_E), 4.21 – 4.13 (m, 4H, H_C), 3.89 (dd, J = 5.6, 3.8 Hz, 4H, H_B), 3.76 (s, 4H, H_A); **^{13}C NMR** (126 MHz, $CDCl_3$); δ 160.93, 157.67, 152.87, 128.09, 126.28, 123.43, 113.67, 112.77, 101.41, 70.96, 69.52, 68.06, 53.43; **HRMS** (ESI +ve) m/z= 543.12341 ([M + Na]$^+$, $C_{24}H_{20}O_8N_6{}^{23}Na$, calc= 543.12348).

Alkene Boc-Coumarin 2.18



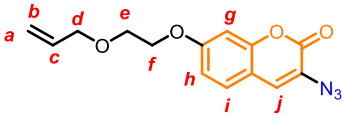
Tosyl-alkene **2.17** (310 mg, 1.21 mmol, 1.05 eq) was added to a mixture of coumarin **2.12** (369 mg, 1.33 mmol, 1.1 eq) and K_2CO_3 (268 mg, 1.94 mmol, 1.6 eq) dissolved in dry MeCN (10 mL). The solution was heated to reflux for 12 h. The solvent was then removed *in vacuo* and the crude residue dissolved in $CHCl_3$ (20 mL). The solution was washed with water (3 x 20 mL), brine (20 mL), dried over $MgSO_4$, filtered and had the solvents removed *in vacuo*. The crude was then purified by column chromatography (eluent: MeOH:CH_2Cl_2 1:99 *v/v*) to yield a yellow powder (222 mg, 51 %). **^{1}H NMR** (400 MHz, $CDCl_3$); δ 8.23 (s, 1H, H_k), 7.35 (d, *J* = 8.6 Hz, 1H, H_i), 7.29 (s, 1H, H_j), 6.90 (dd, *J* = 8.6, 2.5 Hz, 1H, H_h), 6.84 (d, *J* = 2.5 Hz, 1H, H_g), 6.00 – 5.87 (m, 1H, H_c), 5.31 (dq, *J* = 17.2, 1.6 Hz, 1H, H_b), 5.22 (dq, *J* = 10.4, 1.4 Hz, 1H, H_a), 4.21 – 4.13 (m, 2H, H_f), 4.10 (dt, *J* = 5.7, 1.4 Hz, 2H, H_d), 3.86 – 3.78 (m, 2H, H_e), 1.52 (s, 9H, H_l); **^{13}C NMR** (126 MHz, $CDCl_3$); δ 159.94, 158.90, 152.61, 150.85, 134.36, 128.08, 122.22, 121.23, 117.58, 113.51, 113.48, 101.43, 81.48, 72.45, 68.19, 67.98, 28.24; **HRMS** (ESI +ve) m/z= 384.14179 ($[M + Na]^+$, $C_{19}H_{23}O_6N^{23}Na$, calc= 384.14176).

Alkene Coumarin-Amine 2.19



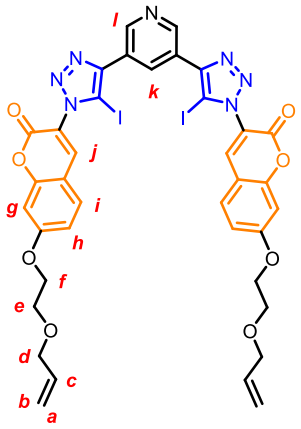
Alkene BOC-coumarin **2.18** (63 mg, 0.17 mmol) was dissolved in CH_2Cl_2 (1.5 mL) and cooled to 0 °C using an ice bath before TFA (1.5 mL) was slowly added. The mixture was left to heat to rt over 3 h. The solvent was removed *in vacuo*, the residue dissolved in $CHCl_3$ (20 mL) and washed with a saturated solution of $NaHCO_3$ (3 x 20 mL), water (20 mL) and brine (20 mL). The organic phase was dried over $MgSO_4$, filtered and had the solvent removed *in vacuo* to yield a yellow solid (45 mg, 0.17 mmol, 99 %). **^{1}H NMR** (400 MHz, $CDCl_3$) δ 7.18 (dd, *J* = 8.1, 0.8 Hz, 1H, H_i), 6.86 – 6.82 (m, 2H, $H_{h,g}$), 6.69 (s, 1H, H_j), 5.94 (ddt, *J* = 17.2, 10.4, 5.7 Hz, 1H, H_c), 5.31 (dq, *J* = 17.2, 1.6 Hz, 1H, H_a), 5.22 (dq, *J* = 10.4, 1.4 Hz, 1H, H_b), 4.17 – 4.12 (m, 2H, H_f), 4.10 (dt, *J* = 5.7, 1.4 Hz, 2H, H_d), 4.05 (br s, 2H, H_k) 3.83 – 3.79 (m, 2H, H_e); **^{13}C NMR** (126 MHz, $CDCl_3$); δ 159.73, 158.21, 150.22, 134.42, 129.79, 125.80, 117.54, 114.56, 113.09, 112.16, 101.51, 72.43, 68.28, 67.90; **HRMS** (ESI +ve) m/z= 262.10748 ($[M + H]^+$, $C_{14}H_{16}O_4N$, calc= 262.10738).

Alkene Coumarin Azide 2.20



Alkene coumarin-amine **2.19** (20 mg, 0.077 mmol) was dissolved in dry MeCN (1 mL) and sonicated. The solution was cooled to 0 °C using an ice bath before *t*-$BuNO_2$ (17 µL, 0.12 mmol), followed by $TMSN_3$ (15 µL, 0.10 mmol) were added, the mixture was left to stir for 2 h. The solvent was removed *in vacuo* to yield an orange powder (22 mg, 0.077 mmol, 99 %). **^{1}H NMR** (400 MHz, $CDCl_3$); δ 7.31 (d, *J* = 8.7 Hz, 1H, H_i), 7.16 (s, 1H, H_j), 6.90 (dd, *J* = 8.6, 2.4 Hz, 1H, H_h), 6.85 (d, *J* = 2.4 Hz, 1H, H_g), 5.93 (m, 1H, H_c), 5.31 (m, H_a), 5.22 (m, H_b), 4.18 (t, *J* = 4.7 Hz, 2H, H_f), 4.09 (d, *J* = 5.8 Hz, 2H, H_d), 3.82 (t, *J* = 4.7 Hz, 2H, H_e); **^{13}C NMR** (126 MHz, $CDCl_3$); δ 159.09, 155.81, 151.00, 132.39, 126.17, 124.45, 121.47, 115.72, 111.84, 110.85, 99.50, 70.54, 66.20, 66.18; **HRMS** (ESI +ve) m/z= 310.07990 ($[M + H]^+$, $C_{14}H_{13}O_4N_3{}^{23}Na$, calc= 310.07983).

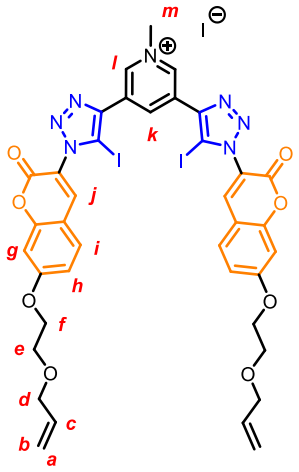
Pyridine Bis-Alkene 2.21



Alkene coumarin-azide **2.20** (820 mg, 2.85 mmol, 2.2 eq), 3,5-bis(iodoethynyl)pyridine **2.4** (492 mg, 1.30 mmol, 1 eq), TBTA (138 mg, 0.259 mmol, 0.2 eq) and $Cu(CH_3CN)_4.PF_6$ (145 mg, 0.39 mmol, 0.3 eq) were dissolved in dry degassed THF (40 mL) and left to stir under N_2 at 60 °C for 72 h. The solvent was removed *in vacuo* and the crude mixture dissolved in $CHCl_3$ (40 mL) and washed with 0.1 M EDTA dissolved in aqueous 1 M NH_4OH (3 x 40 mL) followed by water (40 ml). The combined organic phase was dried over $MgSO_4$, filtered, concentrated *in vacuo* and purified by preparative TLC plate (eluent: MeOH:CH_2Cl_2 4:96 *v/v*) to yield an orange solid (1.20 g, 89 %). **^{1}H NMR** (400 MHz, $CDCl_3$): δ 9.28 (d, *J* = 2.1 Hz, 2H, H_l), 8.93 (t, *J* = 2.1 Hz,

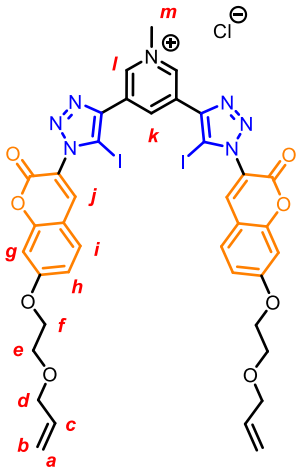
1H, H_k), 8.01 (s, 1H, H_j), 7.50 (d, *J* = 8.7 Hz, 1H, H_i), 6.96 (dd, *J* = 8.7, 2.4 Hz, 1H, H_h), 6.91 (d, *J* = 2.3 Hz, 1H, H_g), 5.88 (m, 1H, H_c), 5.26 (m, 1H, H_b), 5.18 (m, 1H, H_a), 4.23 – 4.17 (m, 2H, H_f), 4.05 (m, 2H, H_d), 3.83 – 3.77 (m, 2H, H_e); **^{13}C NMR** (126 MHz, $CDCl_3$); δ 164.09, 156.42, 156.25, 148.31, 147.40, 142.85, 134.22, 132.84, 130.42, 125.90, 120.51, 117.77, 114.55, 111.19, 101.77, 80.66, 72.50, 68.45, 67.98; **HRMS** (ESI +ve) m/z= 954.02380 ($[M + H]^+$, $C_{37}H_{30}O_8N_7{}^{127}I_2$, calc= 954.02397).

Iodide Pyridinium Bis-Alkene 2.22



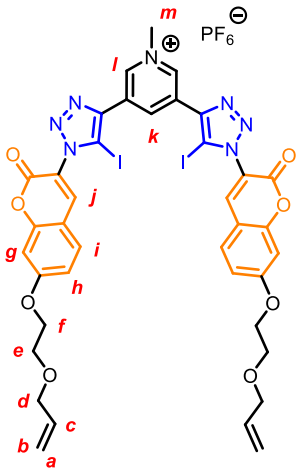
Pyridine bis-alkene **2.21** (100 mg, 0.104 mmol, 1 eq) was dissolved in CH_2Cl_2 (4 mL) and the suspension sonicated to aid solubility. Excess MeI (0.3 mL) was then added and the solution was left to stir for 72 h at rt. The solvent was removed *in vacuo* and an white solid isolated (112, 99%). **^{1}H NMR** (400 MHz, DMSO-d_6): δ 9.77 (t, J = 1.6 Hz, 1H, H_k), 9.70 (d, J = 1.6 Hz, 2H, H_l), 8.74 (s, 2H, H_j), 7.85 (d, J = 8.8 Hz, 2H, H_i), 7.25 (d, J = 2.4 Hz, 2H, H_g), 7.16 (dd, J = 8.8, 2.4 Hz, 2H, H_h), 5.97 – 5.87 (m, 2H, H_c), 5.28 (m, 2H, H_b), 5.16 (m, 2H, H_a), 4.60 (s, 3H, H_m), 4.35 – 4.28 (m, 4H, H_f), 4.04 – 4.01 (m, 4H, H_{dd}), 3.81 – 3.74 (m, 4H, H_e); **^{13}C NMR** (126 MHz, DMSO) δ 163.86, 156.45, 155.82, 144.57, 143.01, 142.74, 135.02, 131.34, 130.12, 119.30, 116.67, 114.41, 110.96, 101.69, 92.27, 71.15, 68.39, 67.77, 48.87; **HRMS** (ESI +ve) m/z= 968.03986 ($[M - I^-]^+$, $C_{38}H_{32}O_8N_7{}^{127}I_2$, calc= 968.03962).

Chloride Pyridinium Bis-Alkene 2.23



Iodide pyridinium bis-alkene **2.22** was dissolved in a minimum of DMSO and slowly dropped into a saturated aqueous solution of NH_4Cl where upon it precipitated as the chloride salt. Once the precipitate had settled the clear solution was decanted and replaced with water, after a minimum of six repeated removals of the solution and replacement with water the solvent was removed by N_2 line to yield a white solid, 99%. **^{1}H NMR** (400 MHz, DMSO-d_6): δ 9.88 (t, J = 1.7 Hz, 1H, H_k), 9.69 (d, J = 1.7 Hz, 2H, H_l), 8.73 (s, 2H, H_j), 7.84 (d, J = 8.7 Hz, 2H, H_i), 7.24 (d, J = 2.4 Hz, 2H, H_g), 7.15 (dd, J = 8.7, 2.4 Hz, 2H, H_h), 5.90 (m, 2H, H_c), 5.27 (m, 2H, H_b), 5.20 – 5.12 (m, 2H, H_a), 4.60 (s, 3H, H_m), 4.31 (t, J = 4.6 Hz, 4H, H_f), 4.03 (m, 4H, H_d), 3.77 (t, J = 4.6 Hz, 4H, H_e); **^{13}C NMR** (101 MHz, DMSO-d_6) δ 163.80, 156.46, 155.80, 144.48, 143.14, 135.03, 131.30, 130.21, 119.39, 116.66, 114.37, 110.97, 101.67, 71.14, 68.37, 67.77; **HRMS** (ESI +ve) m/z= 968.03986 ($[M - Cl^-]^+$, $C_{38}H_{32}O_8N_7{}^{127}I_2$, calc= 968.03962).

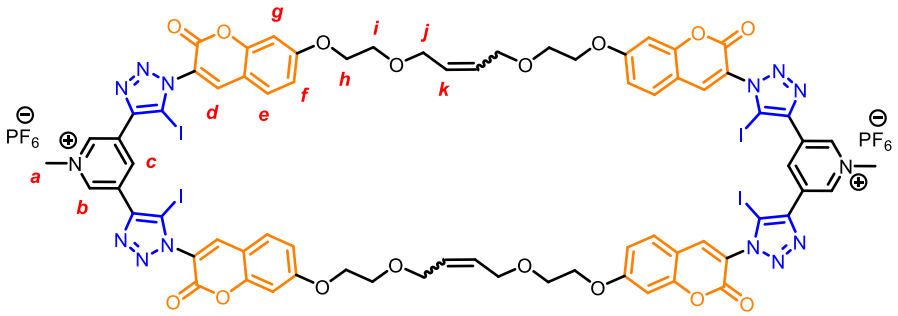
PF_6 Pyridinium Bis-Alkene 2.24



Iodide pyridinium bis-alkene **2.22** dissolved in CH_2Cl_2 (20 mL) was washed with 1M NH_4PF_6 aqueous solution (9 x 20 mL) and water (2 x 20 mL). The organic phase was concentrated *in vacuo* to yield **2.24** as an off-white solid (99%).

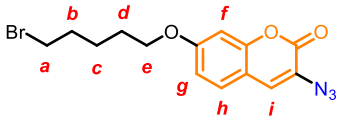
^{1}H NMR (400 MHz, $CDCl_3$) δ 9.52 (s, 1H, H_k), 9.28 (s, 2H, H_l), 8.11 (s, 2H, H_j), 7.57 (d, *J* = 8.8 Hz, 2H, H_i), 6.92 (d, *J* = 8.8 Hz, 2H, H_h), 6.83 (s, 2H, H_g), 5.97 – 5.82 (m, 2H, H_c), 5.32 – 5.25 (m, 2H, H_a), 5.20 – 5.16 (m, 2H, H_b), 4.53 (s, 3H, H_m), 4.20 (s, 4H, H_f), 4.06 (d, *J* = 5.7 Hz, 4H, H_d), 3.80 (s, 4H, H_e); **^{13}C NMR** (101 MHz, DMSO-d_6) δ 163.80, 156.46, 155.80, 144.48, 143.14, 135.03, 131.30, 130.21, 119.39, 116.66, 114.37, 110.97, 101.67, 71.14, 68.37, 67.77; **HRMS** (ESI +ve) m/z= 968.03986 ($[M - Cl^-]^+$, $C_{38}H_{32}O_8N_7{}^{127}I_2$, calc= 968.03962).

[2+2] Coumarin Macrocycle 2.25



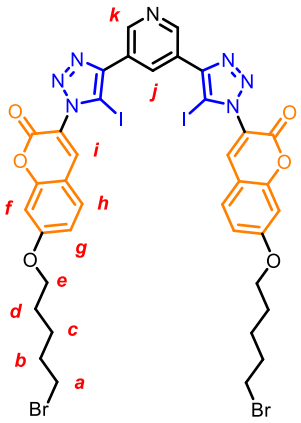
Pyridinium bis-alkene **2.24** (14.4 mg, 12.9 µmol, 1 eq) was dissolved in dry degassed CH_2Cl_2 (12 mL). Hoveyda-Grubbs catalyst (3.6 mg, 5.75 µmol, 0.45 eq) was dissolved in dry degassed CH_2Cl_2 (6 mL) and slowly added via a syringe pump and the reaction mixture left to stir for 24 h. The solvent was removed *in vacuo*, purified via preparative thin layer chromatography (eluent: 10% MeOH/CH_2Cl_2) and isolated as off-white powder (7.8 mg, 27%). **^{1}H NMR** (400 MHz, d_6-DMSO) δ 9.80 (s, 2H), 9.72 (s, 4H), 8.77 (s, 4H), 7.87 (d, *J* = 8.8 Hz, 4H), 7.28 (s, 4H), 7.18 (d, *J* = 8.8 Hz, 4H), 5.84 (s, 4H), 4.63 (s, 4H), 4.34 (s, 4H), 4.07 (s, 4H), 3.80 (s, 4H); **^{13}C NMR** (126 MHz, d_6-DMSO) δ 164.31, 156.89, 156.29, 145.06, 143.59, 143.16, 131.80, 130.53, 129.52, 119.75, 117.13, 114.84, 111.43, 102.14, 70.63, 68.86, 68.17, 49.34, 40.59, 40.50, 40.42, 40.33, 40.26, 40.17, 40.09, 40.00, 39.83, 39.66, 39.50; **HRMS** (ESI +ve) m/z=940.0086 ($[M]^{2+}$, $C_{72}H_{56}I_4N_{14}O_{162}{}^{2+}$, calc=940.0083)

Alkyl-Bromine Coumarin-Azide 2.26



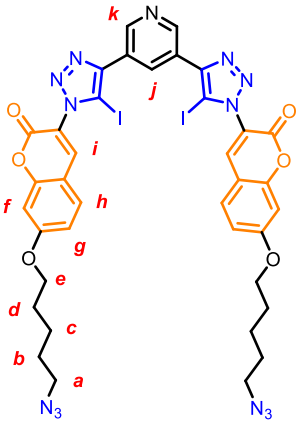
Coumarin azide **2.6** (200 mg, 948 µmol, 1 eq) was dissolved in dry MeCN under N_2 before K_2CO_3 (204 mg, 1.47 mmol, 1.5 eq) and 1,5-dibromopentane (4.52 g, 19.7 mmol, 20 eq) were added. Th reaction was left to stir for 6 h, before the solvent was removed *in vacuo*. Purification was achieved by column chromatography (eluent CH_2Cl_2) to afford the **2.26** (91 mg, 26%) as a brown powder. **^{1}H NMR** (500 MHz, $CDCl_3$) δ 7.23 (d, *J* = 8.6 Hz, 1H, H_h), 7.09 (s, 1H, H_i), 6.78 (dd, *J* = 8.6, 2.4 Hz, 1H, H_g), 6.74 (d, *J* = 2.4 Hz, 1H, H_f), 3.95 (t, *J* = 6.3 Hz, 2H, H_e), 3.38 (t, *J* = 6.7 Hz, 2H, H_a), 1.88 (p, J = 7.0 Hz, 2H, H_d), 1.78 (p, J = 6.7 Hz, 2H, H_b), 1.62 – 1.53 (m, 2H, H_c); **^{13}C NMR** (126 MHz, $CDCl_3$) δ 161.57, 158.12, 153.41, 128.48, 126.80, 123.64, 114.02, 112.95, 101.57, 68.67, 33.82, 32.76, 28.57, 25.12. **HRMS –** *unable to obtain due to decomposition*

Pyridine Bis-Alkyl-Bromine 2.27



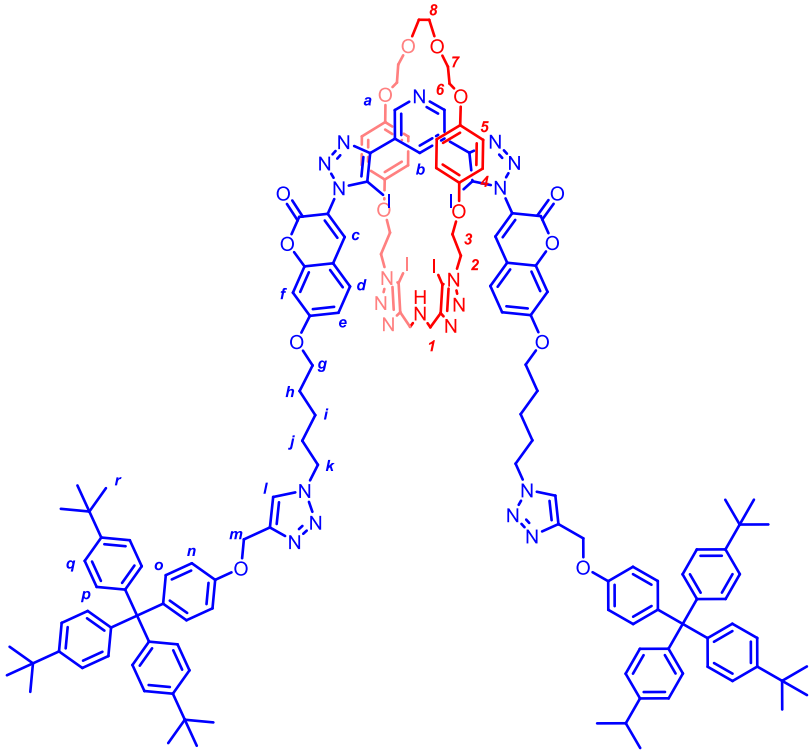
Bis iodo-alkyne **2.4** (40 mg, 105 µmol, 1 eq), TBTA (11 mg, 21 µmol, 0.2 eq), $Cu(MeCN)_4.PF_6$ (12 mg, 32 µmol, 0.3 eq) and coumarin-azide **2.26** (81 mg, 230 mg, 2.2 eq) were dissolved in dry degassed THF (3 mL). The mixture was left to stir for 3 days under N_2 at room temperature. The solvent was removed and the residue redissolved in $CHCl_3$ (20 mL). The organic layer was washed aqueous EDTA solution (4 x 20 mL), and then dried over Na_2SO_4 and the solvent removed *in vacuo*. Purification was achieved via preparative thin layer chromatography (Eluent: 2% MeOH/CH_2Cl_2) affording pyridine bis-alkyl-bromine **2.27** (48 mg, 42%) as a pale brown powder. **^{1}H NMR** (400 MHz, $CDCl_3$) δ 9.35 (s, 2H, H_k), 8.98 (s, 1H, H_j), 8.07 (s, 2H, H_i), 7.56 (d, *J* = 8.7 Hz, 2H, H_h), 6.98 (dd, *J* = 8.7, 2.3 Hz, 2H, H_g), 6.93 (d, *J* = 2.3 Hz, 2H, H_f), 4.11 (t, *J* = 6.3 Hz, 4H, H_e), 3.46 (t, *J* = 6.7 Hz, 4H, H_a), 1.93 (M, 8H, $H_{b,d}$), 1.74 – 1.63 (m, 4H, H_c); **^{13}C NMR** (101 MHz, $CDCl_3$) δ 164.27, 156.46, 156.37, 148.34, 147.42, 142.88, 132.83, 130.44, 125.90, 120.39, 114.45, 111.02, 101.54, 68.71, 33.42, 32.34, 28.12, 24.71; **HRMS** (ESI +ve) m/z=1083.8845 ($[M + H]^+$, $C_{37}H_{32}N_7O_6Br_2I_2$, calc=1083.8848)

Pyridine Bis-Alkyl-Azide 2.28



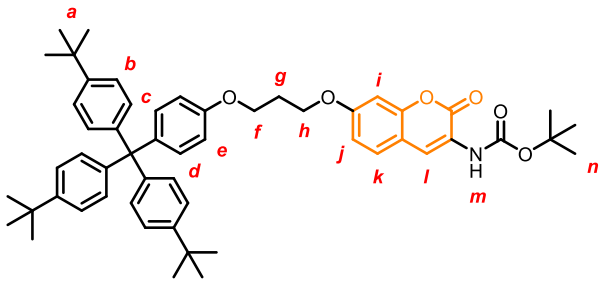
Pyridine bis-alkyl-bromine **2.27** (35 mg, 32 µmol, 1 eq) was dissolved in dry DMF (1.5 mL) under N_2. NaN_3 (8.4 mg, 129 µmol, 4 eq) and NaI (0.97 mg, 6.5 µmol, 0.2 eq) were added and the solution left to stir at room temperature for 16 h. The solvent was removed *in vacuo* and the residue redissolved in Water/EtOAc (20 mL). The product was extracted with EtOAc (3 x 20 mL) and the organic layer dried over Na_2SO_4 before the solvent was removed *in vacuo* to give pyridine bis-alkyl-azide **2.28** (35 mg, 77%) as a brown powder. No further purification required. **^{1}H NMR** (500 MHz, $CDCl_3$) δ 9.35 (d, *J* = 2.2 Hz, 2H, H_k), 8.98 (d, *J* = 2.2 Hz, 1H, H_j), 8.07 (s, 2H, H_i), 7.56 (d, *J* = 8.7 Hz, 2H, H_h), 6.97 (d, J = 8.7 Hz, 2H, H_g), 6.93 (s, 2H, H_f), 4.10 (t, *J* = 6.2 Hz, 4H, H_e), 3.34 (t, *J* = 6.7 Hz, 4H, H_a), 1.95 – 1.85 (m, 4H, H_d), 1.76 – 1.67 (m, 4H, H_b), 1.67 – 1.58 (m, 4H, H_a); **^{13}C NMR** (126 MHz, $CDCl_3$) δ 164.67, 156.77, 148.70, 147.79, 143.27, 130.83, 126.31, 120.79, 114.84, 111.41, 101.93, 69.10, 51.68, 30.10, 29.01, 28.89, 23.72; **HRMS** (ESI +ve) m/z=1008.0682 ($[M + H]^+$, $C_{37}H_{32}N_{13}O_6I_2$, calc = 1008.0687)

Coumarin Rotaxane 2.29



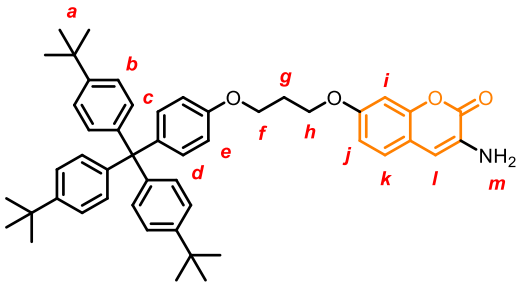
XB macrocycle (11.4 mg, 13.9 µmol, 1 eq) and $Cu(MeCN)_4.PF_6$ (5.2 mg, 13.9 µmol, 1 eq) were dissolved in dry degassed CH_2Cl_2 (0.7 mL). Stopper alkyne **2.31** (45.3 mg, 83.4 µmol, 6 eq) was added followed by pyridine bis-alkyl-azide **2.28** (42 mg, 41.7 µmol, 3 eq) dissolved in dry degassed CH_2Cl_2 (0.7 mL). The reaction mix was left to stir at room temperature for 4 days. The solvent was removed *in vacuo* and the residue redissolved in $CDCl_3$ and washed with aqueous EDTA solution (3 x 20 mL). The organic layer was dried over Na_2SO_4, and the solvent removed *in vacuo*. Purification was achieved via preparative thin layer chromatography (eluent: 5% $MeOH/CH_2Cl_2$) affording rotaxane **2.29** (3.5 mg, 9%) as a white solid. **^{1}H NMR** (400 MHz, $CDCl_3$) δ 9.25 (s, 2H, H_a), 8.74 (s, 1H, H_b) 7.82 (s, 2H, H_c), 7.65 (s, 2H, H_l), 7.47 (d, *J* = 8.8 Hz, 2H, H_d), 7.23 (d, *J* = 8.4 Hz, 12H, H_p), 7.11 (d, *J* = 8.8 Hz, 4H, H_o), 7.07 (d, *J* = 8.3 Hz, 12H, H_q), 6.86 (d, *J* = 8.6 Hz, 6H, $H_{n,e}$), 6.75 (s, 2H, H_f) 6.33 (s, 8H, $H_{4,5}$), 5.18 (s, 4H, H_m), 4.66 (s, 4H, H_2), 4.40 (t, *J* = 7.1 Hz, 4H, H_k), 4.10 (m, 4H, H_3), 3.99 (m, 4H, $H_{g,6}$), 3.91 (s, 4H, H_1), 3.80 (d, *J* = 9.4 Hz, 4H, H_7), 3.78 (s, 4H, H_8), 2.00 (m, 4H, H_j), 1.84 (s, 4H, H_h), 1.52 (m, 4H, H_i) 1.30 (s, 54H, H_r); **^{13}C NMR** (126 MHz, $CDCl_3$) δ 163.91, 156.58, 156.12, 152.89, 151.60, 148.39, 144.44, 144.06, 140.24, 132.37, 130.73, 124.08, 122.65, 114.84, 114.67, 114.20, 113.23, 111.08, 70.80, 69.76, 68.41, 67.51, 66.69, 63.08, 62.08, 50.20, 34.32, 31.40, 29.72; **HRMS** (ESI +ve) m/z=1455.9257 ($[M + 2H]^{2+}$, $C_{145}H_{156}N_{20}O_{14}I_4$, calc=1455.9233)

BOC-Coumarin Stopper 2.34



Bromine-stopper **2.33** (971 mg, 1.55 mmol, 1 eq) was added to a mixture of coumarin **2.12** (474 mg, 1.71 mmol, 1.1 eq), K_2CO_3 (429 mg, 3.11 mmol, 2 eq) and NaI (23 mg, 0.16 mmol, 0.1 eq) dissolved in dry MeCN (20 mL) . The solution was heated at reflux for 16 h. The solvent was then removed *in vacuo* and the crude residue dissolved in $CHCl_3$ (20 mL). The solution was washed with water (3 x 20 mL), brine (20 mL), dried over $MgSO_4$, filtered and had the solvents removed *in vacuo*. The crude was then purified by silica column chromatography (eluent: CH_2Cl_2) to yield a yellow powder (845 mg, 67 %). **^{1}H NMR** (400 MHz, $CDCl_3$); δ 8.23 (s, 1H, H_m), 7.34 (d, *J* = 8.6 Hz, 1H, H_k), 7.29 (s, 1H, H_l), 7.25 – 7.20 (m, 6H, H_c), 7.10 – 7.05 (m 8H, $H_{b,d}$), 6.86 (dd, *J* = 8.6, 2.4 Hz, 1H, H_j), 6.83 (d, *J* = 2.4 Hz, 1H, H_i), 6.80 – 6.75 (m, 2H, H_e), 4.20 (m, 2H, H_h), 4.14 (m, 2H, H_f), 2.27 (m, 2H, H_g), 1.53 (s, 9H, H_n), 1.30 (s, 27H, H_a); **^{13}C NMR** (126 MHz, $CDCl_3$); δ 160.03, 156.52, 152.62, 150.93, 148.31, 144.11, 139.81, 132.29, 130.71, 128.09, 124.04, 122.14, 121.26, 113.34, 112.94, 101.33, 65.04, 63.88, 63.05, 53.43, 34.30, 31.39, 29.17, 28.24; **HRMS** (ESI +ve) m/z= 822.47314 ($[M + H]^+$, $C_{54}H_{64}O_6N$, calc= 822.47282).

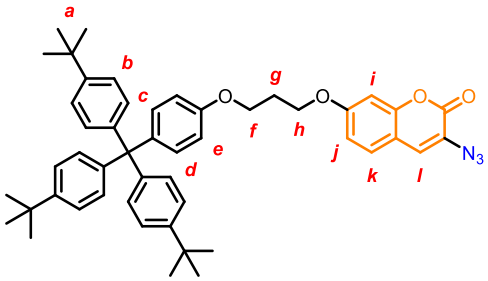
Coumarin-Amine Stopper 2.35



BOC-coumarin stopper **2.34** (147 mg, 0.179 mmol, 1 eq) was dissolved in CH_2Cl_2 (1.0 mL) and cooled to 0 °C using an ice bath before TFA (1.0 mL) was slowly added. The mixture was left to heat to rt over 3 h. $CHCl_3$ (20 mL) was then added and the solution and washed with a saturated solution of $NaHCO_3$ (3 x 20 mL), water (20 mL) and brine (20 mL). The organic phase was dried over $MgSO_4$, filtered and had the solvent removed *in vacuo* to yield an off white

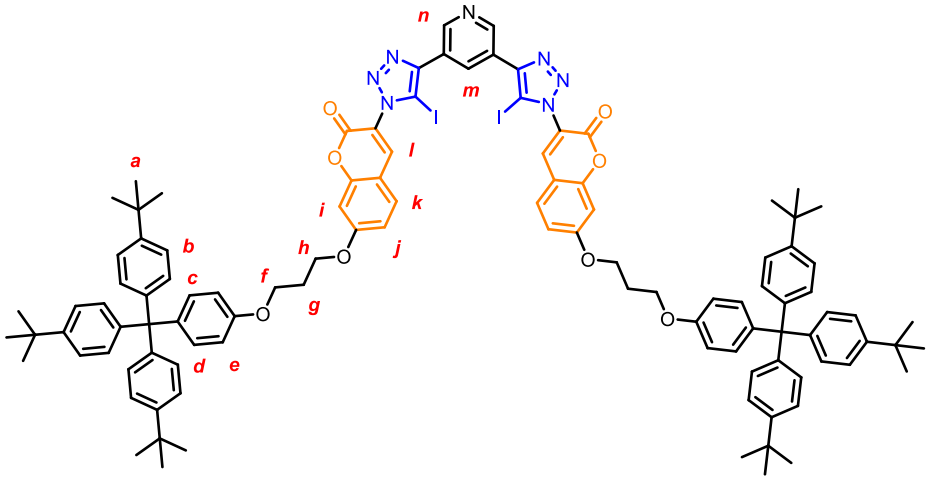
solid (128 mg, 99 %). **^{1}H NMR** (500 MHz, $CDCl_3$); δ 7.24 – 7.19 (m, 6H, H_c), 7.18 (d, *J* = 8.4 Hz, 1H, H_k), 7.10 – 7.05 (m, 8H, $H_{b,d}$), 6.84 – 6.76 (m, 4H, $H_{e,l,j}$), 6.68 (s, 1H, H_l), 4.17 (m, 2H, H_h), 4.13 (m, 2H, H_f), 4.04 (s, 2H, H_m), 2.26 (m, 2H, H_g), 1.30 (s, 29H, H_a); **^{13}C NMR** (126 MHz, $CDCl_3$); δ 159.73, 158.32, 156.56, 150.32, 148.30, 144.12, 139.76, 132.28, 130.71, 129.71, 125.81, 124.04, 114.41, 112.95, 112.85, 112.23, 101.47, 64.95, 63.98, 63.05, 34.30, 31.39, 29.22; **HRMS** (ESI +ve) m/z= 722.42035 ($[M + H]^+$, $C_{49}H_{56}O_4N$, calc= 722.42039).

Coumarin-Azide Stopper 2.36



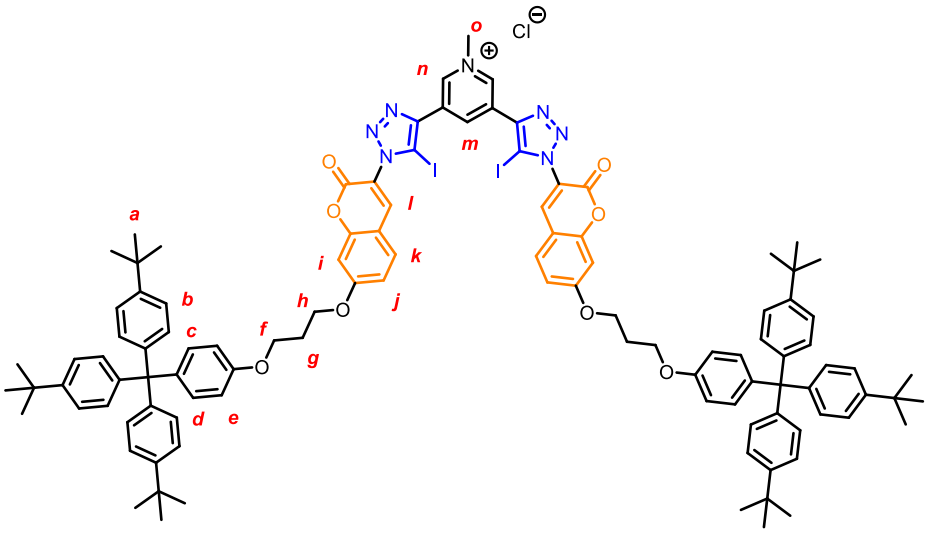
Coumarin-amine stopper **2.35** (506 mg, 0.716 mmol, 1 eq) was dissolved in THF (10 mL), sonicated and cooled to 0 °C in an ice bath. *t*-$BuNO_2$ (0.13 mL, 1.07 mmol, 1.6 eq) and $TMSN_3$ (0.71 mL, 1.29 mmol, 1.8 eq) were sequentially added slowly. The mixture was left to warm up to rt over 2 h. The solvent was removed *in vacuo* to yield a yellow solid (0.512 mg, 96 %), no further purification needed. **^{1}H NMR** (500 MHz, $CDCl_3$) δ 7.32 – 7.27 (m, 1H, H_k), 7.26 – 7.19 (m, 6H, H_c), 7.16 (s, 1H, H_l), 7.13 – 7.04 (m, 8H, $H_{b,d}$), 6.87 – 6.84 (m, 2H, $H_{i,j}$), 6.80 – 6.75 (m, 2H, H_e), 4.21 (t, *J* = 6.1 Hz, 2H, H_h), 4.13 (t, *J* = 5.9 Hz, 2H, H_f), 3.78 – 3.71 (m, 2H, H_g), 1.30 (s, 27H, H_a); **^{13}C NMR** (126 MHz, $CDCl_3$) δ 161.23, 157.87, 156.63, 153.14, 148.48, 144.24, 140.01, 132.44, 130.85, 128.23, 126.52, 124.19, 123.46, 113.68, 113.08, 112.79, 101.53, 68.12, 65.34, 63.94, 63.20, 34.44, 31.53, 29.26, 25.77, 2.09; **HRMS** (ESI +ve) m/z= 770.39331 ($[M + Na]^+$, $C_{49}H_{53}O_4N_3{}^{23}Na$, calc= 770.39283).

Pyridine Coumarin Axle 2.37



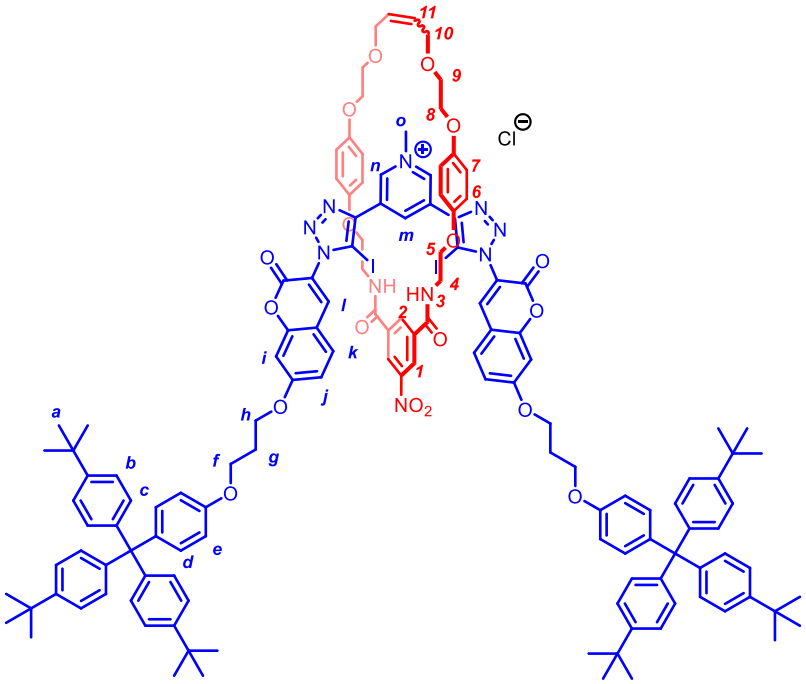
Coumarin-azide stopper **2.36** (445 mg, 0.595 mmol, 2.2 eq), bis-iodo-alkyne **2.4** (102 mg, 0.270 mmol, 1 eq), TBTA (36 mg, 0.054 mmol, 0.25 mmol) and $Cu(CH_3CN)_4.PF_6$ (30 mg, 0.081 mmol, 0.3 eq) were dissolved in dry, degassed THF (10 mL) and left to stir for 72 h in darkness. The solvent was removed *in vacuo* and the crude dissolved in $CHCl_3$ (15 mL) and washed with 0.1 M EDTA solution (3 x 15 mL) and H_2O (15 mL). The combined organic phases were dried over $MgSO_4$, filtered and concentrated *in vacuo*. The crude was then purified by silica column chromatography (eluent: CH_2Cl_2:MeOH 2:98 *v/v*) to yield a yellow powder (236 mg, 57 %). **^{1}H NMR** (500 MHz, $CDCl_3$) δ 9.37 (s, 2H, H_n), 9.01 (s, 1H, H_m), 8.05 (s, 2H, H_l), 7.55 (d, *J* = 8.6 Hz, 2H, H_k), 7.23 (d, *J* = 8.5 Hz, 12H, H_c), 7.11 (d, *J* = 8.8 Hz, 4H, H_d), 7.08 (d, *J* = 8.5 Hz, 12H, H_b), 7.03 – 6.96 (m, 4H, $H_{i,j}$), 6.80 (d, *J* = 8.8 Hz, 4H, H_e), 4.31 (t, *J* = 6.1 Hz, 4H, H_h), 4.17 (t, *J* = 5.9 Hz, 4H, H_f), 2.35 – 2.31 (m, 4H, H_g), 1.30 (s, 54H, H_a); **^{13}C NMR** (126 MHz, $CDCl_3$) δ 156.59, 156.51, 148.51, 144.23, 142.89, 140.12, 132.48, 130.85, 130.54, 124.21, 120.63, 114.49, 113.09, 101.90, 77.41, 77.16, 76.90, 65.77, 63.79, 63.21, 34.45, 31.53, 29.19. **HRMS –** *unable to obtain due to decomposition*

Pyridium Coumarin Axle Chloride 2.38



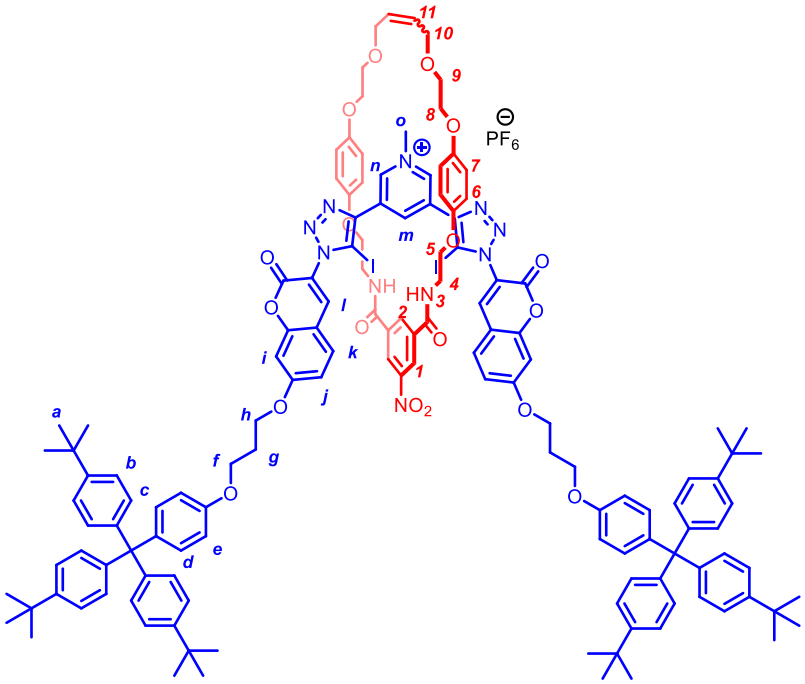
Pyridine coumarin axle **2.37** (236 mg, 0.126 mmol, 1 eq) was dissolved in dry CH_2Cl_2 (2 mL). MeI (0.16 mL, >10 eq) was slowly added and the reaction left to stir in darkness for 24 h. The solvent was removed *in vacuo* and the crude dissolved in $CHCl_3$ (10 mL) and washed with $NH_4Cl_{(aq)}$ solution (4 x 10 mL) and brine (2 x 10 mL). The organic phase was then dried *in vacuo* yielding a yellow solid (236 mg, 97%). **^{1}H NMR** (400 MHz, $CDCl_3$) δ 9.78 (s, 1H, H_m), 9.41 (s, 2H, H_n), 8.38 (s, 2H, H_l), 7.68 (s, 2H, H_i), 7.23 – 7.19 (m, 12H, H_b), 7.10 – 7.07 (m, 16H, $H_{c,d}$), 6.92 – 6.88 (m, 4H, $H_{i,j}$), 6.78 – 6.74 (m, 4H, H_e), 4.68 (s, 3H, H_o), 4.25 (s, 4H, H_h), 4.12 (s, 4H, H_f), 2.28 (s, 4H, H_g), 1.28 (s, 54H, H_a); **^{13}C NMR** (101 MHz, $CDCl_3$) δ 164.20, 156.57, 156.38, 148.43, 144.25, 140.01, 132.45, 130.85, 124.19, 113.10, 65.80, 63.93, 63.20, 34.43, 31.55, 29.16; **HRMS** (ESI +ve) m/z= 1888.66101 ($[M - Cl^-]^+$, $C_{108}H_{112}O_8N_7{}^{127}I_2$, calc= 1888.66563).

Coumarin Rotaxane 2.39



Pyridium coumarin axle **2.38** (60 mg, 31 µmol, 1 eq) and bis-alkene (40.5 mg, 62 µmol, 2 eq, 6 mM) were dissolved in dry de-gassed CH_2Cl_2 (10.4 mL) and left degassing for 30 min. Grubbs' II catalyst (5 mg) was then added and the mixture was left to stir for 2 days before further Grubbs' II catalyst (3 mg) was added. The mixture was then left to stir for a further 2 days at rt. The solvent was removed *in vacuo* and the product purified by preparative TLC plate (5% MeOH in CH_2Cl_2) to afford an off-white solid (21 mg, 27 %). **^{1}H NMR** (400 MHz, 6:4 $CDCl_3$:MeOH-d_4); δ 9.47 (s, 2H, H_n), 9.32 (s, 1H, H_m), 8.67 (s, 2H, H_1), 8.40 (s, 1H, H_2), 8.04 (s, 2H, H_l), 7.59 (d, *J* = 8.8 Hz, 2H, H_k), 7.20 (d, *J* = 8.6 Hz, 12H, H_c), 7.04-7.10 (m, 16H, $H_{b,d}$), 7.02 (dd, *J* = 8.8 Hz, 1.4 Hz, 2H, H_j), 6.88 (d, , *J* = 1.4 Hz, 2H, H_i), 6.81 (d, *J* = 8.7 Hz, 4H, H_e), 6.47 (d, *J* = 8.7 Hz, 4H, H_6), 6.28 (m, 2H, H_3) 6.01 (d, *J* = 8.7 Hz, 4H, H_7), 4.59 (s, 3H, H_o), 4.31 (m, 4H, H_h), 4.20 (m, 4H, H_f), 4.14 (m, 8H, $H_{4,10}$), 3.87 (m, 4H, H_5), 3.71 (m, 4H, H_8), 3.62 (m, 4H, H_9), 2.34 (m, 4H, H_g), 1.26 (s, 54H, H_a); **^{13}C NMR** (126 MHz, 6:4 $CDCl_3$:MeOH-d_4): δ 164.49, 164.37, 156.82, 156.51, 155.94, 152.62, 152.16, 151.86, 148.24, 144.16, 143.42, 142.79, 139.79, 135.21, 132.19, 130.87, 130.64, 128.84, 128.05, 126.20, 123.96, 119.35, 115.09, 114.40, 113.93, 113.00, 110.59, 101.33, 66.39, 65.72, 63.95, 63.01, 60.57, 34.11, 31.09, 29.55, 28.90, 13.76; **HRMS** (ESI +ve) m/z= 2509.89160 ($[M - Cl^-]^+$, $C_{140}H_{147}O_{18}N_{10}{}^{127}I_2$, calc= 2509.89787).

Coumarin Rotaxane 2.40

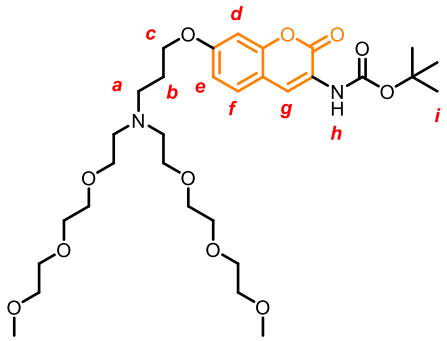


Coumarin rotaxane **2.39** (21 mg, 8.25 µmol, 1 eq) was dissolved in $CHCl_3$ (10 mL) and washed with $NH_4Cl_{(aq)}$ solution (4 x 10 mL) and brine (2 x 10 mL). The organic phase was then dried *in vacuo* yielding a yellow solid (22 mg, 99%). **^{1}H NMR** (400 MHz, 6:4 $CDCl_3$:MeOH-d_4) δ 9.24 (s, 2H, H_n), 8.89 (s, 1H, H_m), 8.76 (s, 1H, H_1), 8.64 (s, 2H, H_2), 8.15 (s, 2H, H_l), 7.64 (d, *J* = 8.8 Hz, 2H, H_k), 7.21 (d, *J* = 8.3 Hz, 12H, H_c), 7.10 – 7.02 (m, 18H, $H_{b,d,j}$), 6.91 (d, *J* = 2.4 Hz, 2H, H_i), 6.87 – 6.77 (m, 4H, H_e), 6.39 (d, *J* = 8.6 Hz, 4H, H_6), 6.21 (d, *J* = 8.6 Hz, 4H, H_7), 6.13 (s, 2H, H_3), 4.59 (s, 3H, H_o), 4.31 (t, *J* = 6.1 Hz, 4H, H_h), 4.18 (t, *J* = 5.9 Hz, 4H, H_f), 4.14 – 4.06 (m, 4H, $H_{4,10}$), 3.90 (s, 4H, H_5), 3.78 – 3.71 (m, 8H, $H_{8,9}$), 2.37 – 2.29 (m, 4H, H_g), 1.27 (s, 54H, H_a); **^{19}F NMR** (376 MHz, 6:4 $CDCl_3$:MeOH-d_4) δ -72.78, -74.67; **^{13}C NMR** (101 MHz, 6:4 $CDCl_3$:MeOH-d_4) δ 166.03, 165.21, 157.49, 157.04, 156.72, 153.19, 152.89, 148.82, 148.78, 144.70, 144.55, 143.11, 140.43, 136.63, 132.75, 131.53, 131.18, 130.73, 125.84, 124.51, 119.61, 116.20, 115.65, 115.26, 114.89, 113.53, 111.37, 102.02, 71.42, 69.83, 68.25, 67.11, 66.26, 64.37, 63.56, 40.67, 34.66, 32.36, 31.61, 30.09, 29.44, 23.09; **HRMS** (ESI +ve) m/z= 2509.89160 ($[M - Cl^-]^+$, $C_{140}H_{147}O_{18}N_{10}{}^{127}I_2$, calc= 2509.89787).

6.4. Synthesis from Chapter 3

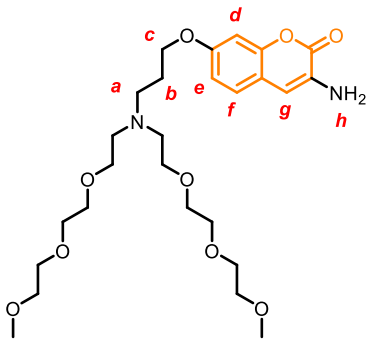
The synthesis of compounds **3.1**,[16] **3.2**,[16] **3.3**,[16] **3.7**,[17] **3.8**,[17] **3.9**,[17] **3.13**,[18] **3.14**,[18] and **3.15**[18] have been described previously.

BOC-Coumarin 3.4



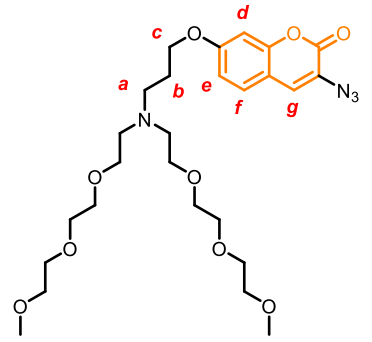
Boc-protected coumarin **2.12** (599 mg, 2.16 mmol, 1 eq), PEG chloride **3.3** (1000 mg, 2.59 mmol, 1.2 eq), K_2CO_3 (895.2 mg, 6.48 mmol, 3 eq) and NaI (64.2 mg, 0.432 mmol, 0.2 eq) were dissolved in MeCN (20 mL) and heated under reflux for 36 hours. The solvent was removed *in vacuo* and the crude dissolved between H_2O (40 mL) and $CHCl_3$ (40 mL). The product was extracted by $CHCl_3$ (3 x 40 mL) and the combined organic phases washed with brine (100 mL). The organic phase was then dried over $MgSO_4$, filtered and the solvent removed *in vacuo*. The product was purified *via* column chromatography (eluent: MeOH/CH_2Cl_2 5:95 *v/v)* affording coumarin **3.4** (1.17g, 87%) as a yellow oil. **^{1}H NMR** (400 MHz, $CDCl_3$) δ 8.22 (s, 1H, H_g), 7.33 (d, *J* = 8.6 Hz, 1H, H_f), 7.28 (s, 1H, H_h), 6.85 (dd, J = 8.6, 2.4 Hz, 1H, H_e), 6.80 (d, *J* = 2.4 Hz, 1H, H_f), 4.04 (t, *J* = 6.2 Hz, 2H, H_c), 3.65 – 3.50 (m, 20H, OCH_2), 3.36 (s, 6H, OCH_3), 2.76 (m, 6H, H_a, NCH_2), 1.94 (m, 2H, H_b), 1.52 (s, 9H, H_i); **^{13}C NMR** (126 MHz, $CDCl_3$) δ 160.36, 159.03, 152.74, 151.08, 128.18, 122.18, 121.45, 113.53, 113.31, 101.35, 81.57, 72.06, 70.73, 70.65, 70.55, 66.58, 59.15, 54.19, 51.74, 28.36; **HRMS** (ESI +ve) m/z= 627.357 ($[M + H]^+$, $C_{31}H_{51}N_2O_{11}$, calc= 627.349).

Coumarin-Amine 3.5



Boc-coumarin **3.4** (1.17 g, 1.87 mmol, 1 eq) was dissolved in CH_2Cl_2 (4.7 mL) and cooled to 0°C. TFA (4.7 ml, excess) was slowly added dropwise and the reaction left to warm up to room temperature over 2 h. Saturated aqueous $NaHCO_3$ solution was added till neutral, and the product extracted with CH_2Cl_2 (5 x 30 mL). The combined organic layers were dried over $MgSO_4$, filtered and the solvent removed *in vacuo* to afford coumarin (0.99 g, 90%) as a viscous yellow oil. **^{1}H NMR** (400 MHz, $CDCl_3$) δ 7.18 (d, J = 9.3 Hz, 1H, H_f), 6.81 – 6.76 (m, 2H, $H_{d,e}$), 6.69 (s, 1H, H_g), 4.05 (s, 2H, H_h), 4.02 (t, J = 6.1 Hz, 2H, H_c), 3.64 – 3.50 (m, 20H, OCH_2), 3.36 (s, 6H, OCH_3), 2.79 (m, 6H, H_a, NCH_2), 1.97 (s, 2H, H_b); **^{13}C NMR** – *unable to obtain due to decomposition*; **HRMS** (ESI +ve) m/z= 527.300 ($[M + H]^+$, $C_{26}H_{43}N_2O_9$, calc= 527.310).

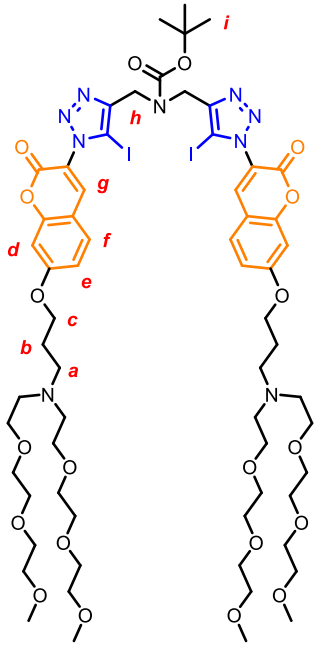
Coumarin-Azide 3.6



Coumarin-amine **3.5** (985 mg, 1.87 mmol, 1 eq) was dissolved in 15% $HCl_{(aq)}$ (15 mL) at 0 °C. $NaNO_2$ (155 mg, 2.25 mmol, 1.2 eq) was then slowly added and the reaction mixture left to stir for 30 minutes. A solution of NaN_3 (195 mg, 3.0 mmol, 1.6 eq) in H_2O (25 mL) was slowly added dropwise and the reaction mixture left to stir for a further 1 hour at 0 °C. The reaction was neutralised with $NaHCO_3$ and product extracted with EtOAc (3 x 60 mL). The combined organic layers were dried over $MgSO_4$, filtered and had the solvent removed *in vacuo* to yield coumarin (845 mg, 81%) as a deep red oil. **^{1}H NMR** (400 MHz, $CDCl_3$) δ 7.30 (d, J = 8.4 Hz, 1H,

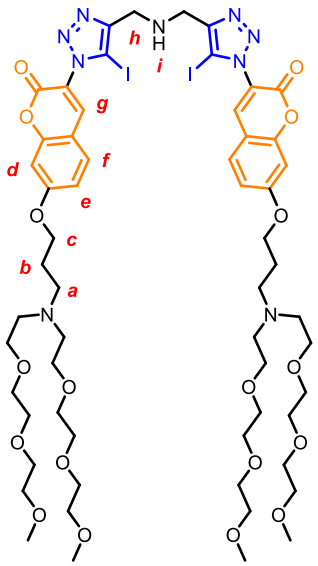
H_f), 7.16 (s, 1H, H_g), 6.87 – 6.82 (m, 2H, $H_{d,e}$), 4.06 (t, *J* = 6.2 Hz, 2H, H_c), 3.66 – 3.49 (m, 20H, OCH_2), 3.37 (s, 6H, OCH_3), 2.73 (t, *J* = 6.5 Hz, 6H, H_a, NCH_2), 1.93 (p, *J* = 6.5 Hz, 2H, H_b); **^{13}C NMR** (126 MHz, $CDCl_3$) δ 153.18, 128.21, 126.61, 113.81, 101.37, 72.08, 70.76, 70.68, 70.57, 66.75, 59.18, 54.19, 31.08; **HRMS** (ESI +ve) m/z= 553.295 ($[M + H]^+$, $C_{26}H_{41}N_4O_9$, calc= 553.287).

Boc-Protected Compound 3.10



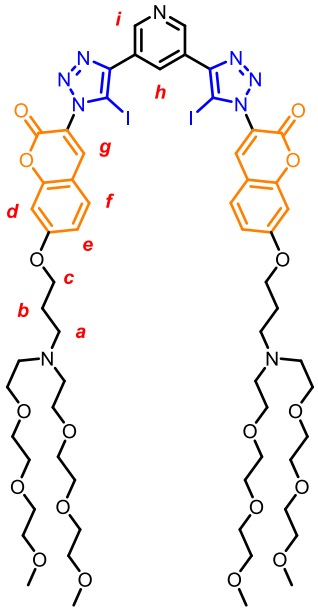
Coumarin-azide **3.10** (70 mg, 0.127 mmol, 2.2 eq), bis-iodo alkyne **2.4** (25.6 mg, 0.0575 mmol, 1 eq), TBTA (5.18 mg, 0.0098 mmol, 0.17 eq), and $Cu(CH_3CN)_4.PF_6$ (6.44 mg, 0.0173 mmol, 0.3 eq) were dissolved in dry degassed THF (3.5 mL) and left to stir at room temperature under N_2 for 3 days. The solvent was then removed *in vacuo*, the crude dissolved in $CHCl_3$ (25 mL) and washed with EDTA solution (3 x 25 mL) whilst extracting all washes again with $CHCl_3$ (15 mL). The combined organic phases were dried over $MgSO_4$, filtered and the solvent removed *in vacuo*. Purification was achieved *via* preparative thin layer chromatography (eluent: $MeOH/CH_2Cl_2$ 1:9 *v/v*) affording the desired product (12 mg, 13 %) as a viscous yellow oil. **^{1}H NMR** (400 MHz, Chloroform-d) δ 7.99 (s, 2H, H_g), 7.52 (d, *J* = 8.6 Hz, 2H, H_f), 6.96 (dd, *J* = 8.6, 2.3 Hz, 2H, H_e), 6.93 (d, *J* = 2.3 Hz, 2H, H_d), 4.85 – 4.68 (m, 4H, H_h), 4.15 (t, J = 6.2 Hz, 4H, H_c), 3.67 – 3.50 (m, 40H, OCH_2), 3.37 (s, 12H, OCH_3), 2.80 – 2.69 (m, 12H, H_a, NCH_2), 1.98 (s, br, 4H, H_b), 1.50 (s, 9H, H_i); **^{13}C NMR** (126 MHz, $CDCl_3$) δ 164.24, 156.47, 156.27, 155.20, 148.63, 142.61, 130.30, 120.43, 114.32, 110.99, 101.53, 80.85, 71.95, 70.65, 70.55, 70.45, 67.01, 59.05, 54.09, 51.43, 29.71, 28.53; **HRMS** (ESI +ve) m/z= 1550.46990 ($[M + H]^+$, $C_{63}H_{94}I_2N_9O_{20}$, calc= 1550.46899).

Receptor 3.11



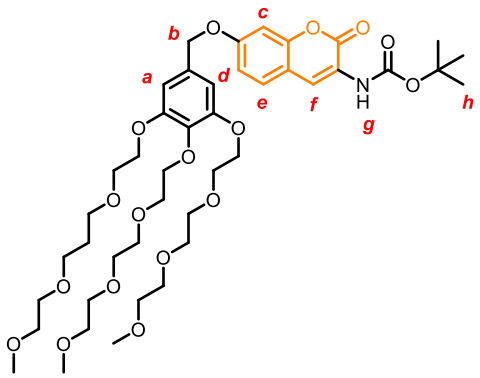
Boc-protected compound **3.10** (1.8 mg, 7.61 mmol, 1eq) was dissolved in CH_2Cl_2 (0.5 mL). TFA (0.5 mL, excess) was added, and the reaction left to stir at room temperature for 2 h. The mixture was brought to a neutral pH with saturated aqueous $NaHCO_3$ solution before the product was extracted 5 times with CH_2Cl_2 (20 mL). The organic layer was dried over Na_2SO_4 and the solvent removed *in vacuo* to afford product (11.9 mg, 99%) as a viscous yellow oil. **^{1}H NMR** (400 MHz, $CDCl_3$) δ 7.90 (s, 2H, H_g), 7.44 (d, J = 8.6 Hz, 2H, H_f), 6.89 (dd, J = 8.6, 2.6 Hz, 2H, H_e), 6.87 (d, J = 2.6 Hz, 2H, H_d), 4.09 (t, J = 6.3 Hz, 4H, H_c), 3.97 (s, 4H, H_h), 3.62 – 3.41 (m, 40H, OCH_2), 3.30 (s, 12H, OCH_3), 2.76 – 2.63 (m, 12H, H_a, NCH_2), 1.95 – 1.87 (m, 6H, H_b); **^{13}C NMR** (101 MHz, $CDCl_3$) δ 163.27, 155.42, 155.26, 149.31, 141.36, 129.24, 119.45, 113.33, 109.95, 100.55, 81.25, 70.95, 69.64, 69.54, 69.44, 68.81, 66.03, 58.02, 53.11, 52.39, 50.39, 43.09, 28.68; **HRMS** (ESI +ve) m/z= 726.800 ($[M + 2H]^+$, $C_{58}H_{87}I_2N_9O_{18}$, calc = 726.705).

Receptor 3.12



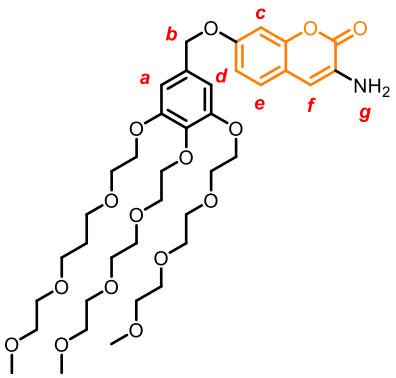
Coumarin-azide **3.6** (126 mg, 0.228 mmol, 2.2eq), bis-iodo-alkyne **2.4** (39.2 mg, 0.1036 mmol, 1 eq), TBTA (11.0 mg, 0.0207 mmol, 0.2 eq), and $Cu(CH_3CN)_4.PF_6$ (11.6 mg, 0.0311 mmol, 0.3 eq) were dissolved in dry degassed THF (6 mL) and left to stir at room temperature under N_2 for 3 days. The solvent was removed *in vacuo,* the crude dissolved in $CHCl_3$ (25 mL) and washed with EDTA solution (3 x 30 mL). The organic phase was dried over $MgSO_4$, and the solvent removed *in vacuo*. Purification was achieved via preparative thin layer chromatography using 93% CH_2Cl_2 / 7% MeOH, yielded **3.12** (109 mg, 71%) as a viscous yellow oil. **^{1}H NMR** (400 MHz, Chloroform-d) δ 9.29 (d, *J* = 2.1 Hz, 2H, H_i), 8.96 (t, *J* = 2.1 Hz, 1H, H_h), 8.06 (s, 2H, H_g), 7.54 (d, *J* = 8.6 Hz, 2H, H_f), 6.96 (dd, *J* = 8.6, 2.3 Hz, 2H, H_e), 6.93 (d, *J* = 2.3 Hz, 2H, H_d), 4.13 (t, *J* = 6.2 Hz, 4H, H_c), 3.62 – 3.48 (m, 40H, OCH_2), 3.33 (s, 12H, OCH_3), 2.77 – 2.69 (m, 12H, , H_a, NCH_2), 1.96 (p, J = 6.7 Hz, 4H, H_b); **^{13}C NMR** (126 MHz, Chloroform-d) δ 164.60, 156.62, 156.52, 148.43, 147.53, 143.03, 130.52, 120.42, 114.64, 111.03, 101.72, 72.06, 70.76, 70.66, 70.55, 69.84, 67.20, 59.18, 54.19, 51.47, 29.84; **HRMS** (ESI +ve) m/z= 1506.38296 ($[M + Na]^+$ $C_{61}H_{83}I_2N_9O_{18}Na$, calc = 1506.38376).

Boc-Coumarin 3.16



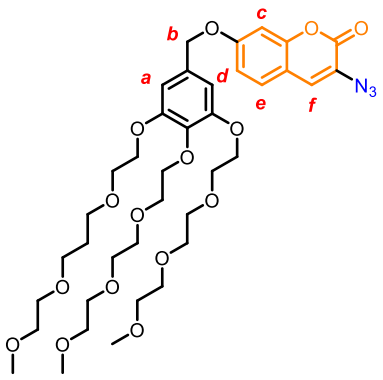
Coumarin **2.12** (369 mg, 1.33 mmol, 1.2 eq), PEG chloride **3.15** (678 mg, 1.11 mmol, 1 eq) K_2CO_3 (368 mg, 2.66 mmol, 2.4 eq) and NaI (17 mg, 0.11 mmol, 0.1 eq) were dissolved in MeCN (15 mL) and heated to 65 °C for 24 hours. The solvent was then removed *in vacuo*, the crude dissolved in H_2O (40 mL) and the product extracted with CH_2Cl_2 (3 x 40 mL) washes. The organic layers were combined and washed with brine (50 mL), dried over $MgSO_4$, filtered and the solvent removed *in vacuo.* The crude product was purified *via* column chromatography (eluent: EtOAc/CH_2Cl_2 1:1 *v/v* followed by MeOH/CH_2Cl_2 4:96 *v/v*) and the desired product was isolated as a yellow oil (707 mg, 75%). **^{1}H NMR** (500 MHz, $CDCl_3$) δ 8.24 (s, 1H, H_g), 7.36 (d, *J* = 8.6 Hz, 1H, H_e), 7.29 (s, 1H, H_f), 6.92 (dd, *J* = 8.6, 2.4 Hz, 1H, H_d), 6.87 (d, *J* = 2.4 Hz, 1H, H_c), 6.66 (s, 2H, H_a), 4.98 (s, 2H, H_b), 4.17 – 4.12 (m, 6H, OCH_2), 3.86 – 3.83 (m, 4H, OCH_2), 3.78 – 3.77 (m, 2H, OCH_2), 3.73 – 3.70 (m, 6H, OCH_2), 3.68 – 3.60 (m, 12H, OCH_2), 3.55 – 3.52 (m, 6H, OCH_2), 3.37 (s, 3H, OCH_3), 3.36 (s, 6H, OCH_3), 1.52 (s, 9H, H_h); **^{13}C NMR** (126 MHz, $CDCl_3$) δ 159.69, 158.86, 152.90, 152.60, 150.84, 138.41, 131.36, 128.15, 122.29, 121.17, 113.67, 113.61, 107.20, 101.75, 72.34, 71.95, 71.93, 70.82, 70.69, 70.56, 70.53, 70.51, 69.72, 68.92, 59.03, 53.43, 28.23; **HRMS** (ESI +ve) m/z=853.416 ($[M + H]^+$, $C_{42}H_{63}NO_{17}$, calc=854.415)

Coumarin-Amine 3.17



Boc-coumarin **3.16** (707 mg, 0.828 mmol, 1 eq) was dissolved in CH_2Cl_2 and cooled to 0 °C in an ice bath. CF_3CO_2H (0.5 mL, excess) was slowly added dropwise and the reaction left to stir and warm up to rt over 2 hours. The solution was quenched with saturated aqueous $NaHCO_3$ (50 mL) solution and extracted with CH_2Cl_2 (5 x 50 mL). The combined organic layers were dried over Mg_2SO_4, filtered and the solvent removed *in vacuo* to obtain the desired product (619 mg, 99%) as a yellow oil with no need for further purification. **^{1}H NMR** (400 MHz, $CDCl_3$) δ 7.19 (d, 1H, 9.07 Hz, H_e), 6.88 – 6.84 (m, 2H, $H_{c,d}$), 6.69 (s, 1H, H_f), 6.65 (s, 2H, H_a), 4.96 (s, 2H, H_b), 4.16 – 4.14 (m, 6H, OCH_2), 4.07 (s, 2H, H_g), 3.85 – 3.83 (m, 4H, OCH_2), 3.80 – 3.78 (m, 2H, OCH_2), 3.75 – 3.68 (m, 6H, OCH_2), 3.69 – 3.60 (m, 12H, OCH_2), 3.57 – 3.50 (m, 6H, OCH_2), 3.37 (s, 4H, OCH_3), 3.36 (s, 6H, OCH_3); **^{13}C NMR** (126 MHz, $CDCl_3$) δ 159.68, 157.96, 152.85, 150.20, 138.31, 131.68, 129.88, 125.85, 114.72, 113.23, 112.04, 107.16, 101.87, 72.33, 71.95, 71.93, 70.81, 70.68, 70.55, 70.53, 70.50, 70.48, 69.72, 68.90, 59.02; **HRMS** (ESI +ve) m/z=776.34639 ($[M + Na]^+$, $C_{37}H_{55}NO_{15}$, calc=776.34583)

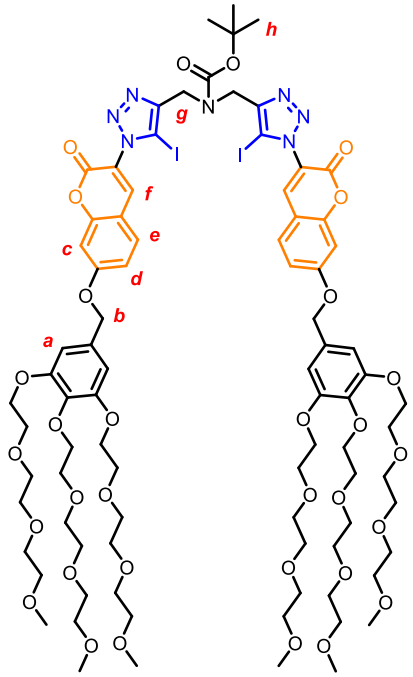
Coumarin-Azide 3.18



Coumarin-amine **3.17** (376 mg, 0.50 mmol, 1 eq) was dissolved in 15% $HCl_{(aq)}$ (8 mL) and cooled to 0 °C in an ice bath. $NaNO_2$ (41.4 mg, 0.60 mmol, 1.2 eq) was added slowly and the solution left to stir for 30 minutes. NaN_3 (52 mg, 30.80 mmol, 1.6 eq) in H_2O (2 mL) was slowly added dropwise and the solution left to stir at 0°C for 1 hour. The reaction was neutralised with a saturated aqueous solution of $NaHCO_3$ and the product extracted with EtOAc (5 x 30 mL). The organic layers were combined, dried over $MgSO_4$ and the solvent removed *in vacuo* to yield the desired product (366 mg, 94%) as an orange oil. **^{1}H NMR** (400 MHz, $CDCl_3$) δ 7.25 (d, *J* = 8.6 Hz, 1H, H_e), 7.10 (s, 1H, H_f), 6.85 (dd, *J* = 8.6, 2.4 Hz, 1H, H_d), 6.82 (d, *J* = 2.4 Hz, 1H, H_d), 6.58 (s, 2H, H_a), 4.93 (s, 2H, H_b), 4.09 (m, 6H, OCH_2), 3.78 (m, 4H, OCH_2), 3.72 (m, 2H, OCH_2), 3.65 (m, 6H, OCH_2), 3.58 (m, 12H, OCH_2), 3.47 (m, 6H), 3.30 (s, 3H, OCH_3), 3.30 (s, 6H, OCH_3); **^{13}C NMR** (126 MHz, CDCl3) δ 160.71, 157.67, 152.94, 152.91, 138.54, 131.07, 128.16, 126.30,

123.50, 113.90, 112.90, 107.24, 101.79, 72.34, 71.96, 71.94, 70.82, 70.70, 70.61, 70.56, 70.54, 70.52, 69.72, 68.96, 59.03; **HRMS** (ESI +ve) m/z=802.33689 ($[M + Na]^+$, $C_{37}H_{53}N_3O_{15}$, calc=802.33646)

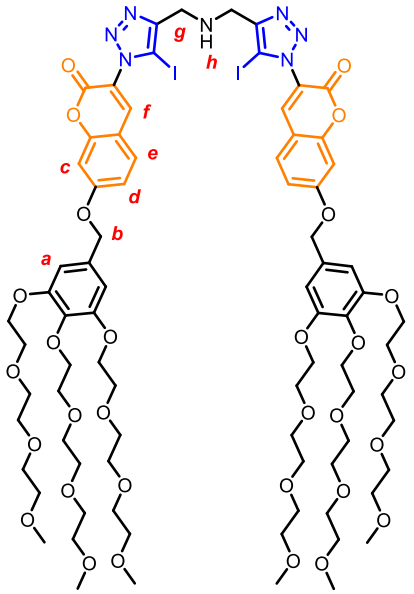
Boc-protected Receptor 3.19



3-Peg coumarin azide **3.18** (80.0 mg, 0.10 mmol, 2.2 eq), bis-iodo-alkyne **2.4** (20.8 mg, 0.047 mmol, 1 eq), TBTA (5 mg, 0.0094 mmol, 0.2 eq), and $Cu(CH_3CN)_4.PF_6$ (5.3 mg, 0.014 mmol, 0.3 eq) dissolved in 1.4 ml dry degassed THF, left to stir at room temperature under N_2 for 3 days. Solvent removed on rotary evaporator then product dissolved in CH_2Cl_2. Washed 3 times with EDTA solution, extracting all washes multiple times with $CHCl_3$. Organic phases combined and dried over $MgSO_4$, solvent removed in vacuo. Purification *via* preparative thin layer chromatography using 90% DCM 10% MeOH yielded the product (55 mg, 59%) as a viscous yellow oil. **^{1}H NMR** (500 MHz, $CDCl_3$) δ 8.00 (s, 2H, H_f), 7.55 (d, *J* = 8.7 Hz, 2H, H_e), 7.03 (dd, *J* = 8.6, 2.4 Hz, 2H, H_d), 6.98 (d, *J* = 2.4 Hz, 2H, H_c), 6.67 (s, 4H, H_a), 5.07 (s, 4H, H_b), 4.77 (d, *J* = 40.2 Hz, 4H, H_g), 4.19 – 4.16 (m, 12H, OCH_2), 3.87 – 3.85 (m, 8H, OCH_2), 3.81 – 3.79 (m, 4H, OCH_2), 3.75 – 3.72 (m, 12H, OCH_2), 3.67 – 3.63 (m, 24H, OCH_2), 3.56 – 3.53 (m, 12H, OCH_2), 3.37 (s, 6H, OCH_3), 3.37 (s, 12H, OCH_3), 1.51 (s, 9H, H_h); **^{13}C NMR** (176 MHz, $CDCl_3$) δ 163.55, 156.36, 156.12, 155.17, 153.00, 148.69, 142.47, 138.66, 130.64, 130.42, 120.77, 114.51, 111.39, 107.30, 102.07, 80.87, 72.37, 71.96, 71.94, 70.91, 70.82, 70.69, 70.56, 70.54, 70.52, 69.71,

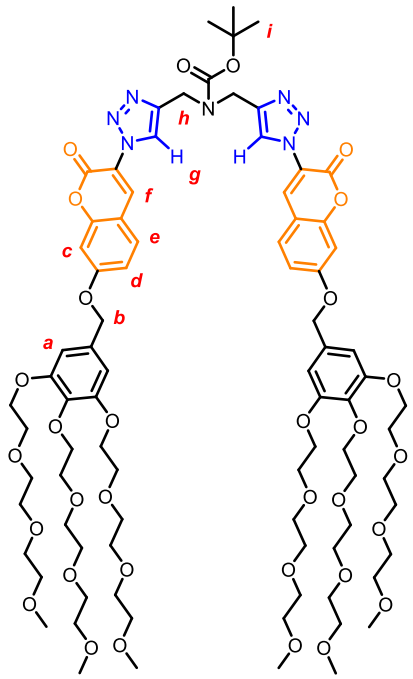
68.98, 59.04, 28.53; **HRMS** (ESI +ve) m/z=2004.60618 ([M + H]$^+$, $C_{85}H_{120}I_2N_7O_{32}$, calc=2004.60226)

XB Amine Receptor 3.20



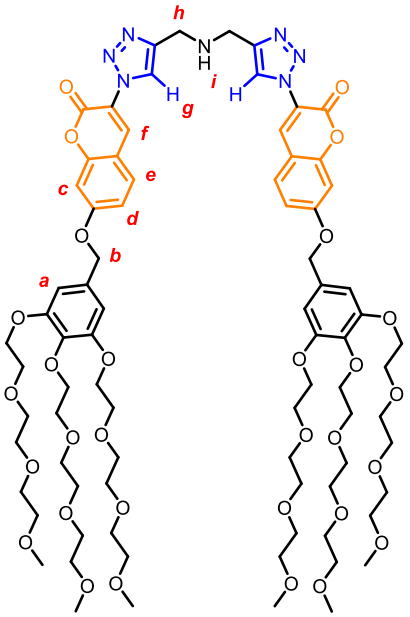
*B*oc-protected receptor **3.19** (50.0 mg, 0.025 mmol, 1 eq) was dissolved in CH_2Cl_2 (0.3 mL) and cooled to 0°C. TFA (0.5 mL, excess) was added and the reaction left to stir to room temperature over 3 h. Saturated aqueous $NaHCO_3$ solution was added till neutral and the product extracted with CH_2Cl_2 (5 x 10 mL). The combined organic layers were dried over Na_2SO_4, filtered and the solvent removed *in vacuo* to afford the desired product (40.0 mg, 84%) as a viscous yellow oil. **^{1}H NMR** (500 MHz, $CDCl_3$) δ 7.98 (s, 2H, H_f), 7.54 (d, *J* = 8.7 Hz, 2H, H_e), 7.03 (dd, *J* = 8.7, 2.4 Hz, 2H, H_d), 6.98 (d, *J* = 2.4 Hz, 2H, H_c), 6.67 (s, 4H, H_a), 5.07 (s, 4H, H_b), 4.20 – 4.14 (m, 12H, OCH_2), 4.04 (s, 4H, H_g), 3.86 – 3.84 (m, 8H, OCH_2), 3.81 – 3.78 (m, 4H, OCH_2), 3.74 – 3.71 (m, 12H, OCH_2), 3.68 – 3.62 (m, 24H, OCH_2), 3.56 – 3.52 (m, 12H, OCH_2), 3.37 (s, 6H, OCH_3), 3.37 (s, 12H, OCH_3); **^{13}C NMR** (126 MHz, $CDCl_3$) δ 163.56, 156.36, 156.11, 153.01, 150.35, 142.31, 138.64, 130.62, 130.38, 120.77, 114.55, 111.37, 107.28, 102.09, 82.24, 72.37, 71.96, 71.94, 70.92, 70.83, 70.70, 70.57, 70.55, 70.53, 69.72, 68.97, 59.05, 44.10, 29.74; **Fluorescence** (H_2O, 10 mM HEPES): λ_{ex}= 342 nm; λ_{em}= 412 nm; **HRMS** (ESI +ve) m/z=1904.55375 ([M + H]$^+$, $C_{80}H_{112}I_2N_7O_{30}$, calc=1904.54083)

Boc-protected Receptor 3.21



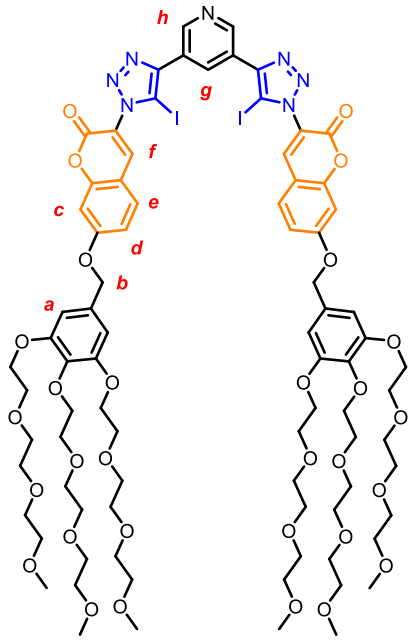
3-Peg coumarin azide **3.18** (40.0 mg, 0.05 mmol, 2.2 eq), bis-iodo-alkyne **2.4** (4.5 mg, 0.023 mmol, 1 eq), TBTA (2.5 mg, 0.005 mmol, 0.2 eq), and $Cu(CH_3CN)_4.PF_6$ (2.6 mg, 0.007 mmol, 0.3 eq) were dissolved in dry degassed THF (1.4 mL) and left to stir at room temperature under N_2 for 3 days. The solvent was removed *in vacuo*, the crude dissolved in CH_2Cl_2 (10 mL) and washed with EDTA solution (3 x 10 mL). The combined organic phases were dried over $MgSO_4$, filtered and the solvent removed *in vacuo*. Purification was achieved *via* preparative thin layer chromatography (eluent: MeOH/CH_2Cl_2 1:19 *v/v*) affording the desired product (34 mg, 83%) as a viscous yellow oil. **^{1}H NMR** (500 MHz, $CDCl_3$) δ 8.60 – 8.48 (m, 4H, $H_{f,g}$), 7.60 (d, *J* = 8.7 Hz, 2H, H_e), 7.06 (dd, *J* = 8.7, 2.4 Hz, 2H, H_d), 6.99 (d, *J* = 2.4 Hz, 2H, H_c), 6.70 (s, 4H, H_a), 5.08 (s, 4H, H_b), 4.73 (d, *J* = 24.4 Hz, 4H, H_h), 4.19 – 4.13 (m, 12H, OC*H*$_2$), 3.87– 3.84 (m, 8H, OC*H*$_2$), 3.81 – 3.78 (m, 4H, OC*H*$_2$), 3.74 – 3.71 (m, 12H, OC*H*$_2$), 3.67 – 3.63 (m, 24H, OC*H*$_2$), 3.56 – 3.53 (m, 12H, OC*H*$_2$), 3.37 (s, 6H, OC*H*$_3$), 3.37 (s, 12H, OC*H*$_3$), 1.54 (s, 9H, H_i); **^{13}C NMR** (126 MHz, $CDCl_3$) δ 162.65, 156.10, 155.20, 154.59, 153.00, 138.62, 133.80, 130.77, 130.00, 120.54, 114.56, 111.84, 107.29, 101.78, 80.92, 72.37, 71.97, 71.94, 70.83, 70.71, 70.58, 70.55, 70.53, 69.73, 68.97, 59.05, 53.44, 42.28, 41.82, 28.46; **HRMS** (ESI +ve) m/z=1774.79484 ($[M + Na]^+$, $C_{85}H_{121}N_7O_{32}$, calc=1774.79556)

HB Amine Receptor 3.22



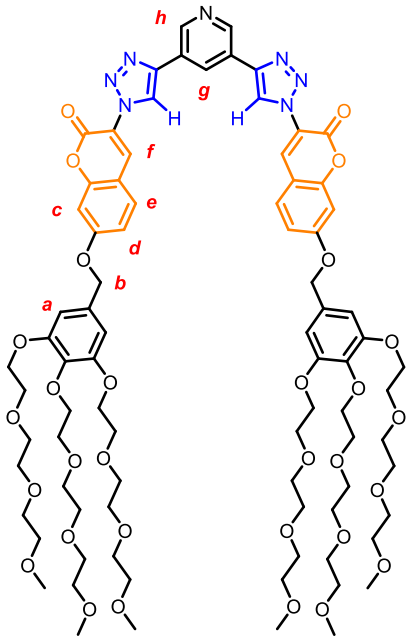
N-boc-protected receptor **3.21** (17 mg, 0.01 mmol, 1 eq) was dissolved in CH_2Cl_2 (0.2 mL) and cooled to 0°C. TFA (0.4 mL, excess) was added and the reaction left to stir to room temperature over 5 h. Saturated aqueous $NaHCO_3$ solution was added till neutral and the product extracted with CH_2Cl_2 (5 x 10 mL). The combined organic layers were dried over $MgSO_4$, filtered and the solvent removed *in vacuo* to afford the desired product (4 mg, 24 %) as a viscous yellow oil. **^{1}H NMR** (500 MHz, $CDCl_3$) δ 8.58 (d, 2H, H_g), 8.51 (d, 2H, H_f), 7.57 (d, *J* = 8.7 Hz, 2H, H_e), 7.03 (dd, *J* = 8.7, 2.4 Hz, 2H, H_d), 6.96 (d, *J* = 2.4 Hz, 2H, H_c), 6.67 (s, 4H, H_a), 5.05 (s, 4H, H_b), 4.19 – 4.11 (m, 12H, OCH_2), 3.87 – 3.82 (m, 8H, OCH_2), 3.81 – 3.77 (m, 4H, OCH_2), 3.74 – 3.70 (m, 12H, OCH_2), 3.67 – 3.62 (m, 24H, OCH_2), 3.55 – 3.52 (m, 12H, OCH_2), 3.49 (s, 4H, H_h), 3.37 – 3.36 (m, 18H, OCH_3); **^{13}C NMR** (126 MHz, $CDCl_3$) δ 162.67, 156.13, 154.60, 152.99, 152.72, 145.88, 138.59, 137.83, 136.65, 133.79, 130.77, 130.00, 123.22, 120.51, 114.59, 111.83, 107.27, 106.68, 101.78, 72.36, 72.27, 71.96, 71.94, 70.83, 70.78, 70.72, 70.70, 70.57, 70.55, 70.52, 69.83, 69.72, 68.96, 68.86, 65.33, 59.05, 43.66, 31.94, 29.71, 22.71, 14.14, 1.03; **Fluorescence** (H_2O, 10 mM HEPES): λ_{ex}= 342 nm; λ_{em}= 484 nm; **HRMS** (High resolution ESI +ve) m/z=1652.76046 ($[M + H]^+$, $C_{80}H_{114}N_7O_{30}$, calc=1652.76113)

XB Pyridine Receptor 3.23



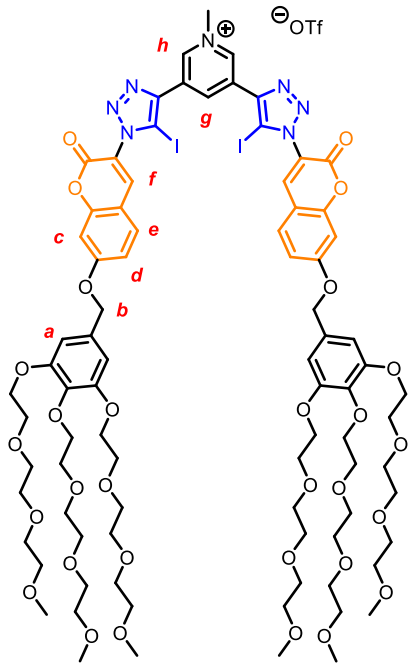
3-Peg coumarin azide **3.18** (95.0 mg, 0.12 mmol, 2.2 eq), bis-iodo-alkyne **2.4** (21.0 mg, 0.055 mmol, 1 eq), TBTA (5.8 mg, 0.011 mmol, 0.2 eq), and $Cu(CH_3CN)_4.PF_6$ (4.1 mg, 0.06 mmol, 0.2 eq) were dissolved in dry degassed THF (0.8 mL) and left to stir at room temperature under N_2 for 3 days. The solvent was removed *in vacuo*, the crude dissolved in CH_2Cl_2 (15 mL) and washed with EDTA solution (3 x 15 mL). The combined organic phases were dried over $MgSO_4$, filtered and the solvent removed *in vacuo*. Purification was achieved *via* preparative thin layer chromatography (eluent: MeOH/CH_2Cl_2 1:19 *v/v*) affording the desired product (71 mg, 66%) as a viscous yellow oil. **^{1}H NMR** (500 MHz, $CDCl_3$) δ 9.39 (d, *J* = 2.1 Hz, 2H, H_h), 9.02 (d, *J* = 2.1 Hz, 1H, H_g), 8.10 (s, 2H, H_f), 7.60 (d, *J* = 8.7 Hz, 2H,H_e), 7.08 (dd, *J* = 8.7, 2.4 Hz, 2H, H_d), 7.03 (d, *J* = 2.4 Hz, 2H, H_c), 6.71 (s, 4H, H_a), 5.11 (s, 4H, H_b), 4.22 – 4.17 (m, 12H, OCH_2), 3.90 – 3.87 (m, 8H, OCH_2), 3.83 – 3.81 (m, 4H, OCH_2), 3.77- 3.74 (m, 12H, OCH_2), 3.71 – 3.66 (m, 24H, OCH_2), 3.58 – 3.56 (m, 12H, OCH_2), 3.40 – 3.39 (m, 18H, OCH_3); **^{13}C NMR** (126 MHz, $CDCl_3$) δ 163.75, 156.38, 156.24, 153.01, 148.36, 147.45, 142.79, 138.63, 132.87, 130.59, 130.49, 125.90, 120.63, 114.70, 111.31, 107.26, 102.17, 72.36, 71.95, 71.93, 70.94, 70.82, 70.69, 70.56, 70.54, 70.52, 69.71, 68.96, 59.05; **Fluorescence** (H_2O, 10 mM HEPES): λ_{ex}= 344 nm; λ_{em}= 414 nm; **HRMS** (ESI +ve) m/z= 1938.53697 ($[M + H]^+$, $C_{83}H_{110}N_7O_{30}I_2$, calc= 1938.53810)

HB Pyridine Receptor 3.24



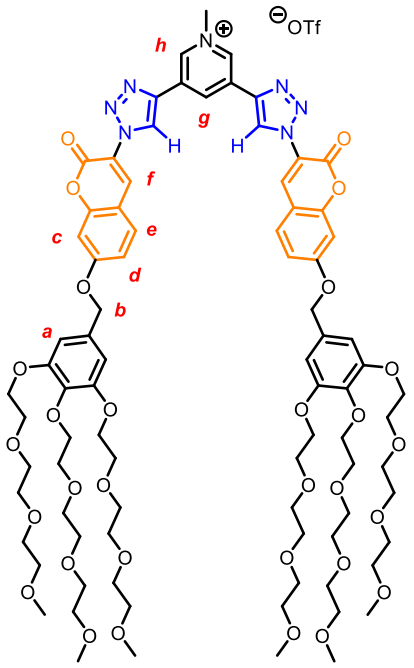
3-Peg coumarin azide **3.18** (348 mg, 0.47 mmol, 2.2 eq), bis-alkyne **2.2** (25.8 mg, 0.203 mmol, 1 eq), TBTA (21.5 mg, 0.04 mmol, 0.2 eq), and $Cu(CH_3CN)_4.PF_6$ (15.1 mg, 0.04 mmol, 0.2 eq) were dissolved in dry degassed THF (3 mL) and left to stir at room temperature under N_2 for 3 days. The solvent was removed *in vacuo*, the crude dissolved in CH_2Cl_2 (50 mL) and washed with EDTA solution (3 x 40 mL) and brine (50 mL). The combined organic phases were dried over $MgSO_4$, filtered and the solvent removed *in vacuo*. Purification was achieved *via* column chromatography (eluent: MeOH/CH_2Cl_2 1:19 *v/v*) affording the desired product (104 mg, 30%) as a viscous yellow oil. **^{1}H NMR** (500 MHz, $CDCl_3$) δ 9.17 (d, *J* = 2.1 Hz, 2H, H_i), 9.06 (s, 2H, H_g), 8.76 (t, *J* = 2.2 Hz, 1H, H_h), 8.64 (s, 2H, H_f), 7.63 (d, *J* = 8.8 Hz, 2H, H_e), 7.06 (dd, *J* = 8.8, 2.4 Hz, 2H, H_d), 6.99 (d, *J* = 2.4 Hz, 2H, H_c), 6.68 (s, 4H, H_a), 5.07 (s, 2H, H_b), 4.19 – 4.16 (m, 12H, OCH_2), 3.89 – 3.85 (m, 8H, OCH_2), 3.81 – 3.79 (m, 4H, OCH_2), 3.76 – 3.70 (m, 12H, OCH_2), 3.70 – 3.62 (m, 24H, OCH_2), 3.56 – 3.54 (m, 12H, OCH_2), 3.38 – 3.37 (m, 18H, OCH_3); **^{13}C NMR** (126 MHz, $CDCl_3$) δ 163.00, 156.27, 154.76, 152.95, 146.44, 144.49, 138.40, 134.27, 130.95, 130.41, 130.29, 126.72, 121.53, 120.16, 114.87, 111.80, 107.18, 101.89, 72.38, 71.94, 71.92, 70.89, 70.80, 70.65, 70.57, 70.51, 70.49, 69.73, 68.89, 59.02, 50.56; **Fluorescence** (H_2O, 10 mM HEPES): λ_{ex}= 342 nm; λ_{em}= 498 nm; **HRMS** (ESI +ve) m/z= 1686.7401 ($[M + H]^+$, $C_{83}H_{111}N_7O_{30}$, calc= 1686.7448)

XB Pyridinium Receptor 3.25



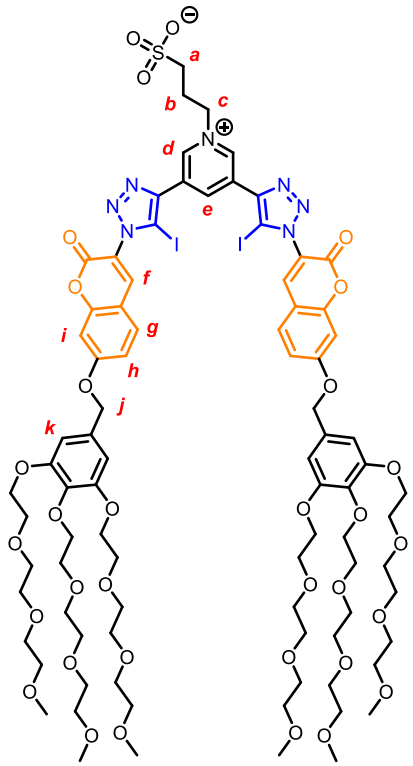
Receptor **3.23** (20.2 mg, 0.01 mmol, 1 eq) was dissolved in dry CH_2Cl_2 (0.1 mL) and cooled to 0 °C. MeI (0.2 mL) was added and the reaction left to stir for 16 h under N_2. The solvent was removed *in vacuo* and anion exchange to the triflate salt was achieved by passing through an Amberlite (triflate) column (11.6 mg, 53%). **^{1}H NMR** (400 MHz, $CDCl_3$) δ 9.59 (s, 3H, $H_{h,g}$), 8.11 (s, 2H, H_f), 7.59 (d, *J* = 8.8 Hz, 2H, H_e), 7.06 (dd, *J* = 8.8, 2.3 Hz, 2H, H_d), 6.92 (d, *J* = 2.3 Hz, 2H, H_c), 6.61 (s, 4H, H_a), 5.04 (s, 4H, H_b), 4.76 (s, 3H, H_i), 4.13 – 4.04 (m, 12H, OCH_2), 3.83 – 3.78 (m, 8H, OCH_2), 3.78 – 3.65 (m, 32H, OCH_2), 3.64 – 3.59 (m, 8H, OCH_2), 3.59 – 3.54 (m, 4H, OCH_2), 3.54 – 3.48 (m, 8H), 3.33 (s, 6H, OCH_3), 3.30 (s, 12H, OCH_3); **^{13}C NMR** (126 MHz, $CDCl_3$) δ 164.02, 156.70, 156.25, 152.41, 143.49, 142.97, 142.64, 137.68, 133.17, 130.95, 130.35, 129.30, 128.22, 121.75, 119.87, 119.20, 114.80, 111.19, 106.57, 102.14, 86.11, 72.33, 71.97, 71.92, 70.93, 70.84, 70.71, 70.69, 70.49, 69.75, 68.57, 58.96, 58.92, 53.80, 49.40; **^{19}F NMR** (377 MHz, $CDCl_3$) δ -77.86; **Fluorescence** (H_2O, 10 mM HEPES): λ_{ex}= 344 nm; λ_{em}= 408 nm; **HRMS** (ESI +ve) m/z= 1952.5531 ([M]$^+$, $C_{84}H_{112}I_2N_7O_{30}$+, calc= 1952.5537)

HB Pyridinium Receptor 3.26



Receptor **3.24** (9 mg, 5.34 µmol, 1 eq) was dissolved in dry CH_2Cl_2 (0.5 mL) and cooled to 0 °C. MeI (0.5 mL) was added and the reaction left to stir for 16 h under N_2. The solvent was removed *in vacuo* and anion exchange to the triflate salt was achieved by passing through an Amberlite (triflate) column (7.7 mg, 78%). **^{1}H NMR** (500 MHz, $CDCl_3$) δ 9.43 (s, 2H, H_h), 9.26 (s, 2H, H_g), 9.25 (s, 1H, H_h), 8.44 (s, 2H, H_f), 7.59 (d, *J* = 8.8 Hz, 2H, H_e), 7.09 (dd, *J* = 8.8, 2.4 Hz, 2H, H_d), 6.85 (d, *J* = 2.4 Hz, 2H, H_c), 6.55 (s, 4H, H_a), 4.91 (s, 4H, H_b), 4.68 (s, 3H, H_j), 4.17 – 4.13 (m, 8H, OCH_2), 4.01 – 3.98 (m, 4H, OCH_2), 3.83 – 3.80 (m, 8H, OCH_2), 3.77 – 3.70 (m, 22H, OCH_2), 3.69 – 3.67 (m, 7H, OCH_2), 3.65 – 3.61 (m, 8H, OCH_2), 3.60 – 3.56 (m, 3H, OCH_2), 3.52 – 3.48 (m, 8H, OCH_2), 3.29 (s, 11H, OCH_3), 3.28 (s, 6H, OCH_3); **^{13}C NMR** (126 MHz, $CDCl_3$) δ 162.86, 155.95, 154.75, 152.35, 141.35, 141.05, 137.67, 135.48, 134.74, 130.81, 130.62, 130.57, 124.32, 122.14, 119.91, 119.59, 114.70, 111.49, 105.85, 101.43, 72.14, 71.95, 71.90, 70.91, 70.76, 70.71, 70.68, 70.58, 70.53, 70.50, 70.34, 69.73, 68.43, 58.93, 58.81, 48.72; **Fluorescence** (H_2O, 10 mM HEPES): λ_{ex}= 354 nm; λ_{em}= 426 nm; **HRMS** (ESI +ve) m/z= 1700.7563 ($[M]^+$, $C_{84}H_{114}N_7O_{30}$+, calc= 1700.7605)

Zwitter-ion Receptor 3.27

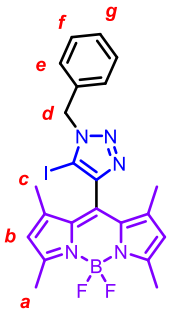


XB receptor **3.23** (19 mg, 0.001 mmol, 1 eq) was dissolved in 1,2-dichloroethane (0.2 mL). 1,3-Propane sultone (6.06 mg, 0.050 mmol, 5 eq) was added and the reaction was left to stir at 40 ˚C for 24 h. The solvent was removed in vacuo and the crude purified via preparative TLC (eluent: 10% MeOH in CH_2Cl_2) affording zwitter ion **3.27** as a yellow liquid (4.3 mg, 20%). **^{1}H NMR** (500 MHz, 4:2:1 D_2O:CD_3CN:MeOD) δ 10.03 (s, 1H, H_e), 9.92 (s, 2H, H_d), 8.80 (s, 2H, H_f), 8.15 (d, *J* = 8.6 Hz, 2H, H_g), 7.53 (m, 4H, $H_{h,i}$), 7.19 (s, 4H, H_k), 5.55 (s, 4H, H_j), 5.36 (s, 2H, H_c), 4.55 – 4.46 (m, 12H, OC*H*$_2$), 4.22 – 4.09 (m, 12H, OC*H*$_2$), 4.06 – 3.82 (m, 48H, OC*H*$_2$), 3.66 (s, 6H, OC*H*$_3$), 3.63 (s, 12H, OC*H*$_3$), 3.40 – 3.36 (m, 2H, H_b), 2.98 – 2.90 (m, 2H, H_a); **^{13}C NMR** (126 MHz, $CDCl_3$) δ 163.89, 156.62, 156.20, 152.87, 144.05, 138.33, 131.23, 130.80, 119.80, 114.54, 111.39, 107.27, 101.97, 72.33, 71.94, 71.92, 70.97, 70.76, 70.66, 70.52, 70.46, 69.69, 68.89, 59.03, 29.72, 1.04; **HRMS** (ESI +ve) m/z= 2060.5424 ($[M+H]^+$, $C_{86}H_{116}I_2N_7O_{33}S$, calc= 2060.5419)

6.5. Synthesis from Chapter 4

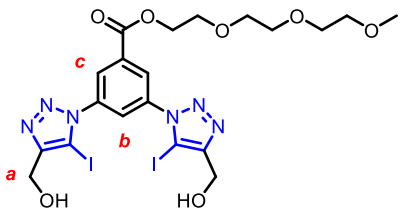
The synthesis of compounds **4.2**,[19] **4.3**,[19] **4.4**,[19] **4.18**,[20] **4.19**,[20] **4.25**[21] have been described previously.

BODIPY Receptor 4.1



Di-methyl pyrrole (0.25 mL, 2.42 mmol, 2.05 eq) and iodo-triazole aldehyde (370 mg, 1.18 mmol, 1 eq) were dissolved in dry CH_2Cl_2 (100 mL) in an N_2 atmosphere. A catalytic amount of TFA (13 µL) was then added and the reaction mixture left to stir at rt for 48 h in the dark. *p*-Chloranil (291 mg, 1.18 mmol, 1 eq) in dry CH_2Cl_2 (20 mL) was then added and the reaction left to stir for a further 1 h. NEt_3 (2.47 mL, 17.7 mmol, 15 eq) followed by $BF_3.OEt_2$ (2.33 mL, 18.9 mmol, 16 eq) were added and left to stir for another 2 h. The solvent was removed *in vacuo* and the crude dissolved in CH_2Cl_2 (50 mL) and washed with H_2O (3 x 50 mL) and brine (50 mL). The organic phase was then dried over $MgSO_4$, filtered and had the solvent removed *in vacuo*. The product was purified by column chromatography (eluent: CH_2Cl_2) to afford a gold solid (150 mg, 24%). **^{1}H NMR** (400 MHz, $CDCl_3$); δ 7.30 – 7.28 (m, 5H, $H_{e,f,g}$), 5.90 (s, 2H, H_b), 5.61 (s, 2H, H_d), 2.47 (s, 6H, H_a), 1.30 (s, 6H, H_f); **^{13}C NMR** (126 MHz, $CDCl_3$); δ 157.11, 146.46, 142.39, 133.95, 132.16, 128.91, 128.88, 128.02, 81.40, 54.92, 53.43, 14.77, 13.77; **HRMS** (ESI +ve) m/z= 532.0972 ($[M+H]^+$, $C_{22}H_{21}BF_2IN_5$, calc= 532.0.978)

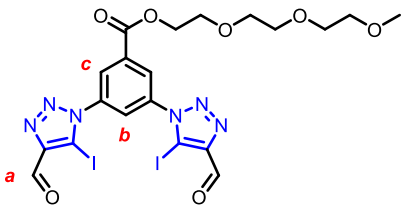
Bis-alcohol 4.5



3,5-Bisazide **4.4** (184 mg, 0.525 mmol, 1 eq), NaI (630 mg, 4.20 mmol, 8 eq) and $Cu(ClO_4).H_2O$ (778 mg, 2.1 mmol, 4 eq) were dissolved in dry degassed THF (3.3 mL) and stirred in darkness

for 10 min. TBTA (13.8 mg, 0.03 mmol, 0.05 eq), DBU (157 µL, 1.05 mmol, 2 eq) dissolved in MeCN (3.3 mL), and propargyl alcohol (65 µL, 1.10 mmol, 2.1 eq) were added sequentially and the reaction mixture left to stir for 2 d in darkness and under N_2. The solvent was removed *in vacuo* and the crude dissolved in CH_2Cl_2 (20 mL) and washed with EDTA solution (3 x 20 mL), saturated NaCl solution (20 mL). The organic phase was dried over Na_2SO_4, filtered and concentrated *in vacuo*. Purification was achieved by column chromatography (eluent: MeOH:CH_2Cl_2 5:95 *v/v*) to afford a yellow solid (147 mg, 39%); **^{1}H NMR** (400 MHz, $CDCl_3$) δ 8.48 (d, *J* = 2.0 Hz, 2H, H_c), 8.05 (t, *J* = 2.0 Hz, 1H, H_b), 4.91 – 4.77 (m, 4H, H_a), 4.58 – 4.54 (m, 2H, *OCH₂*), 3.88 – 3.84 (m, 2H, *OCH₂*), 3.76 – 3.56 (m, 6H, *OCH₂*), 3.51 (m, 2H, *OCH₂*), 3.35 (s, 3H, *OCH₃*); **^{13}C NMR** (126 MHz, $CDCl_3$) δ 163.62, 151.95, 137.64, 133.04, 128.11, 127.09, 71.87, 70.73, 70.67, 70.56, 68.90, 65.43, 59.02, 56.70, 56.68; **HRMS** (ESI +ve) m/z= 714.9862 ($[M+H]^+$, $C_{20}H_{24}I_2N_6O_7$, calc= 714.9869)

Bis-aldehyde 4.6

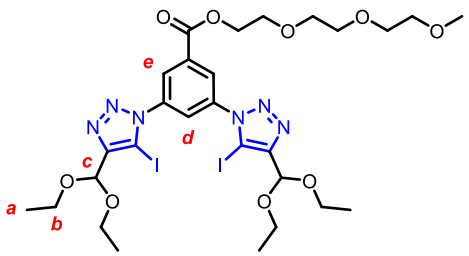


Oxalyl chloride (171 µL, 2.03 mmol, 10 eq) and dry DMSO (288 µL, 4.06 mmol, 20 eq) were dissolved in dry CH_2Cl_2 (4.5 mL), cooled to -78 °C and stirred for 15 min. Bis-iodotriazole alcohol **4.5** (145 mg, 0.20 mmol, 1 eq) in dry CH_2Cl_2 (3 mL) was added and the reaction mixture left to stir for 15 min. NEt_3 (849 µL, 6.09 mmol, 30 eq) was added and the reaction mixture left to stir for 1 h. The reaction mixture with quenched with 1M HCl (30 mL) and washed with CH_2Cl_2 (3 x 30 mL). The combined organic phase was dried over Na_2SO_4, filtered and concentrated *in vacuo*. Purification was achieved by column chromatography (eluent: MeOH:CH_2Cl_2 5:95 *v/v*) to afford a yellow solid (61 mg, 42%).

Bis-acetal **4.7** (360 mg, 0.42 mmol, 1 eq) and iodine (5.3 mg, 0.042 mmol, 0.1 eq) were dissolved in acetone (14 mL) and the reaction mixture left to stir for 2 h. The solvent was removed *in vacuo* and the crude dissolved in CH_2Cl_2 (20 mL) and washed with 1 M $Na_2S_2O_3$ solution (3 x 20 mL). The organic phase was dried over Na_2SO_4, filtered and concentrated *in vacuo*, yielding a yellow solid (298 mg, 99 %). **^{1}H NMR** (400 MHz, $CDCl_3$) δ 10.23 (s, 2H, H_a), 8.56 (d, *J* = 2.1 Hz, 2H, H_c), 8.10 (t, *J* = 2.1 Hz, 1H, H_c), 4.62 – 4.54 (m, 2H, *OCH₂*), 3.90 – 3.83

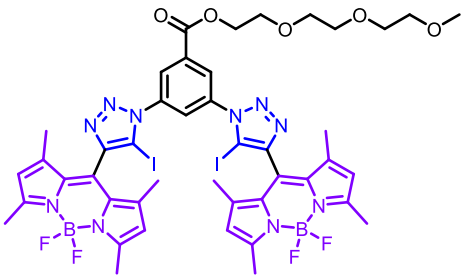
(m, 2H, *OCH₂*), 3.74 – 3.68 (m, 2H, *OCH₂*), 3.68 – 3.58 (m, 6H, *OCH₂*), 3.53 – 3.47 (m, 2H, *OCH₂*), 3.34 (s, 3H, *OCH₃*). **^{13}C NMR** (126 MHz, $CDCl_3$) δ 183.87, 163.22, 147.95, 136.81, 133.46, 128.97, 127.59, 82.62, 71.90, 70.74, 70.72, 70.61, 68.86, 65.70, 60.39, 59.02, 21.05, 14.20. **HRMS** (ESI +ve) m/z= 710.9549 ($[M+H]^+$, $C_{20}H_{20}I_2N_6O_7$, calc= 710.9556)

Bis-acetal 4.7



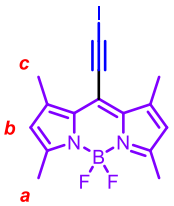
3,5-Bisazide **4.4** (260 mg, 0.74 mmol, 1 eq), NaI (890 mg, 5.94 mmol, 8 eq) and $Cu(ClO_4).H_2O$ (1100 mg, 2.97 mmol, 4 eq) were dissolved in dry degassed THF (4.6 mL) and stirred in darkness for 10 min. TBTA (20 mg, 0.04 mmol, 0.05 eq), DBU (222 µL, 1.48 mmol, 2 eq) dissolved in MeCN (4.6 mL), and 3,3-diethoxy-1-propyne (230.4 µL, 1.56 mmol, 2.1 eq) were added sequentially and the reaction mixture left to stir for 2 d in darkness and under N_2. The solvent was removed *in vacuo* and the crude dissolved in CH_2Cl_2 (20 mL) and washed with EDTA solution (3 x 20 mL), saturated NaCl solution (20 mL). The organic phase was dried over Na_2SO_4, filtered and concentrated *in vacuo*. Purification was achieved by column chromatography (eluent: MeOH:CH_2Cl_2 2:98 *v/v*) to afford a yellow solid (381 mg, 60%). **^{1}H NMR** (500 MHz, $CDCl_3$) δ 8.46 (d, *J* = 2.0 Hz, 2H, H_e), 8.00 (t, *J* = 2.0 Hz, 1H, H_d), 5.75 (s, 2H, H_c), 4.60 – 4.50 (m, 2H, OC*H₂*), 3.88 – 3.84 (m, 2H, *OCH₂*), 3.83 – 3.75 (m, 4H, *OCH₂*), 3.75 – 3.60 (m, 10H, H_b, OC*H₂*), 3.52 – 3.49 (m, 2H, OCH_2), 3.35 (s, 3H, OC*H₃*), 1.31 (t, *J* = 7.0 Hz, 12H, H_a). **^{13}C NMR** (126 MHz, $CDCl_3$) δ 163.62, 151.95, 137.64, 133.04, 128.11, 127.09, 71.87, 70.73, 70.67, 70.56, 68.90, 65.43, 59.02, 56.70, 56.68. **HRMS** (ESI +ve) m/z= 881.08352 ($[M+Na]^+$, $C_{28}H_{40}I_2N_6O_9Na$, calc= 881.08383).

BODIPY Receptor 4.8



Di-methyl pyrrole (145 µL, 1.41 mmol, 5 eq) and bis-aldehyde **4.6** (222 mg, 0.31 mmol, 1 eq) were dissolved in dry CH_2Cl_2 (3.5 mL) in an N_2 atmosphere. A catalytic amount of TFA (5 µL) was then added and the reaction mixture left to stir at rt for 3 h in the dark. *p*-Chloranil (159 mg, 0.63 mmol, 2 eq) in dry CH_2Cl_2 (4 mL) was then added and the reaction left to stir for a further 1 h. NEt_3 (302 µL, 2.17 mmol, 7 eq) followed by $BF_3.OEt_2$ (268 µL, 2.17 mmol, 7 eq) were added and left to stir for another 1 h. The solvent was removed *in vacuo* and the crude dissolved in CH_2Cl_2 (30 mL) and washed with H_2O (3 x 30 mL) and brine (30 mL). The organic phase was then dried over $MgSO_4$, filtered and had the solvent removed *in vacuo*. The product was purified by column chromatography (eluent: MeOH:CH_2Cl_2 2:98 *v/v*) to afford a gold solid (4.9 mg, 2%). **^{1}H NMR** (500 MHz, $CDCl_3$) δ 8.58 (d, *J* = 2.0 Hz, 2H, H_e), 8.19 (t, *J* = 2.0 Hz, 1H, H_d), 6.07 (s, 4H, H_b), 4.65 – 4.60 (m, 2H, *OCH*$_2$), 3.93 – 3.87 (m, 2H, *OCH*$_2$), 3.75 – 3.73 (m, 2H, *OCH*$_2$), 3.70 – 3.65 (m, 2H, *OCH*$_2$), 3.65 – 3.57 (m, 2H, *OCH*$_2$), 3.55 – 3.47 (m, 2H, *OCH*$_2$), 3.31 (s, 3H, *OCH*$_3$), 2.59 (s, 6H, H_a), 1.59 (s, 6H, H_c). **^{13}C NMR** (126 MHz, $CDCl_3$) δ 163.50, 157.70, 147.61, 142.15, 137.66, 133.33, 132.19, 127.71, 126.58, 126.34, 121.93, 82.44, 71.85, 70.77, 70.73, 70.65, 68.96, 65.73, 58.96, 29.71, 29.34, 22.71, 14.87, 14.06. **HRMS** (ESI +ve) m/z= 1167.18516 ($[M + Na]^+$, $C_{44}H_{46}B_2F_4I_2N_{10}O_5$, calc= 1167.18291.

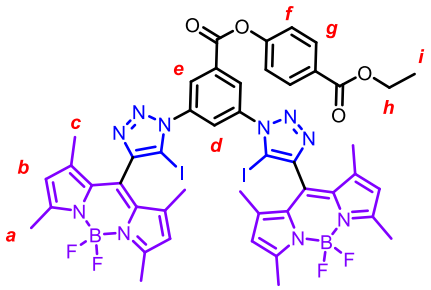
BODIPY Iodo-Alkyne 4.10



BODIPY TMS-alkyne **4.9** (60 mg, 0.174 mmol, 1 eq) and AgF (22 mg, 0.174 mmol, 1 eq) were dissolved in dry degassed MeCN (3 mL). NIS (42 mg, 0.174 mmol, 1 eq) was added and the reaction mixture left to stir in darkness for 5 h. The mixture was filtered through a silica plug

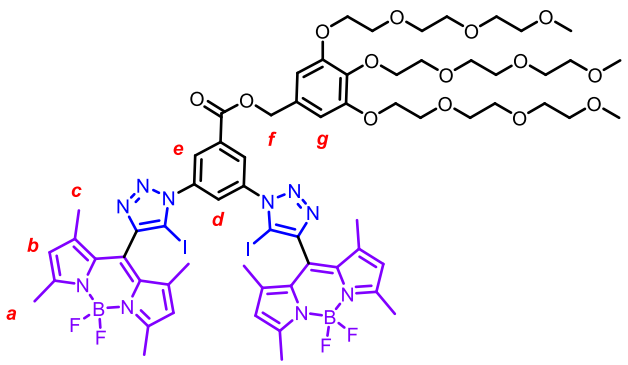
and the filtrate reduced in vacuo. The crude was dissolved in CH_2Cl_2 (20 mL) and washed with H_2O (3 x 20 mL) before drying over Na_2SO_4. The solvent was removed in vacuo and the product was isolated as a red powder without further purification (69 mg, 99%). **^{1}H NMR** (500 MHz, $CDCl_3$) δ 6.06 (s, 2H, H_b), 2.51 (s, 6H, H_a), 2.41 (s, 6H, H_c). **^{19}F NMR** (471 MHz, $CDCl_3$) δ -145.90, -145.99, -146.05; **^{13}C NMR** (126 MHz, $CDCl_3$) δ 155.03, 142.21, 134.10, 121.08, 119.68, 90.46; **HRMS –** *unable to obtain due to decomposition*

XB BODIPY Activated Ester 4.14



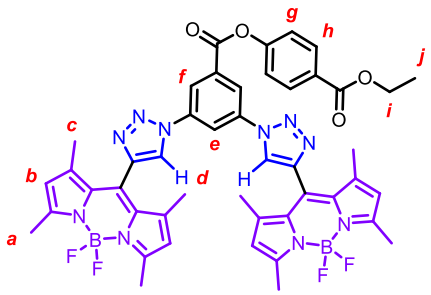
3,5-diazidoactive ester **4.13** (23 mg, 0.0655 mmol, 1 eq), BODIPY-iodoalkyne **4.10** (60 mg, 0.151 mmol, 2.3 eq), $Cu(CH_3CN)_4PF_6$ (5 mg, 0.0131 mmol, 0.2 eq) and TBTA (7 mg, 0.0131 mmol, 0.2 eq) were dissolved in anhydrous CH_2Cl_2 (5 mL) and stirred for 16 h under N_2 in the dark. TLC indicated incomplete reaction, thus more $Cu(CH_3CN)_4PF_6$ (5 mg, 0.0131 mmol, 0.2 eq) and TBTA (7 mg, 0.0131 mmol, 0.2 eq) were added and the reaction stirred for a further 16 h. The reaction mixture was then washed with a aqueous EDTA solution (2 x 20 mL), followed by washing with water (2 x 20 mL). The organic phase was dried over $MgSO_4$, reduced *in vacuo* and the product purified by preparative TLC (3% EtOAc in CH_2Cl_2) affording **4.14** as a red solid (74 mg 0.0645 mmol, 98%). **^{1}H NMR** (400 MHz, $CDCl_3$) δ 8.70 (d, *J* = 2.0 Hz, 2H, H_e), 8.26 (t, *J* = 2.0 Hz, 1H, H_d), 8.23 – 8.15 (m, 2H, H_f), 7.42 – 7.30 (m, 2H, H_g), 6.07 (s, 4H, H_b), 4.41 (q, *J* = 7.1 Hz, 2H, H_h), 2.59 (s, 12H, H_a), 1.57 (s, 12H, H_c), 1.42 (t, *J* = 7.1 Hz, 3H, H_i); **^{13}C NMR** (126 MHz, $CDCl_3$) δ 165.71, 162.23, 157.51, 153.76, 142.58, 142.34, 138.49, 133.54, 132.44, 131.62, 129.22, 127.02, 122.06, 121.56, 121.54, 121.02, 116.43, 61.47, 14.93, 14.74, 14.48; **HRMS** (ESI +ve) m/z= 1129.1453 ($[M–F^-]^+$, $C_{46}H_{40}B_2F_3I_2N_{10}O_4$, calc= 1129.1462).

XB BODIPY Receptor 4.15



Active ester **4.14** (30 mg, 0.026 mmol, 1 eq) and PEG-benzyl alcohol **3.14** (31 mg, 0.052 mmol, 2 eq) were dissolved in anhydrous 1,2-dichloroethane (4 mL). Three drops of triethylamine were added, and the reaction was stirred at 50 °C under N_2 in the dark for 2 d. The solution was then partitioned between CH_2Cl_2 (30 mL) and water (30 mL) and washed with water (2 x 30 mL), whereafter the organic phase was dried over $MgSO_4$ and reduced *in vacuo*. The product was then purified and isolated by preparative TLC (5% MeOH in CH_2Cl_2) as a red solid (6.5 mg, 0.004 mmol, 16%). **^{1}H NMR** (400 MHz, $CDCl_3$) δ 8.55 (d, *J* = 2.1 Hz, 2H, H_e), 8.19 (t, *J* = 2.0 Hz, 1H, H_d), 6.72 (s, 2H, H_g), 6.07 (s, 4H, H_b), 5.39 (s, 2H, H_f), 4.18 – 4.13 (m, 6H, OCH_2), 3.86 – 3.74 (m, 8H, OCH_2), 3.74 – 3.48 (m, 29H, OCH_2), 3.36 (s, 3H, OCH_3), 3.35 (s, 6H, OCH_3), 2.59 (s, 12H, H_a), 1.58 (s, 12H, H_c); **^{13}C NMR** (126 MHz, $CDCl_3$) δ 163.34, 157.70, 154.70, 152.90, 152.24, 147.62, 142.14, 139.12, 137.72, 136.64, 133.40, 132.18, 130.32, 127.74, 126.48, 123.25, 122.53, 121.95, 108.64, 82.55, 72.41, 71.97, 71.92, 70.83, 70.71, 70.66, 70.54, 69.72, 69.13, 68.18, 59.04, 29.72; **HRMS:** (ESI +ve) m/z= 1599.3924 ($[M+Na]^+$, $C_{65}H_{80}B_2F_4I_2N_{10}O_{14}Na$, calc= 1599.3965).

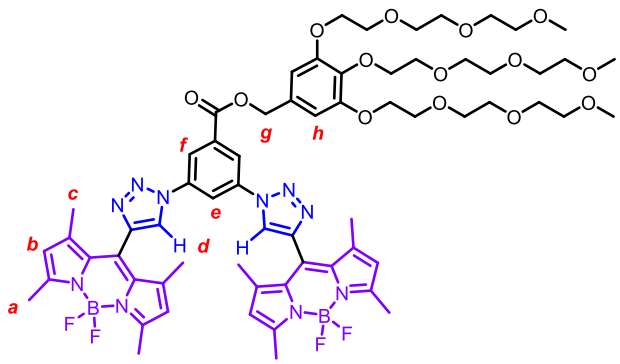
HB BODIPY Activated Ester 4.16



3,5-Diazidoactive ester **4.13** (29 mg, 0.083 mmol, 1 eq), BODIPY-alkyne **4.11** (52 mg, 0.191 mmol, 2.3 eq), $Cu(CH_3CN)_4PF_6$ (6.2 mg, 0.0166 mmol, 0.2 eq) and TBTA (8.8 mg, 0.0166 mmol,

0.2 eq) were dissolved in anhydrous CH_2Cl_2 (5 mL) and stirred overnight under N_2 in the dark. The reaction mixture was then washed with aqueous EDTA solution (2 x 10 mL), followed by washing with water (2 x 10 mL). The organic phase was dried over $MgSO_4$, reduced *in vacuo* and the product purified by preparative TLC (eluent: 4% EtOAc in CH_2Cl_2) affording **4.14** as a red solid (69.5 mg, 0.0775 mmol, 93%). **^{1}H NMR** (400 MHz, $CDCl_3$) δ 8.85 (t, *J* = 2.1 Hz, 1H, H_e), 8.68 (d, *J* = 2.1 Hz, 2H, H_f), 8.31 (s, 2H, H_d), 8.19 (d, *J* = 8.8 Hz, 2H, H_g), 7.35 (d, *J* = 8.8 Hz, 2H, H_h), 6.05 (s, 4H, H_b), 4.41 (q, *J* = 7.1 Hz, 2H, H_i), 2.58 (s, 12H, H_a), 1.58 (s, 12H, H_c), 1.42 (t, *J* = 7.1 Hz, 4H, H_j); **^{13}C NMR** (126 MHz, $CDCl_3$) δ 165.71, 162.23, 157.51, 153.76, 142.58, 142.34, 138.49, 133.54, 132.44, 131.62, 129.22, 127.02, 122.06, 121.56, 121.54, 121.02, 116.43, 61.47, 14.93, 14.74, 14.48; **HRMS:** (ESI +ve) m/z= 877.3518 ($[M–F^-]^+$: $C_{46}H_{42}B_2F_3N_{10}O_4$, calc= 877.3529).

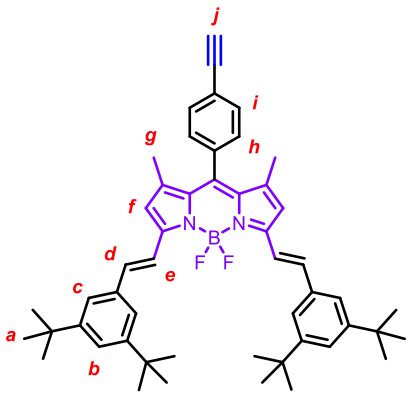
HB BODIPY Receptor 4.17



Active ester **4.16** (30 mg, 0.0335 mmol, 1 eq) and PEG-benzyl alcohol **3.14** (40 mg, 0.067 mmol, 2 eq) were dissolved in anhydrous 1,2-dichloroethane (4 mL). Triethylamine (10 mg, 14 µL, 0.1 mmol, 3 eq) was added and the reaction stirred under N_2 in the dark overnight. TLC indicated only minor conversion, thus the reaction was heated to 50 °C for 2 d. The solution was then partitioned between CH_2Cl_2 (30 mL) and water (30 mL) and washed with water twice (2 x 30 mL), whereafter the organic phase was dried over $MgSO_4$ and reduced *in vacuo*. The product was then obtained by preparative TLC (Eluent: 5% MeOH in CH_2Cl_2) as a red solid (25 mg, 0.0189 mmol, 56%). **^{1}H NMR** (400 MHz, $CDCl_3$) δ 8.78 (t, *J* = 2.1 Hz, 1H, H_e), 8.52 (d, *J* = 2.1 Hz, 2H, H_f), 8.32 (s, 2H, H_d), 6.73 (s, 2H, H_h), 6.03 (s, 4H, H_b), 5.35 (s, 2H, H_g), 4.19 – 4.13 (m, 6H, OCH_2), 3.85 – 3.76 (m, 6H, OCH_2), 3.74 – 3.67 (m, 6H, OCH_2), 3.67 – 3.58 (m, 12H, OCH_2), 3.56 – 3.47 (m, 6H, OCH_2), 3.36 (s, 3H, OCH_3), 3.34 (s, 6H, OCH_3), 2.57 (s, 12H, H_a) 1.56 (s, 12H, H_c); **^{13}C NMR** (126 MHz, $CDCl_3$) δ 163.87, 157.42, 153.01, 142.67, 142.14, 138.24, 134.48, 132.47, 130.27, 127.25, 123.54, 122.01, 121.63, 120.66, 115.85, 109.25, 72.52, 72.09,

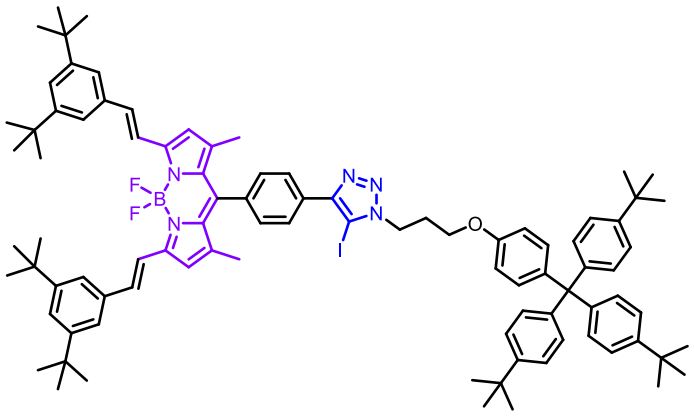
72.04, 70.93, 70.80, 70.67, 69.88, 69.20, 68.52, 59.17, 59.14, 14.92, 14.73; **HRMS:** (ESI +ve) m/z= 1347.6000 ($[M+Na]^+$, $C_{65}H_{82}B_2F_4N_{10}O_{14}Na$, calc= 1347.6046).

BODIPY Alkyne Stopper 4.20



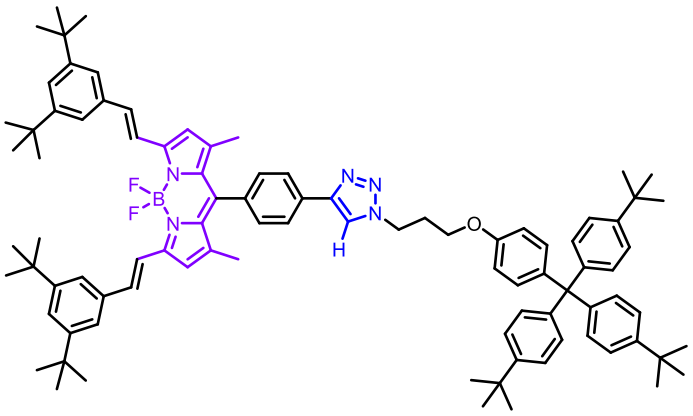
To a solution of BODIPY alkyne **4.19** (20 mg, 0.057 mmol, 1 eq) in dry MeCN (3 mL), $MgSO_4$ (68 mg, 0.57 mmol, 10 eq), 3,5-di-tert-butylbenzaldehyde (63 mg, 0.29 mmol, 5 eq), pyrrolidine (48 µL, 0.57 mmol, 10 eq) and glacial acetic acid (33 µL, 0.57 mmol, 10 eq) were added. The reaction was immersed in an oil bath at 80 °C, upon which a colour change from orange to red was observed, for 30 minutes. The solvent was removed *in vacuo* and the crude dissolved in CH_2Cl_2 (15 mL) and washed with 0.05 M HCl (15 mL), saturated $NaHCO_3$ solution (15 mL) and brine (15 mL). The organic phase was dried over $MgSO_4$, filtered and the solvents removed *in vacuo*. Purification was achieved by column chromatography (eluent: Hexane/CH_2Cl_2 1:1) to afford a blue powder (23 mg, 53%). **^{1}H NMR** (400 MHz, $CDCl_3$) δ 7.77 (d, *J* = 16.3 Hz, 2H, H_e), 7.65 (d, *J* = 8.3 Hz, H_i), 7.45 (d, *J* = 1.8 Hz, 4H, H_c), 7.41 (t, *J* = 1.8 Hz, 2H, H_b), 7.35 (d, *J* = 8.3 Hz, 2H, H_h), 7.29 (d, *J* = 16.3 Hz, 2H, H_d), 6.65 (s, 2H, H_f), 3.19 (s, 1H, H_j), 1.48 (s, 6H, H_g), 1.37 (s, 36H, H_a). **^{13}C NMR** (126 MHz, $CDCl_3$) δ 153.03, 151.25, 141.84, 137.44, 136.01, 135.96, 133.02, 132.93, 128.83, 123.71, 122.93, 121.95, 118.98, 117.87, 83.10, 78.68, 35.01, 31.75, 31.55, 22.82, 15.04, **^{19}F NMR** (376 MHz, $CDCl_3$) δ -138.43, -138.52, -138.61, -138.69. **HRMS** (ESI +ve) m/z= 748.4748 ($[M + H]^+$, $C_{51}H_{59}BF_2N_2$, calc= 748.4752).

XB BODIPY Axle 4.21



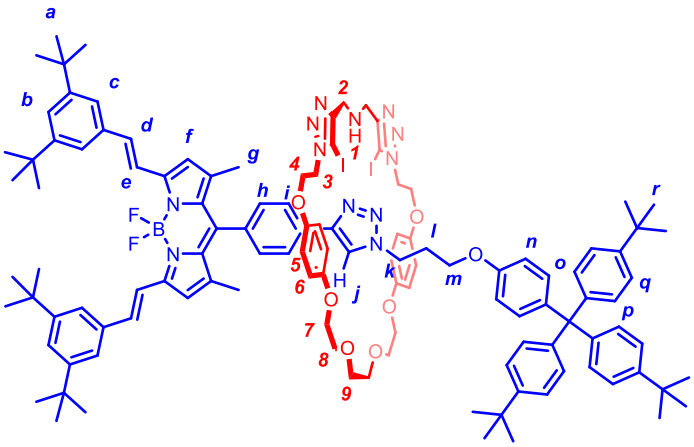
NaI (11 mg, 0.074 mmol, 4 eq) and $Cu(ClO_4).6H_2O$ (14 mg, 0.038 mmol, 2 eq) were suspended in dry THF (0.3 mL) and stirred for 5 min. Stopper azide (11 mg, 0.02 mmol, 1.05 eq), TBTA (0.3 mg, 0.6 µmol, 0.03 eq), DBU (2.8 µL, 0.02 mmol, 1 eq) and BODIPY alkyne **4.20** (15 mg, 0.10 mmol, 1.05 eq) were added and the reaction mixture topped up with MeCN (0.3 mL). The reaction was left to stir for 72 h before the solvent was removed *in vacuo*. The crude was dissolved in CH_2Cl_2 (5 mL) and washed with EDTA solution (3 x 5 mL) and brine (5 mL). The organic phase was concentrated *in vacuo* and purified *via* column chromatography (eluent: CH_2Cl_2) and the desired product was isolated as a red solid (4 mg, 14%). **^{1}H NMR** (400 MHz, $CDCl_3$) δ 8.13 (d, *J* = 8.2 Hz, 2H, H_i), 7.79 (d, *J* = 16.3 Hz, 2H, H_e), 7.49 – 7.44 (m, 6H, $H_{b,h}$), 7.41 (t, *J* = 1.8 Hz, 2H, H_c), 7.29 (d, *J* = 16.1 Hz, 3H, H_d), 7.25 – 7.22 (m, 6H, H_o), 7.13 – 7.07 (m, 8H, $H_{n,p}$), 6.79 (d, *J* = 8.9 Hz, 2H, H_m), 6.66 (s, 2H, H_f), 4.71 (t, *J* = 7.0 Hz, 2H, H_j), 4.08 (t, *J* = 5.7 Hz, 2H, H_l), 2.51 – 2.44 (m, 2H, H_k), 1.38 (s, 36H, H_a), 1.45 (s, 6H, H_g), 1.30 (s, 27H, H_q). **^{13}C NMR** (126 MHz, $CDCl_3$) δ 156.22, 152.91, 151.24, 149.07, 148.44, 144.16, 142.01, 140.18, 138.01, 137.29, 136.01, 135.60, 133.23, 132.43, 131.08, 130.79, 128.91, 128.04, 124.21, 123.66, 121.93, 119.05, 117.80, 113.16, 63.97, 63.14, 48.23, 42.03, 35.01, 34.44, 32.08, 31.55, 31.51, 29.86, 29.53, 22.86, 15.07, 14.32; **^{19}F NMR** (376 MHz, $CDCl_3$) δ -138.42, -138.51, -138.60, -138.68. **HRMS** (ESI +ve) m/z= 1462.7676 ($[M + H]^+$, $C_{91}H_{107}BF_2IN_5O$, calc= 1462.7654).

HB BODIPY Axle 4.22



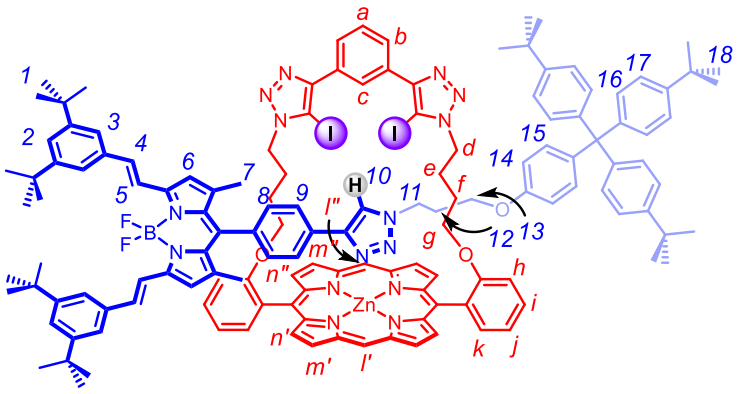
BODIPY stopper **4.20** (5.1 mg, 6.8 mmol, 1 eq), azide stopper (4.6 mg, 6.8 mmol 1 eq), TBTA (0.36 mg, 0.68 mmol, 0.1 eq) and $Cu(CH_3CN)_4.PF_6$ (0.38 mg, 1.02 mmol, 0.15 eq) were dissolved in dry degassed THF (0.5 mL) and left to stir for 48 h in darkness. CH_2Cl_2 (5 mL) was added and the mixture washed with EDTA solution (3 x 5 mL) and H_2O (5 mL). The organic phase was dried over Na_2SO_4, filtered and concentrated *in vacuo*. The crude product was purified *via* column chromatography (eluent: CH_2Cl_2) and the desired product was isolated as a red solid (7.6 mg, 85%). **^{1}H NMR** (400 MHz, $CDCl_3$) δ 7. 97 (d, *J* = 8.3 Hz, 2H, H_i), 7.88 (s, 1H, H_j), 7.79 (d, *J* = 16.3 Hz, 2H, H_e), 7.46 (d, *J* = 1.8 Hz, 4H, H_c), 7.44 – 7.38 (m, 4H, $H_{b,h}$), 7.29 (d, *J* = 16.1 Hz, 2H, H_d), 7.25 – 7.21 (m, 6H, H_p), 7.12 (d, *J* = 8.8 Hz, 2H, H_n), 7.10 – 7.05 (m, 6H, H_q), 6.80 (d, *J* = 8.8 Hz, 2H, H_o), 6.65 (s, 2H, H_f), 4.68 (t, *J* = 6.8 Hz, 2H, H_k), 4.02 (t, *J* = 5.6 Hz, 2H, H_m), 2.48 – 2.24 (m, 2H, H_l), 1.52 (s, 6H, H_g), 1.38 (s, 36H, H_a), 1.30 (s, 27H, H_r). **^{13}C NMR** (126 MHz, $CDCl_3$) δ 156.28, 152.87, 151.24, 148.50, 147.14, 144.11, 141.99, 140.30, 138.15, 137.24, 136.01, 135.15, 133.26, 132.51, 131.35, 130.79, 129.23, 126.38, 124.22, 123.65, 121.92, 120.73, 119.06, 117.76, 113.02, 63.83, 63.14, 47.45, 35.01, 34.86, 34.44, 31.55, 31.50, 30.19, 15.10. **^{19}F NMR** (376 MHz, $CDCl_3$) δ -138.50, -138.60, -138.68, -156.63; **HRMS** (ESI +ve) m/z= 1336.8682 ($[M + H]^+$, $C_{91}H_{108}BF_2N_5O$, calc= 1336.8688).

BODIPY Rotaxane 4.23



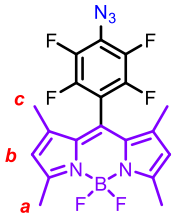
Macrocycle (20 mg, 0.0122 mmol, 1 eq) and $Cu(CH_3CN)_4PF_6$ (4.5 mg, 0.0122 mmol, 1 eq) were dissolved in dry degassed CH_2Cl_2 (1 mL). Stopper BODIPY alkyne **4.20** (36.62 mg, 0.049 mmol, 4 eq) and stopper azide (28.7 mg, 0.049 mmol, 4 eq) were subsequently added the reaction was left to stir for 3 days. The solvent was removed in vacuo and the crude was purified via preparative TLC (eluent 5% MeOH in CH_2Cl_2) affording rotaxane 4.23 as a blue powder (5.2 mg, 20 %). **^{1}H NMR** (400 MHz, $CDCl_3$) δ 7.94 (d, *J* = 7.9 Hz, 2H, H_i), 7.90 (s, 1H, H_j), 7.80 (d, *J* = 16.3 Hz, 2H, H_e), 7.46 (d, *J* = 1.8 Hz, 4H, H_c), 7.41 (t, *J* = 1.8 Hz, 2H, H_b), 7.38 (d, *J* = 7.9 Hz, 2H, H_h), 7.30 (d, *J* = 16.3 Hz, 2H, H_d), 7.28 – 7.23 (m, 6H, H_p), 7.17 – 7.09 (m, 8H, $H_{n,q}$), 6.66 (s, 2H, H_f), 6.54 – 6.45 (m, 6H, $H_{5,o}$), 6.41 (d, *J* = 9.1 Hz, 4H, H_6), 4.67 – 4.63 (m, 2H, H_3), 4.21 – 4.18 (m, 4H, H_4), 3.89 (s, 4H, H_2), 3.85 – 3. 81 (m, 6H, $H_{k,7}$), 3.71 – 3.68 (m, 4H, H_8), 3.63 (s, 4H, H_9), 3.35 (t, *J* = 5.8 Hz, 2H, H_m), 1.73 – 1.68 (m, 2H, H_l) 1.38 (s, 36H, H_a), 1.31 (s, 27H, H_r). **^{13}C NMR** (101 MHz, $CDCl_3$) δ 156.37, 153.17, 152.93, 151.95, 151.29, 149.80, 148.47, 144.40, 139.82, 137.27, 136.11, 133.40, 132.33, 130.84, 129.11, 126.43, 124.30, 123.65, 121.94, 117.77, 115.56, 115.22, 113.25, 80.89, 70.98, 69.93, 67.84, 66.88, 63.25, 49.74, 44.43, 35.03, 34.49, 31.58, 29.86, 29.55, 15.13. **HRMS** (ESI +ve) m/z= 2152.92871 ($[M + H]^+$, $C_{119}H_{142}O_7N_{12}{}^{10}BF_2{}^{127}I_2$, calc= 2152.93058.

BODIPY-Porphyrin Rotaxane 4.24



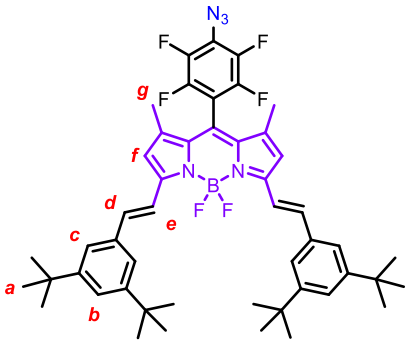
Strapped porphyrin macrocycle (10 mg, 0.009 mmol, 1 eq) and $[Cu(CH_3CN)_4]PF_6$ (3.3 mg, 0.009 mmol, 1 eq) were dissolved in dry and degassed CH_2Cl_2 (0.8 mL) in a sealed vial and the mixture was stirred at room temperature under N_2 for 15 minutes. A solution of terphenyl-stoppered azide (26 mg, 0.044 mmol, 5 eq) in CH_2Cl_2 (0.5 mL) was added into the reaction vial, followed by addition of BODIPY-stoppered alkyne **4.20** (33 mg, 0.044 mmol, 5 eq) dissolved in CH_2Cl_2 (0.5 mL). The reaction mixture was stirred at 40°C in dark for two days. The crude was diluted with CH_2Cl_2 (20 mL) and washed with basic aqueous EDTA (20 mL). The aqueous layer was back-extracted with CH_2Cl_2 (10 mL × 3) to minimise the loss of products. The combined organic layer was dried with anhydrous $MgSO_4$, filtered and concentrated on rotary evaporator. The crude solid residue obtained was purified by preparative TLC (4% EtOAc in CH_2Cl_2) to afford [2]rotaxane **4.24** as blue powder (7.6 mg, 35%). **^{1}H NMR** (500 MHz, $CDCl_3$) □ (ppm): 10.10 (s, 1H; *l'*), 9.77 (s, 1H; *l''*), 9.26 (d, *J* = 4.4 Hz, 2H; *m'*), 9.11 (d, *J* = 4.4 Hz, 2H; *m''*), 8.98 (d, *J* = 4.4 Hz, 2H; *n'*), 8.95 (d, *J* = 4.4 Hz, 2H; *n''*), 8.02 (dd, *J* = 7.3, 1.8 Hz, 2H; *b*), 7.80 (d, *J* = 16.2 Hz, 2H; *4*), 7.76 (t, *J* = 8.0 Hz, 2H; *i*), 7.56 (dd, *J* = 7.7, 1.8 Hz, 2H; *k*), 7.47 (d, *J* = 1.8 Hz, 4H; *3*), 7.42 (t, *J* = 1.8 Hz, 2H; *2*), 7.38 (t, *J* = 7.6 Hz, 1H; *a*), 7.35 (d, *J* = 8.5 Hz, 2H; *h*), 7.33 – 7.29 (m, 9H; *c*,*5*,*16*), 7.28 (d, *J* = 9.0 Hz, 2H; *15*), 7.24 – 7.14 (m, 4H; *j*,*14*), 7.12 – 7.06 (m, 6H; *17*), 6.66 (s, 2H; *6*), 6.56 (s, 1H; 10^{Trz}), 6.37 (d, *J* = 8.3 Hz, 2H; *8*), 4.22 – 4.13 (m, 2H; *9*), 4.09 – 3.99 (m, 4H; *d*), 3.79 – 3.69 (m, 4H; *g*), 1.73 – 1.57 (m, 4H, *e*), 1.47 (s, 6H; *7*) 1.39 (s, 36H; *1*), 1.36 (s, 27H; *18*), 0.86 – 0.76 (m, 4H, *f*). (Signals of proton *11*–*13* missing due to peaks overlap); **^{13}C NMR** (126 MHz, $CDCl_3$) □ (ppm): 158.80, 152.91, 151.30, 150.33, 150.13, 149.48, 149.38, 148.53, 148.33, 144.46, 142.03, 137.24, 137.04, 136.15, 134.52, 133.37, 132.16, 132.08, 131.99, 131.76, 131.57, 130.88, 130.80, 130.06, 129.61, 128.97, 128.86, 127.05, 125.88, 125.65, 124.37, 123.64, 121.96, 119.99, 119.20, 117.75, 115.78, 113.37, 112.85, 105.95, 105.84, 68.87, 63.05, 53.57, 49.98, 44.65, 35.04, 34.54, 31.66, 31.59, 29.86, 25.82, 25.61, 22.85, 15.20, 14.28; **HRMS** (ESI +ve) m/z: 2466.94248 ($[M+H]^+$, $C_{141}H_{148}O_3N_{15}BF_2I_2Zn$ calc=2466.93668).

BODIPY Azide 4.26



2,4-Dimethylpyrrole (472 µL, 4.68 mmol, 2.05 eq) and 4-azido-tetrafluorobenzaldehyde (500 mg, 2.28 mmol, 1 eq) were dissolved in dry CH_2Cl_2 (150 mL), 2 drops of TFA were added and the mixture was left to stir for 12 h. *p*-Chloranil (561 mg, 2.28 mmol, 1 eq) was added and the reaction mixture was left to stir for a further 3 h before NEt_3 (2.22 mL, 15.96 mmol, 7 eq) followed by BF_3OEt_2 (2.25 mL, 18.24 mmol, 8 eq) were added in succession. The mixture was left to stir for a further 0.5 h before the solvent was removed *in vacuo*. The crude was purified by silica gel column chromatography (eluent: CH_2Cl_2:*n*-hexane 2:3 v/v) to afford the product as a red solid (356 mg, 35%). **^{1}H NMR** (400 MHz, $CDCl_3$) δ 6.05 (s, 2H, H_b), 2.57 (s, 6H, H_a), 1.64 (s, 6H; H_c); **^{13}C NMR** (151 MHz, $CDCl_3$) δ 157.78, 144.04, 141.73, 141.18, 131.21, 123.44, 122.30, 32.08, 29.85, 14.94, 13.81; **^{19}F NMR** (376 MHz, $CDCl_3$) δ -139.77, -139.91 (m), -146.16 (q, *J* = 32.2 Hz), -149.95 – -150.14 (m); **HRMS** (ESI +ve) m/z= 438.1317 ($[M + H]^+$, $C_{19}H_{15}N_5B_1F_6$, calc = 438.1321).

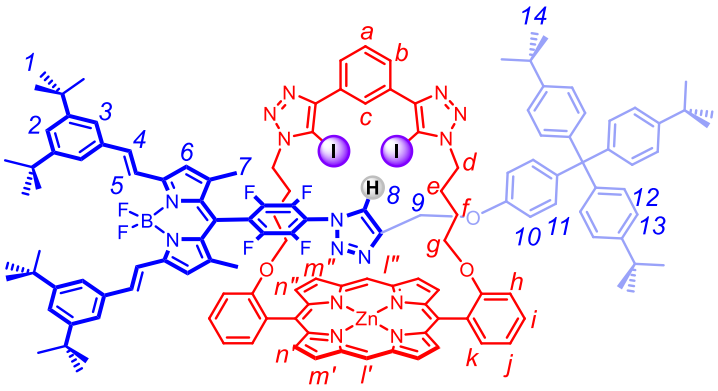
BODIPY Azide Stopper 4.27



To a mixture of azide-BODIPY **4.26** (100 mg, 0.23 mmol, 1 eq) in MeCN (10 mL), $MgSO_4$ (275 mg, 2.3 mmol, 10 eq), aldehyde (200 mg, 0.91 mmol, 4 eq), pyrrolidine (163 mg, 2.3 mmol, 10 eq) and glacial acetic acid (132 µL, 2.3 mmol, 10 eq) were added. The reaction was immersed in an oil bath at 60 °C, upon which a colour change from orange to blue was observed, for 1 h. The solvent was removed *in vacuo* and the crude dissolved in CH_2Cl_2 (10 mL) and washed with 0.05 M HCl (10 mL), saturated $NaHCO_3$ solution (10 mL) and brine (10 mL). The combined

organics were dried over $MgSO_4$, filtered and the solvents removed *in vacuo*. Purification was achieved by column chromatography (eluent: CH_2Cl_2:Hexane 3:2 *v/v*) to afford a blue powder (58 mg, 30%). **^{1}H NMR** (400 MHz, $CDCl_3$) δ 7.76 (d, *J* = 16.3 Hz, 2H, H_d), 7.48 – 7.41 (m, 6H, $H_{c,b}$), 7.33 (d, *J* = 16.3 Hz, 2H, H_e), 6.71 (s, 2H, H_f), 1.54 (s, 6H, H_h), 1.38 (s, 36H, H_a). **^{19}F NMR** (376 MHz, $CDCl_3$) δ -138.44, -138.53, -138.61, -138.70, -139.20, -139.22, -139.26, -139.28, -150.20, -150.23, -150.26, -150.29. **^{13}C NMR** (126 MHz, $CDCl_3$) δ 154.09, 151.27, 140.07, 138.59, 135.77, 132.99, 123.97, 122.01, 119.38, 118.73, 118.52, 34.90, 31.95, 31.42, 29.72, 29.38, 22.71, 14.14, 13.94. **HRMS** (ESI +ve) m/z= 836.4301 ($[M + H]^+$, $C_{51}H_{59}BF_2N_2$, calc = 836.4300).

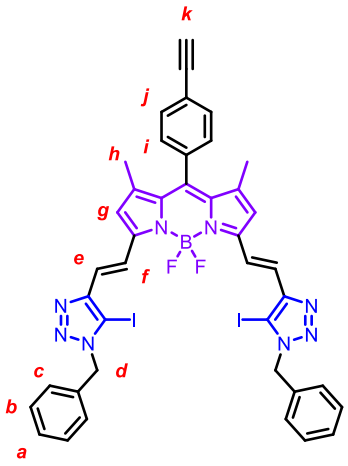
BODIPY-Porphyrin Rotaxane 4.28



Strapped porphyrin macrocycle (10 mg, 0.009 mmol, 1 eq) and $[Cu(CH_3CN)_4]PF_6$ (3.3 mg, 0.009 mmol, 1 eq) were dissolved in dry and degassed CH_2Cl_2 (0.8 mL) in a sealed vial and the mixture was stirred at room temperature under N_2 for 15 minutes. A solution of terphenyl-stoppered alkyne **2.31** (24 mg, 0.044 mmol, 5 eq) in CH_2Cl_2 (0.5 mL) was added into the reaction vial, followed by addition of BODIPY-stoppered azide **4.27** (37 mg, 0.044 mmol, 5 eq) dissolved in CH_2Cl_2 (0.5 mL). The reaction mixture was stirred at 40°C in dark for two days. The crude was diluted with CH_2Cl_2 (20 mL) and washed with basic aqueous EDTA (20 mL). The aqueous layer was back-extracted with CH_2Cl_2 (10 mL × 3) to minimise the loss of products. The combined organic layer was dried with anhydrous $MgSO_4$, filtered and concentrated on rotary evaporator. The crude solid residue obtained was purified by preparative TLC (0.5% EtOAc in CH_2Cl_2) to afford [2]rotaxane **4.28** as blue powder (8 mg, 37%). **^{1}H NMR** (400 MHz, CD_2Cl_2) δ (ppm): 9.98 (s, 1H; *l'*), 9.57 (s, 1H; *l''*), 9.21 (d, *J* = 4.5 Hz, 2H; *m'*), 9.03 (d, *J* = 4.5 Hz, 2H; *m''*), 8.93 (d, *J* = 4.4 Hz, 2H; *n'*), 8.91 (d, *J* = 4.4 Hz, 2H; *n''*), 7.92 (d, *J* = 6.5 Hz, 2H; *b*), 7.80 (t, *J* = 7.5 Hz, 2H; *i*), 7.75 (d, *J* = 16.3 Hz, 2H; *4*), 7.51 – 7.46 (m, 7H; *2,3,a*), 7.45 – 7.34 (m, 12H; *5,12,h,k*),

7.25 (d, *J* = 8.6 Hz, 6H; *13*), 7.21 (d, *J* = 7.8 Hz, 2H; *j*), 7.13 (t, *J* = 1.8 Hz, 1H; *c*), 6.76 (s, 2H; *6*), 6.70 (d, *J* = 8.8 Hz, 2H; *11*), 6.15 (s, 1H; *8*), 4.61 (d, *J* = 8.7 Hz, 2H; *10*), 4.25 – 4.03 (m, 4H; *d*), 3.96 – 3.73 (m, 4H; *g*), 1.63 (s, 6H; *7*), 1.39 (s, 36H; *1*), 1.38 (s, 27H; *14*), 0.56 (s, 2H; *9*); **^{13}C NMR** (126 MHz, $CDCl_3$) δ (ppm): 158.74, 154.38, 151.42, 150.29, 150.08, 149.52, 149.19, 149.08, 148.38, 148.17, 144.46, 140.07, 139.73, 138.91, 137.31, 135.89, 132.61, 132.36, 131.99, 131.71, 131.47, 131.18, 130.78, 130.68, 129.43, 128.65, 127.33, 126.54, 124.40, 124.17, 123.12, 122.19, 119.92, 118.82, 118.77, 118.55, 115.54, 113.14, 112.93, 105.63, 105.58, 68.72, 63.15, 50.28, 35.04, 34.55, 31.67, 31.56, 29.85, 25.96, 25.74, 25.65, 14.01, 1.17; **^{19}F NMR** (376 MHz, CD_2Cl_2) δ (ppm): -137.70 – -137.87 (m), -138.35 (q, *J* = 32.6 Hz), -145.01 – -145.18 (m); **HRMS** (ESI +ve) m/z: 2510.8677 ($[M+H]^+$ $C_{139}H_{140}BF_6I_2N_{15}O_3Zn$ calc=2510.8670).

XB BODIPY Receptor 4.28



To a solution of BODIPY alkyne **4.19** (8.4 mg, 0.024 mmol, 1 eq) in dry MeCN (1 mL), $MgSO_4$ (29 mg, 0.23 mmol, 10 eq), iodotriazole-aldehyde (30 mg, 0.096 mmol, 5 eq), pyrrolidine (20 µL, 0.23 mmol, 10 eq) and glacial acetic acid (14 µL, 0.23 mmol, 10 eq) were added. The reaction was immersed in an oil bath at 80 °C, upon which a colour change from orange to ruby red was observed, for 1 h. The solvent was removed *in vacuo* and the crude dissolved in CH_2Cl_2 (15 mL) and washed with 0.05 M HCl (15 mL), saturated $NaHCO_3$ solution (15 mL) and brine (15 mL). The combined organics were dried over $MgSO_4$, filtered and the solvents removed *in vacuo*. Purification was achieved by column chromatography (eluent: EtOAc:CH_2Cl_2 5:95 *v/v*) to afford a blue powder (8.1 mg, 36%). **^{1}H NMR** (400 MHz, DMSO-d_6); δ 7.93 (d, *J* = 16.1 Hz, 2H, H_f), 7.70 (d, *J* = 8.0 Hz, 2H, H_j), 7.52 (d, *J* = 8.0 Hz, 2H, H_i), 7.43 – 7.31 (m, 6H, $H_{a,b}$), 7.28 – 7.20 (m, 6H, $H_{f,c}$), 7.13 (s, 2H, H_g), 5.73 (s, 4H, H_d), 4.38 (s, 1H, H_k), 1.46 (s, 6H, H_h). **^{13}C NMR** (151 MHz, d_6-Acetone) δ 132.76, 128.81, 128.18, 127.58, 123.75, 53.69,

14.05 – *poor solubility hindered full spectroscopic characterisation*; **^{19}F NMR** (565 MHz, d_6-Acetone) δ -137.46, -137.52, -137.57, -137.63. **HRMS** (ESI +ve) m/z: 938.0943 ($[M+H]^+$ $C_{41}H_{31}BF_2I_2N_8$ calc=938.0944).

6.6. References

1 B. Y. Lee, S. R. Park, H. B. Jeon and K. S. Kim, *Tetrahedron Lett.*, 2006, **47**, 5105–5109.

2 A. Hassner and M. Stern, *Angew. Chem. Int. Ed. English*, 1986, **25**, 478–479.

3 A. Hassner, M. Stern, H. Gottlieb and F. Frolow, *J. Org. Chem.*, 1990, **55**, 2304–2306.

4 A. Dalmia, R. F. Savinell and C. C. Liu, *J. Electrochem. Soc.*, 1996, **143**, 1827–1833.

5 D. Brynn Hibbert and P. Thordarson, *Chem. Commun.*, 2016, **52**, 12792–12805.

6 P. Thordarson, *Chem. Soc. Rev.*, 2011, **40**, 1305–1323.

7 S. W. Robinson and P. D. Beer, *Org. Biomol. Chem.*, 2017, **15**, 153–159.

8 L. Yi, J. Shi, S. Gao, S. Li, C. Niu and Z. Xi, *Tetrahedron Lett.*, 2009, **50**, 759–762.

9 K. Muthuramu, N. Ramnath and V. Ramamurthy, *J. Org. Chem.*, 1983, **48**, 1872–1876.

10 K. M. Bonger, R. J. B. H. N. van den Berg, L. H. Heitman, A. P. IJzerman, J. Oosterom, C. M. Timmers, H. S. Overkleeft and G. A. van der Marel, *Bioorganic Med. Chem.*, 2007, **15**, 4841–4856.

11 A. A. Kudale, J. Kendall, C. C. Warford, N. D. Wilkins and G. J. Bodwell, *Tetrahedron Lett.*, 2007, **48**, 5077–5080.

12 J. F. Ayme, J. Lux, J. P. Sauvage and A. Sour, *Chem. Eur. J.*, 2012, **18**, 5565–5573.

13 H. W. Gibson, S. H. Lee, P. T. Engen, P. Lecavalier, J. Sze, Y. X. Shen and M. Bheda, *J. Org. Chem.*, 1993, **58**, 3748–3756.

14 V. Aucagne, K. D. Hänni, D. A. Leigh, P. J. Lusby and D. B. Walker, *J. Am. Chem. Soc.*, 2006, **128**, 2186–2187.

15 H. Zheng, W. Zhou, J. Lv, X. Yin, Y. Li, H. Liu and Y. Li, *Chem. Eur. J.*, 2009, **15**, 13253–13262.

16 H. Zhu, M. Lin & Z. Xuan, *US-201916729882 20191230*, 2020.

17 X. Li, J. Y. C. Lim and P. D. Beer, *Chem. Eur. J.*, 2018, **24**, 17788–17795.

18 K. C. Elbert, D. Jishkariani, Y. Wu, J. D. Lee, B. Donnio and C. B. Murray, *Chem. Mater.*, 2017, **29**, 8737–8746.

19 A. Borissov, J. Y. C. Lim, A. Brown, K. E. Christensen, A. L. Thompson, M. D. Smith and P. D. Beer, *Chem. Commun.*, 2017, **53**, 2483–2486.

20 X. Wu, W. Wu, X. Cui, J. Zhao and M. Wu, *J. Mater. Chem. C*, 2016, **4**, 2843–2853.

21 J. F. W. Keana and S. X. Cai, *J. Org. Chem.*, 2002, **55**, 3640–3647.